UC Berkeley
UC Berkeley Electronic Theses and Dissertations

Title
Ion Transport in Nanostructured Block Copolymer/Ionic Liquid Membranes

Permalink
https://escholarship.org/uc/item/3xh5n289

Author
Hoarfrost, Megan Lane

Publication Date
2012

Peer reviewed|Thesis/dissertation

eScholarship.org Powered by the California Digital Library
University of California

Ion Transport in Nanostructured Block Copolymer/Ionic Liquid Membranes

By

Megan Lane Hoarfrost

A dissertation submitted in partial satisfaction of the

requirements for the degree in

Doctor of Philosophy

in

Chemical Engineering

in the

Graduate Division

of the

University of California, Berkeley

Committee in Charge:

Professor Rachel A. Segalman, Chair
Professor Jeffrey A. Reimer
Professor John S. Newman
Professor John Arnold

Spring 2012

Ion Transport in Nanostructured Block Copolymer/Ionic Liquid Membranes

© 2012

by Megan Lane Hoarfrost

Abstract

Ion Transport in Nanostructured Block Copolymer/Ionic Liquid Membranes

by

Megan Lane Hoarfrost

Doctor of Philosophy in Chemical Engineering

University of California, Berkeley

Professor Rachel A. Segalman, Chair

Incorporating an ionic liquid into one block copolymer microphase provides a platform for combining the outstanding electrochemical properties of ionic liquids with a number of favorable attributes provided by block copolymers. In particular, block copolymers thermodynamically self-assemble into well-ordered nanostructures, which can be engineered to provide a durable mechanical scaffold and template the ionic liquid into continuous ion-conducting nanochannels. Understanding how the addition of an ionic liquid affects the thermodynamic self-assembly of block copolymers, and how the confinement of ionic liquids to block copolymer nanodomains affects their ion-conducting properties is essential for predictable structure-property control.

The lyotropic phase behavior of block copolymer/ionic liquid mixtures is shown to be reminiscent of mixtures of block copolymers with selective molecular solvents. A variety of ordered microstructures corresponding to lamellae, hexagonally close-packed cylinders, body-centered cubic, and face-centered cubic oriented micelles are observed in a model system composed of mixtures of imidazolium bis(trifluoromethylsulfonyl)imide ([Im][TFSI]) and poly(styrene-*b*-2-vinyl pyridine) (PS-*b*-P2VP). In contrast to block copolymer/molecular solvent mixtures, the interfacial area occupied by each PS-*b*-P2VP chain decreases upon the addition of [Im][TFSI], indicating a considerable increase in the effective segregation strength of the PS-*b*-P2VP copolymer with ionic liquid addition.

The relationship between membrane structure and ionic conductivity is illuminated through the development of scaling relationships that describe the ionic conductivity of block copolymer/ionic liquid mixtures as a function of membrane composition and temperature. It is shown that the dominant variable influencing conductivity is the overall volume fraction of ionic liquid in the mixture, which means there is incredible freedom in designing the block copolymer architecture in order to optimize the mechanical and other properties of the membrane without sacrificing conductivity. The derived scaling relationships are shown to be general for many block copolymer and ionic liquid chemistries.

In certain cases, the mechanism of ion conduction in the ionic liquid is affected by block copolymer nanoconfinement. The introduction of excess neutral imidazole to [Im][TFSI]

leads to enhanced proton conductivity as well as a high H^+ transference number due to facilitated proton hopping between imidazole molecules. We show that there is increased proton hopping when the nonstoichiometric ionic liquid is confined to lamellar block copolymer nanodomains, which we hypothesize is due to changes in the hydrogen bond structure of the ionic liquid under confinement. This, in combination with unique ion aggregation behavior, leads to a lower activation energy for macroscopic ion transport compared to that in a corresponding homopolymer/ionic liquid mixture.

Through this work, we further the understanding of the relationship between membrane composition, structure, and ion transport. The findings presented herein portend the rational design of nanostructured membranes having improved mechanical properties and conductivity.

Table of Contents

List of Figures iv

List of Tables vii

Acknowledgements viii

Chapter 1. Introduction 1

1.1. Electrochemical Applications of Ionic Liquid-Containing Membranes 1

1.2. Routes for Combining Polymers with Ionic Liquids 3

1.3. Self-Assembly of Mixtures of Block Copolymers with Ionic Liquids 6

1.3.1. Dilute Solutions of Block Copolymers in Ionic Liquids 9

1.3.2. Concentrated Solutions of Block Copolymers in Ionic Liquids 12

1.4. Relationship between Structure and Conductivity 14

1.5. Understanding Ion Transport in Nanostructured Mixtures of Block Copolymers with Ionic Liquids 17

1.6. References 18

Chapter 2. Effect of an Ionic Liquid Solvent on the Phase Behavior of Block Copoolymers 25

2.1. Introduction 25

2.2. Experimental Section 26

2.3. Results and Discussion 29

2.3.1. Thermal Properties of PS-*b*-P2VP/[Im][TFSI] System 29

2.3.2. Domain Spacing 31

2.3.3. Lyotropic Phase Behavior 35

2.3.4. Thermotropic Phase Behavior 38

2.4. Conclusions 41

2.5. Acknowledgements 41

2.6. Appendix: Supporting DSC, SAXS, and SANS 42

2.7. References 46

Chapter 3. Ionic Conductivity of Nanostructured Block Copolymer/Ionic Liquid Membranes 48

3.1. Introduction 48

3.2. Experimental Section 50

3.3. Results and Discussion 56

3.3.1. Ionic Conductivity of PS-*b*-P2VP/[Im][TFSI] 56

3.3.2. Universality of Ionic Conductivity of Block Copolymer/Ionic Liquid Mixtures 61

3.4. Conclusions 65

3.5. Acknowledgements 65

3.6. Appendix: Supporting SAXS and AC Impedance Spectroscopy 66

3.7. References 70

Chapter 4. Conductivity Scaling Rules for Nanostructured Block Copolymer/Ionic Liquid Membranes 72

4.1. Introduction 72

4.2. Experimental Section 73

4.3. Results and Discussion 78

4.4. Conclusions 81

4.5. Acknowledgements 81

4.6. References 82

Chapter 5. Proton Hopping and Long-range Transport in the Protic Ionic Liquid [Im][TFSI], Probed by Pulsed-Field Gradient NMR and Quasi-Elastic Neutron Scattering 84

5.1. Introduction 84

5.2. Experimental Section 85

5.3. Results and Discussion 88

5.4. Conclusions 99

5.5. Acknowledgements 102

5.6. Appendix: Supporting PGSE NMR and QENS 103

5.7. References 105

Chapter 6. Effect of Confinement on Proton Transport Mechanisms in Block Copolymer/Ionic Liquid Membranes 107

6.1. Introduction 107

6.2. Experimental Section 109

6.3. Results and Discussion 114

6.4. Conclusions 125

6.5. Acknowledgements 125

6.6. Appendix: Supporting SAXS, PGSE NMR, and QENS 127

6.7. References 131

Chapter 7. Conclusion and Future Outlook 134

List of Figures

Figure 1.1. Ionic Liquids 2

Figure 1.2. Proton Hopping in Imidazole 2

Figure 1.3. Routes for Incorporating Ionic Liquids into Polymers 4

Figure 1.4. Diblock Copolymer Morphologies 7

Figure 1.5. Doubly Thermoresponsive Micellization 11

Figure 1.6. Thermoresponsive Micellar Shuttles 11

Figure 1.7. Effect of Morphology on Conductivity 16

Figure 2.1. Chemical Structures of [Im][TFSI] and PS-*b*-P2VP 27

Figure 2.2. Glass Transition Temperature of P2VP/[Im][TFSI] Phase 30

Figure 2.3. SAXS Profiles of PS-*b*-P2VP/[Im][TFSI] Mixtures 32

Figure 2.4. Lyotropic Phase Diagrams of PS-*b*-P2VP/[Im][TFSI] Mixtures 34

Figure 2.5. Domain Spacing Scaling Analysis: Effect of Concentration 37

Figure 2.6. Domain Spacing Scaling Analysis: Effect of Molecular Weight 37

Figure 2.7. Temperature Dependent SAXS Profiles 40

Figure 2.A.1. DSC Heating Scans of PS-*b*-P2VP/[Im][TFSI] Mixtures 42

Figure 2.A.2. SANS Profiles of PS-*b*-P2VP/[Im][TFSI] Mixtures 43

Figure 2.A.3. SAXS Profiles of Mixtures with Fixed N_{P2VP} 44

Figure 2.A.4. Expanded SAXS Profiles 45

Figure 3.1. Chemical Structures of [Im][TFSI], [EMIm][TFSI], and PS-*b*-P2VP 52

Figure 3.2. DSC Heating Scans of PS-*b*-P2VP/Ionic Liquid Mixtures 54

Figure 3.3. Glass Transition Temperatures of P2VP/Ionic Liquid Phases 54

Figure 3.4. Domain Spacing Scaling Analysis of PS-*b*-P2VP/Ionic Liquid Mixtures 55

Figure 3.5. Ionic Conductivity of PS-*b*-P2VP/Ionic Liquid Mixtures 57

Figure 3.6. Concentration Dependence of Conductivity 59

Figure 3.7. Evidence that Conductivity Strongly Depends on ϕ_{IL} 60

Figure 3.8. Master Conductivity Curve 62

Figure 3.9. Conductivity and Glass Transition Temperature as a Function of Molecular Weight 64

Figure 3.A.1. SAXS Profiles of PS-*b*-P2VP/[EMIm][TFSI] Mixtures 66

Figure 3.A.2. Expanded PS-*b*-P2VP/[EMIm][TFSI] SAXS Profiles 67

Figure 3.A.3. Nyquist Plots 68

Figure 3.A.4. Evidence that Morphology Does Not Strongly Impact Conductivity 69

Figure 4.1. SAXS Profiles of Block Copolymer/Ionic Liquid Mixtures 75

Figure 4.2. Selectivity of [Im][TFSI] for PMMA 77

Figure 4.3. Ionic Conductivity of PS-*b*-PMMA/[Im][TFSI] Mixtures 79

Figure 4.4. Normalized Ionic Conductivity 80

Figure 4.5. Concentration Dependence of Ionic Conductivity 80

Figure 5.1. Chemical Structure of Imidazole, HTFSI, and Imidazolium and TFSI Ions 87

Figure 5.2. Proton Hopping in [Im][TFSI] 89

Figure 5.3. Mean Squared Displacement of Protons in [Im][TFSI] 91

Figure 5.4. HFBS QENS Profiles for [Im][TFSI] 93

Figure 5.5. HFBS QENS Fits for [Im][TFSI] 93

Figure 5.6. Dependence of DCS Quasi-elastic Scattering on Scattering Vector 95

Figure 5.7. Dependence of HFBS Quasi-elastic Scattering on Scattering Vector 96

Figure 5.8. Proton Diffusion in [Im][TFSI] 97

Figure 5.9. Fraction of Fast Proton Diffusion Process 98

Figure 5.10. Quasi-elastic Scattering of 4:1 [Im][TFSI] and 4:1 [*d*Im][TFSI] 100

Figure 5.11. Diffusion in [Im][TFSI] 101

Figure 5.12. Ionic Conductivity of [Im][TFSI] 101

Figure 5.A.1. PGSE NMR Data and Fits for [Im][TFSI] 103

Figure 5.A.2. DCS QENS Profiles of [Im][TFSI] 104

Figure 5.A.3. DCS QENS Fits for [Im][TFSI] 104

Figure 6.1. Chemical Structure of Nonstoichiometric [Im][TFSI] 110

Figure 6.2. Cation and Anion Diffusion as a Function of Temperature 115

Figure 6.3. Proton Diffusion Enhancement by Proton Hopping 117

Figure 6.4. QENS Profiles of Polymer/Ionic Liquid Mixtures 118

Figure 6.5. QENS Fits of *d*P2VP/[*d*Im][TFSI] Mixtures 119

Figure 6.6. Dependence of Quasi-elastic Scattering on Scattering Vector 121

Figure 6.7. MAS ^{1}H NMR Spectra of Polymer/Ionic Liquid Mixtures 122

Figure 6.8. Comparison of Conductivity and NMR Measurements 124

Figure 6.A.1. SAXS Profiles of Mixtures of PS-*b*-P2VP with Nonstoichiometric [Im][TFSI 127

Figure 6.A.2. PGSE NMR Data and Fits 128

Figure 6.A.3. Evidence that Diffusion Coefficients Do Not Depend on Diffusion Time in PGSE NMR Experiments 128

Figure 6.A.4. Cation and Anion Diffusion of Stoichiometric Mixtures 129

Figure 6.A.5. QENS Scattering Fits of *d*PS-*b*-*d*P2VP/[*d*Im][TFSI] Mixtures 130

List of Tables

Table 2.1. Characteristics of Block Copolymers Studied 27

Table 2.2. $f_{PS,eff}$ for Mixtures of [Im][TFSI] and PS-*b*-P2VP Copolymers with Constant N_{P2VP} 36

Table 2.3. γas a Function of IL:2VP 39

Table 3.1. Polymer Compositions and Morphologies of Block Copolymer/Ionic Liquid Mixtures 52

Table 4.1. Degree of Polymerization, Volume Fraction, and PDI of PS-*b*-P2VP and PS-*b*-PMMA Polymers Studied 75

Table 6.1. Degree of Polymerization, Volume Fraction, and PDI of Polymers Studied 110

Acknowledgements

I would like to thank my advisor, Professor Rachel Segalman, for being a wonderful mentor over the past five years. She has imparted me with vast knowledge about being a scientist, and given me the freedom to explore my intellectual curiosities. I would also like to thank my unofficial co-advisor, Professor Jeffrey Reimer, who has been deeply influential through his endless support and scientific guidance. My present and former labmates in both the Segalman and Reimer labs have also been incredibly encouraging, and I would like to thank them all for inspirational scientific discussions and, more importantly, their friendship. I am so lucky to have spent the last five years with such a talented, supportive, and fun group of individuals. I would especially like to thank Justin Virgili, who did fantastic work studying the self-assembly of mixtures of block copolymers with ionic liquids before I arrived at Berkeley, and patiently mentored me during my first few years of graduate school. Thank you also to Joel Stettler, with whom I spent an innumerable number of hours figuring out how to measure self-diffusion coefficients using NMR. I have also had the pleasure of working with some very talented undergraduates who have certainly challenged me intellectually and scientifically, and I hope I have done the same for them: Kevin Ng, Jay Bhatnagar, and Yuping Li. I would like to thank John Newman, Nitash Balsara, Clay Radke, Arun Majumdar, and John Arnold for the advice and guidance they have provided me through serving on my qualifying exam and thesis committees, as well as through many very helpful scientific discussions. I would also like to thank John Kerr for allowing me to do work in his laboratory, and for teaching me about electrochemistry. Thank you as well to Madhu Tyagi, who was hugely involved in guiding the quasi-elastic neutron scattering work. Finally, I would like to express great appreciation for the support of several members of the College of Chemistry staff: Aileen Harris, Rocio Sanchez, Fred Deakin, Cheryn Gliebe, and Carlet Altamirano.

Chapter 1: Introduction

Incorporating an ionic liquid into one block copolymer microphase provides a platform for combining the outstanding electrochemical properties of ionic liquids with a number of favorable attributes provided by block copolymers. In particular, block copolymers thermodynamically self-assemble into well-ordered nanostructures, which can be engineered to provide a durable mechanical scaffold, template the ionic liquid into continuous ion-conducting nanochannels, block gas transport, or incorporate a complementary functionality into the second ordered phase. Understanding how the addition of an ionic liquid affects the thermodynamic self-assembly of block copolymers and how the confinement of ionic liquids to block copolymer nanodomains affects their ion-conducting properties is essential for predictable structure-property control.

1.1. Electrochemical Applications of Ionic Liquid-Containing Membranes

Ionic liquids are salts that have low melting temperatures, where "low" generally means below 100 ºC.[1] The low melting temperatures stem from efficient charge delocalization by ring structures or strong electron-withdrawing groups in the anions and cations. Example structures are shown in Figure 1.1. Because ionic liquids are composed completely of ions, they have negligible volatility, which has garnered them attention as "green" solvents for synthesis and catalysis.[2-5] Reaction products can be distilled or extracted from ionic liquids using an immiscible solvent, and the ionic liquid can be reused. Furthermore, ionic liquids are good solvents for a wide range of organic and inorganic materials, where the solvent properties can be "tuned" by choosing one of several hundred (and counting) anion/cation pairs and by mixing different ionic liquids. They are capable of solubilizing macromolecules or combinations of chemically dissimilar reactants for which there are otherwise very few (or no) solvent choices. For instance, cellulose, currently one of the most important biorenewable materials, is insoluble in water and most molecular organic solvents, but is soluble in several ionic liquids.[6-8] Ionic liquids also demonstrate interesting gas separation properties, particularly with respect to CO_2 and SO_2 separation.[9, 10] In addition, most ionic liquids have excellent thermal and chemical stability.[1]

This combination of properties suggests that ionic liquids may be promising components in electrochemical devices.[11, 12] Inherently high ion densities and low melting temperatures lead to high ionic conductivities. Devices containing ionic liquids have wide operating temperature ranges due to the low volatility and thermal stability of ionic liquids, especially in comparison to devices with aqueous electrolytes. Furthermore, low volatility leads to flame retardancy, making ionic liquids safe and long-lasting electrolyte choices. Ionic liquids also have wide electrochemical windows, often in excess of 5 V.[13] Durable membranes exhibiting the favorable electrochemical properties of ionic liquids can be obtained by incorporating an ionic liquid into a compatible polymer. Such membranes are useful for a wide variety of electrochemical devices, including battery electrolytes,[14-18] fuel cells,[19-26] dye-sensitized solar cells,[27, 28] electrochemical sensors,[29] double layer capacitors,[30] actuators,[31] and transistors.[32] Particularly exciting is the potential for ionic liquids to replace water as a proton-conducting medium in proton

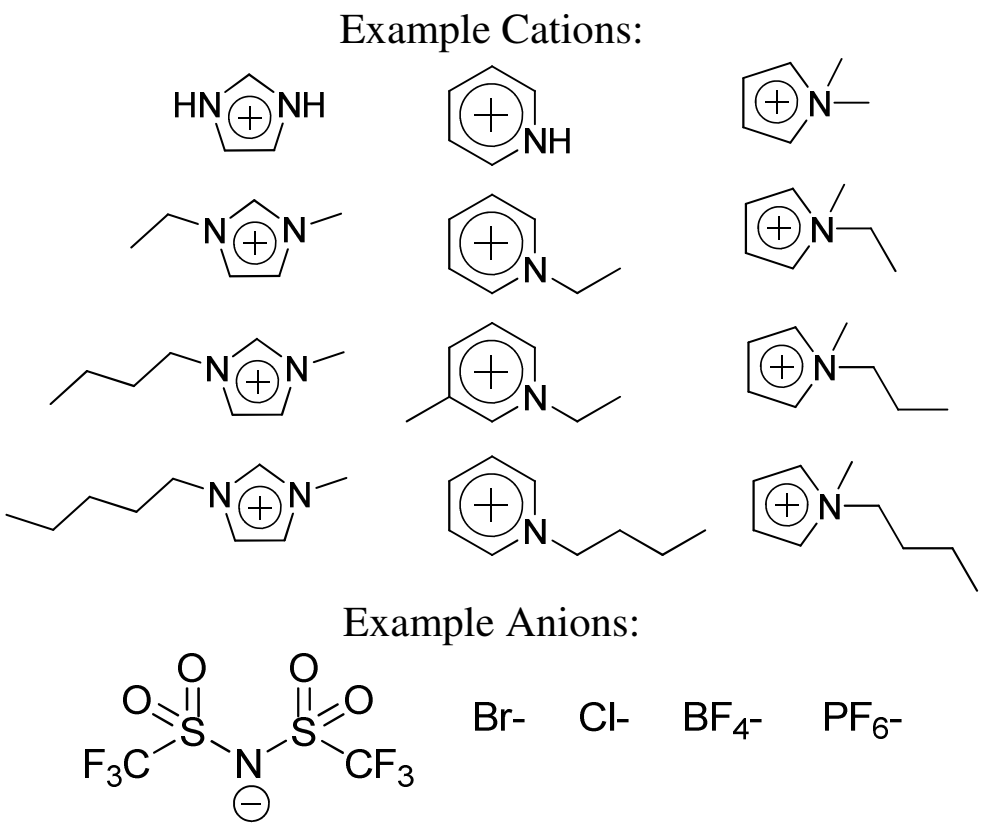


Figure 1.1. Ionic Liquids.

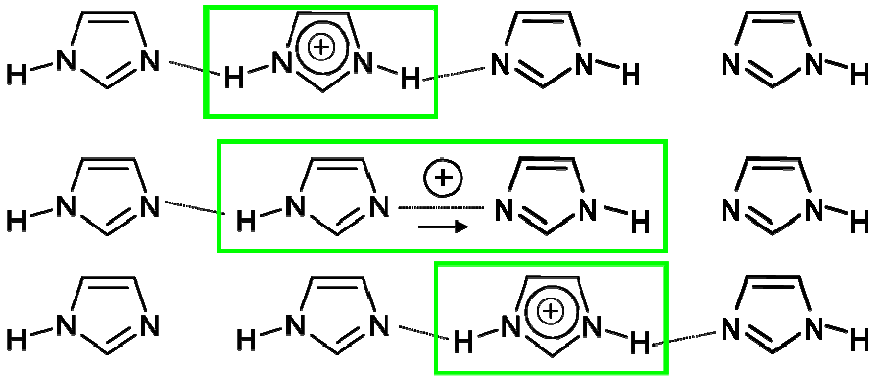


Figure 1.2. Proton Hopping in Imidazole.

exchange membranes (PEMs), for instance in fuel cells. Fuel cell membranes utilizing ionic liquids rather than water could operate at higher temperatures without complex water management, thus improving catalyst activity and reducing poisoning from carbon monoxide.[33] Furthermore, membranes containing ionic liquid could be designed to take advantage of the interesting gas separation properties of ionic liquids to block reactant and product gases from passing through the membrane. Imidazolium or pyrazolium-based ionic liquids are particularly suitable for these applications. Analogous to the Grotthuss mechanism in water,[34] imidazole and pyrazole molecules facilitate intermolecular proton transfer termed "proton hopping" (depicted for imidazole in Figure 1.2.), which leads to very high proton conductivity.[20, 35, 36] Using pulsed-field gradient (PFG) NMR to measure selectively the diffusion coefficients of acidic protons and imidazole molecules in imidazolium bis(trifluoromethylsulfonyl)imide ([Im][TFSI]), it has been shown that proton hopping enhances acidic proton diffusion by up to 40% vis-à-vis proton transport by molecular diffusion alone.[20]

1.2. Routes for Combining Polymers with Ionic Liquids

Ionic liquids can be incorporated into polymer membranes by several routes (Figure 1.3). The most straightforward approach is simply to blend an ionic liquid with a homopolymer to create an essentially homogeneous composite material. There is a wide variety of compatible homopolymer/ionic liquid systems owing to the "tunability" of the solvent properties of ionic liquids.[37]

Homopolymer membranes containing ionic liquids achieve significantly higher conductivities than traditional polymer electrolytes that are composed of polymers like poly(ethylene oxide) (PEO) doped with small amounts of salt such as lithium [TFSI] (LiTFSI). In these traditional polymer electrolytes, the presence of salt induces ionic crosslinks that increase the glass transition temperature, T_g, of the polymer.[38] Thus, the addition of salt increases ion concentration but decreases ion mobility, leading to a maximum in conductivity at some relatively low salt concentration. Because ionic liquids typically plasticize rather than stiffen compatible polymers, the addition of ionic liquid simultaneously leads to high ion concentration and high ion mobility.[39] Watanabe and coworkers first demonstrated that highly conductive membranes can be achieved by combining polycations with ionic liquids composed of either 1-butylpyridinium bromide or 1-butylpyridinium chloride and aluminum chloride.[40-42] The conductivities of these membranes monotonically increase with ionic liquid concentration. They reach values on the order of 10^{-3} S/cm at room temperature, comparable to that of optimal PEO/LiTFSI polymer electrolytes at temperatures in excess of 110 ºC.[38] (At room temperature, the PEO/LiTFSI polymer electrolytes have conductivities orders of magnitude lower.) High conductivities have also been achieved in mixtures of a variety of homopolymers with imidazolium, pyridinium, and pyrrolidinium-based ionic liquids.[23, 43-49]

While the conductivities of mixtures of homopolymers with ionic liquids increase monotonically with increasing ionic liquid loading, the mechanical properties of the membranes tend to worsen with increasing ionic liquid loading.[50] One way to improve

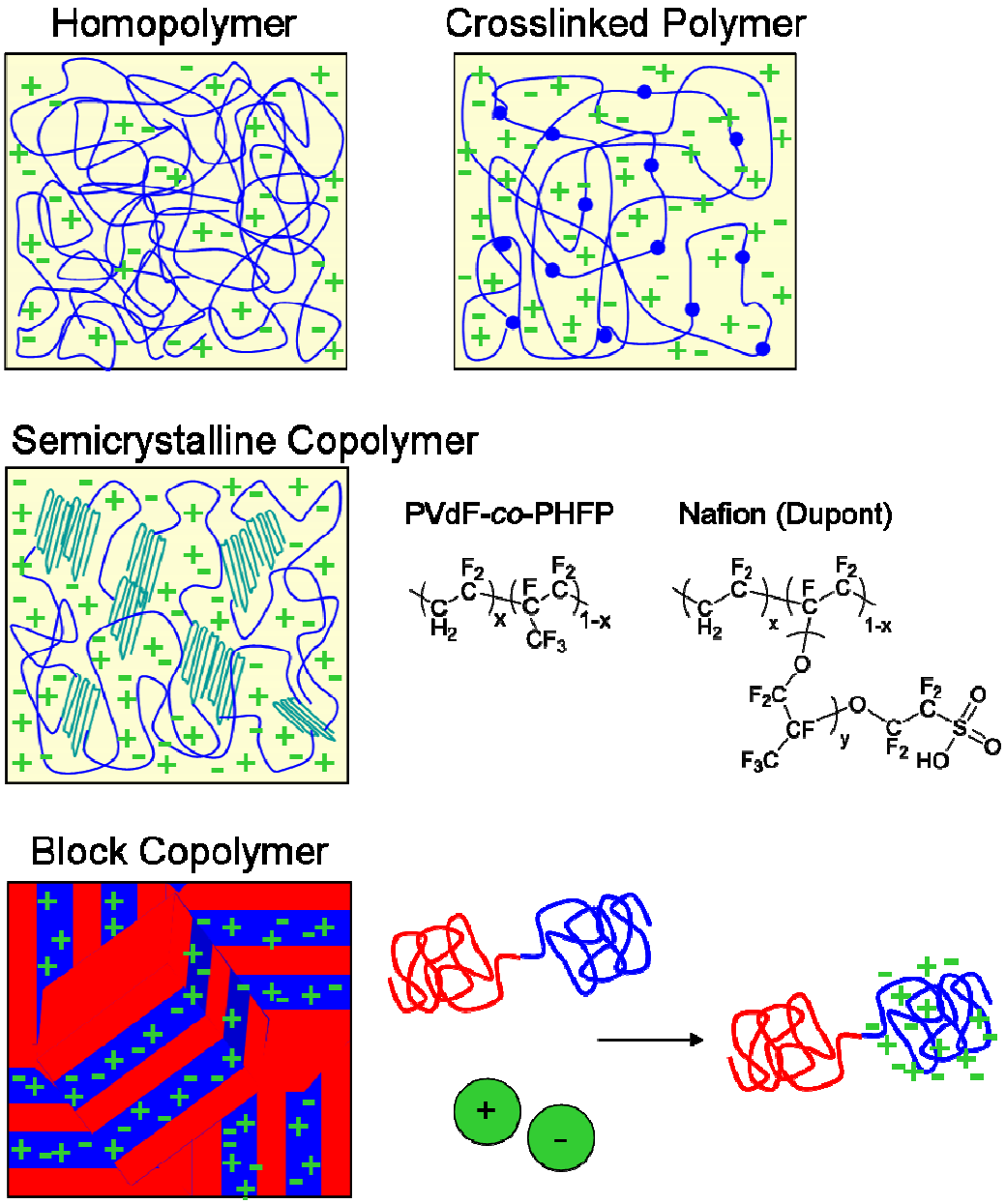


Figure 1.3. Routes for Incorporating Ionic Liquids into Polymers.

mechanical properties while maintaining high conductivity is to polymerize a crosslinked polymer network directly in an ionic liquid solvent to form an "ion gel". It is possible to polymerize a wide variety of vinyl monomers in ionic liquids.[51-54] Using this route, up to 60% 1-butylpyrridinium tetrafluoroborate ([BP][BF_4]) and 40% 1-ethyl-3-methylimidazolium [BF_4] ([EMIm][BF_4]) can be incorporated into crosslinked poly(2-hydroxyethyl methacrylate) to produce solid membranes with conductivities of 10^{-3} and 10^{-4} S/cm, respectively, at 30 °C.[44] Ion gels made up of crosslinked poly(methyl methacrylate) (PMMA) in [EMIm][TFSI] exhibit conductivities reaching 10^{-2} S/cm at 30 °C.[46, 48, 55] Highly lithium-conducting membranes are synthesized by polymerizing crosslinked poly(acrylonitrile) in the presence of a mixture of N,N-methyl butyl pyrrolidinium [TFSI] ([MBP][TFSI]) and LiTFSI.[56]

Another route for achieving simultaneous high conductivity and mechanical strength is to mix an ionic liquid with a random copolymer, where the comonomers are chosen to facilitate compatibility with the ionic liquid as well as provide mechanical durability. Poly(vinylidine fluoride-*co*-hexafluoropropene) (PVdF-*co*-PHFP) is a particularly attractive copolymer matrix. The fluorinated copolymer is stable in a large number of chemical environments, making it especially useful for lithium batteries or dye-sensitized solar cells.[57, 58] PVdF-*co*-PHFP is semicrystalline, where crystalline regions lead to freestanding films with good mechanical properties, and amorphous regions facilitate the uptake of a wide variety of hydrophilic and hydrophobic ionic liquids.[47, 57-63] Due to their semicrystalline nature, composite PVdF-*co*-PHFP/ionic liquid membranes have a microphase-separated morphology, where the ionic liquid forms a percolated network through the membrane. The addition of different amounts and types of ionic liquid affects the film morphology, and in turn the morphology affects the mechanical properties and conductivity.[63] While PVdF-*co*-PHFP/ionic liquid membranes have generally been shown to demonstrate favorable properties, we still lack a thorough understanding of their governing structure-property relationships.

Nafion (Dupont) is another attractive copolymer matrix for ionic liquids. Nafion is the industry standard proton exchange membrane material.[64] In the presence of water, the randomly placed hydrophilic side chains phase separate from the hydrophobic fluorinated backbone to form hydrated proton-conducting channels with dimensions on the nanometer length scale. Similar to PVdF-*co*-PHFP, Nafion is semicrystalline, and has exceptional mechanical properties owing to the semicrystallinity of the backbone. At high hydration levels, the ionic conductivity reaches 10^{-1} S/cm. For many applications, however, it is desirable to operate the proton exchange membrane at high temperatures, which requires complex water management systems to maintain membrane hydration. For this reason, the incorporation of ionic liquids into Nafion has been explored.[19, 65-68] Conductivities as high as 10^{-1} S/cm have been achieved between 100 and 200 °C.[19] Like the PVdF-*co*-PHFP/ionic liquid membranes, the conductivity of ionic liquid-impregnated Nafion is affected by the morphology of the membrane, which is sensitive to the hydrophilicity of the ionic liquid, ionic liquid concentration, and film preparation method.[65, 66, 68] The presence of the ionic liquid also affects the mechanism of proton transport in Nafion.[65, 66] The dissociation of protons from the sulfonic acid groups in Nafion is affected by the dielectric constant of the ionic liquid and the propensity for

ionic liquid cations to interact with sulfonic acid groups and exchange with the acidic protons. Furthermore, proton transport is thought to occur through a hopping mechanism, where exchanged protons hop between sulfonic acid groups and ionic liquid anions.

Additional random copolymer chemistries have been studied with themes similar to the PVdF-*co*-PHFP and Nafion studies.[65, 69] It has generally been found that the morphology of the membrane is strongly affected by the presence of the ionic liquid. In turn, the morphology, particularly the connectivity of the conducting domains and phase contrast between the conducting and structural domains, has a significant impact on mechanical and conductive properties. However, it has proven very difficult to study structure-property relationships in detail because fully characterizing the morphology of random copolymer films is not straightforward and the morphology is extremely sensitive to film preparation methods.[68]

Recently, ion-conducting membranes composed of mixtures of block copolymers with ionic liquids have been investigated because they can be designed to have carefully controlled, coexisting conducting and structural domains with well-defined morphologies that are easily characterizable by standard techniques.[70-77] The morphology is easily controlled by changing the length of the block copolymer, the relative volume fractions of each block copolymer phase, as well as the ionic liquid concentration. Therefore, block copolymer/ionic liquid membranes provide an opportunity to design membranes with optimal composition and morphology for the desired conductive and mechanical properties, as well as an opportunity to study fundamental structure-property relationships.

1.3. Self-Assembly of Mixtures of Block Copolymers with Ionic Liquids

Block copolymers are composed of two or more polymers covalently bound together at their ends. Block copolymer self-assembly results from the free energy minimization of enthalpic interactions between the dissimilar polymer segments and the entropic penalty from chain stretching at the interface where dissimilar polymer blocks are joined.[78] Ordered phases are exhibited above a certain segregation strength, where the segregation strength is defined as a combination of the Flory-Huggins interaction parameter for the specific block copolymer chemistry, χ_{AB}, which is an inverse function of temperature, and the degree of polymerization, N. In combination with the segregation strength, the relative volume fraction of one block, f_A, determines the morphology. Diblock copolymers demonstrate a variety of morphologies depicted in Figure 1.4, including spheres on an ordered body-centered cubic lattice (S_{BCC}), hexagonally packed cylinders (C), a bicontinuous gyroid structure (G), and lamellae (LAM).

The presence of an additional component such as an ionic liquid affects block copolymer self-assembly. Because an ionic liquid is conceptually both a solvent and a salt, it is expected that the self-assembly of block copolymer/ionic liquid mixtures shares some traits with the self-assembly of mixtures of block copolymers with molecular solvents and salts, both of which have been studied in detail. The addition of a solvent or salt to a diblock copolymer introduces two new interaction parameters, one to describe the

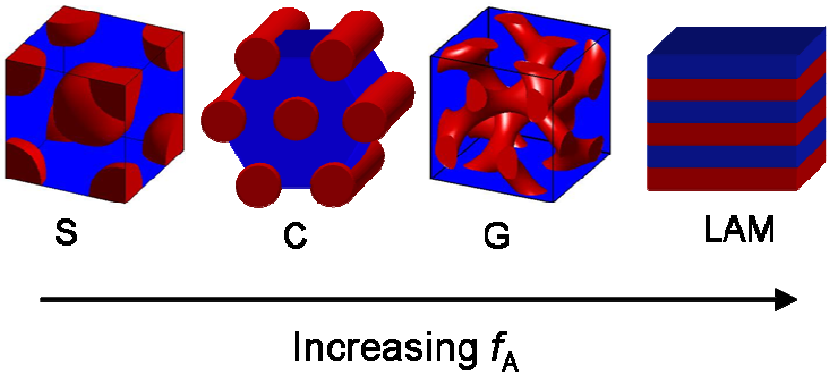


Figure 1.4. Diblock Copolymer Morphologies. With increasing relative volume fraction of component "A", f_A, spheres of A on a body-centered cubic lattice (S_{BCC}), hexagonally packed cylinders of A (C), a bicontinuous gyroid structure (G), and lamellae (LAM) are observed. Component A is colored red in the cartoons.

interactions between each block and the additional component, χ_{AS} and χ_{BS}. In the case of mixtures of block copolymers with molecular solvents, the effect of the relative selectivity of the solvent for each component of the block copolymer (the difference between χ_{AS} and χ_{BS}) is well understood. For a neutrally favorable solvent, one for which $\chi_{AS} = \chi_{BS}$, the self-assembly is described well by combining all of the interaction parameters into a single effective interaction parameter between each solvated microphase, χ_{eff}, where χ_{eff} is expected to decrease with increasing solvent content due to the screening of unfavorable interactions between each polymer microphase by the solvent. The simple "dilution approximation" has been proposed, which predicts that $\chi_{eff} = \chi_{AB}N\phi_P$, where ϕ_P is the volume fraction of polymer in the mixture.[79] The order-disorder transition temperature, T_{ODT}, would also then scale with $\chi_{AB}N\phi_P$. The dilution approximation does not, however, account for chain swelling, where the polymer coil has dimensions greater than it would in a random walk due to favorable enthalpic interactions between the polymer and solvent.[80] Incorporation of chain swelling effects leads to the scaling of the T_{ODT} with $\chi_{AB}^{1.59}N\phi_P$ in the weak segregation limit.[81-83] The screening of unfavorable interactions between the two polymer microphases by a neutral solvent has two additional effects on self-assembly. One is the slight accumulation of solvent at the block copolymer interface.[81, 83] The second is the reduction of chain stretching at the block copolymer interface, which leads to a decrease in the domain spacing of the ordered morphology, d, which follows the scaling $d \sim \chi_{AB}^{1/6}N^{2/3}\phi_P^{1/6}$ in the strong segregation limit.[84]

When the solvent is selective for one of the block copolymer microphases ($\chi_{AS} \neq \chi_{BS}$), the mixtures demonstrate rich lyotropic phase behavior depending on f_A, ϕ_P, and the selectivity of the solvent (the difference between χ_{AS} and χ_{BS}). When the solvent selectivity is small, the T_{ODT} and d decrease with increasing solvent concentration.[85-87] In contrast, when the solvent selectivity is large, the T_{ODT} and d increase with increasing solvent concentration.[85, 87] The domain spacing has been shown theoretically and experimentally to scale with ϕ_P according to $d \sim \phi_P^{\alpha}$, where α depends on the selectivity of the solvent and the morphology.[87] The addition of a selective solvent to block copolymers also induces lyotropic phase transitions due to the combination of the change in effective segregation strength of the system as well as the change in the relative volume fractions of each phase.[88, 89] For instance, the addition of a selective solvent to a symmetric block copolymer induces lyotropic phase transitions from LAM to C to S_{BCC}.[89] The phase behavior of mixtures of block copolymers with selective solvents has been mapped out as a function of f_A, ϕ_P, and T for many different combinations of χ_{AB}, $\chi_{AS,}$ and χ_{BS}.[87, 89, 90] At high selective solvent concentrations, morphologies are observed that are not normally observed in neat block copolymer systems, including spheres on a face-centered cubic lattice (S_{FCC}) and a variety of disordered micellar structures, including spherical micelles, wormlike micelles, and vesicles.[87, 90, 91]

Most studies of mixtures of block copolymers with salts have focused on systems where the salt is selective for one component of the block copolymer. In these systems it has been shown that the T_{ODT} and d increase with increasing salt loading, in qualitative similarity with observations of mixtures of block copolymers with selective solvents.[75, 92-

[96] Like the selective solvent mixtures, increased segregation strength and to some extent a change in the relative volume fractions of each phase lead to these effects. Insight into the phase behavior also comes from considering the competition between the entropic driving force for ions to distribute evenly between the two polymer phases and the enthalpic driving force for ions to selectively enter the lower dielectric phase. Mean field theory has been developed recently that captures this competition.[97] The theory predicts an increase in effective segregation strength with increasing salt concentration and decreasing anion size, which has been validated experimentally.[75, 97] The effective segregation strength of polystyrene-*b*-PMMA (PS-*b*-PMMA)/lithium chloride mixtures becomes less temperature dependent at high salt concentrations, suggesting that entropic factors dominate in this regime.[94]

In addition to these factors, coordination between the salt and polymer also affects self-assembly. It is well known that salts generally increase the T_g of polymers due to ionic crosslinking.[38] Ion coordination can also affect the statistical segment length of the polymer, which has profound effects on self-assembly.[98] For instance, a large increase in the statistical segment length of PMMA-*b*-poly(oligo oxyethylene methacrylate) was observed in the disordered state when mixed with lithium trifluoromethane sulfonate, presumably due to ion coordination.[93] In another case, intra- versus inter-chain ion coordination in mixtures of cadmium chloride with PS-*b*-poly(2-vinyl pyridine) (PS-*b*-P2VP) and PS-*b*-poly(4-vinyl pyridine), respectively, led to profound differences in *d*.[99] A method was recently proposed for distinguishing the effects of increased segregation strength and polymer/salt coordination on the T_{ODT}, which involves assuming that the segregation strength is constant at the T_{ODT} for block copolymers containing different salt concentrations, and analyzing the effect of salt concentration on *d* at the T_{ODT}.[100]

1.3.1. Dilute Solutions of Block Copolymers in Ionic Liquids

As expected, many of the features of the self-assembly of block copolymers with solvents and salts are found in the self-assembly of block copolymers with ionic liquids. However, the low volatility and tunable solvent properties of ionic liquids allow for new examinations of the phase behavior of block copolymer solutions and more complex self-assembly behavior in block copolymer/ionic liquid mixtures.

Investigation of the phase behavior of block copolymer/ionic liquid mixtures began with studies of micelle formation in dilute solutions.[101-104] Studying micelle formation of surfactants in ionic liquids opened up new possibilities for understanding the thermodynamic driving forces for micelle formation, since ionic liquids have tunable polarities and hydrogen bonding behavior, and can be studied over a wide range of temperatures.[105, 106] The first comprehensive studies of block copolymer micelle formation in ionic liquids were performed by Lodge and coworkers.[107, 108] They showed that block copolymers exhibit the "universal" block copolymer micelle morphologies in ionic liquids, ranging from spheres to wormlike micelles to vesicles with decreasing chain length of the soluble component.

As in aqueous solution, block copolymer micelle formation in ionic liquids is kinetically as well as thermodynamically controlled, as evidenced by the coexistence of different micelle morphologies as well as the dependence of micelle morphology on the preparation procedure.[107, 109, 110] Owing to the nonvolatility of ionic liquids, the ergodicity of block copolymer micelles can be uniquely studied in ionic liquids by thermal annealing and new preparation methods. For example, poly(butadiene)-*b*-PEO (PB-*b*-PEO) or PS-*b*-PEO micelles in [EMIm][TFSI] or [BMIm][TFSI] reach two distinct monodisperse radii based on whether the block copolymer is directly dissolved in the ionic liquid or whether the block copolymer and ionic liquid are first dissolved in a cosolvent, followed by cosolvent evaporation.[109, 110] Thermal annealing leads to the relaxation of large aggregates formed by the direct dissolution method into smaller, monodisperse spherical micelles. The rate of relaxation increases with increasing copolymer concentration, suggesting that fusion/fission is the main mechanism of micelle relaxation. In contrast, thermal annealing has no effect on the even smaller, monodisperse spherical micelles formed by the cosolvent evaporation method. These smaller spherical micelles result from the lower interfacial energy between the PB or PS cores and the ionic liquid/cosolvent mixture compared to the ionic liquid solvent alone. Once the cosolvent evaporates, mechanisms for micelle growth are energetically unfavorable. Micelle coalescence is unfavorable due to strong steric repulsion between micelle coronas, and micelle evaporation is an activated process with a large energy barrier. Furthermore, expulsion of chains from a given micelle (in order to add to another) opposes the micelle's own thermodynamic driving force for growth.

The diversity of ionic liquid chemistries provides a vast playground for tuning the temperature-dependent solvent quality for various polymers. Thus, there are many block copolymer micelle systems that exhibit interesting thermoresponsive behavior in ionic liquids. Furthermore, the low volatility of ionic liquids allows micelle transitions to be probed over a large temperature range. For example, PMMA-*b*-Poly(benzyl methacrylate) demonstrates a lower critical micellization temperature (LCMT) in [EMIm][TFSI] between 110 and 120 ºC.[111] The LCMT can be easily tuned by mixing [EMIm][TFSI] with various amounts of [BMIm][TFSI].[112] A doubly thermosensitive system can be designed by choosing a block copolymer with one component demonstrating lower critical solution behavior and the second demonstrating upper critical solution behavior (depicted in Figure 1.5).[113, 114] Temperature-sensitive solubility in ionic liquids can also be exploited to manipulate the morphology of block copolymer thin films. For example, the temperature-sensitive solubility of P2VP in [BMIm][CF_3SO_3] leads to the formation of thin films of PS-*b*-P2VP micelles upon heating a film with a LAM morphology on a silicon substrate immersed in ionic liquid and in free-floating thin films floating on the surface of ionic liquid.[115, 116]

The thermoresponsive behavior of block copolymers in ionic liquids can also be employed to create "micellar shuttles" between immiscible ionic liquid and aqueous phases.[117-120] Such systems are interesting, for instance, as recoverable delivery vehicles. The first micellar shuttle consisted of PB-*b*-PEO micelles reversibly switching between aqueous and [BMIm][PF_6] phases.[118, 120] At ambient temperature, water is a slightly better solvent for PEO than [BMIm][PF_6], causing PB-*b*-PEO micelles to reside in the

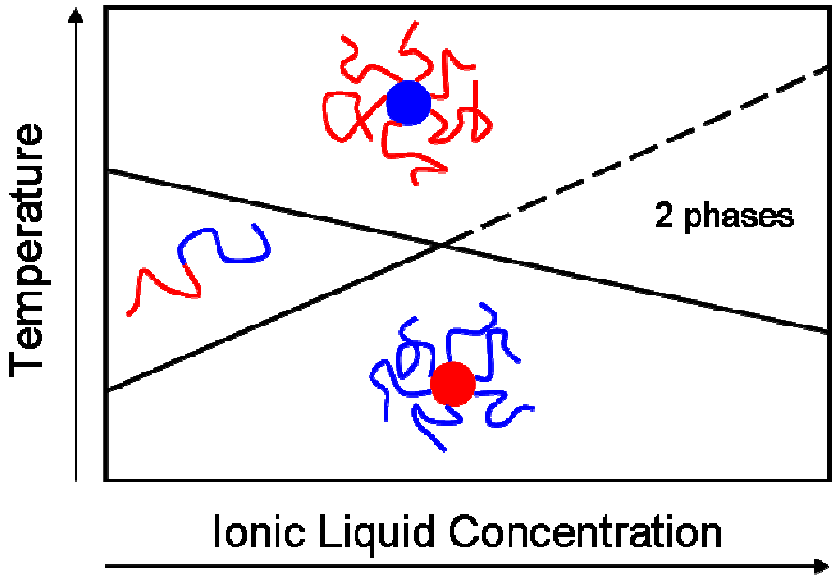


Figure 1.5. Doubly Thermoresponsive Micellization. (Modified from Reference 113.) The red component of the block copolymer demonstrates upper critical solution temperature behavior in the ionic liquid, while the blue component demonstrates lower critical solution behavior.

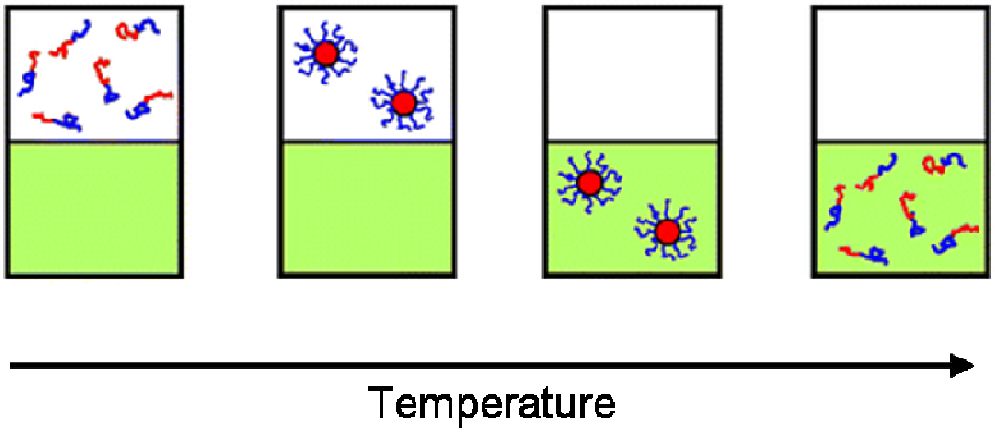


Figure 1.6. Thermoreponsive Micellar Shuttles. (Modified from Reference 121.)

aqueous phase. At high temperatures (75-90 ºC), water becomes a poorer solvent for PEO, and the micelles transfer to the ionic liquid phase (which is a good solvent for PEO over the entire temperature range). Upon cooling back to ambient temperature, the micelles reversibly enter the aqueous phase. The transfer temperature can be tuned by using ionic liquids with different polarity and by adding ionic or nonionic additives to the aqueous phase to change the solvent quality of water for PEO.[117] Additional thermoresponsivity can also be programmed into the micellar shuttles by using block copolymer components with lower and/or upper critical solution temperature behavior, for example by using poly(*N*-isopropyl acrylamide)-*b*-PEO (PNIPAm-*b*-PEO) as a shuttle between water and [BMIm][PF_6].[121] At low temperatures, PNIPAm-*b*-PEO exists as free dissolved chains in water. Upon heating, micelles are formed in water, then the micelles are transferred to [BMIm][PF_6], and finally the micelles disintegrate into free chains dissolved in [BMIm][PF_6] (Figure 1.6). Dissipative particle dynamics simulation of this system predicts micelle morphologies and transition temperatures that are fairly consistent with the experimental findings, indicating that this type of simulation tool may be useful for further investigating micellar shuttle systems.[122] Micellar shuttles are useful as reversible delivery vehicles, i.e. to transfer various cargos between ionic liquid and aqueous phases.[123, 124] For example, homopolymers can be extracted from an ionic liquid phase by loading them into micelles and washing the micelle-containing ionic liquid phase with water.[123] In addition, hydrophobic dyes loaded in hydrophobic micelle cores can be reversibly transferred between ionic liquid and water phases using a temperature stimulus.[123, 124]

By using triblock copolymers rather than diblock copolymers, where the endblocks are insoluble in ionic liquid and the midblocks are soluble in ionic liquid, ion gels can be formed via the self-assembly of a very small amount of polymer in ionic liquid (ca. 4 wt%).[125] Thermoreversible ion gels are formed by incorporating endblocks with temperature-sensitive solubility in the ionic liquid. For instance, mixtures of PNIPAm-*b*-PEO-*b*-PNIPAm with [EMIm][TFSI] form ion gels that "melt" into viscous liquids around 17 °C, and reversibly cool to reform the ion gel.[126] The transition temperature can be adjusted between 17 and 48 °C by incorporating PS blocks of varying molecular weight on either side of the PEO midblock, i.e. by creating pentablocks, PNIPAm-*b*-PS-*b*-PEO-*b*-PS-*b*-PNIPAm.[127] Thermoreversible ion gels with much higher transition temperatures are created via an alternate route utilizing hydrogen bonding interactions.[128-130] Triblock copolymers with P2VP endblocks in combination with poly(4-vinylphenol) (PVPh) and an ionic liquid form gels at low temperatures due to hydrogen bonding between P2VP and PVPh. The transition temperature to a viscous liquid can be tuned in the range of 119 to 163 °C by varying the P2VP block lengths and the ratio of triblock copolymer to homopolymer since these variables influence the number of hydrogen bonds on a P2VP/PVPh association. Interestingly, in contrast to the simple triblock copolymer gels without the hydrogen bonding gelation mechanism, the mechanical strength of the hydrogen-bonded gels is strongly dependent on temperature below the gelation point, which is attributed to the increasing strength of the hydrogen bonds with decreasing temperature.

1.3.2. Concentrated Solutions of Block Copolymers in Ionic Liquids

Concentrated mixtures of block copolymers in ionic liquids have even more diverse phase behavior than dilute solutions, where the ionic liquid can be templated into well-defined nanochannels of various size and shape. Work in this area, however, is much less developed compared to investigations of dilute solution self-assembly. The first investigation of the lyotropic phase behavior of concentrated block copolymer/ionic liquid solutions mapped out the phase behavior of PB-*b*-PEO in two different ionic liquids, [EMIm][TFSI] and [BMIm][PF_6], where f_{PEO} was varied between 0.20 and 0.33.[77] The phase behavior resembles that of a block copolymer mixed with a selective solvent, as expected since the ionic liquids are good solvents for PEO and poor solvents for PB. Lyotropic phase transitions occur upon the addition of ionic liquid as a result of the volume fraction increase of the PEO/ionic liquid phase. In addition to the classical diblock copolymer microstructures (LAM, C and S_{BCC}), there are regions of coexistence between LAM and C, as well as a disordered network structure consisting of branched PB cylinders in a matrix of PEO/ionic liquid. Notably missing from the phase behavior is the G microstructure, where coexisting LAM/C takes its place at the relevant block copolymer and ionic liquid compositions. It has been proposed that the large effective segregation strength of the system prevents the frustrated packing of the G structure. The extra degree of freedom introduced by the addition of the ionic liquid allows the system to rearrange instead into coexisting LAM/C. The strong selectivity of the ionic liquids for the PEO phase is confirmed by the scaling of the lamellar domain spacing, *d*, with ionic liquid concentration. The expected $d \sim \phi_P^{\alpha}$ scaling for a block copolymer in a solvent is demonstrated, where α ranges from -0.17 to -0.52 for block copolymers of different PEO volume fraction in the two ionic liquids (the domain spacing increased with increasing ionic liquid concentration). The negative values for α confirm that the ionic liquids act as selective solvents. Comparing the values of α provides a simple way to compare the selectivity of the ionic liquids, and in this case it shows that [BMIm][PF_6] is a more selective solvent than [EMIm][TFSI].

A handful of other systems has been investigated where the ionic liquid is selectively incorporated into one phase of the block copolymer.[70-76] Values for α as low as -3 have been reported for nearly symmetric PS-*b*-P2VP block copolymers with [Im][TFSI].[73] This is the most negative value that has been reported for α, and indicates that [Im][TFSI] is extremely selective for the P2VP phase of the block copolymer. Small angle neutron scattering (SANS) data confirm the strong selectivity, showing that the partition function of the ionic liquid is <0.1 (where the partition function is defined as the ratio of the volume fractions of ionic liquid in the PS versus P2VP phase).[74] The selectivity of ionic liquids for one block copolymer microphase is associated with an increase in the effective segregation strength upon addition of the ionic liquid.[71, 72, 75]

The lyotropic phase behavior observed in the above studies is in qualitative agreement with the phase behavior observed in the original study of PB-*b*-PEO mixtures.[77] However, several additional interesting regions of coexistence have also been observed. Coexisting lamellar phases having two different domain sizes are exhibited by certain mixtures of PS-*b*-P2VP with [Im][TFSI] as well as mixtures of PS-*b*-PEO with [EMIm][TFSI].[73, 76] It was proposed that the two lamellar phases contain unequal

amounts of ionic liquid, or perhaps come about due to cocrystallization of the polymer and ionic liquid in the case of the PS-*b*-PEO/[EMIm][TFSI] mixtures. Another mixture of PS-*b*-PEO with [EMIm][TFSI] demonstrates coexistence between LAM, C, and G microphases.[76] The coexistence of the G microphase is particularly interesting since this morphology is missing from the PB-*b*-PEO/[EMIm][TFSI] and PB-*b*-PEO/[BMIm][PF_6] phase diagrams, presumably due to the strong segregation strength of those systems. It is expected that PS-*b*-PEO/[EMIm][TFSI] is also very strongly segregated, making this observation surprising. Low molecular weight PS-*b*-PEO/[Im][TFSI] mixtures also demonstrate coexisting LAM and G phases, as well as pure G phases.[75] This is less surprising given the low molecular weight of the block copolymer and the vicinity of these phases to disordered phases on the phase diagram.

Thermotropic investigations of block copolymer/ionic liquid mixtures also reveal interesting behavior.[73] While neat PS-*b*-P2VP (M_N=28 kg/mol) demonstrates a reversible order-disorder transition around 250 ºC, mixtures of the block copolymer with ca. 10-55 vol% ionic liquid undergo irreversible transitions from ordered LAM, C, or coexisting LAM/C phases to nonperiodic disordered structures or disordered micelles upon heating around a similar temperature. This behavior in combination with the prevalence of coexisting phases brings up the issue of equilibrium in block copolymer/ionic liquid mixtures. It is possible that the strong segregation of many of these systems as well as the preparation processes (usually a cosolvent evaporation method) lead to kinetically trapped, non-equilibrium or metastable structures, where coexistence is especially prevalent due to the third component ionic liquid. A thorough investigation of the path-dependence and equilibrium or non-equilibrium nature of block copolymer micelles in ionic liquids has been performed, which was described in the previous section.[109, 110] Similar studies have not yet been performed for concentrated mixtures of block copolymers with ionic liquids, although the preparation-dependent self-assembly of PS-*b*-PMMA/[EMIm][TFSI] mixtures has been noted.[70] Greater understanding of the kinetic versus thermodynamic driving forces for self-assembly in concentrated mixtures of block copolymers with ionic liquids is needed. Furthermore, it is clear that concentrated mixtures of block copolymers with ionic liquids have rich lyotropic and thermotropic phase behavior. Greater understanding of the universal driving forces for self-assembly in these complex systems is essential for controlling the morphology of membranes incorporating different ionic liquid and block copolymer chemistries. The morphology has an incredible impact on membrane properties of interest, as described in the next section.

1.4. Relationship between Structure and Conductivity

Incorporating an ionic liquid into a nanostructured block copolymer matrix is especially interesting for electrochemical applications, since the desirable electrochemical properties of the ionic liquid can be templated into ion-conducting nanochannels within a durable polymer matrix.[32, 70, 71, 76, 131-143] The morphology of the membrane is expected to have significant impact on conductivity, and research in this area is just emerging.[70, 71, 76, 133, 135, 138, 141-143] Insight into the relationship between structure and conductivity in block

copolymer/ionic liquid membranes can be gained by examining the effect of structure on conductivity in other nanostructured, ion-conducting materials.

Figure 1.7 depicts several ways in which structure affects conductivity in nanostructured materials. One is phase contrast. In general, stronger segregation between the structural and conducting domains leads to better conductivity. This is nicely illustrated by comparing the conductivity of Nafion, which is fully fluorinated other than the sulflonic acid groups on its randomly placed sidechains, to two similar copolymers, one being partially fluorinated and one being completely unfluorinated. For a given hydration, the conductivity increases in the order nonfluorinated<partially fluorinated<fully fluorinated, presumably due to the increasing degree of phase segregation with increasing fluorination level.[144] Similarly, the conductivity of self-assembled amphiphilic polymers with proton-conducting groups incorporated into one portion of the polymer is orders of magnitude higher than the conductivity of analogous polymers that contain a greater number of proton-conducting groups, but lack the capacity for self-assembly.[131]

Another morphological trait that has significant impact on conductivity is phase continuity. Clearly, well-connected conducting domains provide continuous pathways for ion conduction, leading to improved conductivity. In evidence, a order-order transition from LAM to S_{BCC} (conducting spheres) in lithium-conducting dendrons upon heating corresponds to a three-order-of-magnitude decrease in conductivity.[145] Furthermore, a transition from LAM to C (conducting cylinders) corresponds to an order-of-magnitude decrease in conductivity, and a transition from C (conducting cylinders) to a bicontinuous cubic phase corresponds to an order-of-magnitude increase in conductivity, both of which may also be the result of changes in conducting phase continuity. For instance, it is quite plausible that the bicontinuous cubic structure has greater phase connectivity than hexagonally-packed cylinders. However, little is actually known about the grain connectivity of certain common block copolymer morphologies, such as C and LAM, and connectivity is difficult to probe.

Another factor contributing to the latter two step changes in conductivity could be changes in the dimensionality of the morphology. For instance, it is expected that there is one-dimensional transport within a cylinder, two-dimensional transport within a lamellar sheet, and three-dimensional transport within a bicontinuous cubic structure, which presumably leads to a decrease in conductivity by one half through a LAM to C (conducting cylinders) transition, and an increase in conductivity by a factor of three through a C to bicontinuous cubic morphology transition.[146] However, this dimensional analysis requires that the morphologies have perfect geometrical form within grains, whereas in reality many block copolymer structures are wavy, and/or have point defects and dead ends.[147] No change was observed in the conductivity of PS-*b*-PEO doped with LiTFSI through a LAM to G transition, whereas dimensional analysis would predict an increase in conductivity by 50%.[148] It should be noted, however, that the LAM to G transition occurred over a broad temperature range, and it is possible that any change in conductivity was "smeared" through this temperature range. "In-situ" techniques for simultaneously measuring conductivity and morphology will be very useful for gaining a more detailed and accurate understanding of the effect of morphology on conductivity.

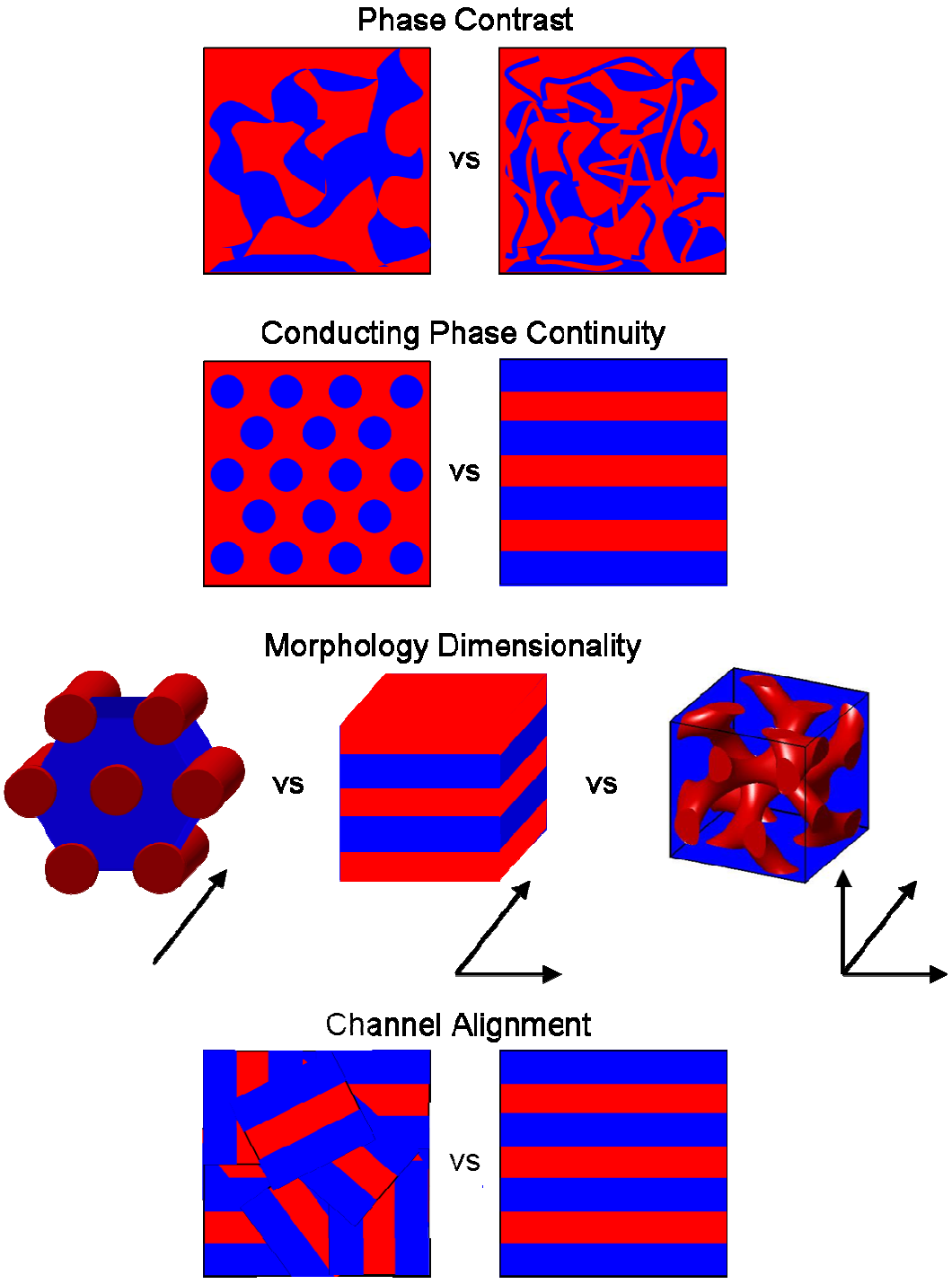


Figure 1.7. Effect of Morphology on Conductivity.

For instance, in the same study, no discontinuity in conductivity was observed in the vicinity of the T_{ODT} (measured separately by SAXS and Birefringence). However, more recent in-situ, simultaneous SAXS and conductivity measurements on a very similar PS-*b*-PEO/LiTFSI system revealed a clear discontinuous increase in conductivity above the T_{ODT}. Very few other in-situ studies have been performed thus far.[149]

While the exact effects of the dimensionality of the morphology on conductivity are still unclear, it is clear that reducing the overall dimensionality or tortuosity of the morphology through grain alignment can improve conductivity in the direction of alignment. Many groups have shown that conductivity increases in the direction of grain alignment, where alignment has been induced by a magnetic field,[150] an electric field,[151] solvent casting,[70] shearing,[132, 151] stretching,[147, 152-154] or pressing.[151] Compared to unaligned samples, conductivities up to an order of magnitude higher have been observed for conducting cylinders, and conductivities up to about two times as high have been observed for LAM samples.[147, 150-154] Transport anisotropy, defined as the ratio of the conductivity in the direction of alignment to the conductivity perpendicular to the direction of alignment, increases linearly with the degree of alignment by stretching in Nafion.[152]

In addition to the effects of channel geometry on molecular transport in nanostructured membranes, the confinement of charge carriers has also been shown to affect the mechanism of charge transport. For example, it has been shown that hydrogen bonding in water is significantly different at the walls of confined domains,[155-158] and that such effects have significant implications for proton transport in hydrated Nafion.[63, 159-162] Remarkably, sulfonated block copolymer membranes with hydrophilic channel sizes less than 5 nm take up increasing amounts of water with increasing temperature (at a fixed relative humidity), which consequently leads to increasing proton conductivity.[163] Furthermore, chain stretching at the PS-*b*-PEO block copolymer interface affects how lithium ions are coordinated to PEO, and consequently affects lithium ion conductivity in lamellar membranes.[164] Finally, specific chemical interactions between imidazole and the walls of conducting nanochannels formed by aluminum porous coordination polymers affect the rate of proton transport.[165] Clearly there are many examples of confinement affecting charge transport mechanisms, although the full impact of confinement on conductivity is still not grasped. Many of the above examples were deduced largely based on bulk conductivity measurements. In one case, NMR experiments also provided clues as to how the local dynamics change,[165] but determining exactly how confinement affects the molecular mechanisms of conductivity remains difficult.

1.5. Understanding Ion Transport in Nanostructured Mixtures of Block Copolymers with Ionic Liquids

Prior work has demonstrated that mixtures of block copolymers with ionic liquids are exceptional membrane candidates for a wide variety of electrochemical applications due to the ability to template the desirable electrochemical properties of ionic liquids into well-defined nanochannels within a durable polymer matrix. The properties of such membranes promise to be easily tuned by varying the block copolymer architecture and

ionic liquid content. However, the self-assembly of these materials is complex, and the relationship between structure and ionic conductivity was previously not fully understood. Detailed understanding of the effect of the ionic liquid on the thermodynamic self-assembly of the block copolymer, as well as the effect of the nanostructure of the resulting membrane on the ion-conducting properties of the ionic liquid, is essential for predictable structure and property control, as well as the ability to design optimal membranes for a given application.

This thesis discusses the relationship between composition, morphology, and ionic conductivity in nanostructured mixtures of block copolymers with ionic liquids. Chapter 2 describes the lyotropic and thermotropic phase behavior of a model block copolymer/ionic liquid system for a wide range of block copolymer architectures and ionic liquid concentrations. The relationship between membrane structure and ionic conductivity of the model system is detailed in Chapter 3, where scaling relationships are presented that accurately describe the conductivity of any mixture. These scaling relationships are shown to be general to a wide variety of block copolymer and ionic liquid chemistries in Chapter 4. In Chapter 5, the mechanisms of proton conductivity in ionic liquids are characterized, and the effects of block copolymer nanoconfinement on these mechanisms are presented in Chapter 6. Finally, the impact of this work and the outlook for future research of nanostructured, ion-conducting membranes are discussed in Chapter 7.

1.6. References

1. Wasserchеid, P.; Welton, T., *Ionic Liquids in Synthesis*. Wiley-VCH: Verlag, 2003.
2. Freemantle, M. *Chemical & Engineering News* **1998,** 76, (13), 32-37.
3. Holbrey, J. D.; Rooney, D.; Seddon, K. R. *Abstracts of Papers of the American Chemical Society* **1999,** 218, U800-U800.
4. Seddon, K. R. *Journal of Chemical Technology and Biotechnology* **1997,** 68, (4), 351-356.
5. Welton, T. *Chemical Reviews* **1999,** 99, (8), 2071-2083.
6. Swatloski, R. P.; Spear, S. K.; Holbrey, J. D.; Rogers, R. D. *Journal of the American Chemical Society* **2002,** 124, (18), 4974-4975.
7. Fukaya, Y.; Hayashi, K.; Wada, M.; Ohno, H. *Green Chemistry* **2008,** 10, (1), 44-46.
8. Wu, J.; Zhang, J.; Zhang, H.; He, J. S.; Ren, Q.; Guo, M. *Biomacromolecules* **2004,** 5, (2), 266-268.
9. Bara, J. E.; Carlisle, T. K.; Gabriel, C. J.; Camper, D.; Finotello, A.; Gin, D. L.; Noble, R. D. *Industrial & Engineering Chemistry Research* **2009,** 48, (6), 2739-2751.
10. Jiang, Y. Y.; Zhou, Z.; Jiao, Z.; Li, L.; Wu, Y. T.; Zhang, Z. B. *Journal of Physical Chemistry B* **2007,** 111, (19), 5058-5061.
11. Ohno, H., *Electrochemical Aspects of Ionic Liquids*. Wiley-Interscience: New York, 2005.
12. Armand, M.; Endres, F.; MacFarlane, D. R.; Ohno, H.; Scrosati, B. *Nature Materials* **2009,** 8, (8), 621-629.

13. Buzzeo, M. C.; Evans, R. G.; Compton, R. G. *Chemphyschem* **2004,** 5, (8), 1106-1120.
14. Sakaebe, H.; Matsumoto, H. *Electrochemistry Communications* **2003,** 5, (7), 594-598.
15. Shin, J. H.; Henderson, W. A.; Passerini, S. *Electrochemistry Communications* **2003,** 5, (12), 1016-1020.
16. Garcia, B.; Lavallee, S.; Perron, G.; Michot, C.; Armand, M. *Electrochimica Acta* **2004,** 49, (26), 4583-4588.
17. Seki, S.; Kobayashi, Y.; Miyashiro, H.; Ohno, Y.; Mita, Y.; Usami, A.; Terada, N.; Watanabe, M. *Electrochemical and Solid State Letters* **2005,** 8, (11), A577-a578.
18. Kim, G. T.; Appetecchi, G. B.; Alessandrini, F.; Passerini, S. *Journal of Power Sources* **2007,** 171, (2), 861-869.
19. Doyle, M.; Choi, S. K.; Proulx, G. *Journal of the Electrochemical Society* **2000,** 147, (1), 34-37.
20. Noda, A.; Susan, A. B.; Kudo, K.; Mitsushima, S.; Hayamizu, K.; Watanabe, M. *Journal of Physical Chemistry B* **2003,** 107, (17), 4024-4033.
21. Xu, W.; Angell, C. A. *Science* **2003,** 302, (5644), 422-425.
22. Belieres, J. P.; Gervasio, D.; Angell, C. A. *Chemical Communications* **2006**, (46), 4799-4801.
23. Fernicola, A.; Panero, S.; Scrosati, B.; Tamada, M.; Ohno, H. *Chemphyschem* **2007,** 8, (7), 1103-1107.
24. Sekhon, S. S.; Lalia, B. S.; Park, J. S.; Kim, C. S.; Yamada, K. *Journal of Materials Chemistry* **2006,** 16, (23), 2256-2265.
25. Lee, S. Y.; Ogawa, A.; Kanno, M.; Nakamoto, H.; Yasuda, T.; Watanabe, M. *Journal of the American Chemical Society* **2010,** 132, (28), 9764-9773.
26. Lee, S. Y.; Yasuda, T.; Watanabe, M. *Journal of Power Sources* **2010,** 195, (18), 5909-5914.
27. Gorlov, M.; Kloo, L. *Dalton Transactions* **2008**, (20), 2655-2666.
28. Zakeeruddin, S. M.; Gratzel, M. *Advanced Functional Materials* **2009,** 19, (14), 2187-2202.
29. Zhao, F.; Wu, X.; Wang, M. K.; Liu, Y.; Gao, L. X.; Dong, S. J. *Analytical Chemistry* **2004,** 76, (17), 4960-4967.
30. McEwen, A. B.; McDevitt, S. F.; Koch, V. R. *Journal of the Electrochemical Society* **1997,** 144, (4), L84-L86.
31. Lu, W.; Fadeev, A. G.; Qi, B. H.; Smela, E.; Mattes, B. R.; Ding, J.; Spinks, G. M.; Mazurkiewicz, J.; Zhou, D. Z.; Wallace, G. G.; MacFarlane, D. R.; Forsyth, S. A.; Forsyth, M. *Science* **2002,** 297, (5583), 983-987.
32. Lee, J.; Panzer, M. J.; He, Y. Y.; Lodge, T. P.; Frisbie, C. D. *Journal of the American Chemical Society* **2007,** 129, (15), 4532-+.
33. Li, Q. F.; He, R. H.; Jensen, J. O.; Bjerrum, N. J. *Chemistry of Materials* **2003,** 15, (26), 4896-4915.
34. Agmon, N. *Chemical Physics Letters* **1995,** 244, (5-6), 456-462.
35. Kreuer, K. D.; Fuchs, A.; Ise, M.; Spaeth, M.; Maier, J. *Electrochimica Acta* **1998,** 43, (10-11), 1281-1288.
36. Munch, W.; Kreuer, K. D.; Silvestri, W.; Maier, J.; Seifert, G. *Solid State Ionics* **2001,** 145, (1-4), 437-443.

37. Winterton, N. *Journal of Materials Chemistry* **2006,** 16, (44), 4281-4293.
38. Robitaille, C. D.; Fauteux, D. *Journal of the Electrochemical Society* **1986,** 133, (2), 315-325.
39. Ueki, T.; Watanabe, M. *Macromolecules* **2008,** 41, (11), 3739-3749.
40. Watanabe, M.; Yamada, S.; Sanui, K.; Ogata, N. *Journal of the Chemical Society-Chemical Communications* **1993**, (11), 929-931.
41. Watanabe, M.; Yamada, S.; Ogata, N. *Electrochimica Acta* **1995,** 40, (13-14), 2285-2288.
42. Ogata, N.; Sanui, K.; Rikukawa, M.; Yamada, S.; Watanabe, M. *Synthetic Metals* **1995,** 69, (1-3), 521-524.
43. Lewandowski, A.; Swiderska, A. *Solid State Ionics* **2004,** 169, (1-4), 21-24.
44. Noda, A.; Watanabe, M. *Electrochimica Acta* **2000,** 45, (8-9), 1265-1270.
45. Pyati, R.; Murray, R. W. *Journal of the Electrochemical Society* **1996,** 143, (2), 401-405.
46. Seki, S.; Susan, A. B. H.; Kaneko, T.; Tokuda, H.; Noda, A.; Watanabe, M. *Journal of Physical Chemistry B* **2005,** 109, (9), 3886-3892.
47. Singh, B.; Sekhon, S. S. *Chemical Physics Letters* **2005,** 414, (1-3), 34-39.
48. Susan, M. A.; Kaneko, T.; Noda, A.; Watanabe, M. *Journal of the American Chemical Society* **2005,** 127, (13), 4976-4983.
49. Forsyth, M.; Sun, J. Z.; MacFarlane, D. R. *Electrochimica Acta* **2000,** 45, (8-9), 1249-1254.
50. Scott, M. P.; Brazel, C. S.; Benton, M. G.; Mays, J. W.; Holbrey, J. D.; Rogers, R. D. *Chemical Communications* **2002**, (13), 1370-1371.
51. Lu, J. M.; Yan, F.; Texter, J. *Progress in Polymer Science* **2009,** 34, (5), 431-448.
52. Kubisa, P. *Progress in Polymer Science* **2009,** 34, (12), 1333-1347.
53. Klingshirn, M. A.; Spear, S. K.; Subramanian, R.; Holbrey, J. D.; Huddleston, J. G.; Rogers, R. D. *Chemistry of Materials* **2004,** 16, (16), 3091-3097.
54. Snedden, P.; Cooper, A. I.; Scott, K.; Winterton, N. *Macromolecules* **2003,** 36, (12), 4549-4556.
55. Tiyapiboonchaiya, C.; MacFarlane, D. R.; Sun, J. Z.; Forsyth, M. *Macromolecular Chemistry and Physics* **2002,** 203, (13), 1906-1911.
56. Patel, M.; Gnanavel, M.; Bhattacharyya, A. J. *Journal of Materials Chemistry* **2011,** 21, (43), 17419-17424.
57. Tarascon, J. M.; Gozdz, A. S.; Schmutz, C.; Shokoohi, F.; Warren, P. C. *Solid State Ionics* **1996,** 86-8, 49-54.
58. Wang, P.; Zakeeruddin, S. M.; Exnar, I.; Gratzel, M. *Chemical Communications* **2002**, (24), 2972-2973.
59. Singh, B.; Sekhon, S. S. *Journal of Physical Chemistry B* **2005,** 109, (34), 16539-16543.
60. Fuller, J.; Breda, A. C.; Carlin, R. T. *Journal of the Electrochemical Society* **1997,** 144, (4), L67-L70.
61. Fuller, J.; Breda, A. C.; Carlin, R. T. *Journal of Electroanalytical Chemistry* **1998,** 459, (1), 29-34.
62. De Long, H. C.; Trulove, P. C.; Sutto, T. E. *Ionic Liquids as Green Solvents: Progress and Prospects* **2003,** 856, 478-494.

63. Yeon, S. H.; Kim, K. S.; Choi, S.; Cha, J. H.; Lee, H. *Journal of Physical Chemistry B* **2005,** 109, (38), 17928-17935.
64. Mauritz, K. A.; Moore, R. B. *Chemical Reviews* **2004,** 104, (10), 4535-4585.
65. Cho, E.; Park, J. S.; Sekhon, S. S.; Park, G. G.; Yang, T. H.; Lee, W. Y.; Kim, C. S.; Park, S. B. *Journal of the Electrochemical Society* **2009,** 156, (2), B197-B202.
66. Bennett, M. D.; Leo, D. J.; Wilkes, G. L.; Beyer, F. L.; Pechar, T. W. *Polymer* **2006,** 47, (19), 6782-6796.
67. Bennett, M. D.; Leo, D. J. *Sensors and Actuators a-Physical* **2004,** 115, (1), 79-90.
68. Sekhon, S. S.; Park, J. S.; Cho, E.; Yoon, Y. G.; Kim, C. S.; Lee, W. Y. *Macromolecules* **2009,** 42, (6), 2054-2062.
69. Brown, R. H.; Duncan, A. J.; Choi, J. H.; Park, J. K.; Wu, T. Y.; Leo, D. J.; Winey, K. I.; Moore, R. B.; Long, T. E. *Macromolecules* **2010,** 43, (2), 790-796.
70. Gwee, L.; Choi, J. H.; Winey, K. I.; Elabd, Y. A. *Polymer* **2010,** 51, (23), 5516-5524.
71. Kim, S. Y.; Yoon, E.; Joo, T.; Park, M. J. *Macromolecules* **2011,** 44, (13), 5289-5298.
72. Miranda, D. F.; Russell, T. P.; Watkins, J. J. *Macromolecules* **2010,** 43, (24), 10528-10535.
73. Virgili, J. M.; Hexemer, A.; Pople, J. A.; Balsara, N. P.; Segalman, R. A. *Macromolecules* **2009,** 42, (13), 4604-4613.
74. Virgili, J. M.; Nedoma, A. J.; Segalman, R. A.; Balsara, N. P. *Macromolecules* **2010,** 43, (8), 3750-3756.
75. Wanakule, N. S.; Virgili, J. M.; Teran, A. A.; Wang, Z. G.; Balsara, N. P. *Macromolecules* **2010,** 43, (19), 8282-8289.
76. Simone, P. M.; Lodge, T. P. *Acs Applied Materials & Interfaces* **2009,** 1, (12), 2812-2820.
77. Simone, P. M.; Lodge, T. P. *Macromolecules* **2008,** 41, (5), 1753-1759.
78. Bates, F. S.; Fredrickson, G. H. *Physics Today* **1999,** 52, (2), 32-38.
79. Helfand, E.; Tagami, Y. *Journal of Chemical Physics* **1972,** 56, (7), 3592-&.
80. Flory, P. J., *Principles of Polymer Chemistry*. Cornell University Press: Ithaca, 1953.
81. Fredrickson, G. H.; Leibler, L. *Macromolecules* **1989,** 22, (3), 1238-1250.
82. Delacruz, M. O. *Journal of Chemical Physics* **1989,** 90, (3), 1995-2002.
83. Lodge, T. P.; Pan, C.; Jin, X.; Liu, Z.; Zhao, J.; Maurer, W. W.; Bates, F. S. *Journal of Polymer Science Part B-Polymer Physics* **1995,** 33, (16), 2289-2293.
84. Balsara, N. P.; Eastman, C. E.; Foster, M. D.; Lodge, T. P.; Tirrell, M. *Makromolekulare Chemie-Macromolecular Symposia* **1991,** 45, 213-235.
85. Lai, C. J.; Russel, W. B.; Register, R. A. *Macromolecules* **2002,** 35, (10), 4044-4049.
86. Banaszak, M.; Whitmore, M. D. *Macromolecules* **1992,** 25, (13), 3406-3412.
87. Hanley, K. J.; Lodge, T. P.; Huang, C. I. *Macromolecules* **2000,** 33, (16), 5918-5931.
88. Birshtein, T. M.; Zhulina, E. B. *Polymer* **1990,** 31, (7), 1312-1320.
89. Huang, C. I.; Lodge, T. P. *Macromolecules* **1998,** 31, (11), 3556-3565.
90. Lodge, T. P.; Pudil, B.; Hanley, K. J. *Macromolecules* **2002,** 35, (12), 4707-4717.

91. Israelachvili, J., *Intermolecular & Surface Forces*. 2 ed.; Academic Press: London, 1991.
92. Epps, T. H.; Bailey, T. S.; Pham, H. D.; Bates, F. S. *Chemistry of Materials* **2002,** 14, (4), 1706-1714.
93. Ruzette, A. V. G.; Soo, P. P.; Sadoway, D. R.; Mayes, A. M. *Journal of the Electrochemical Society* **2001,** 148, (6), A537-a543.
94. Wang, J. Y.; Chen, W.; Russell, T. P. *Macromolecules* **2008,** 41, (13), 4904-4907.
95. Young, W. S.; Epps, T. H. *Macromolecules* **2009,** 42, (7), 2672-2678.
96. Naidu, S.; Ahn, H.; Gong, J.; Kim, B.; Ryu, D. Y. *Macromolecules* **2011,** 44, (15), 6085-6093.
97. Wang, Z. G. *Journal of Physical Chemistry B* **2008,** 112, (50), 16205-16213.
98. Matsen, M. W.; Bates, F. S. *Journal of Polymer Science Part B-Polymer Physics* **1997,** 35, (6), 945-952.
99. Lee, D. H.; Kim, H. Y.; Kim, J. K.; Huh, J.; Ryu, D. Y. *Macromolecules* **2006,** 39, (6), 2027-2030.
100. Gunkel, I.; Thurn-Albrecht, T. *Macromolecules* **2012,** 45, (1), 283-291.
101. Anderson, J. L.; Pino, V.; Hagberg, E. C.; Sheares, V. V.; Armstrong, D. W. *Chemical Communications* **2003**, (19), 2444-2445.
102. Atkin, R.; Warr, G. G. *Journal of the American Chemical Society* **2005,** 127, (34), 11940-11941.
103. Araos, M. U.; Warr, G. G. *Journal of Physical Chemistry B* **2005,** 109, (30), 14275-14277.
104. Wang, L. Y.; Chen, X.; Chai, Y. C.; Hao, J. C.; Sui, Z. M.; Zhuang, W. C.; Sun, Z. W. *Chemical Communications* **2004**, (24), 2840-2841.
105. Evans, D. F.; Yamauchi, A.; Roman, R.; Casassa, E. Z. *Journal of Colloid and Interface Science* **1982,** 88, (1), 89-96.
106. Evans, D. F.; Yamauchi, A.; Wei, G. J.; Bloomfield, V. A. *Journal of Physical Chemistry* **1983,** 87, (18), 3537-3541.
107. He, Y. Y.; Li, Z. B.; Simone, P.; Lodge, T. P. *Journal of the American Chemical Society* **2006,** 128, (8), 2745-2750.
108. Simone, P. M.; Lodge, T. P. *Macromolecular Chemistry and Physics* **2007,** 208, (4), 339-348.
109. Meli, L.; Lodge, T. P. *Macromolecules* **2009,** 42, (3), 580-583.
110. Meli, L.; Santiago, J. M.; Lodge, T. P. *Macromolecules* **2010,** 43, (4), 2018-2027.
111. Tamura, S.; Ueki, T.; Ueno, K.; Kodama, K.; Watanabe, M. *Macromolecules* **2009,** 42, (16), 6239-6244.
112. Lee, H. N.; Lodge, T. P. *Journal of Physical Chemistry B* **2011,** 115, (9), 1971-1977.
113. Lee, H. N.; Bai, Z. F.; Newell, N.; Lodge, T. P. *Macromolecules* **2010,** 43, (22), 9522-9528.
114. Ueki, T.; Watanabe, M.; Lodge, T. P. *Macromolecules* **2009,** 42, (4), 1315-1320.
115. Lu, H. Y.; Lee, D. H.; Russell, T. P. *Langmuir* **2010,** 26, (22), 17126-17132.
116. Lu, H. Y.; Akgun, B.; Wei, X. Y.; Li, L.; Satija, S. K.; Russell, T. P. *Langmuir* **2011,** 27, (20), 12443-12450.
117. Bai, Z. F.; He, Y. Y.; Lodge, T. P. *Langmuir* **2008,** 24, (10), 5284-5290.

118. Bai, Z. F.; Lodge, T. P. *Journal of Physical Chemistry B* **2009,** 113, (43), 14151-14157.
119. Guerrero-Sanchez, C.; Gohy, J. F.; D'Haese, C.; Thijs, H.; Hoogenboom, R.; Schubert, U. S. *Chemical Communications* **2008**, (24), 2753-2755.
120. He, Y. Y.; Lodge, T. P. *Journal of the American Chemical Society* **2006,** 128, (39), 12666-12667.
121. Bai, Z. F.; He, Y. Y.; Young, N. P.; Lodge, T. P. *Macromolecules* **2008,** 41, (18), 6615-6617.
122. Soto-Figueroa, C.; Rodriguez-Hidalgo, M. D.; Vicente, L. *Soft Matter* **2012,** 8, (6), 1871-1877.
123. Bai, Z. F.; Lodge, T. P. *Langmuir* **2010,** 26, (11), 8887-8892.
124. Guerrero-Sanchez, C.; Wouters, D.; Hoeppener, S.; Hoogenboom, R.; Schubert, U. S. *Soft Matter* **2011,** 7, (8), 3827-3831.
125. He, Y. Y.; Boswell, P. G.; Buhlmann, P.; Lodge, T. P. *Journal of Physical Chemistry B* **2007,** 111, (18), 4645-4652.
126. He, Y. Y.; Lodge, T. P. *Chemical Communications* **2007**, (26), 2732-2734.
127. He, Y.; Lodge, T. P. *Macromolecules* **2008,** 41, (1), 167-174.
128. Noro, A.; Matsushita, Y.; Lodge, T. P. *Macromolecules* **2008,** 41, (15), 5839-5844.
129. Noro, A.; Matsushita, Y.; Lodge, T. P. *Macromolecules* **2009,** 42, (15), 5802-5810.
130. Lei, Y.; Lodge, T. P. *Soft Matter* **2012,** 8, (7), 2110-2120.
131. Chen, Y. B.; Thorn, M.; Christensen, S.; Versek, C.; Poe, A.; Hayward, R. C.; Tuominen, M. T.; Thayumanavan, S. *Nature Chemistry* **2010,** 2, (6), 503-508.
132. Huang, Y. J.; Cong, Y. H.; Li, J. J.; Wang, D. L.; Zhang, J. T.; Xu, L.; Li, W. L.; Li, L. B.; Pan, G. Q.; Yang, C. L. *Chemical Communications* **2009**, (48), 7560-7562.
133. Choi, I.; Ahn, H.; Park, M. J. *Macromolecules* **2011,** 44, (18), 7327-7334.
134. Cho, J. H.; Lee, J.; He, Y.; Kim, B.; Lodge, T. P.; Frisbie, C. D. *Advanced Materials* **2008,** 20, (4), 686-+.
135. Suga, T.; Takeuchi, S.; Nishide, H. *Advanced Materials* **2011,** 23, (46), 5545-+.
136. Cho, J. H.; Lee, J.; Xia, Y.; Kim, B.; He, Y. Y.; Renn, M. J.; Lodge, T. P.; Frisbie, C. D. *Nature Materials* **2008,** 7, (11), 900-906.
137. Lee, J.; Kaake, L. G.; Cho, J. H.; Zhu, X. Y.; Lodge, T. P.; Frisbie, C. D. *Journal of Physical Chemistry C* **2009,** 113, (20), 8972-8981.
138. Lee, K. H.; Zhang, S. P.; Lodge, T. P.; Frisbie, C. D. *Journal of Physical Chemistry B* **2011,** 115, (13), 3315-3321.
139. Yoon, J.; Kang, D. K.; Won, J.; Park, J. Y.; Kang, Y. S. *Journal of Power Sources* **2012,** 201, 395-401.
140. Imaizumi, S.; Kokubo, H.; Watanabe, M. *Macromolecules* **2012,** 45, (1), 401-409.
141. Zhang, S. P.; Lee, K. H.; Frisbie, C. D.; Lodge, T. P. *Macromolecules* **2011,** 44, (4), 940-949.
142. Zhang, S. P.; Lee, K. H.; Sun, J. R.; Frisbie, C. D.; Lodge, T. P. *Macromolecules* **2011,** 44, (22), 8981-8989.
143. Kim, S. Y.; Kim, S.; Park, M. J. *Nature Communications* **2010,** 1.
144. Kim, Y. S.; Pivovar, B. S. *Annual Review of Chemical and Biomolecular Engineering, Vol 1* **2010,** 1, 123-148.

145. Cho, B. K.; Jain, A.; Gruner, S. M.; Wiesner, U. *Science* **2004,** 305, (5690), 1598-1601.
146. Sax, J.; Ottino, J. M. *Polymer Engineering and Science* **1983,** 23, (3), 165-176.
147. Hou, J. B.; Li, J.; Madsen, L. A. *Macromolecules* **2010,** 43, (1), 347-353.
148. Wanakule, N. S.; Panday, A.; Mullin, S. A.; Gann, E.; Hexemer, A.; Balsara, N. P. *Macromolecules* **2009,** 42, (15), 5642-5651.
149. Mullin, S. A.; Stone, G. M.; Teran, A. A.; Hallinan, D. T.; Hexemer, A.; Balsara, N. P. *Nano Letters* **2012,** 12, (1), 464-468.
150. Majewski, P. W.; Gopinadhan, M.; Jang, W. S.; Lutkenhaus, J. L.; Osuji, C. O. *Journal of the American Chemical Society* **2010,** 132, (49), 17516-17522.
151. Park, M. J.; Balsara, N. P. *Macromolecules* **2010,** 43, (1), 292-298.
152. Li, J.; Park, J. K.; Moore, R. B.; Madsen, L. A. *Nature Materials* **2011,** 10, (7), 507-511.
153. Li, J.; Wilmsmeyer, K. G.; Madsen, L. A. *Macromolecules* **2009,** 42, (1), 255-262.
154. Park, J. K.; Li, J.; Divoux, G. M.; Madsen, L. A.; Moore, R. B. *Macromolecules* **2011,** 44, (14), 5701-5710.
155. Scatena, L. F.; Brown, M. G.; Richmond, G. L. *Science* **2001,** 292, (5518), 908-912.
156. Piletic, I. R.; Moilanen, D. E.; Spry, D. B.; Levinger, N. E.; Fayer, M. D. *Journal of Physical Chemistry A* **2006,** 110, (34), 10369-10369.
157. Moilanen, D. E.; Levinger, N. E.; Spry, D. B.; Fayer, M. D. *Journal of the American Chemical Society* **2007,** 129, (46), 14311-14318.
158. Guegan, R. *Journal of Colloid and Interface Science* **2011,** 358, (2), 485-490.
159. Moilanen, D. E.; Piletic, I. R.; Fayer, M. D. *Journal of Physical Chemistry C* **2007,** 111, (25), 8884-8891.
160. Eikerling, M.; Kornyshev, A. A.; Kuznetsov, A. M.; Ulstrup, J.; Walbran, S. *Journal of Physical Chemistry B* **2001,** 105, (17), 3646-3662.
161. Mafe, S.; Manzanares, J. A.; Ramirez, P. *Physical Chemistry Chemical Physics* **2003,** 5, (2), 376-383.
162. Paddison, S. J.; Paul, R. *Physical Chemistry Chemical Physics* **2002,** 4, (7), 1158-1163.
163. Park, M. J.; Downing, K. H.; Jackson, A.; Gomez, E. D.; Minor, A. M.; Cookson, D.; Weber, A. Z.; Balsara, N. P. *Nano Letters* **2007,** 7, (11), 3547-3552.
164. Singh, M.; Odusanya, O.; Wilmes, G. M.; Eitouni, H. B.; Gomez, E. D.; Patel, A. J.; Chen, V. L.; Park, M. J.; Fragouli, P.; Iatrou, H.; Hadjichristidis, N.; Cookson, D.; Balsara, N. P. *Macromolecules* **2007,** 40, (13), 4578-4585.
165. Bureekaew, S.; Horike, S.; Higuchi, M.; Mizuno, M.; Kawamura, T.; Tanaka, D.; Yanai, N.; Kitagawa, S. *Nature Materials* **2009,** 8, (10), 831-836.

Chapter 2. Effect of an Ionic Liquid Solvent on the Phase Behavior of Block Copolymers

Reproduced with permission from Justin M. Virgili, Megan L. Hoarfrost, and Rachel A. Segalman, Macromolecules, 2010, 43(12), pp. 5417-5423. 2009 American Chemical Society

The phase behavior of concentrated mixtures of block copolymers with an ionic liquid has been studied using a large series of block copolymers with various molecular weights and volume fractions to gain a thorough understanding of the thermodynamics of self-assembly. The lyotropic phase behavior of mixtures of poly(styrene-*b*-2-vinyl pyridine) (PS-*b*-P2VP) block copolymers with the ionic liquid imidazolium bis(trifluoromethylsulfonyl)imide ([Im][TFSI]) is reminiscent of block copolymer/selective molecular solvent mixtures, and ordered microstructures corresponding to lamellae, hexagonally close-packed cylinders, body-centered cubic, and face-centered cubic oriented micelles are observed. Scaling analysis reveals that, in contrast to observations of block copolymer/molecular solvent mixtures, the interfacial area occupied by each PS-*b*-P2VP chain decreases upon the addition of [Im][TFSI], indicating a considerable increase in the effective segregation strength of the PS-*b*-P2VP copolymer with ionic liquid addition.

2.1. Introduction

Ionic liquids are an exciting class of materials due to unique properties including high thermal and electrochemical stability, negligible volatility, and high ionic conductivity.[1] This exceptional combination of properties makes them candidates for a variety of applications such as fuel cells,[2-6] transistors,[7, 8] and battery electrolytes,[9, 10] for which it would be desirable to integrate the ionic liquid into a solid polymeric matrix. Such a material can be realized by selectively incorporating the ionic liquid into a continuous block copolymer phase, forming a membrane in which the second phase provides mechanical stability.[11] Fundamental understanding of block copolymer/ionic liquid interactions and the resulting self-assembly is essential for predictable structure and property control.

Both "solvent-like" and "salt-like" properties of ionic liquid have been observed in block copolymer/ionic liquid mixtures.[12] Addition of a molecular solvent to a block copolymer typically results in lyotropic phase transitions, changes in characteristic domain spacing (d), and changes in the order-disorder transition temperature (T_{ODT}).[13-18] In the case of block copolymer/salt mixtures, changes in the phase behavior relative to the neat copolymer have been interpreted as changes in the effective segregation strength, chain statistics, or intermolecular coordination.[19-22] Recently, Wang has developed an analytical expression for an effective interaction parameter, χ_{eff}, in homopolymer blend/salt mixtures that incorporates ion solvation and entropic effects.[23] Previous experimental studies of the self-assembly of dilute[24] and concentrated[11] poly(1,2-butadiene-*b*-ethylene oxide)/ionic liquid mixtures have highlighted the similarity of the phase behavior of the mixtures to that of block copolymer/molecular solvent mixtures.

However, studies of the thermal properties of poly(styrene-*b*-2-vinylpyridine) (PS-*b*-P2VP)/ionic liquid mixtures have shown an increased glass transition temperature (T_g) of the poly(2-vinyl pyridine) (P2VP) phase at low ionic liquid concentrations due to a salt-like physical cross linking, while at high ionic liquid concentrations the T_g of the P2VP block was depressed as it would be in the presence of a molecular solvent.[12]

In this work the effect of block copolymer volume fraction, f_{PS}, and degree of polymerization, N_T, on the phase behavior of concentrated PS-*b*-P2VP copolymer mixtures with the ionic liquid imidazolium bis(trifluoromethylsulfonyl)imide ([Im][TFSI]) (Figure 2.1) is explored to gain a thorough understanding of the thermodynamics of self-assembly in this complex system. In particular, thermal characterization of PS-*b*-P2VP/[Im][TFSI] mixtures reveals an unusual composition dependence of T_g not predicted by either the Gordon-Taylor or Fox equations for polymer/molecular solvent mixtures. The lyotropic phase behavior of the mixtures is studied using small-angle X-ray scattering (SAXS) and small-angle neutron scattering (SANS) and compared to that of mixtures of block copolymers in selective molecular solvents. Scaling analysis of the structural length scales and studies of the thermotropic phase behavior of the PS-*b*-P2VP/[Im][TFSI] mixtures reveal a substantial increase in segregation strength upon the addition of ionic liquid compared to block copolymer/selective molecular solvent mixtures. It is anticipated that the increased segregation strength is due to the enthalpic driving force for ions to reside in the high dielectric P2VP phase of the block copolymer.[23]

2.2. Experimental Section

Polymer Synthesis and Characterization. PS-*b*-P2VP copolymers and P2VP homopolymer were synthesized via anionic polymerization using standard methods.[25] The molecular weight of the polystyrene (PS) hompolymer was determined using gel permeation chromatography (GPC) and the total molecular weight of the block copolymer was determined via ^{1}H NMR (Bruker AVB-300). The molecular weight of the P2VP homopolymer was determined using ^{1}H NMR end-group analysis. The polydispersity of each polymer was assessed using GPC. The PS-*b*-P2VP copolymers are designated PS-*b*-P2VP(*xx*-*yy*) and the P2VP homopolymer is designated P2VP(*yy*), where '*xx*' and '*yy*' refer to the number averaged molecular weights in kg/mol of the PS and P2VP blocks, respectively. The total molecular weight, volume fraction of polystyrene, f_{PS}, and polydispersity index (PDI) of the polymers are given in Table 2.1. One of the ten polymers, *d*PS-*b*-P2VP(7.1-6.8), was synthesized with *d*8-styrene monomer obtained from Polymer Source.

Ionic Liquid Purification. Imidazole (≥95%) and bis(trifluoromethylsulfonyl)imide (HTFSI, ≥95%) were purchased from Sigma Aldrich and purified by sublimation under vacuum. Differential scanning calorimetry (DSC) and ^{1}H NMR were used to assess the purity of the two starting materials. Purified imidazole and HTFSI were combined in equimolar quantities in a glove box, sealed, and heated in an oven outside the glove box to 100 °C for 2 to 3 hours to prepare the ionic liquid [Im][TFSI]. The composition of the ionic liquid was confirmed by comparing the measured melting point of the compound

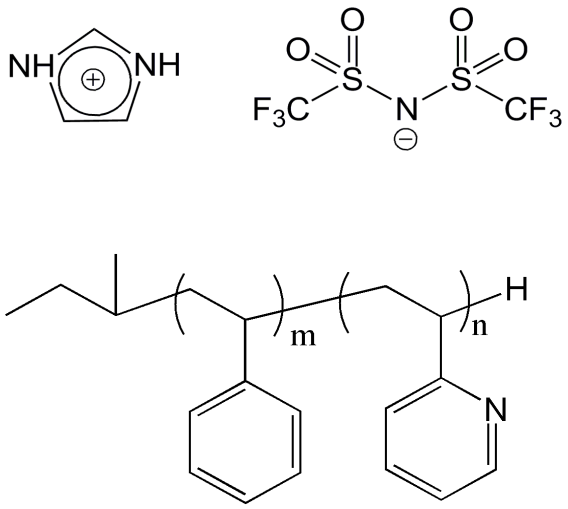


Figure 2.1. Chemical Structures of [Im][TFSI] and PS-*b*-P2VP.

Table 2.1. Characteristics of Block Copolymers Studied.

Constant N_T			
Sample	**Total MW (g/mol)**	f_{PS}	**PDI**
PS-*b*-P2VP(4.4-10.8)	15,200	0.29	1.07
PS-*b*-P2VP(4.9-6.6)	11,500	0.43	1.13
*d*PS-*b*-P2VP(7.1-6.8)	13,900	0.50	1.10
Constant N_{P2VP}			
Sample	**Total MW (g/mol)**	f_{PS}	**PDI**
PS-*b*-P2VP(4.4-10.8)	15,200	0.29	1.07
PS-*b*-P2VP(8.7-12.0)	20,800	0.42	1.02
PS-*b*-P2VP(12.0-12.4)	24,300	0.49	1.19
PS-*b*-P2VP(18.4-11.4)	29,800	0.62	1.10
PS-*b*-P2VP(28.5-10.7)	39,200	0.73	1.04
P2VP(13.1)	13,100	0.00	1.06

with literature.[2] Care was taken to limit air and water exposure of the hydroscopic ionic liquid by handling the material in an argon glove box and sealed sample holders.

Scattering Sample Preparation and Methods. Dichloromethane was degassed using three freeze, pump, thaw cycles, stirred over CaH_2 overnight, then distilled into a collection flask, brought into a glove box, and stored on molecular sieves. All further sample preparation was performed within an argon glove box. Predetermined quantities of [Im][TFSI] and PS-*b*-P2VP were weighed into glass vials, ca. 5 wt% solutions were prepared by dissolving in dichloromethane, and the solutions were stirred overnight. Samples were cast one drop at a time into sample cells formed by an aluminum spacer sealed onto a Kapton window on one side until a ca. 1 mm solid sample was obtained. Samples were heated to 60 °C (above the boiling point of dichloromethane) for ca. 18 hours to remove remaining solvent. A second Kapton window was glued to seal the samples. Samples were sealed in jars containing desiccant in the argon glove box for transportation to the beamline. Samples are designated by the value of the polymer volume fraction, ϕ_P, assuming ideal mixing. The density of [Im][TFSI] was estimated to be 1.67 g/cm^3 from scattering length density fits of SANS intensity profiles[26] and the densities of both PS and P2VP were taken to be 1.05 g/cm^3.

SAXS was performed on beamline 7.3.3 of the Advanced Light Source (ALS) and beamline 1-4 of the Stanford Synchrotron Radiation Lightsource (SSRL). At the ALS, the beamline was configured with an X-ray wavelength of λ=1.240 Å and focused to a 50 by 300 µm spot. Samples were equilibrated within the beamline at 145 ºC for 20 to 30 minutes before data was gathered. Full two-dimensional scattering patterns were collected on an ADSC CCD detector with an active area of 188 by 188 mm. The scattering patterns were radially averaged and the scattering intensity corrected with the post-ion chamber intensity using Nika version 1.18. At the SSRL, the beamline was configured with an X-ray wavelength λ=1.488 Å and focused to a 0.5 mm diameter spot. A single quadrant of a two-dimensional scattering pattern was collected on a CCD detector with an active area of 25.4 by 25.4 mm. The scattering patterns were radially averaged and corrected for detector null signal, dark current, and empty cell scattering.

SANS measurements of mixtures of *d*PS-*b*-P2VP(7.1-6.8) with [Im][TFSI] were performed at Oak Ridge National Laboratory on the SANS-I instrument. Neutrons with a λ=6.0 Å wavelength and a sample to detector distance of 4 and 10 m were utilized. Data from room temperature samples was collected and the intensity corrected for instrumental background, empty cell scattering, sample transmission, and incoherent background, and placed on an absolute intensity scale by use of a porous carbon standard (Al4).[27] In some samples, a small positive scattering intensity, typically on the order of 0.1 cm^{-1}, remained after this data reduction procedure, likely due to incoherent scattering.[28] In these cases, the residual intensity was removed by subtracting the average intensity over the range $0.085<q<0.100$ Å^{-1}.

Differential Scanning Calorimetry (DSC). DSC was performed on a TA Instruments DSC 2920. Samples were solution cast in a glove box into aluminum DSC pans from the same solutions used to prepare scattering samples. The samples were heated to 60 °C for

ca. 18 hours to remove remaining solvent. The samples were then crimped within the glove box using hermetically sealed pans and placed inside a container with desiccant for transfer to the DSC. Indium and dodecane were used as calibration standards for the DSC. Samples underwent three heating and cooling cycles and glass transitions recorded upon the second heating were reported.

2.3. Results and Discussion

2.3.1. Thermal Properties of PS-*b*-P2VP/[Im][TFSI] System

The thermal properties of PS-*b*-P2VP/[Im][TFSI] mixtures highlight the complex effect of the addition of an ionic liquid to a block copolymer. In the neat PS-*b*-P2VP copolymers, a single T_g is observed in the vicinity of 100 °C, due to the similarity of the T_g of the PS and P2VP homopolymers. While the T_g of the PS phase remains in the viscinity of 100 °C upon the addition of ionic liquid, the presence of a sufficient amount of ionic liquid (>4 wt%) leads to a decrease in the T_g of the P2VP-rich phase due to the high selectivity of [Im][TFSI] for this phase.[26] In Figure 2.2, the low temperature T_g is plotted as a function of weight fraction of ionic liquid in the P2VP-rich phase, w_{IL} (where w_{IL} and w_{P2VP} sum to one), assuming all ionic liquid partitions into the P2VP-rich phase. Representative DSC scans, used to determine the T_g of the PS and P2VP phases of the mixtures, are included in the Appendix, Figure 2.A.1. The ratio of [Im][TFSI] to P2VP is found to be predictive of the P2VP/[Im][TFSI] T_g, regardless of the f_{PS} and N_T of the PS-*b*-P2VP copolymers, as indicated by the collapse of the data onto a single curve. The Gordon-Taylor[29] and Fox[30] equations (Equations 2.1 and 2.2, respectively) have been routinely used to describe the T_g of polymer/molecular solvent mixtures and polymer ion gels[31] and are given by:

$$T_g = v_{IL} * T_{g,IL} + v_{P2VP} * T_{g,P2VP} \tag{2.1}$$

$$\frac{1}{T_g} = \frac{w_{IL}}{T_{g,IL}} + \frac{w_{P2VP}}{T_{g,P2VP}} \tag{2.2}$$

where v_{P2VP} *and* v_{IL} are the volume fractions of P2VP and [Im][TFSI] in the P2VP/[Im][TFSI] phase. The T_g of [Im][TFSI] is below the range of our DSC (-40 to 725 ºC) and also not available from literature. Thus, the [Im][TFSI] T_g was used as a fitting parameter to compare equations 1 and 2 to the P2VP/[Im][TFSI] T_g data. Neither the Gordon-Taylor nor the Fox equations capture the composition dependence of the T_g data. Both equations predict a monotonically decreasing relationship between the T_g of a polymer and the solvent weight or volume fraction with a concave-up curve shape. In contrast, an unusual concave-down curve shape is observed in Figure 2.2. It is conceivable that specific interactions between [Im][TFSI] and P2VP that are not captured by the Gordon-Taylor or the Fox equations lead to the unique composition dependence of the T_g of the P2VP phase observed in Figure 2.2.

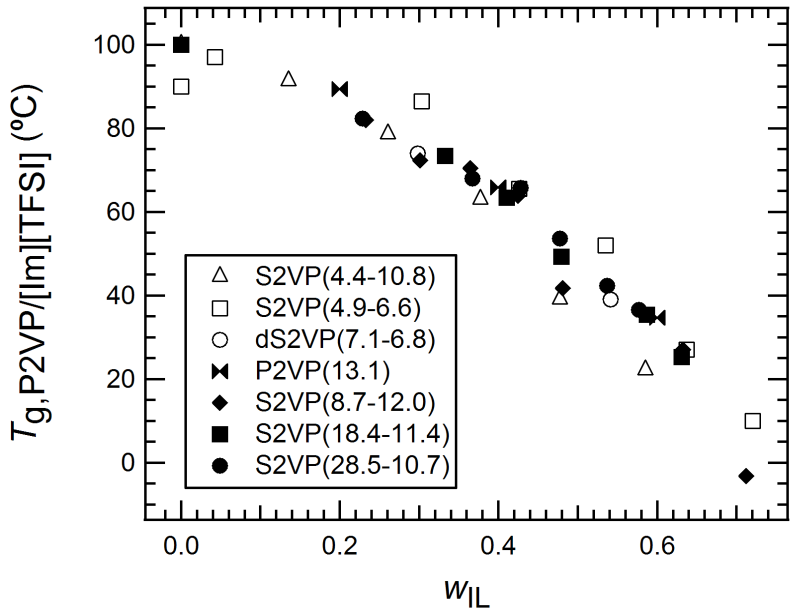


Figure 2.2. Glass Transition Temperature of P2VP/[Im][TFSI] Phase. T_g of the P2VP/[Im][TFSI] phase as a function of w_{IL} determined by DSC.

2.3.2. Lyotropic Phase Behavior

The phase behavior of mixtures of [Im][TFSI] with two series of PS-*b*-P2VP copolymers, one with constant N_T and one with constant N_{P2VP} (Table 2.1), demonstrates the similarity between mixtures of block copolymers with a selective molecular solvent and mixtures with an ionic liquid. Representative SAXS profiles are shown in Figure 2.3 from mixtures of PS-*b*-P2VP copolymers of both series with [Im][TFSI] to highlight specific lyotropic phase transitions. Additional SAXS and SANS data is included in the Appendix, Figures 2.A.2 and 2.A.3, and Figure 2.A.4 features expanded SAXS profiles such that detailed higher order peaks and other features are more visible. In Figure 2.3a, the neat PS-*b*-P2VP(4.4-10.8) copolymer with f_{PS}=0.29 exhibits a hexagonally-close-packed (HCP) cylinder morphology with a domain spacing (d) of 14.9 nm (110 scattering plane). As expected, the addition of ionic liquid (ϕ_P=0.95-0.48) increases d, indicating that [Im][TFSI] acts as a selective solvent in the PS-*b*-P2VP copolymer.[12] At a composition of ϕ_P=0.42, the higher order scattering peaks reveal a lyotropic transition to spheres packed on a body-centered cubic (BCC) lattice. The presence of the $\sqrt{7}q^*$ scattering peak, as well as the higher scattering intensity of the $\sqrt{3}q^*$ peak compared to the $\sqrt{2}q^*$ peak differentiates the observed SAXS profile from that of spherical micelles oriented on a simple cubic (SC) lattice.[32] It appears that the coexistence window required by Gibb's phase rule between the two phases is small ($\Delta\phi_P \leq 0.06$).[33] As ϕ_P is decreased to ϕ_P=0.37 and ϕ_P=0.34, distinct shoulders are observed on the primary scattering peak. At ϕ_P=0.23 the q^* peak narrows and the higher order scattering peaks corresponding to BCC-packed spheres persist, indicating that the ϕ_P=0.34 and ϕ_P=0.37 mixtures consist of coexisting BCC-packed spheres with slightly incommensurate unit cells. This finding suggests that long equilibration times are necessary for the formation of stable, ordered micellar structures in block copolymer/ionic liquid mixtures, in agreement with previous experimental observations[34] as well as suggestions that when micellar phases form lattices that are not at equilibrium spacings the driving force for recovery is exceedingly small.[35]

In a more nearly symmetric PS-*b*-P2VP(4.9-6.6) copolymer with f_{PS}=0.43 the neat lamellar structure swells to form HCP cylinder phases when $0.62 \leq \phi_P \leq 0.86$ (Figure 2.3b). At ϕ_P=0.52, a distinctive broadening of the q^*, $\sqrt{3}q^*$, $\sqrt{7}q^*$ and $3q^*$ scattering peaks suggests a lyotropic transition; however, the likelihood of coexistence makes phase identification impossible. Upon further decreasing ϕ_P to ϕ_P=0.29, reflections at $\sqrt{3}q^*$, $\sqrt{4}q^*$, $\sqrt{8}q^*$, and $\sqrt{20}q^*$ are observed corresponding to a lyotropic transition to PS spheres on a face-centered cubic (FCC) lattice.

Figure 2.3c illustrates the qualitative differences in the lyotropic phase behavior of copolymers with a PS-majority phase. The HCP P2VP cylinders observed in the neat f_{PS}=0.73 PS-*b*-P2VP(28.5-10.7) copolymer undergo a lyotropic phase transition to a lamellar microstructure at ϕ_P=0.95. At ϕ_P=0.70, a dramatic broadening of the q^* peak is observed along with weak, undulating higher order scattering peaks revealing micelles with liquid-like order (DM) that persist as ϕ_P is further reduced to ϕ_P=0.28. The asymmetry of the PS and P2VP blocks in the f_{PS}=0.73 PS-*b*-P2VP(28.5-10.7) copolymer

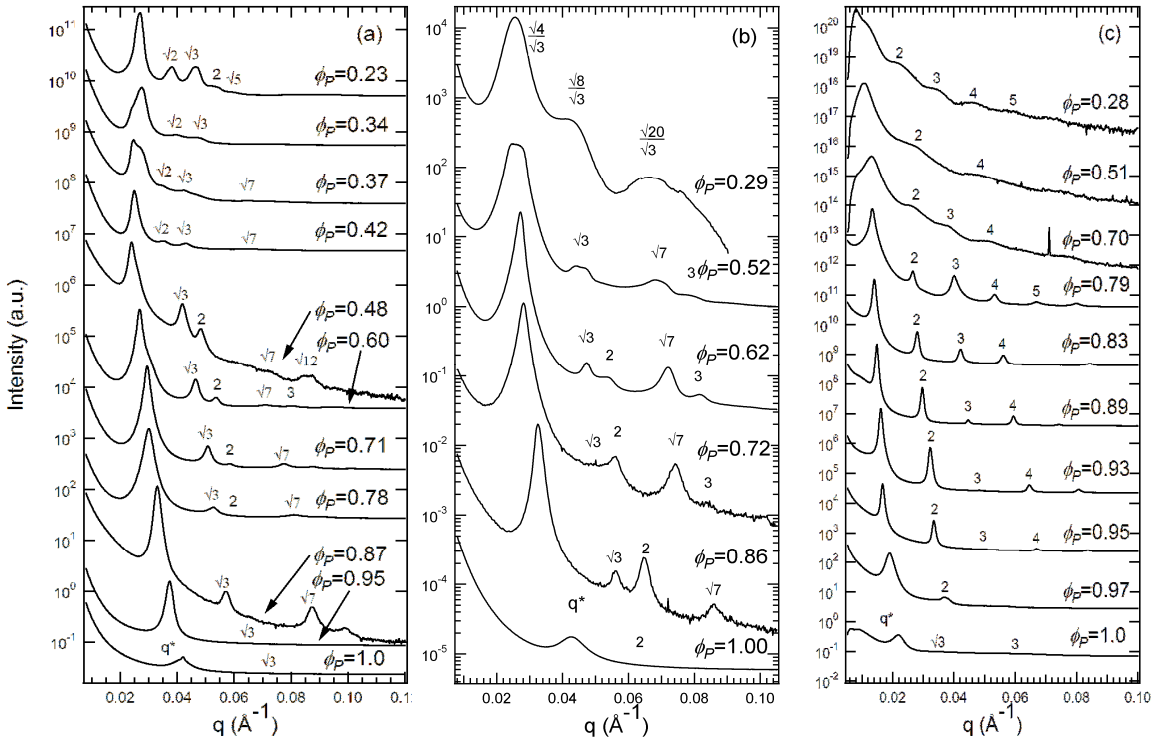


Figure 2.3. SAXS Profiles of PS-*b*-P2VP/[Im][TFSI] Mixtures. SAXS profiles of varying ϕ_P for (a) PS-*b*-P2VP(4.4-10.8), (b) PS-*b*-P2VP(4.9-6.6), and (c) PS-*b*-P2VP(28.5-10.7) copolymers. In all cases, peak labels correspond to the q/q^* for scattering peaks and the profiles are recorded at 145 °C.

likely leads to packing frustration in the PS phase upon addition of ionic liquid, which disrupts the formation of long-range order ($\phi_P \leq 0.70$). These findings demonstrate the rich variety of microstructures attainable in PS-*b*-P2VP/[Im][TFSI] mixtures through modification of f_{PS}, N, and ϕ_P. Further, from the sequence of lyotropic phase transitions observed in the f_{PS}=0.29, 0.43, and 0.73 copolymers it is evident that the [Im][TFSI] ionic liquid selectively solvates the P2VP block.

Lyotropic phase diagrams of the PS-*b*-P2VP/[Im][TFSI] mixtures for the series of PS-*b*-P2VP copolymers with constant N_T and N_{P2VP} demonstrate similarities to the lyotropic phase behavior of block copolymer/selective molecular solvent mixtures (Figure 2.4). For example, spheres on a BCC lattice are both predicted and experimentally observed in selective solvent/block copolymer systems in which the corona layer is large relative to the core,[14, 32, 36] and are also observed in PS-*b*-P2VP(4.4-10.8) (f_{PS}=0.29) at low ϕ_P. For "inverted spheres," in which the corona is small relative to the core, FCC and BCC packings have been predicted and observed for block copolymer/selective solvent systems.[14, 15] Block copolymers with thin corona layers in the most highly-selective solvents for the corona tend to form FCC-packed spheres, which is consistent with the behavior of mixtures containing the compositionally symmetric PS-*b*-P2VP(4.9-6.6) and PS-*b*-P2VP(8.7-12.0) copolymers with [Im][TFSI]. For $f_{PS} \geq 0.42$, micelles with liquid-like order are observed in mixtures with the lowest values of ϕ_P characterized. The concentration range for the DM structures increases with increasing $f_{PS,}$ similar to observations in molecular solvent systems.[11, 37, 38]

The lyotropic phase diagrams describing PS-*b*-P2VP/[Im][TFSI] mixtures for constant N_T (Figure 2.4a) and constant N_{P2VP} (Figure 2.4b) are compared to determine the effect of block copolymer degree of polymerization on self-assembly. The lyotropic phase behavior of the constant N_T series and N_{P2VP} series are qualitatively similar with the notable exception of the narrower ϕ_P window between lamellar and micellar phases in the N_{P2VP} series. As the PS blocks of the copolymers in the constant N_{P2VP} series systematically have a higher degree of polymerization at a given f_{PS} than those in the constant N_{PS} series, the entropic penalty associated with packing the long PS chains into HCP-ordered structures may lead to the narrowing of the HCP PS cylinder (C_{PS}) region in favor of the formation of micellar phases. Further, in Figure 2.4b, the complete disappearance of the C_{PS} region and unexpected narrowing of the lamellar window in mixtures with the f_{PS}=0.73 copolymer compared to the less PS-rich copolymers also points to the role that packing frustration of PS chains may play in the rich lyotropic phase behavior of these materials. In block copolymer/selective molecular solvent mixtures, inversion of cylindrical phases has been widely reported. Inversion of cylindrical phases has been recently observed in PB-*b*-PEO/ionic liquid mixtures,[11] although the ionic liquids studied in these mixtures exhibit less selectivity compared to the PS-*b*-P2VP/[Im][TFSI] system. It is anticipated that packing frustration of PS chains in the f_{PS}=0.73 copolymer mixtures in combination with the strong selectivity of the ionic liquid for the P2VP block preclude formation of inverted cylindrical phases on experimental time scales and instead lead to the formation of micelles with liquid-like order.

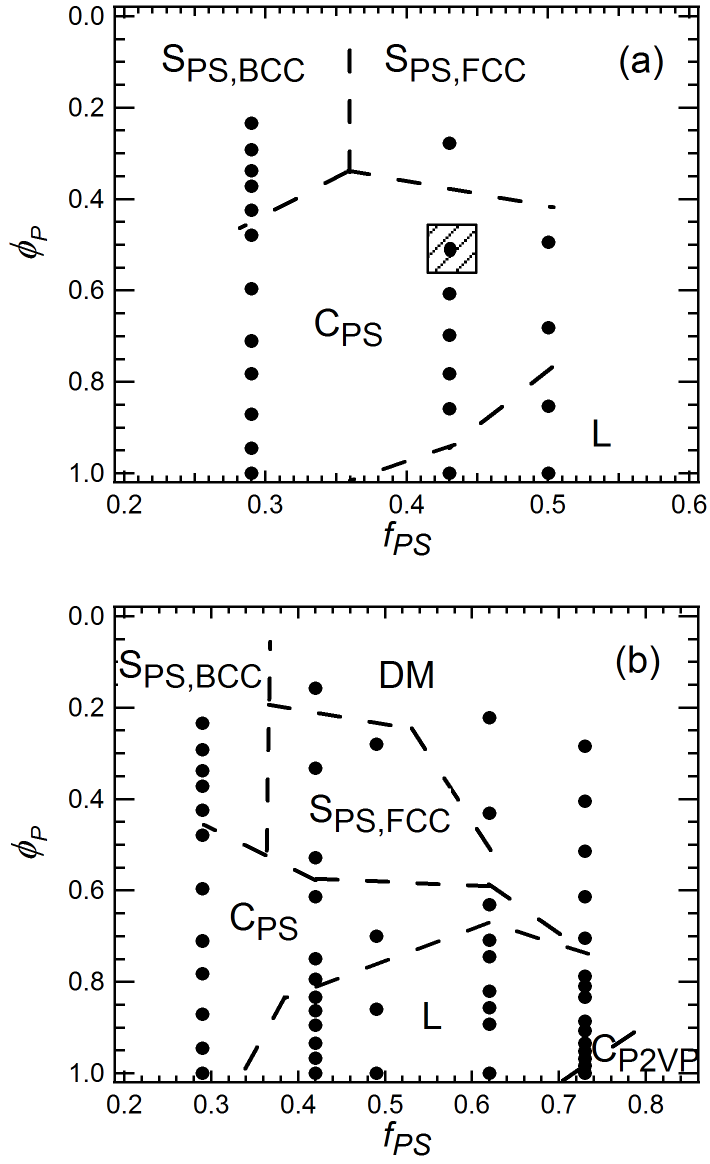


Figure 2.4. Lyotropic Phase Diagrams of PS-*b*-P2VP/[Im][TFSI] Mixtures. (a) Fixed N_T and (b) fixed N_{P2VP} at T=145 °C. Markers indicate phases identified using small-angle scattering and dashed lines are drawn to indicate interpolated phase boundaries. A region of co-existence is indicated with diagonal shading. Phases are labeled as follows: lamellae (L), HCP PS cylinders (C_{PS}), HCP P2VP cylinders (C_{P2VP}), FCC- and BCC-oriented PS spheres ($S_{PS,FCC}$ and $S_{PS,BCC}$, respectively), and micelles with liquid-like order (DM).

From Figures 2.4a and 2.4b it is observed that the ϕ_P at which the lamellae to C_{PS} lyotropic phase transition occurs, $\phi_{P,C\text{-}L}$, decreases monotonically as f_{PS} increases. The lamellar/C_{PS} phase boundary for a neat PS-*b*-P2VP copolymer is determined by f_{PS} and the segregation strength, χN. The values of χN for the neat PS-*b*-P2VP copolymers with constant N_{P2VP} as well as $\phi_{P,C\text{-}L}$ and $f_{PS,eff}$ for the mixtures with [Im][TFSI] are shown in Table 2.2, where $f_{PS,eff}$ is defined as the effective PS volume fraction at the $\phi_{P,C\text{-}L}$ phase transition and was calculated by assuming complete partitioning of the ionic liquid into the P2VP phase. Self-consistent mean-field theory predicts a lamellar/C_{PS} phase boundary between $0.32 \leq f_{PS} \leq 0.33$ for strongly segregated block copolymers and predicts the f_{PS} of this transition to decrease with increasing χN for χN less than about 30.[39] The neat copolymers in Table 2.2 span both of these categories (χN ranges from 24.6-35.6). It is evident in Table 2.2 that $f_{PS,eff}$ for the mixtures is larger than the f_{PS} of the lamellar/C_{PS} phase boundary predicted for strongly segregated copolymers, and that $f_{PS,eff}$ increases with increasing χN rather than decreasing with increasing χN as predicted for neat block copolymers for χN less than 30. It is probable that the addition of ionic liquid alters the statistical segment lengths of the two copolymer blocks, as has been observed in block copolymer/salt mixtures,[22] leading to this set of observations.

2.3.3. Domain Spacing

Theoretical[14] and experimental[14, 17, 41] studies have shown that the addition of a selective molecular solvent to a block copolymer increases *d* following the power law:

$$d \sim \phi_P^{\alpha} \tag{2.3}$$

where α is a measure of the solvent selectivity. Previously, the domain spacing of a symmetric PS-*b*-P2VP block copolymer swollen with [Im][TFSI] was shown to increase according to Equation 2.3 ($\alpha<0$), indicating that the ionic liquid selectively solvates one block of the PS-*b*-P2VP copolymer.[12] In Figure 2.5, a plot of *d* versus ϕ_P for lamellar mixtures of the constant N_{P2VP} copolymer series at 145 ºC is shown to examine the effect of f_{PS} on α. The "affine dilution" limit describes the scenario in which the insoluble block is large compared to the solvated block. In this limit α=-1 and the interfacial area per chain (*A*) remains constant upon the addition of solvent.[17] For a lamellar phase, *A* is given by:

$$A = \frac{V}{d\phi_P} \tag{2.4}$$

where *V* is the volume of the insoluble phase. For mixtures containing the highly asymmetric PS-*b*-P2VP(28.5-10.7) copolymer in [Im][TFSI], α=-1.1 ± 0.1. As f_{PS} decreases, the value of α becomes more negative, in stark contrast to observations of mixtures with molecular solvents.[17, 42] Based on Equations 2.3 and 2.4 and values of α<-1, *A* must decrease with decreasing ϕ_P, revealing that interfacial chain stretching perpendicular to the interface dominates over chain swelling parallel to the interface upon the addition of ionic liquid. While the origin of the increased segregation strengths compared to mixtures of block copolymers with molecular solvents cannot be definitively established from the current data set, it is anticipated that phase immiscibility is increased due to the presence of ions in the high dielectric P2VP phase, which comes about from a higher enthalpic free energy gain from ion solvation in the P2VP phase compared to the

Table 2.2. $f_{PS,eff}$ for Mixtures of [Im][TFSI] and PS-*b*-P2VP Copolymers with Constant N_{P2VP}.

f_{PS} of neat copolymer	χN^*	$\phi_{P,C\text{-}L}^{\dagger}$	$f_{PS,eff}^{\dagger}$
0.42	24.6	0.85 ± 0.02	0.35 ± 0.01
0.49	28.9	0.78 ± 0.09	0.38 ± 0.04
0.62	35.6	0.67 ± 0.04	0.42 ± 0.02

* χN (T=145 ºC) was determined from ref. 40.

† Error in $\phi_{P,C\text{-}L}$ and $f_{PS,eff}$ is related to the range of ϕ_P separating lamellar and C_{PS} samples in Figure 2.4b.

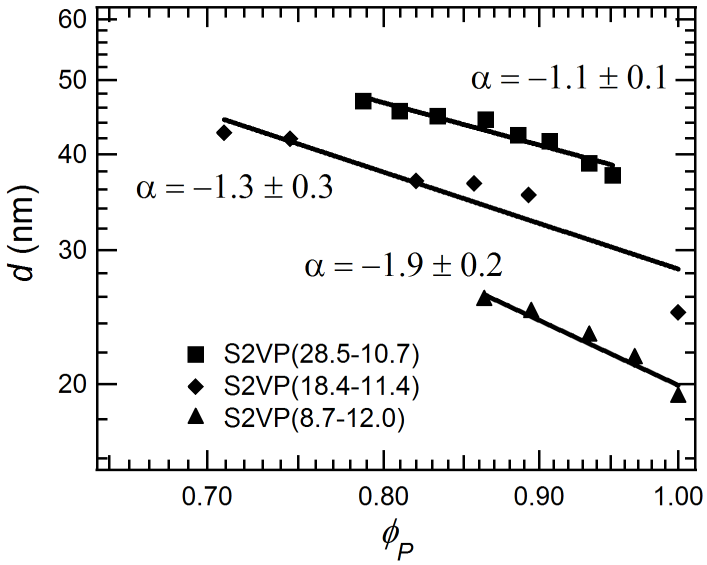


Figure 2.5. Domain Spacing Scaling Analysis: Effect of Concentration. Lamellar domain spacing, d, versus ϕ_P determined from SAXS data at 145 ºC. A power law, $d \sim \phi_P^{\alpha}$, is used to obtain α and the errors represent one standard deviation of the fit.

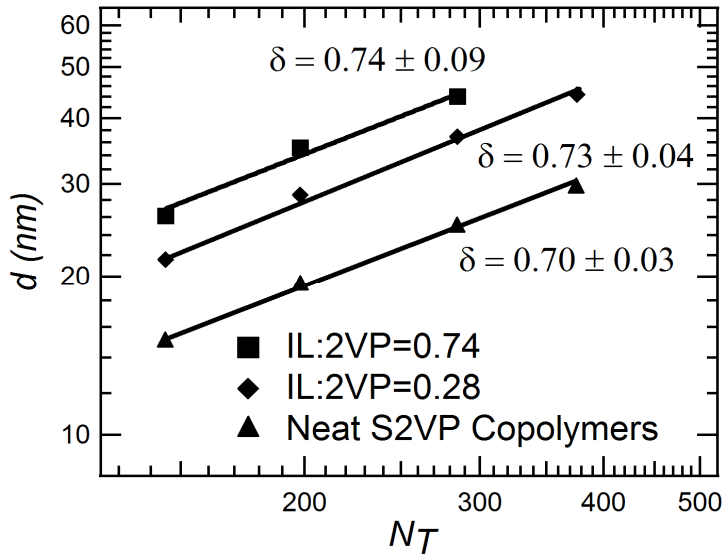


Figure 2.6. Domain Spacing Scaling Analysis: Effect of Molecular Weight. Lamellar domain spacing, d, versus N_T determined by SAXS data at 145 ºC for PS-*b*-P2VP copolymers with fixed N_{P2VP}, for the neat copolymer (▲), IL:2VP=0.74 (■), and IL:2VP=0.28 (♦). A power law fit, $d=\gamma N_T^{\delta}$, is used to obtain δ (reported errors are one standard deviation of the fit).

entropic penalty to confining the ions to a single phase.[23] The strong ion selectivity for the P2VP phase is supported by thermal characterization of the mixtures, in which the T_g of the P2VP phase decreases upon addition of [Im][TFSI] while the T_g of the PS phase remains in the viscinity of the neat T_g.

In Figure 2.6, the domain spacing of the neat PS-*b*-P2VP copolymers with constant N_{P2VP} is shown to vary with N_T as $d=\gamma N_T^{\delta}$, where $\delta=2/3$ within error, in agreement with strong segregation limit (SSL) scaling and experimental observations of the intermediate segregation regime[43-46] ($18\leq\chi N\leq47$ for the neat copolymers at 145 ºC, as calculated from the Flory-Huggins temperature dependence suggested by Schulz et al.[40]). The prefactor, γ, is known to depend on morphology, f_{PS}, the ratio of the two statistical segment lengths (a_{PS}/a_{P2VP}), and χ.[43, 44] Since the SSL scaling behavior of $d\sim N_T^{2/3}$ is also observed for fixed and non-zero values of IL:2VP as shown in Figure 6, where IL:2VP is the molar ratio of [Im][TFSI] to P2VP monomers, γ is a function of IL:2VP. In Table 2.3, γ is tabulated as a function of IL:2VP, where γ was calculated from power law fits to the data in Figure 2.6 with both γ and the N_T power law dependence used as fitting parameters. γ was found to increase monotonically with increasing IL:2VP. While the effective χ is expected to increase with increasing IL:2VP based on the highly negative values of α observed, further studies of chain statistical dimensions are necessary to quantitatively estimate the effective χ from the domain spacing data.

2.3.4. Thermotropic Phase Behavior

It is anticipated that addition of [Im][TFSI] will increase the T_{ODT} of neat PS-*b*-P2VP copolymers due to increased segregation strength of the system. In Figure 2.7a, SAXS profiles are shown for the neat, lamellar PS-*b*-P2VP(4.9-6.6) copolymer at varying temperatures. An ODT is evident at 185 ± 20 °C based on the discontinuous change in the full width at half maximum (fwhm) and intensity of the q^* peak shown in Figure 2.7b. The ODT is fully reversible upon cooling, and in close agreement with the predicted T_{ODT} (197 °C) of a $f_{PS}=0.50$, $N_T=110$ copolymer (as calculated from the Flory-Huggins temperature dependence suggested by Schulz et al.[40]). In Figure 2.7c, SAXS profiles for PS-*b*-P2VP(4.9-6.6)/[Im][TFSI] mixtures for varying ϕ_P at 225 °C are shown. The profiles are remarkably similar to those observed at 145 °C (Figure 3b), and indicate that across a wide-range of ϕ_P, the ordered block copolymer phase is stabilized with respect to temperature by the presence of ionic liquid. While the origin of the increased T_{ODT} in the PS-*b*-P2VP/[Im][TFSI] system cannot be definitively established from the current, limited data set, such behavior could result from one or both of the following possibilities: (1) the PS and P2VP interaction parameters with [Im][TFSI] are strongly temperature-dependent, or (2) as observed from domain scaling analysis, PS-*b*-P2VP/[Im][TFSI] has increased segregation strength compared to PS-*b*-P2VP due to the enthalpically driven presence of ions in the P2VP phase.

Table 2.3. γ as a Function of IL:2VP.

IL:2VP	$\gamma^{\ddagger}$
0.00	0.48 ± 0.07
0.28	0.59 ± 0.12
0.74	0.68 ± 0.35

‡ Error in γ is one standard deviation of the fit.

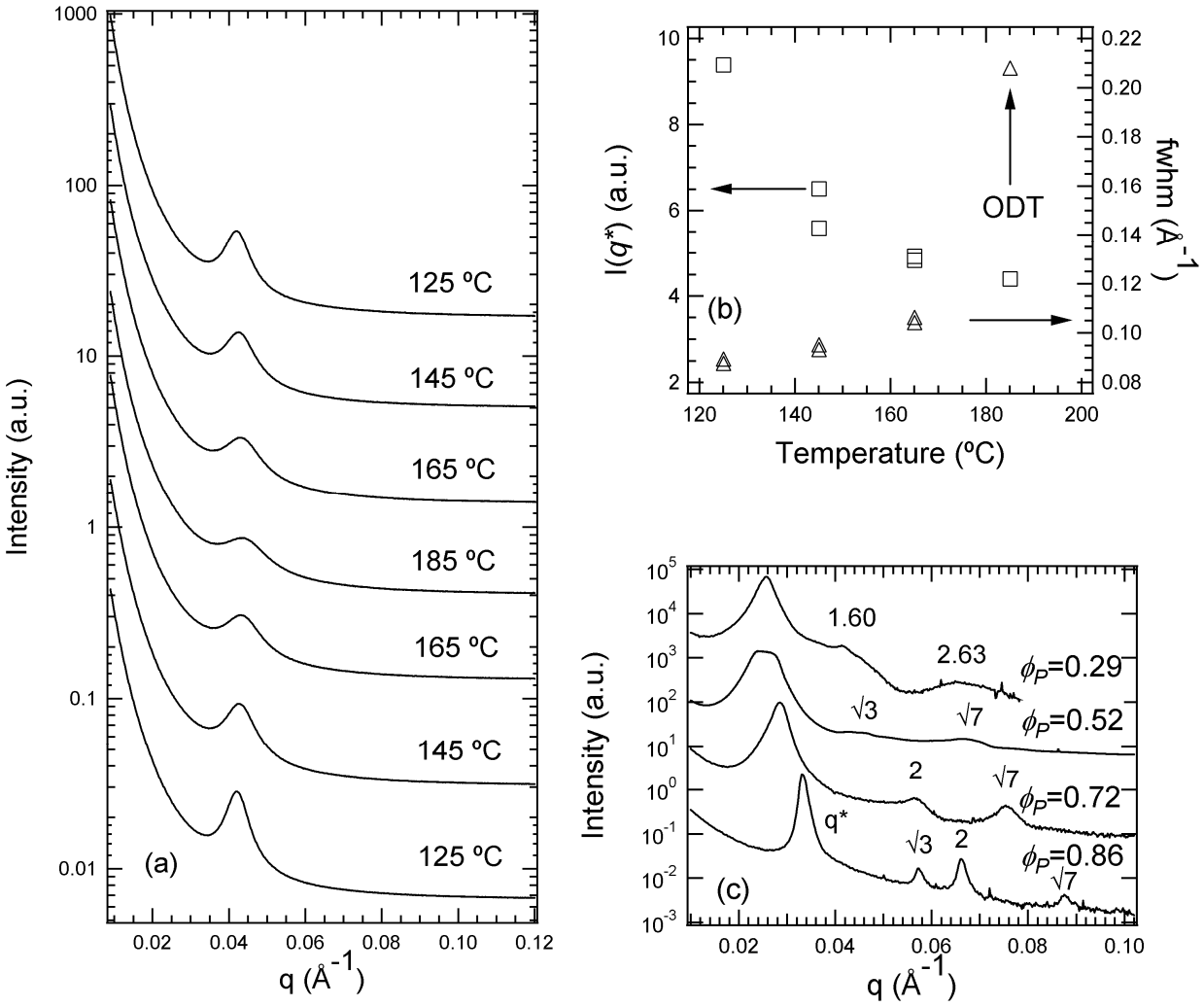


Figure 2.7. Temperature Dependent SAXS Profiles. (a) SAXS profiles (offset for clarity) of ϕ_P=1.00, PS-*b*-P2VP(4.9-6.6) at varying temperatures. (b) Plot of $I(q^*)$ (□) and fwhm (△) versus temperature (°C) of ϕ_P=1.00, PS-*b*-P2VP(4.9-6.6). The ODT is defined as the point at 185 ± 20 °C and overlapping data points at a given temperature were recorded upon heating and cooling. (c) SAXS profiles (offset for clarity) of PS-*b*-P2VP(4.9-6.6)/[Im][TFSI] mixtures at varying ϕ_P at 225 °C.

2.4. Conclusions

The phase behavior of PS-*b*-P2VP/[Im][TFSI] mixtures for copolymers with a wide range of f_{PS} and N_T was studied using SAXS, SANS, and DSC. The observed dependence of the P2VP/[Im][TFSI] phase T_g on IL:2VP was found to be independent of f_{PS} and N_T of the copolymer and cannot be predicted by standard theories for the thermal properties of polymer/molecular solvent mixtures. SAXS and SANS characterization revealed the existence of lamellar, cylindrical, ordered micellar, and disordered micellar phases, in agreement with studies of block copolymer/selective molecular solvent mixtures. Scaling analysis of the PS-*b*-P2VP/[Im][TFSI] mixtures revealed a decrease in the interfacial area occupied by each PS-*b*-P2VP chain upon the addition of ionic liquid, which indicates an increase in segregation strength upon the addition of ionic liquid that is larger than observations of block copolymer/selective molecular solvent mixtures and is due to the enthalpically driven presence of ions in the high dielectric P2VP phase. Across a broad range of IL:2VP ratios, d of the mixtures was found to follow the scaling predicted by SSL theory. An increase in the T_{ODT} of the PS-*b*-P2VP/[Im][TFSI] mixtures compared to the neat copolymer was in qualitative agreement with the scaling analysis.

2.5. Acknowledgements

We gratefully acknowledge support from the Assistant Secretary for Energy Efficiency and Renewable Energy, Office of Hydrogen, Fuel Cell, and Infrastructure Technologies of the U.S. Department of Energy under Contract No. DE-AC02-05CH11231. The authors thank Dr. John Kerr for useful discussions. SAXS experiments were performed at the Advanced Light Source and the Stanford Synchrotron Radiation Laboratory and SANS experiments were conducted at Oak Ridge National Laboratory's (ORNL) High Flux Isotope Reactor. All three are national user facilities supported by the Department of Energy, Office of Basic Energy Sciences. We gratefully acknowledge Dr. Alexander Hexemer, Dr. Cheng Wang, and Dr. Eric Schaible for experimental assistance at the ALS, Dr. John Pople for experimental assistance at the SSRL, and Alisyn Nedoma, Dr. Yuri Melnichenko and Dr. Gang Cheng for experimental assistance at ORNL.

2.6. Appendix: Supporting DSC, SAXS, and SANS

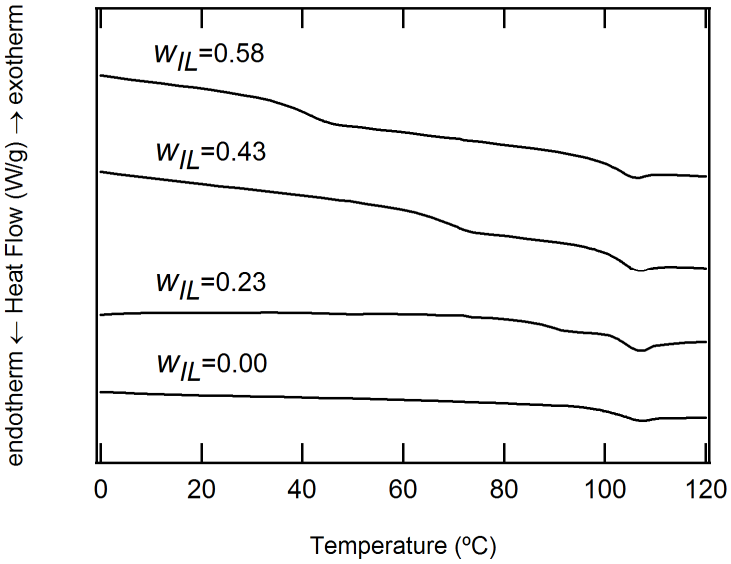


Figure 2.A.1. DSC Heating Scans of PS-*b*-P2VP/[Im][TFSI] Mixtures. DSC heating scans of mixtures of PS-*b*-P2VP(28.5-10.7) and [Im][TFSI] with varying w_{IL}.

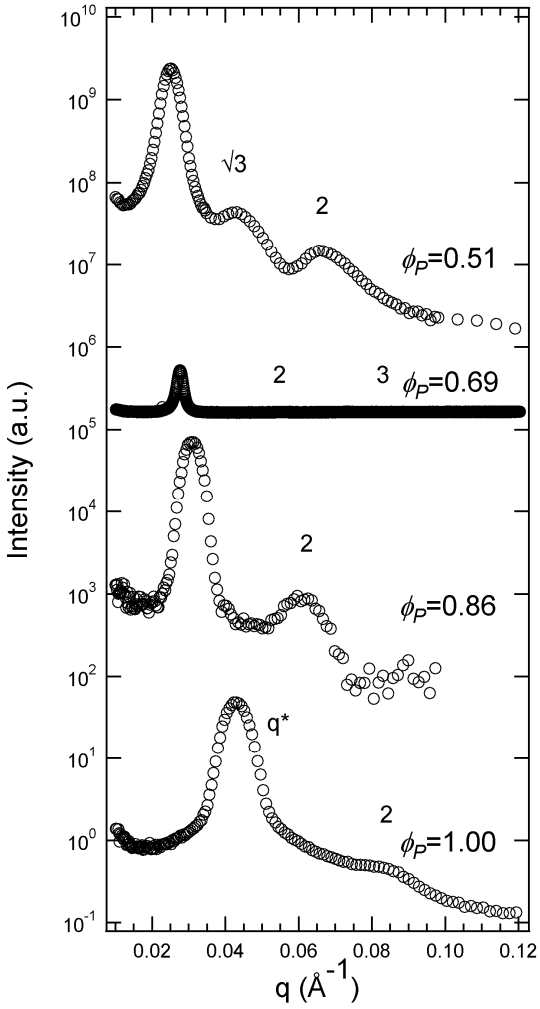


Figure 2.A.2. SANS Profiles of PS-*b*-P2VP/[Im][TFSI] Mixtures. SANS profiles of varying ϕ_P of *d* PS-*b*-P2VP(7.1-6.8) at 30 ºC (a member of the fixed N_T PS-*b*-P2VP series). The peak labels correspond to the q/q^* for scattering peaks.

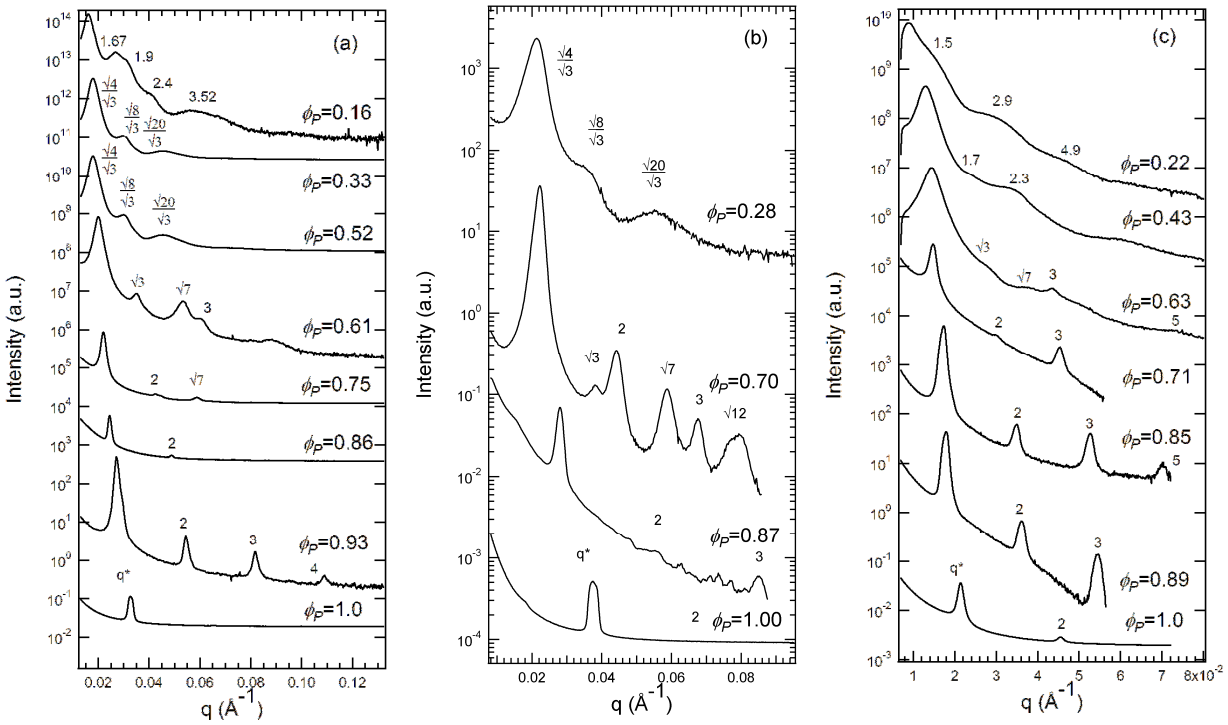


Figure 2.A.3. SAXS Profiles of Mixtures with Fixed N_{P2VP}. SAXS profiles of varying ϕ_P with block copolymers of fixed N_{P2VP} at 145 °C of (a) PS-*b*-P2VP(8.7-12.0), (b) PS-*b*-P2VP(12.0-12.4), and (c) PS-*b*-P2VP(18.4-11.4). In all cases, the peak labels correspond to the q/q^* for scattering peaks.

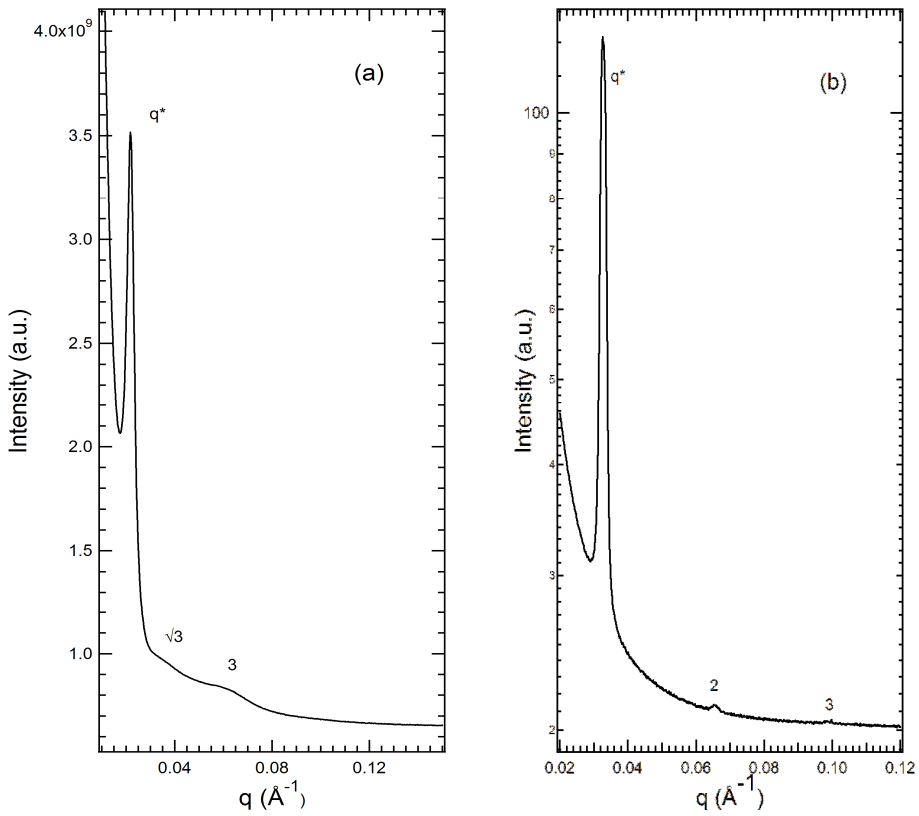


Figure 2.A.4. Expanded SAXS Profiles. Expanded SAXS profiles at 145 ºC for a) PS-*b*-P2VP(28.5-10.7) and b) PS-*b*-P2VP(8.7-12.0).

2.7. References

1. Wasserchеid, P.; Welton, T., *Ionic Liquids in Synthesis*. WILEY-VCH Verlag: Weinheim, 2003.
2. Noda, A.; Susan, M. A. B. H.; Kudo, K.; Mitsushima, S.; Hayamizu, K.; Watanabe, M. *J. Phys. Chem. B* **2003,** 107, (17), 4024-4033.
3. Doyle, M.; Choi, S. K.; Proulx, G. *Journal of the Electrochemical Society* **2000,** 147, (1), 34-37.
4. Fernicola, A.; Panero, S.; Scrosati, B.; Tamada, M.; Ohno, H. *Chemphyschem* **2007,** 8, (7), 1103-1107.
5. Matsuoka, H.; Nakamoto, H.; Susan, M. A. B. H.; Watanabe, M. *Electrochimica Acta* **2005,** 50, (19), 4015-4021.
6. Sekhon, S. S.; Lalia, B. S.; Park, J. S.; Kim, C. S.; Yamada, K. *Journal of Materials Chemistry* **2006,** 16, (23), 2256-2265.
7. Cho, J. H.; Lee, J.; Xia, Y.; Kim, B.; He, Y. Y.; Renn, M. J.; Lodge, T. P.; Frisbie, C. D. *Nature Materials* **2008,** 7, (11), 900-906.
8. Lee, J.; Panzer, M. J.; He, Y. Y.; Lodge, T. P.; Frisbie, C. D. *Journal of the American Chemical Society* **2007,** 129, (15), 4532-+.
9. Kim, G. T.; Appetecchi, G. B.; Alessandrini, F.; Passerini, S. *Journal of Power Sources* **2007,** 171, (2), 861-869.
10. Sakaebe, H.; Matsumoto, H. *Electrochemistry Communications* **2003,** 5, (7), 594-598.
11. Simone, P. M.; Lodge, T. P. *Macromolecules* **2008,** 41, 1753-1759.
12. Virgili, J. M.; Hexemer, A.; Pople, J. A.; Balsara, N. P.; Segalman, R. A. *Macromolecules* **2009,** 42, (13), 4604-4613.
13. Hanley, K. J.; Lodge, T. P. *Journal of Polymer Science Part B-Polymer Physics* **1998,** 36, (17), 3101-3113.
14. Hanley, K. J.; Lodge, T. P.; Huang, C.-I. *Macromolecules* **2000,** 33, (16), 5918-5931.
15. Huang, C. I.; Hsueh, H. Y. *Polymer* **2006,** 47, (19), 6843-6856.
16. Huang, C.-I.; Lodge, T. P. *Macromolecules* **1998,** 31, (11), 3556-3565.
17. Lai, C.; Russel, W. B.; Register, R. A. *Macromolecules* **2002,** 35, (10), 4044-4049.
18. Lai, C.; Russel, W. B.; Register, R. A. *Macromolecules* **2002,** 35, (3), 841-849.
19. Ruzette, A. V. G.; Soo, P. P.; Sadoway, D. R.; Mayes, A. M. *Journal of the Electrochemical Society* **2001,** 148, (6), A537-A543.
20. Epps, T. H.; Bailey, T. S.; Pham, H. D.; Bates, F. S. *Chemistry of Materials* **2002,** 14, (4), 1706-1714.
21. Lee, D. H.; Kim, H. Y.; Kim, J. K.; Huh, J.; Ryu, D. Y. *Macromolecules* **2006,** 39, (6), 2027-2030.
22. Wang, J.-Y.; Chen, W.; Russell, T. P. *Macromolecules* **2008,** 41, (13), 4904-4907.
23. Wang, Z. G. *Journal of Physical Chemistry B* **2008,** 112, (50), 16205-16213.
24. He, Y. Y.; Li, Z. B.; Simone, P.; Lodge, T. P. *Journal of the American Chemical Society* **2006,** 128, (8), 2745-2750.
25. Yokoyama, H.; Mates, T. E.; Kramer, E. J. *Macromolecules* **2000,** 33, (5), 1888-1898.

26. Virgili, J. M.; Nedoma, A. J.; Melnichenko, Y. B.; Cheng, G.; Balsara, N. P.; Segalman, R. A. *Abstracts of Papers of the American Chemical Society* **2009**, In-press.
27. Wignall, G. D.; Bates, F. S. *Journal of Applied Crystallography* **1987,** 20, 28-40.
28. Lodge, T. P.; Hamersky, M. W.; Hanley, K. J.; Huang, C. I. *Macromolecules* **1997,** 30, (20), 6139-6149.
29. Gordon, M.; Taylor, J. S. *Journal of Applied Chemistry* **1952,** 2, (9), 493-500.
30. Fox, T. G. *Bull. Am. Phys. Soc.* **1956,** 1, 123.
31. Susan, M. A.; Kaneko, T.; Noda, A.; Watanabe, M. *Journal of the American Chemical Society* **2005,** 127, (13), 4976-4983.
32. Mcconnell, G. A.; Gast, A. P.; Huang, J. S.; Smith, S. D. *Physical Review Letters* **1993,** 71, (13), 2102-2105.
33. Laughlin, R. G., *The Aqueous Phase Behavior of Surfactants*. Academic Press: San Diego, 1994.
34. Meli, L.; Lodge, T. P. *Macromolecules* **2009,** 42, (3), 580-583.
35. Cavicchi, K. A.; Lodge, T. P. *Journal of Polymer Science Part B-Polymer Physics* **2003,** 41, (7), 715-724.
36. McConnell, G. A.; Gast, A. P. *Macromolecules* **1997,** 30, (3), 435-444.
37. Halperin, A.; Tirrell, M.; Lodge, T. P. *Advances in Polymer Science* **1992,** 100, 31-71.
38. Zhang, L. F.; Eisenberg, A. *Polymers for Advanced Technologies* **1998,** 9, (10-11), 677-699.
39. Cochran, E. W.; Garcia-Cervera, C. J.; Fredrickson, G. H. *Macromolecules* **2006,** 39, (7), 2449-2451.
40. Schulz, M. F.; Khandpur, A. K.; Bates, F. S.; Almdal, K.; Mortensen, K.; Hajduk, D. A.; Gruner, S. M. *Macromolecules* **1996,** 29, (8), 2857-2867.
41. Shibayama, M.; Hashimoto, T.; Kawai, H. *Macromolecules* **1983,** 16, (1), 16-28.
42. Hajduk, D. A.; Kossuth, M. B.; Hillmyer, M. A.; Bates, F. S. *The Journal of Physical Chemistry B* **1998,** 102, (22), 4269-4276.
43. Semenov, A. N. *Macromolecules* **1989,** 22, (6), 2849-2851.
44. Lipic, P. M.; Bates, F. S.; Matsen, M. W. *Journal of Polymer Science Part B-Polymer Physics* **1999,** 37, (16), 2229-2238.
45. Whitmore, M. D.; Vavasour, J. D. *Acta Polymerica* **1995,** 46, (5), 341-360.
46. Almdal, K.; Rosedale, J. H.; Bates, F. S.; Wignall, G. D.; Fredrickson, G. H. *Physical Review Letters* **1990,** 65, (9), 1112-1115.

Chapter 3. Ionic Conductivity of Nanostroctured Block Copolymer/Ionic Liquid Membranes

Reproduced with permission from Megan L. Hoarfrost and Rachel A. Segalman, Macromolecules, 2011, 44(13), pp. 5281-5288. 2011 American Chemical Society

Nanostructured mixtures of ionic liquids and polymers are of great interest for a wide variety of electrochemical applications. Understanding the relationship between composition, structure, and ionic conductivity for these mixtures is essential for designing new materials. In this work, the effect of nanostructure on ionic conductivity, σ, is investigated for model mixtures of diblock copolymers and ionic liquids that are selective for one of the polymer microphases. It is demonstrated that the concentration dependence of σ is a function of the total volume fraction of ionic liquid, and described well by percolation theory. This scaling behavior encourages the design of membranes where the amount of a mechanical component in the block copolymer can be increased to improve the strength of the membrane without sacrificing conductivity. The temperature dependence of σ is a function of the amount of ionic liquid exclusively in the conducting domain. Comparing σ for mixtures of the diblock copolymer poly(styrene-*b*-2-vinylpyridine) (PS-*b*-P2VP) and two different ionic liquids, imidazolium bis(trifluoromethylsulfonyl)imide ([Im][TFSI]) and 1-ethyl-3-methylimidazolium bis(trifluoromethylsulfonyl)imide ([EMIm][TFSI]), reveals that the chemistry of the polymer/ionic liquid pair affects both the activation energy for σ and the maximum attainable σ, but does not affect how σ scales with ionic liquid concentration. The effect of the morphology on σ is also examined, and it is found that as long as the conducting phase morphology is isotropic and well-connected, σ is not affected by morphology.

3.1. Introduction

Ionic liquids, which are salts with low melting temperatures, or equivalently, solvents composed completely of ions, have unique properties including low vapor pressure, high thermal, chemical, and electrochemical stability, and high ionic conductivity.[1] This exceptional combination of properties makes them of significant interest for a variety of electrochemical applications.[2] Combining ionic liquids with polymers is of further interest as the polymer may be designed to impart mechanical strength to the resulting membrane and template the ionic liquid into ion-conducting nanochannels. This can be achieved, for example, by selectively incorporating an ionic liquid into one phase of a diblock copolymer.[3, 4]

When properly designed, nanostructured membranes feature continuous ion-conducting channels, which can lead to enhanced conductivity. Nafion (DuPont), the industry standard material for proton exchange membrane (PEM) fuel cell membranes, is characterized by nanoscale phase-separation into conducting hydrophilic domains and structural hydrophobic domains, which contributes to exceptional conductivity coupled with favorable mechanical properties.[5] Model materials with continuous ordered nanostructures have also been shown to have significantly higher conductivities than comparable non-ordered materials.[6, 7] Understanding the effect of morphology on

conductivity has become increasingly important in recent years as a tool for designing new, improved membranes.[8-12] Using a block copolymer to template the morphology provides an advantage because it affords precise control over the volume fractions of the conducting and structural phases, and the size and shape of the domains.

In dilute electrolyte solutions, ionic conductivity, σ, is simply proportional to the number of ions and the diffusion coefficients of the ionic moieties (Nernst-Einstein equation). In concentrated mixtures of ionic liquids and compatible, neutral homopolymers, it is expected that σ does not scale linearly with the number of ions due to the effect of tortuosity and the need to be above a concentration threshold to form a percolated ionic liquid network. Also, the diffusion coefficients are greatly dependent on how far the temperature is above the glass transition temperature of the mixture, T_g,[13-15] where the T_g is actually a function of the ionic liquid concentration.[16-18] Because the T_g typically decreases with increasing ionic liquid concentration,[16-18] and the number of ions simultaneously increases, the result is a monotonic increase in σ with increasing ionic liquid concentration.[18, 19] This is also the case in nanostructured block copolymer membranes,[20, 21] although ion concentration and T_g are not so intimately coupled. This is because the T_g is determined by the ionic liquid content exclusively in the conducting phase,[22] while the ion concentration depends on the total amount of ionic liquid in the membrane. In this work, the scaling of σ with temperature and composition is decoupled by varying the volume fraction of the structural component in the block copolymer as well as the ionic liquid content. Understanding in detail how conductivity depends on concentration and temperature will provide knowledge about important design parameters for highly conductive polymer/ionic liquid membranes.

Conductivity scaling behavior has been investigated for other types of nanostructured, ion-conducting, polymeric materials, but they are fundamentally different from the block copolymer/ionic liquid membranes. At first, lithium bis(trifluoromethylsulfonyl)imide (LiTFSI) salts in poly(ethylene oxide) (PEO)-based polymer electrolytes appear similar to ionic liquids that contain TFSI as the anion. However, in these systems, Li^+ ions are conducted by movement between oxygen atoms, making the polymer intimately involved in the conductivity mechanism.[23] Furthermore, the addition of LiTFSI salts tends to increase the polymer's T_g, leading to a maximum in conductivity with respect to salt concentration due to the competition between the increase in ion concentration and the concomitant increase in T_g upon the addition of salt.[24] Both hydrated and ionic liquid-containing[25-27] versions of sulfonated polyelectrolytes, like Nafion, are fundamentally different from polymer/ionic liquid membranes due to the presence of sulfonic acid sites, which donate conductive protons. In such materials, protons are conducted via protonation/deprotonation reactions. At high hydration levels, the conductivity of sulfonated polyelectrolytes scales with the percent conducting volume, while at lower hydration levels, the conductivity is a more complicated function of sulfonation level, humidity, and morphology.[9]

In this work, using a model block copolymer/ionic liquid system, we demonstrate that while the temperature dependence of σ is a function of the amount of ionic liquid exclusively in the conducting domain, the concentration dependence of σ is a function of

the total volume fraction of ionic liquid. By comparing σ for mixtures of the diblock copolymer poly(styrene-*b*-2-vinyl pyridine) (PS-*b*-P2VP) and two different ionic liquids, imidazolium bis(trifluoromethylsulfonyl)imide ([Im][TFSI]) and 1-ethyl-3-methylimidazolium bis(trifluoromethylsulfonyl)imide ([EMIm][TFSI]), the universality of this scaling behavior is demonstrated. The effect of morphology on σ is also discussed, and it is shown that morphology does not strongly influence σ, as long as the conducting phase morphology is isotropic and well-connected.

3.2. Experimental Section

Polymer Synthesis and Characterization. PS-*b*-P2VP copolymers and poly(2-vinyl pyridine) (P2VP) homopolymer were synthesized via anionic polymerization as previously described.[28] The molecular weight of the polystyrene (PS) block was determined using gel permeation chromatography (GPC) and the total molecular weight of the block copolymer was determined via ^{1}H NMR (Bruker AVB-300). The molecular weight of the P2VP homopolymer was determined using ^{1}H NMR end-group analysis. GPC was used to assess the polydispersity of the polymers. The volume fraction of the PS block, f_{PS}, degree of polymerization of the P2VP block, N_{P2VP}, total molecular weight, MW, and polydispersity index, PDI, of the polymers are provided in Table 3.1. The structure of the PS-*b*-P2VP copolymer is shown in Figure 3.1.

Ionic Liquid Purification and Preparation. Imidazole (≥95%) and bis(trifluoromethylsulfonyl)imide (HTFSI, ≥95%) were purchased from Sigma Aldrich and purified by sublimation. Differential scanning calorimetry (DSC) and ^{1}H NMR were used to assess the purity of the two starting materials. The melting points of imidazole and HTFSI were compared to literature values of 89 and 55 °C, respectively.[29] To prepare the ionic liquid [Im][TFSI], purified imidazole and HTFSI were combined in equimolar quantities in an argon atmosphere glove box, sealed, heated in an oven outside the glove box at 100 ^{o}C for 2 to 3 hours, and then transferred back to the glove box. The composition of the ionic liquid was confirmed by comparing the measured melting point of the compound with the literature value of 73 ºC.[29] The ionic liquid [EMIm][TFSI] was purchased from EMD Chemicals, Inc. and purified by heating at 100 ºC under vacuum (P≈200 mTorr) for 3 days before it was transferred to an argon atmosphere glove box. Care was taken to limit air and water exposure of the hydroscopic ionic liquids at all times by handling the materials in an argon atmosphere glove box and sealed sample holders. The structures of the ionic liquid ions are shown in Figure 3.1.

Preparation of Polymer/Ionic Liquid Mixtures. Dichloromethane and tetrahydrofuran were degassed using three freeze-pump-thaw cycles, dried by stirring over CaH_2 overnight, then distilled under vacuum, brought into an argon atmosphere glove box, and stored on molecular sieves. All further sample preparation was performed in an argon atmosphere glove box. Specific quantities of [Im][TFSI] or [EMIm][TFSI] and PS-*b*-P2VP or P2VP were weighed into glass vials and were dissolved overnight in dichloromethane (PS-*b*-P2VP mixtures) or tetrahydrofuran (P2VP mixtures) to produce ca. 5 wt% solutions. Samples were cast one drop at a time into sample holders for DSC, small angle X-ray scattering (SAXS), and AC impedance spectroscopy. Samples were

then heated above the boiling point of the solvent (65 and 70 ºC for samples cast from dichloromethane and tetrahydrofuran, respectively) for ca. 18 hours to remove any remaining solvent. Complete solvent removal was confirmed by ^{1}H NMR analysis and the achievement of constant sample mass. Samples were sealed in jars containing desiccant in the glove box for transportation to experimental apparatuses.

Differential Scanning Calorimetry (DSC). DSC samples were crimped in an argon atmosphere glove box using hermetically sealed pans and placed inside a container with desiccant for transfer to the DSC. DSC was performed on a TA Instruments DSC Q20. Indium and dodecane were used as calibration standards. Samples underwent three heating and cooling cycles between -40 and 150 ºC, scanning at 10 ºC per minute, and T_g values recorded upon the second heating scan were reported.

Morphology Characterization. Mixture morphologies were determined using SAXS. Samples were cast in an argon atmosphere glove box into sample cells formed by an aluminum spacer sealed onto a Kapton window on one side until ca. 1 mm solid samples were obtained. After heating to remove solvent, a second Kapton window was glued to seal the samples, and the samples were stored in jars containing desiccant for transportation to the beamline. SAXS was performed on beamline 7.3.3 of the Advanced Light Source (ALS) and beamline 1-4 of the Stanford Synchrotron Radiation Lightsource (SSRL). At the ALS, the beamline was configured with an X-ray wavelength of λ=1.240 Å and focused to a 50 by 300 µm spot. Samples were annealed and equilibrated at 145 ºC for 20 to 30 minutes prior to data acquisition. Full two-dimensional scattering patterns were collected on an ADSC CCD detector with an active area of 188 by 188 mm. The scattering patterns, which reflected isotropic structures in all cases, were radially averaged and the scattering intensity was corrected with the post-ion chamber intensity using Nika version 1.18. At the SSRL, the beamline was configured with an X-ray wavelength λ=1.488 Å and focused to a 0.5 mm diameter spot. A single quadrant of a two-dimensional scattering pattern was collected on a CCD detector with an active area of 25.4 by 25.4 mm. The scattering patterns, which reflected isotropic structures in all cases, were radially averaged and corrected for detector null signal, dark current, and empty cell scattering.

The PS-*b*-P2VP/[Im][TFSI] samples in this study exhibit a variety of morphologies, including lamellae (LAM), hexagonally close-packed (HCP) PS cylinders (C_{PS}), body-centered cubic (BCC) PS spheres ($S_{PS,BCC}$), face-centered cubic (FCC) PS spheres ($S_{PS,BCC}$), and disordered PS micelles (DM), as determined by analysis of SAXS profiles reported in reference 22. For each copolymer, the morphologies are provided in Table 3.1 as a function of the total volume fraction of [Im][TFSI] in the mixtures, $\phi_{[Im][TFSI]}$. The PS-*b*-P2VP /[EMIm][TFSI] samples in this study have LAM and C_{PS} morphologies, as determined from analysis of SAXS measurements. Representative SAXS profiles for mixtures of PS-*b*-P2VP and [EMIm][TFSI] are plotted in Figures 3.A.1 and 3.A.2 in the Appendix, and the morphologies are provided as a function of $\phi_{[EMIm][TFSI]}$ in Table 3.1.

Selectivity of Ionic Liquids for P2VP. It has been previously shown that [Im][TFSI] is very selective for the P2VP phase of PS-*b*-P2VP copolymers,[22, 30] and the same is true of

Table 3.1. Polymer Compositions and Morphologies of Block Copolymer/Ionic Liquid Mixtures.

Polymers with similar N_{P2VP}								
Polymer	f_{PS}	N_{P2VP}	Total MW (kg/mol)	PDI	$\phi_{[Im][TFSI]}$	Morphology	$\phi_{[EMIm][TFSI]}$	Morphology
P2VP	0.00	118	12.4	1.07	0.00≤0.61	-	0.00≤0.33	-
PS-*b*-P2VP	0.29	102	15.2	1.07	0.00≤0.52	C_{PS}	0.44	C_{PS}
					0.58≤0.71	$S_{PS,BCC}$		
PS-*b*-P2VP	0.42	115	20.8	1.02	0.00≤0.17	LAM	0.00≤0.08	LAM
					0.21≤0.39	C_{PS}		
					0.48≤0.67	$S_{PS,FCC}$	0.14≤0.39	C_{PS}
					0.84	DM		
PS-*b*-P2VP	0.62	108	29.8	1.10	0.00≤0.29	LAM	-	-
					0.37	C_{PS}		
					0.58≤0.78	DM		
PS-*b*-P2VP	0.72	101	39.2	1.04	0.05≤0.21	LAM	-	-
					0.30≤0.72	DM		
Polymers with similar f_{PS}								
Polymer	f_{PS}	N_{P2VP}	Total MW (kg/mol)	PDI	$\phi_{[Im][TFSI]}$	Morphology	$\phi_{[EMIm][TFSI]}$	Morphology
PS-*b*-P2VP	0.62	108	29.8	1.10	0.00≤0.29	LAM	-	-
					0.37	C_{PS}		
					0.58≤0.78	DM		
PS-*b*-P2VP	0.62	221	61.7	1.10	0.26	LAM	-	-
PS-*b*-P2VP	0.59	296	75.8	1.10	0.27	LAM	-	-
PS-*b*-P2VP	0.65	451	135.0	1.19	0.24	LAM	-	-

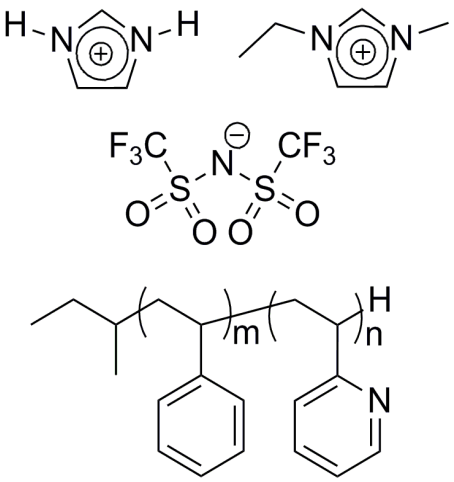


Figure 3.1. Chemical Structures of [Im][TFSI], [EMIm][TFSI], and PS-*b*-P2VP.

[EMIm][TFSI]. This is reflected in the thermal properties of the mixtures. As shown in Figure 3.2, upon the addition of [Im][TFSI] and [EMIm][TFSI] to PS-*b*-P2VP copolymers, the T_g of the ionic liquid-containing P2VP phase, $T_{g,P2VP+IL}$, decreases from that of neat P2VP. $T_{g,P2VP+IL}$ collapses for all copolymers as a function of the weight fraction of ionic liquid exclusively in the P2VP phase, w_{IL}, as shown in Figure 3.3. The T_g of the PS domain, however, remains in the vicinity of 100 ºC with increasing w_{IL} as expected because the ionic liquid selectively enters the P2VP domain. The degree of selectivity of the ionic liquids for the P2VP phase is quantified and found to be very high based on the scaling behavior of the domain spacing of self-assembled microdomains, *d*, with volume fraction polymer, ϕ_P. In Figure 3.4, *d* is plotted as a function of ϕ_P for lamellar PS-*b*-P2VP(f_{PS}=0.72)/[Im][TFSI] and PS-*b*-P2VP(f_{PS}=0.42)/[EMIm][TFSI] mixtures. *d* was calculated as $2\pi/q^*$ where q* is the primary scattering peak from SAXS data. Power law fits through each set of data, $d \sim \phi_P^{\alpha}$, result in α=-1.9 and -1.5 for PS-*b*-P2VP/[Im][TFSI] and PS-*b*-P2VP/[EMIm][TFSI], respectively. Values of $\alpha<0$ (*d* increases upon the addition of ionic liquid) indicate that [Im][TFSI] and [EMIm][TFSI] are both selective for one block of the copolymer.[32] Values of -1.9 and -1.5 for α are both very negative compared to values observed for typical block copolymer/selective molecular solvent mixtures,[22] indicating that [Im][TFSI] and [EMIm][TFSI] are both strongly selective for P2VP. Because of the strong selectivity of the systems, PS-*b*-P2VP/[Im][TFSI] and PS-*b*-P2VP/[EMIm][TFSI] are good model systems for studying block copolymer/ionic liquid mixtures. In addition, the strong selectivities substantiate the simplifying assumption that all ionic liquid enters the P2VP phase of PS-*b*-P2VP copolymers. Samples are designated by w_{IL} as well as the total volume fraction of ionic liquid, ϕ_{IL}, which is calculated by assuming ideal mixing and using densities of 1.67 g/cm^3 for [Im][TFSI], estimated from scattering length density fits of small angle neutron scattering intensity profiles,[30] 1.52 g/cm^3 for [EMIm][TFSI],[33] and 1.05 g/cm^3 for both PS and P2VP.

Ionic Conductivity Measurements. Ionic conductivity was measured using AC impedance spectroscopy. In an argon atmosphere glove box, samples were cast onto stainless steel blocking electrodes. After heating to remove remaining solvent, two sample-coated electrodes were sandwiched together with an annular Kapton spacer placed in between with a thickness of 25μm and an inner diameter of 1.4 cm. The sandwiches were pressed at 105 ºC for one hour in the glove box using a hand press to allow the sample to completely fill the Kapton spacer. The samples were then placed in home-made, air-tight, stainless steel cells with Teflon flanges. The cells were screwed together in the glove box, clamped to maintain constant pressure, and then annealed at 150 ºC for 12 hours in an oven outside the glove box prior to performing measurements. Two-point probe, through-plane AC impedance measurements were performed using a Gamry Reference 600 Potentiostat at descending temperatures. An alternating current signal with an amplitude of 5 mV was applied in the frequency range of 100 to 65,000 Hz. Nyquist plots of the negative imaginary part of the impedance, -*Z*', versus the real part of the impedance, *Z*', were analyzed to find the sample resistance, *R*. Typically, Z' at the minimum in the Nyquist plot (the high x-intercept of the semi-circle portion of the data) was taken as *R*. For highly conductive samples, the semi-circle portion of the data was not observed in the frequency range of the potentiostat, so the x-intercept was taken as *R*.

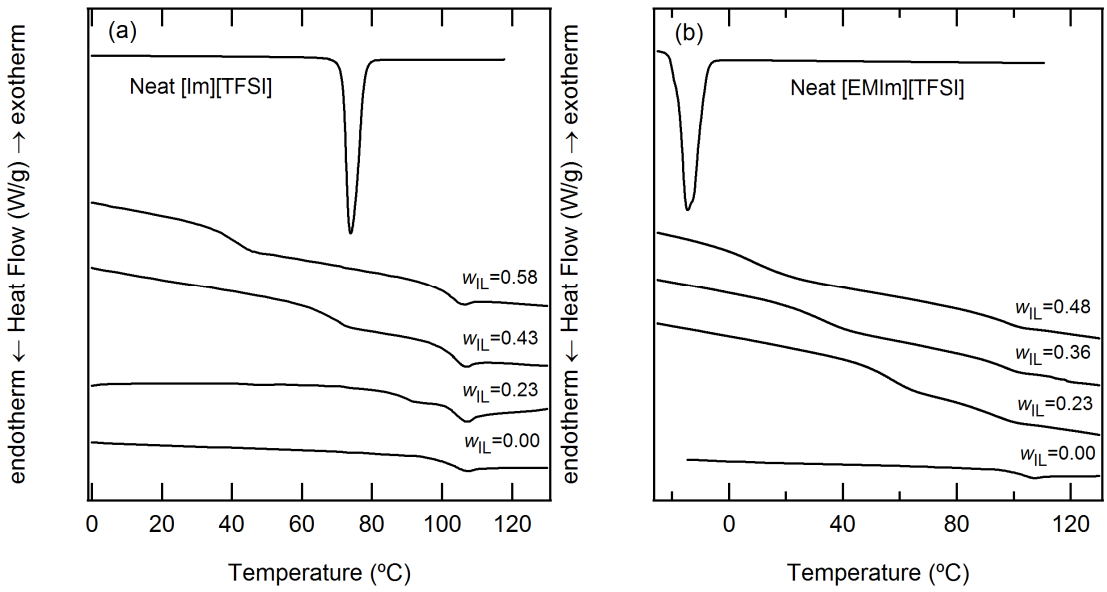


Figure 3.2. DSC Heating Scans of PS-*b*-P2VP/Ionic Liquid Mixtures. Representative DSC heating scans for (a) PS-*b*-P2VP(f_{PS}=0.72)/[Im][TFSI] mixtures and (b) PS-*b*-P2VP(f_{PS}=0.42)/[EMIm][TFSI] mixtures.

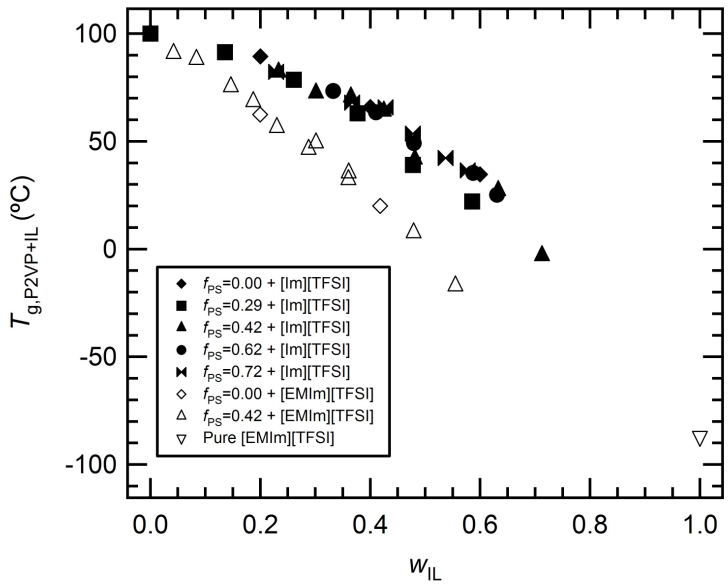


Figure 3.3. Glass Transition Temperatures of P2VP/Ionic Liquid Phases. $T_{g,P2VP+IL}$ as a function of w_{IL} for PS-*b*-P2VP copolymers and P2VP homopolymer mixed with [Im][TFSI] and [EMIm][TFSI]. All T_g values were determined using DSC except for the T_g of [EMIm][TFSI], which is from reference 31.

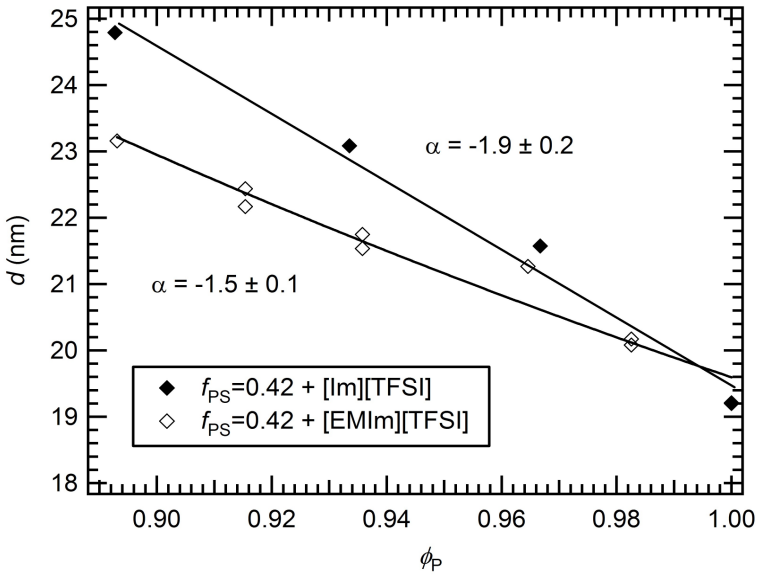


Figure 3.4. Domain Spacing Analysis of PS-*b*-P2VP/Ionic Liquid Mixtures. Lamellar domain spacing, d, determined from SAXS at 145 ºC as a function of ϕ_P for PS-*b*-P2VP(f_{PS}=0.42)/[Im][TFSI] mixtures (solid symbols) and PS-*b*-P2VP(f_{PS}=0.42)/[EMIm][TFSI] mixtures (open symbols). Power law fits, $d \sim \phi_P^{\alpha}$, are used to obtain α, and the errors represent one standard deviation of the fits.

Representative Nyquist plots for each scenario are shown in Figure 3.A.3 in the Appendix. The ionic conductivity, σ, was calculated as t/AR, where t and A are the thickness and area of the sample, respectively, measured after the AC impedance measurements. Specifically, t was determined by measuring the total thickness of the membrane/spacer/electrodes sandwich and subtracting the thicknesses of the electrodes.

Four-point probe measurements in the in-plane direction were performed to confirm that σ was isotropic. For the four-point probe measurements, samples were cast and hot-pressed in the same manner as the samples measured using two-point probe AC impedance, but into a home made, air-tight, poly(ether ether ketone) cell, which contained four stainless steel electrodes and was screwed shut in an argon atmosphere glove box. The working and reference electrodes were 0.7 cm apart and 1.9 cm long, and the samples were cast to be about 0.05 cm thick. The AC impedance spectroscopy parameters were the same as the parameters used for the two-point probe, through-plane measurements, and σ was calculated in the same manner. Values of σ measured using four-point probe measurements were comparable to those measured using two-point probe measurements, confirming isotropic conductivity. Two-point probe measurements are reported.

3.3. Results and Discussion

3.3.1. Ionic Conductivity of PS-*b*-P2VP/[Im][TFSI].

For mixtures of PS-*b*-P2VP block copolymers and [Im][TFSI], σ increases with increasing w_{IL}, and the temperature dependence of σ becomes less steep with increasing w_{IL}, as shown for representative mixtures in Figure 3.5. There are two factors contributing to this behavior: the increase in ion concentration with increasing w_{IL} and the decrease in $T_{g,P2VP+IL}$ with increasing w_{IL}. ($T_{g,P2VP+IL}$ is the important T_g that affects ion mobility since all of the ions reside in and travel through the ionic liquid-containing P2VP phase.) Quantitatively, this translates into an expression for σ with a concentration dependence in terms of the overall volume fraction of ionic liquid, ϕ_{IL}, and a temperature dependence that is in terms of T and w_{IL}. Separation of the temperature and concentration dependencies of σ was accomplished by evaluating σ versus temperature data for mixtures of [Im][TFSI] and PS-*b*-P2VP copolymers (listed in Table 3.1) with similar N_{P2VP} but various f_{PS}. In this manner, ϕ_{IL} and w_{IL} were tuned independently by varying the block copolymer composition (f_{PS}) and ionic liquid content.

The strong influence of the T_g on ionic conductivity is reflected in the Vogel-Tamman-Fulcher (VTF) equation,[34-37]

$$\sigma = A\exp\left(\frac{-B}{R(T-T_0)}\right) \tag{3.1}$$

where A is a fitting parameter that contains the concentration dependence of σ, B contains information about the temperature dependence of σ, and T_0 is the Vogel temperature. While T_0 for polymers has been shown to fluctuate with respect to T_g, a good estimate for T_0 is about 50 K below T_g.[38-40] Assuming T_0=$T_{g,P2VP+IL}$-50 K is a good choice, it is

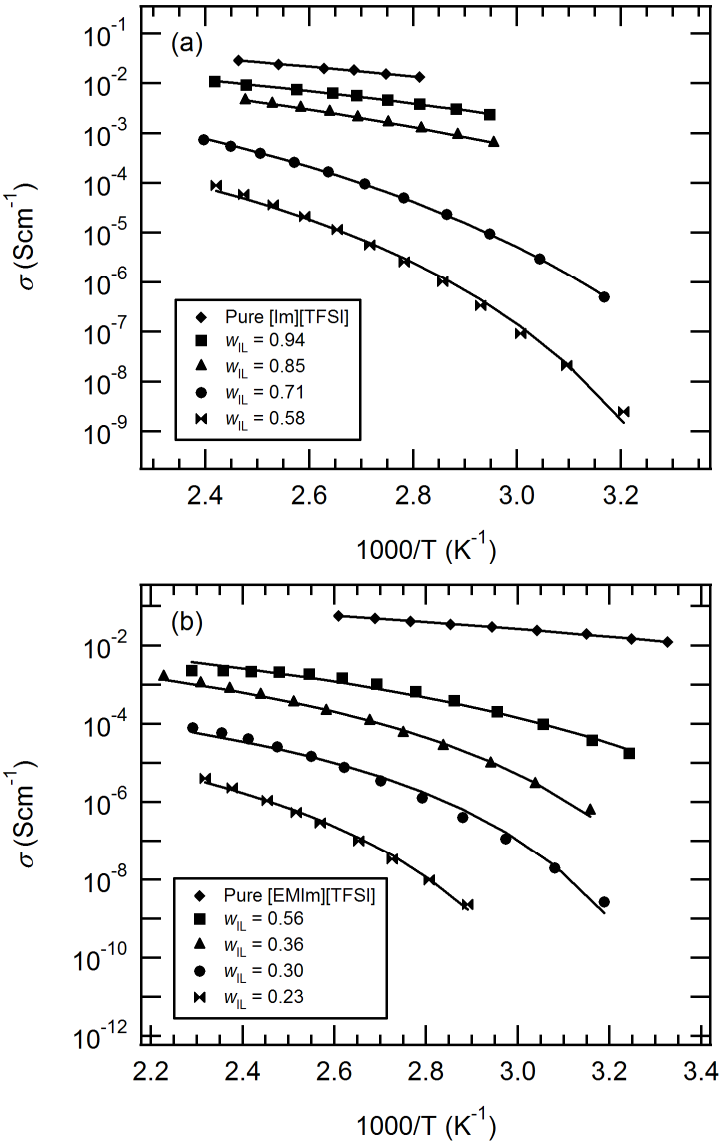


Figure 3.5. Ionic Conductivity of PS-*b*-P2VP/Ionic Liquid Mixtures. Temperature dependence of σ for (a) PS-*b*-P2VP(f_{PS}=0.62, N_{P2VP}=108)/[Im][TFSI] mixtures and (b) PS-*b*-P2VP(f_{PS}=0.42)/[EMIm][TFSI] mixtures with many w_{IL}. The solid lines are VTF fits with *A* and *B* as fitting parameters and T_0=$T_{g,P2VP+IL}$–50 K. The best fit values for *B* are 8.1±1.2 kJ/mol for PS-*b*-P2VP/[ImTFSI] and 6.8±1.2 kJ/mol for PS-*b*-P2VP/[EMIm][TFSI].

expected that one value for B will be obtained for all of the PS-*b*-P2VP/[Im][TFSI] mixtures. As expected, for 24 mixtures of [Im][TFSI] and PS-*b*-P2VP copolymers with different f_{PS} and w_{IL}, the VTF fits (shown in Figure 3.5) result in similar best fits for B: 8.1 kJ/mol with a standard deviation of 1.2 kJ/mol. Therefore, $T_{g,P2VP+IL}$ (which is a function of w_{IL}) is the only factor that determines the temperature dependence of σ for PS-*b*-P2VP/[Im][TFSI] mixtures.

While the temperature dependence of σ is determined by the amount of ionic liquid exclusively in the conducting domain, w_{IL}, the concentration dependence of σ is a function of the *total* volume fraction of ionic liquid in the system, ϕ_{IL}. This is shown in Figure 3.6, where the fitting parameter A from Equation 3.1 collapses as a function of ϕ_{IL} for PS-*b*-P2VP/[Im][TFSI] mixtures containing block copolymers with many different f_{PS} (and thus, w_{IL}) and over a wide range of ϕ_{IL}. In other words, at sufficiently high temperatures, where the dependence of σ on ion concentration is much more important than it is on temperature, similar conductivities are obtained for mixtures containing block copolymers of widely different compositions as long as ϕ_{IL} is kept constant. Figure 3.7 shows that σ is a strong function of ϕ_{IL} even at temperatures as low as 100 ºC. This is an important result to take into account when designing new materials based on mixtures of polymers and ionic liquids, since it means that polymers with high volume fractions of a structural component can be used to impart good mechanical properties without sacrificing ionic conductivity. For example, a lamellar mixture of PS-*b*-P2VP(f_{PS}=0.72) and [Im][TFSI] with ϕ_{IL}=0.20 will have roughly the same ionic conductivity at high temperatures as a mixture of P2VP and [Im][TFSI] with ϕ_{IL}=0.20, even though more than half of the total volume in the block copolymer sample is composed of the structural PS phase. Interestingly, this scaling behavior is similar to that of sulfonated polyelectrolytes at high hydration levels, where conductivity has been shown to collapse as a function of percent conducting volume.[9] At lower temperatures, however, for instance 60 ºC (Figure 3.7), conductivity is a weaker function of ϕ_{IL} due to the stronger effect of $T_{g,P2VP+IL}$.

The fitting parameter A clearly increases nonlinearly with increasing ϕ_{IL}, which is due to the effects of tortuosity and the need to be above a concentration threshold to form a percolated ionic liquid network. The concentration dependence of σ for PS-*b*-P2VP/[Im][TFSI] is modeled well using percolation theory, specifically the power law

$$A = \sigma_0 (\phi_{IL} - \phi_0)^n \tag{3.2}$$

where the prefactor σ_0 depends on the system, ϕ_0 is the percolation threshold volume fraction, and the exponent n is a constant that includes the effect of tortuosity, depends only on the spatial dimensions, and is 1.5 for a 3-D system.[41, 42] For an ideal, continuous, 3-D system, ϕ_0=0.15,[43] but ϕ_0 is easily influenced by the distribution of the conductive phase, as occurs in the case of Nafion, where phase separation causes a percolated hydrophilic network to be formed at low water concentrations (ϕ_0=0.06).[44] For the PS-*b*-P2VP/[Im][TFSI] system, the best fit values for σ_0 and ϕ_0 are 2.0±1.1 S/cm and 0.17±0.02, respectively. The percolation fit is shown in Figure 3.6. Within error, the best fit value for ϕ_0 matches that of the ideal, 3-D system. Thus, self-assembly of PS-*b*-P2VP/[Im][TFSI] mixtures in this study does not lead to a decrease in ϕ_0 compared to the ideal 3-D case as the phase separation of Nafion does. The percolation behavior of A

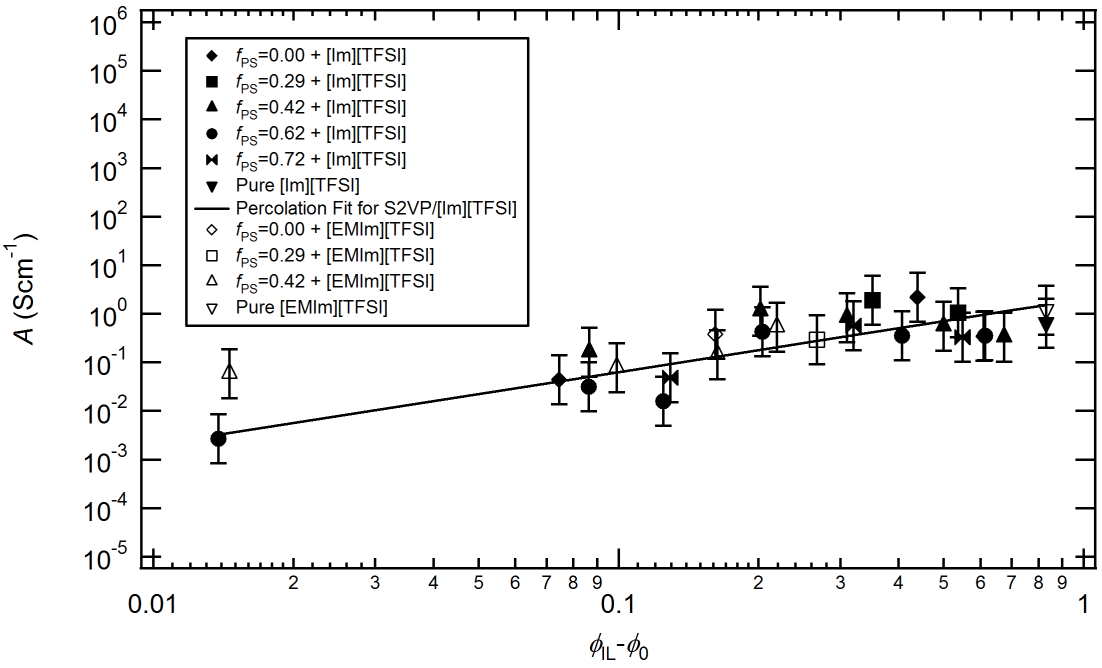


Figure 3.6. Concentration Dependence of Conductivity. *A*, determined by VTF fits with *A* and *B* as fitting parameters and T_0=$T_{g,P2VP+IL}$–50 K, as a function of ϕ_{IL}-ϕ_0 for PS-*b*-P2VP/[Im][TFSI] mixtures (solid symbols) and PS-*b*-P2VP/[EMIm][TFSI] mixtures (open symbols). ϕ_0 is the percolation threshold for conductivity (0.15). The error bars represent reasonable estimates based on the accuracy of AC impedance measurements and data fits. The solid line is the percolation model fit to PS-*b*-P2VP/[Im][TFSI] data with n=1.5, and ϕ_0 and σ_0 as fitting parameters.

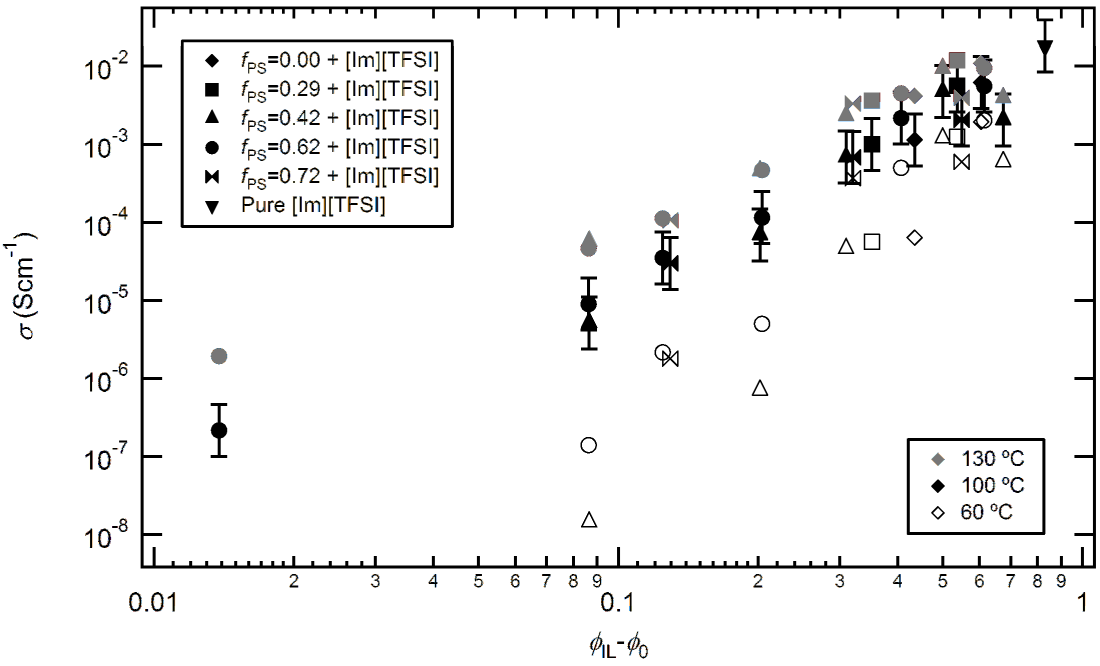


Figure 3.7. Evidence that Conductivity Strongly Depends on ϕ_{IL}. σ versus ϕ_{IL}-ϕ_0 for PS-*b*-P2VP/[Im][TFSI] mixtures at 130 ºC (gray symbols), 100 ºC (solid symbols), and 60 ºC (open symbols). ϕ_0 is the percolation threshold for conductivity. Error bars represent reasonable estimates based on the accuracy of AC impedance measurements, and are shown only for 100 ºC data for clarity.

versus ϕ_{IL} should be taken into account when designing new materials based on polymers and ionic liquids. Because mechanical properties are expected to worsen with increasing ionic liquid concentration, perhaps the nonlinear conductivity dependence on ϕ_{IL} can be exploited in determining an optimal membrane ionic liquid concentration.

Combining the temperature and concentration dependencies of σ for mixtures of PS-*b*-P2VP and [Im][TFSI] results in an equation for the conductivity of any PS-*b*-P2VP/[Im][TFSI] mixture:

$$\sigma = 2.0(\phi_{IL} - 0.17)^{1.5} * \exp\left\{\frac{-8.1}{R\left[T - \left(T_{g,P2VP+IL}(w_{IL}) - 50\right)\right]}\right\} \quad (3.3)$$

The conductivity data for all PS-*b*-P2VP/[Im][TFSI] samples are plotted according to Equation 3.3 in Figure 3.8. While certain parameters in Equation 3.3, for instance σ_0=2.0 S/cm, B=8.1 kJ/mol, and $T_g(w_{IL})$, are specific to the model PS-*b*-P2VP/[Im][TFSI] system, it is expected that the general form of the equation is applicable to other polymer/ionic liquid systems as well.

Morphology does not significantly impact the conductivity of PS-*b*-P2VP/[Im][TFSI] mixtures for a variety of reasons. Phase contrast is high as [Im][TFSI] is strongly selective for the P2VP phase and the system is strongly segregated.[22] Second, there is no preferential alignment of any of the morphologies relative to the electrodes, as indicated by radially symmetric SAXS patterns and similar σ measurements in both in-plane and through-plane directions. Finally, the wide variety of morphologies demonstrated by the mixtures, including lamellae, HCP PS cylinders, BCC and FCC PS spheres, and DM, can all be characterized as having conducting phase continuity, assuming the P2VP/ionic liquid domains in the lamellar samples are well-connected. Scatter in the data for σ is unrelated to the morphology exhibited, as clearly demonstrated in Figure 3.A.4 in the Appendix. Conductivity, then, is unaffected by morphology as long as the conducting phase is well-connected throughout the membrane, and the nanostructure is strongly segregated and isotropic. It is likely that if any of these conditions were not met, σ would not be described by Equation 3.3.[6-9, 45, 46]

The PS-*b*-P2VP/[Im][TFSI] mixtures discussed thus far have only included mixtures with copolymers having N_{P2VP}=113±12. It is expected that conductivity will be independent of P2VP molecular weight as long as it is high enough that $T_{g,P2VP}$ is independent of molecular weight.[13-15] Indeed, for mixtures containing PS-*b*-P2VP with similar f_{PS} (0.62±0.03) and various N_{P2VP} ($108 \leq N_{P2VP} \leq 451$), molecular weight does not affect σ, as shown in Figure 3.9.

3.3.2. Universality of Ionic Conductivity of Block Copolymer/Ionic Liquid Mixtures.

The universality of the conductivity behavior of block copolymer/ionic liquid mixtures has been investigated by comparing σ of PS-*b*-P2VP/[Im][TFSI] to that of mixtures of PS-*b*-P2VP and a second ionic liquid, [EMIm][TFSI]. Changing the base in the ionic liquid from imidazolium to 1-ethyl-3-methylimidazolium results in changes in the

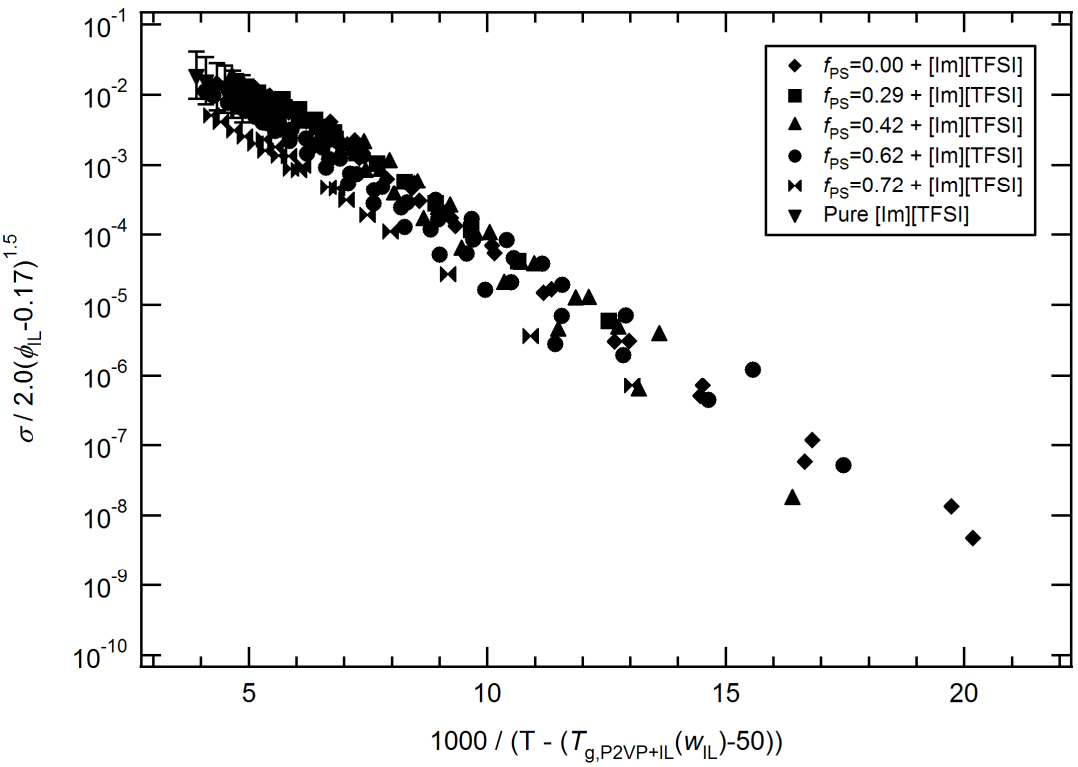


Figure 3.8. Master Conductivity Curve. Conductivity data for all PS-*b*-P2VP/[Im][TFSI] samples, plotted according to Equation 3.3. For graphical clarity, the error bars are shown only for pure [Im][TFSI]. They represent a reasonable estimate based on the accuracy of AC impedance measurements and can be extended to all data points.

temperature dependence of σ and the maximum conductivity of the mixtures, but does not change the overall scaling relationships between σ, ϕ_{IL}, w_{IL}, and T. Consequently, the chemistry of mixtures of block copolymers and ionic liquids can be tuned to improve ionic conductivity while still taking advantage of design parameters universal to all chemistries.

Equation 3.1, which was used to model σ of PS-*b*-P2VP/[Im][TFSI] mixtures, also describes the PS-*b*-P2VP/[EMIm][TFSI] data well (Figure 3.5). Furthermore, B collapses for all of the PS-*b*-P2VP/[EMIm][TFSI] mixtures with T_0=$T_{g,P2VP+IL}$-50 K, just like in the PS-*b*-P2VP/[Im][TFSI] system, confirming the generality of the conclusion that the temperature dependence of σ is only a function of the T_g of the conducting phase in block copolymer/ionic liquid mixtures (within mixtures of a given chemistry). The relationship between $T_{g,P2VP}$ and w_{IL}, though, is different for the two systems. As shown in Figure 3.3, while $T_{g,P2VP}$ collapses as a function of w_{IL} for each type of mixture, $T_{g,P2VP}$ decreases more rapidly with w_{IL} for PS-*b*-P2VP/[EMIm][TFSI] mixtures compared to PS-*b*-P2VP/[Im][TFSI] mixtures. Also, the chemistry of the system affects the value of B. The best fit value of B for PS-*b*-P2VP/[EMIm][TFSI] is 6.8 kJ/mol with a standard deviation of 1.0 kJ/mol compared to 8.1 kJ/mol with a standard deviation of 1.2 kJ/mol for PS-*b*-P2VP/[Im][TFSI]. One likely contributor to PS-*b*-P2VP/[EMIm][TFSI] mixtures exhibiting a lower B value is the existence of different P2VP/ionic liquid interactions in each type of mixture. Unlike [EMIm][TFSI], [Im][TFSI] is protic and likely participates in hydrogen bonding with and protonation of 2VP monomers, slowing down the transport of imidazolium cations compared to ethylmethylimidazolium cations. Another possibility is that ion aggregation occurs to varying degrees as a function of temperature and w_{IL} in the PS-*b*-P2VP/[Im][TFSI] and PS-*b*-P2VP/[EMIm][TFSI] systems.[18, 47] The extent of ion aggregation in the PS-*b*-P2VP/ionic liquid membranes is the subject of future work. Thus, to maximize conductivity at a given temperature and ϕ_{IL}, a block copolymer and ionic liquid pair should be chosen such that the T_g of the host copolymer phase is low and/or greatly depressed upon addition of ionic liquid, and so that B is low.

Percolation theory, which describes the concentration dependence of σ for PS-*b*-P2VP/[Im][TFSI] mixtures, also describes the PS-*b*-P2VP/[EMIm][TFSI] data well (Figure 3.6), suggesting that the concentration dependence of σ being a function of ϕ_{IL} is a general property of mixtures of block copolymers and ionic liquids, at least in systems where morphology does not significantly influence conductivity. It is expected that ϕ_0 and n in Equation 3.2 will be similar for both types of mixtures since they are properties of the geometry of the system, which is confirmed by the PS-*b*-P2VP/[EMIm][TFSI] data points falling very close to the percolation curve fit for PS-*b*-P2VP/[Im][TFSI] mixtures. The value of σ_0 depends on the system, and should be different for each type of mixture. The fact that σ_0 does not appear to be significantly different for PS-*b*-P2VP/[Im][TFSI] and PS-*b*-P2VP/[EMIm][TFSI] most likely reflects the similar ionic conductivities of neat [Im][TFSI] and [EMIm][TFSI].[29, 31]

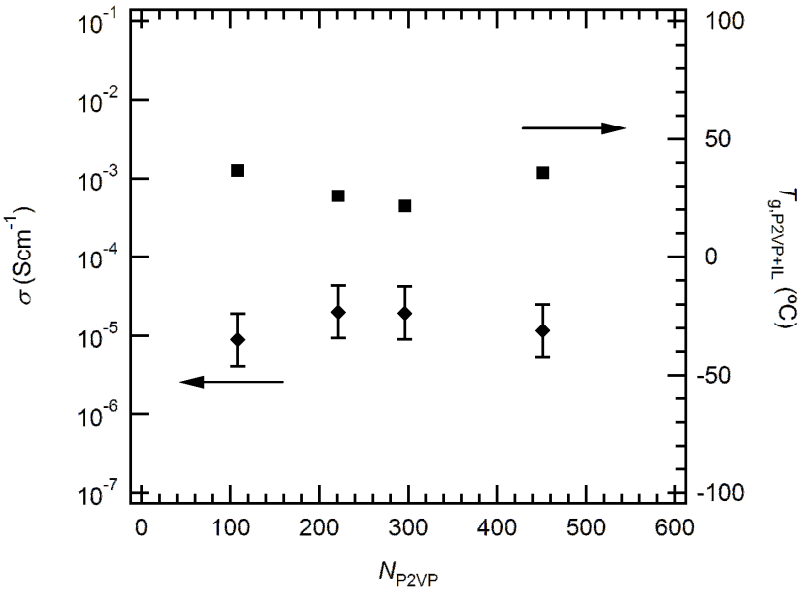


Figure 3.9. Conductivity and Glass Transition Temperature as a Function of Molecular Weight. σ and $T_{g,P2VP+IL}$ as a function of N_{P2VP} for PS-*b*-P2VP/[Im][TFSI] mixtures with f_{PS}=0.62±0.03, ϕ_{IL}=0.25±0.02, and T=100 ºC.

In summary, the general form of Equation 3.3,

$$\sigma = \sigma_0 \left(\phi_{IL} - 0.17\right)^{1.5} * \exp\left\{\frac{-B}{R\left[T - \left(T_g\left(w_{IL}\right) - 50\right)\right]}\right\} \tag{3.4}$$

is predicted to be widely applicable to block copolymer/ionic liquid systems, where the tunable parameters are $T_g(w_{IL})$ and B, which are characteristic of the polymer/ionic liquid pair, and σ_0, which is characteristic of the ionic liquid. It is emphasized that Equation 3.4 is applicable only to systems where the conducting phase morphology is well-connected, isotropic, and strongly segregated from the structural phase.

3.4. Conclusions

Phase separated mixtures of ionic liquids and polymers are of great interest for a wide variety of electrochemical applications. Understanding the relationship between polymer composition, ionic liquid concentration, temperature, and ionic conductivity for these mixtures is essential for designing new materials. In this work, the concentration and temperature dependencies of σ for model mixtures of PS-*b*-P2VP block copolymers and [Im][TFSI] and [EMIm][TFSI] ionic liquids have been successfully decoupled. While the temperature dependence of σ is a function of $T_{g,P2VP+IL}$, which is a function of the amount of ionic liquid exclusively in the P2VP domain of the block copolymer, the concentration dependence of σ is a function of the overall volume fraction of ionic liquid, ϕ_{IL}. This scaling behavior allows for the design of membranes where the amount of a mechanical component in the block copolymer can be increased to improve the strength of the membrane without sacrificing conductivity (as long as ϕ_{IL} is kept high). The chemistry of the system can also be tuned to increase σ at a given temperature and ϕ_{IL} by selecting a block copolymer/ionic liquid pair for which the T_g of the ionic liquid host phase is low and/or greatly depressed upon the addition of ionic liquid and for which the neat ionic liquid has a high σ. Molecular weight and morphology, as long as the conducting phase is isotropic and well-connected, have been found to have negligible effects on σ.

3.5. Acknowledgements

We gratefully acknowledge support from the Assistant Secretary for Energy Efficiency and Renewable Energy, Office of Hydrogen, Fuel Cell, and Infrastructure Technologies of the U.S. Department of Energy under Contract No. DE-AC02-05CH11231. The authors thank Prof. Nitash Balsara, Dr. John Kerr, Dr. Justin Virgili, Dr. Adam Weber, and Prof. John Newman for many useful discussions. SAXS experiments were performed at the Advanced Light Source (ALS) and the Stanford Synchrotron Radiation Lightsource (SSRL). Both are national user facilities supported by the Department of Energy, Office of Basic Energy Sciences. We gratefully acknowledge Dr. Alexander Hexemer, Dr. Cheng Wang, and Dr. Eric Schaible for experimental assistance at the ALS, and Dr. John Pople for experimental assistance at the SSRL.

3.6. Appendix: Supporting SAXS and AC Impedance Spectroscopy

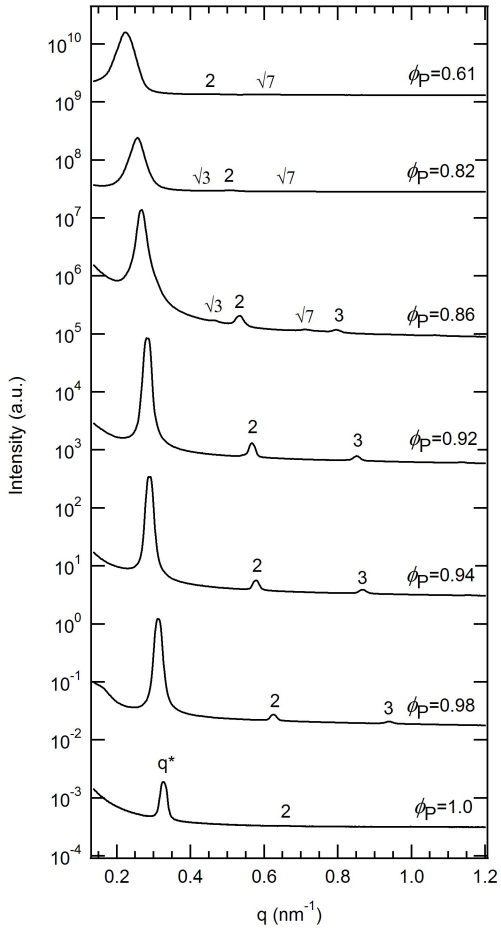


Figure 3.A.1. SAXS Profiles of PS-*b*-P2VP/[EMIm][TFSI] Mixtures. SAXS profiles at 145 ºC for mixtures of PS-*b*-P2VP(f_{PS}=0.42) with [EMIm][TFSI] with many ϕ_P. Scattering peak labels correspond to q/q*. Mixtures with $0.92 \leq \phi_P \leq 1.0$ exhibit a lamellar morphology, and mixtures with $0.92 \leq \phi_P \leq 1.0$ exhibit a HCP PS morphology.

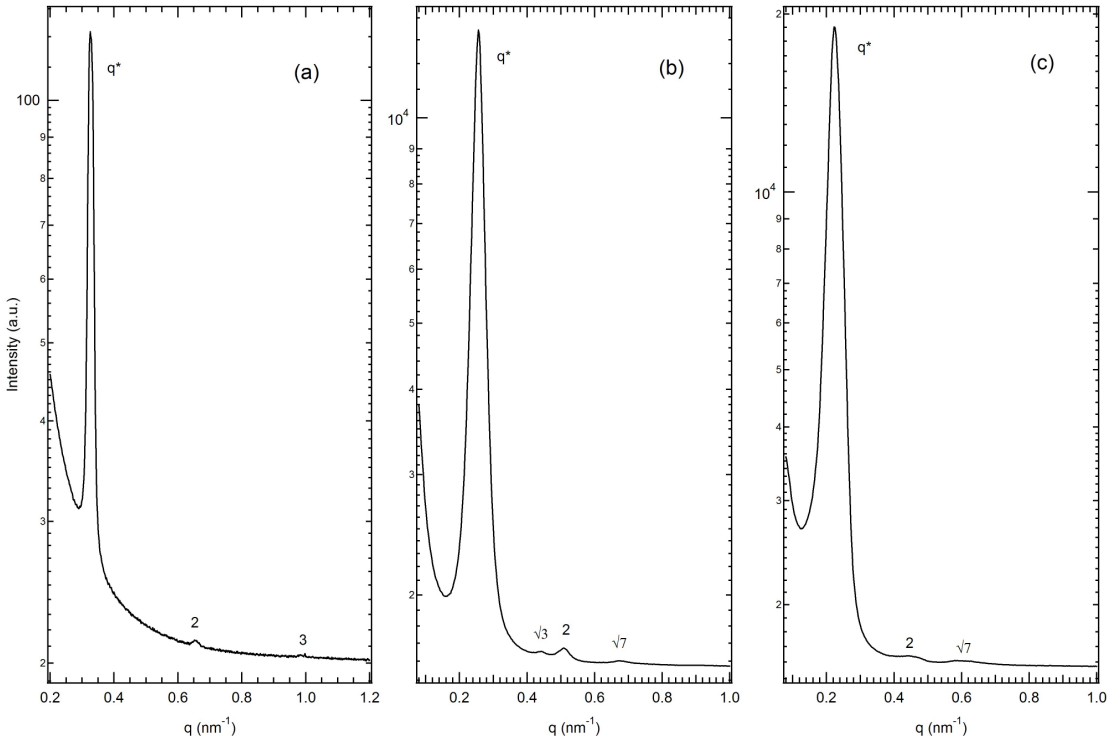


Figure 3.A.2. Expanded PS-*b*-P2VP/[EMIm][TFSI] SAXS Profiles. Expanded SAXS profiles at 145 ºC for a) PS-*b*-P2VP(f_{PS}=0.42) and mixtures of PS-*b*-P2VP(f_{PS}=0.42) with [EMIm][TFSI] with b) ϕ_P=0.82, and c) ϕ_P=0.61.

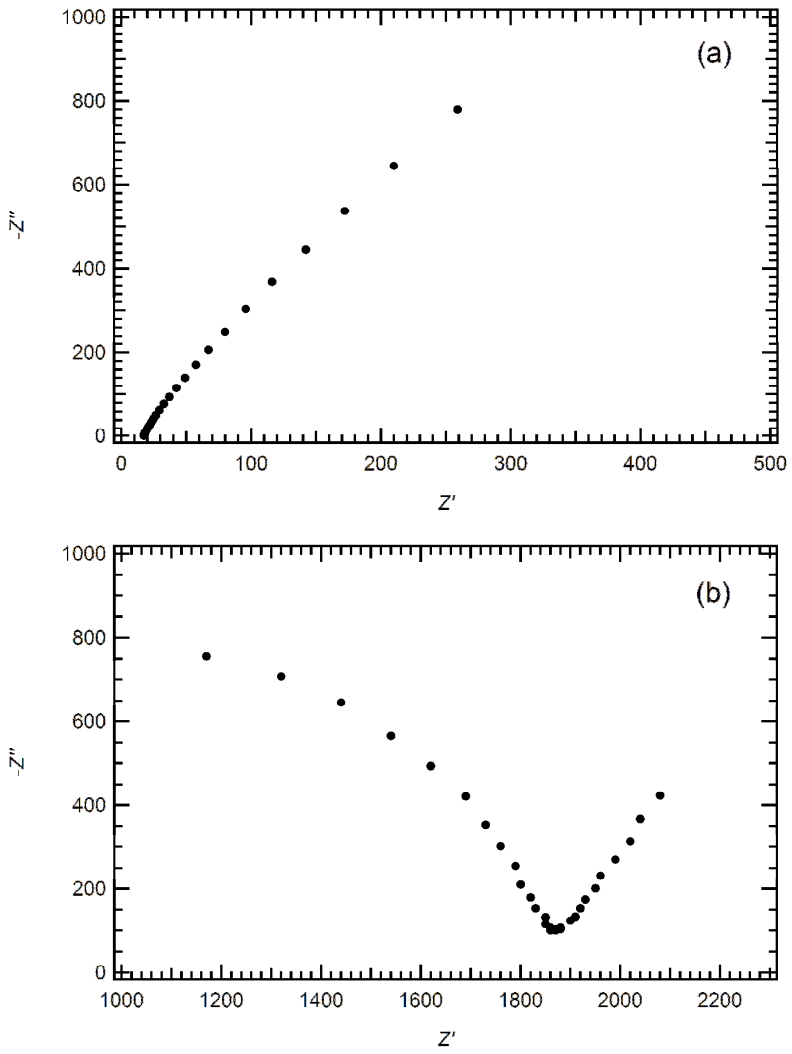


Figure 3.A.3. Nyquist Plots. Representative Nyquist plots of -*Z*'' versus *Z*' from AC impedance spectroscopy measurements of (a) highly conductive and (b) less conductive PS-*b*-P2VP/[Im][TFSI] and PS-*b*-P2VP/[EMIm][TFSI] membranes. *R* is generally taken as the minimum in the Nyquist plot (a), or as the Z'-intercept in highly conductive samples (b).

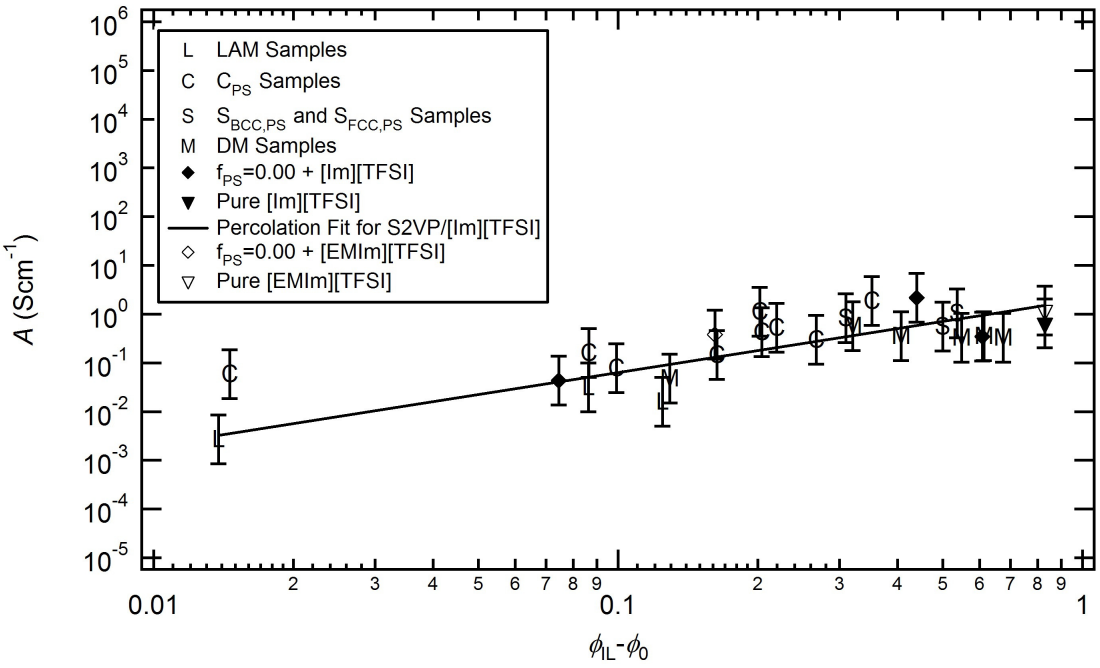


Figure 3.A.4. Evidence that Morphology Does Not Strongly Impact Conductivity. A, determined by VTF fits with A and B as fitting parameters and $T_o = T_{g,P2VP+IL}-50$ K, as a function of ϕ_{IL}-ϕ_0 for mixtures of PS-*b*-P2VP with [Im][TFSI] and [EMIm][TFSI]. Copolymer mixtures are labeled by morphology to demonstrate that scatter is unrelated to the nanoscale morphology. The error bars represent a reasonable estimate based on the accuracy of AC Impedance measurements and data fits.

3.7. References

1. Wasserscheid, P.; Welton, T., *Ionic Liquids in Synthesis*. WILEY-VCH Verlag: Weinheim, 2003.
2. Ohno, H., *Electrochemical Aspects of Ionic Liquids*. Wiley-Interscience: New York, 2005.
3. Simone, P. M.; Lodge, T. P. *Macromolecules* **2008,** 41, (5), 1753-1759.
4. Virgili, J. M.; Hexemer, A.; Pople, J. A.; Balsara, N. P.; Segalman, R. A. *Macromolecules* **2009,** 42, (13), 4604-4613.
5. Mauritz, K. A.; Moore, R. B. *Chemical Reviews* **2004,** 104, (10), 4535-4585.
6. Chen, Y. B.; Thorn, M.; Christensen, S.; Versek, C.; Poe, A.; Hayward, R. C.; Tuominen, M. T.; Thayumanavan, S. *Nature Chemistry* **2010,** 2, (6), 503-508.
7. Ichikawa, T.; Yoshio, M.; Hamasaki, A.; Mukai, T.; Ohno, H.; Kato, T. *Journal of the American Chemical Society* **2007,** 129, (35), 10662-+.
8. Cho, B. K.; Jain, A.; Gruner, S. M.; Wiesner, U. *Science* **2004,** 305, (5690), 1598-1601.
9. Kim, Y. S.; Pivovar, B. S. *Annual Review of Chemical and Biomolecular Engineering* **2010,** 1, 123-148.
10. Rubatat, L.; Li, C. X.; Dietsch, H.; Nykanen, A.; Ruokolainen, J.; Mezzenga, R. *Macromolecules* **2008,** 41, (21), 8130-8137.
11. Ruzette, A. V. G.; Soo, P. P.; Sadoway, D. R.; Mayes, A. M. *Journal of the Electrochemical Society* **2001,** 148, (6), A537-a543.
12. Wanakule, N. S.; Panday, A.; Mullin, S. A.; Gann, E.; Hexemer, A.; Balsara, N. P. *Macromolecules* **2009,** 42, (15), 5642-5651.
13. Fujita, H.; Kishimoto, A.; Matsumoto, K. *Transactions of the Faraday Society* **1960,** 56, (3), 424-437.
14. Vrentas, J. S.; Duda, J. L. *Journal of Polymer Science Part B-Polymer Physics* **1977,** 15, (3), 403-416.
15. Vrentas, J. S.; Duda, J. L. *Journal of Polymer Science Part B-Polymer Physics* **1977,** 15, (3), 417-439.
16. Lodge, T. P.; Mok, M. M.; Liu, X. C.; Bai, Z. F.; Lei, Y. *Macromolecules* **2011,** 44, (4), 1016-1025.
17. Scott, M. P.; Brazel, C. S.; Benton, M. G.; Mays, J. W.; Holbrey, J. D.; Rogers, R. D. *Chemical Communications* **2002**, (13), 1370-1371.
18. Susan, M. A.; Kaneko, T.; Noda, A.; Watanabe, M. *Journal of the American Chemical Society* **2005,** 127, (13), 4976-4983.
19. Seki, S.; Susan, A. B. H.; Kaneko, T.; Tokuda, H.; Noda, A.; Watanabe, M. *Journal of Physical Chemistry B* **2005,** 109, (9), 3886-3892.
20. Simone, P. M.; Lodge, T. P. *Acs Applied Materials & Interfaces* **2009,** 1, (12), 2812-2820.
21. Winey, K. I.; Gwee, L.; Choi, J. H.; Elabd, Y. A. *Polymer* **2010,** 51, (23), 5516-5524.
22. Virgili, J. M.; Hoarfrost, M. L.; Segalman, R. A. *Macromolecules* **2010,** 43, (12), 5417-5423.
23. Gray, F. M., *Solid Polymer Electrolytes: Fundamentals and Technological Applications*. VCH Publishers, Inc.: New York, 1991.

24. Robitaille, C. D.; Fauteux, D. *Journal of the Electrochemical Society* **1986,** 133, (2), 315-325.
25. Cho, E.; Park, J. S.; Sekhon, S. S.; Park, G. G.; Yang, T. H.; Lee, W. Y.; Kim, C. S.; Park, S. B. *Journal of the Electrochemical Society* **2009,** 156, (2), B197-B202.
26. Doyle, M.; Choi, S. K.; Proulx, G. *Journal of the Electrochemical Society* **2000,** 147, (1), 34-37.
27. Kim, S. Y.; Kim, S.; Park, M. J. *Nature Communications* **2010,** 1.
28. Yokoyama, H.; Mates, T. E.; Kramer, E. J. *Macromolecules* **2000,** 33, (5), 1888-1898.
29. Noda, A.; Susan, A. B.; Kudo, K.; Mitsushima, S.; Hayamizu, K.; Watanabe, M. *Journal of Physical Chemistry B* **2003,** 107, (17), 4024-4033.
30. Virgili, J. M.; Nedoma, A. J.; Segalman, R. A.; Balsara, N. P. *Macromolecules* **2010,** 43, (8), 3750-3756.
31. Tokuda, H.; Hayamizu, K.; Ishii, K.; Susan, M. A. B. H.; Watanabe, M. *Journal of Physical Chemistry B* **2005,** 109, (13), 6103-6110.
32. Hanley, K. J.; Lodge, T. P.; Huang, C. I. *Macromolecules* **2000,** 33, (16), 5918-5931.
33. Krummen, M.; Wasserscheid, P.; Gmehling, J. *Journal of Chemical and Engineering Data* **2002,** 47, (6), 1411-1417.
34. Fulcher, G. S. *Journal of the American Ceramic Society* **1925,** 8, (12), 789-794.
35. Fulcher, G. S. *Journal of the American Ceramic Society* **1925,** 8, (6), 339-355.
36. Tammann, G.; Hesse, W. *Zeitschrift Fur Anorganische Und Allgemeine Chemie* **1926,** 156, (4).
37. Vogel, H. *Physikalische Zeitschrift* **1921,** 22, 645-646.
38. Adam, G.; Gibbs, J. H. *Journal of Chemical Physics* **1965,** 43, (1), 139-&.
39. Ferry, J. D., *Viscoelastic Properties of Polymers*. 3 ed.; John Wiley & Sons, Inc.: 1980.
40. Passaglia, E.; Kevorkian, H. K. *Journal of Applied Physics* **1963,** 34, (1), 90-&.
41. Kirkpatr.S. *Reviews of Modern Physics* **1973,** 45, (4), 574-588.
42. Hunt, A. G.; Ewing, R. P., *Percolation Theory for Flow in Porous Media, Lecture Notes in Physics*. Springer: Berlin, 2009.
43. Scher, H.; Zallen, R. *Journal of Chemical Physics* **1970,** 53, (9), 3759-&.
44. Morris, D. R.; Sun, X. D. *Journal of Applied Polymer Science* **1993,** 50, (8), 1445-1452.
45. Maki-Ontto, R.; de Moel, K.; Polushkin, E.; van Ekenstein, G. A.; ten Brinke, G.; Ikkala, O. *Advanced Materials* **2002,** 14, (5), 357-361.
46. Park, M. J.; Balsara, N. P. *Macromolecules* **2010,** 43, (1), 292-298.
47. Noda, A.; Hayamizu, K.; Watanabe, M. *Journal of Physical Chemistry B* **2001,** 105, (20), 4603-4610.

Chapter 4. Conductivity Scaling Relationships for Nanostructured Block Copolymer/Ionic Liquid Membranes

Reproduced with permission from Megan L. Hoarfrost and Rachel A. Segalman (2012) *In Preparation.*

Understanding the relationship between membrane composition, structure, and ionic conductivity is essential for optimizing the properties of nanostructured mixtures of block copolymers and ionic liquids. It was previously demonstrated that the conductivity of mixtures of poly(styrene-*b*-2-vinyl pyridine) (PS-*b*-P2VP) with two different ionic liquids can be described by a single expression, which combines percolation theory with the Vogel-Tamman-Fulcher (VTF) equation. Percolation theory describes the power law dependence of conductivity on the overall volume fraction of ionic liquid, while the VTF equation takes into account the effect of the glass transition temperature of the conducting phase on the temperature dependence. In this work, the ionic conductivity of mixtures of poly(styrene-*b*-methyl methacrylate) (PS-*b*-PMMA) with imidazolium bis(trifluoromethylsulfonyl)imide ([Im][TFSI]) is compared to that of the PS-*b*-P2VP mixtures to demonstrate that the previously developed scaling relationships are general across multiple block copolymer chemistries, showing that there is incredible flexibility in designing block copolymer/ionic liquid membranes for applications requiring high conductivity.

4.1. Introduction

Ionic liquids, which are salts with low melting temperatures, or equivalently, solvents composed completely of ions, have unique properties including low vapor pressure, high thermal, chemical, and electrochemical stability, and high ionic conductivity.[1] This exceptional combination of properties makes them outstanding candidates for ion-conducting media in a variety of electrochemical applications.[2] Combining ionic liquids with block copolymers allows for tunable mechanical properties and the confinement of ionic liquid to nanoscopic conducting channels.[3-12]

Understanding the relationship between composition, structure, and ionic conductivity in the resulting block copolymer/ionic liquid membranes is essential for optimizing their properties. In contrast to dilute electrolyte solutions, where ionic conductivity, σ, is simply proportional to the number of ions and the diffusion coefficients of the ionic moieties (Nernst-Einstein equation), σ scales nonlinearly with ion concentration in concentrated block copolymer/ionic liquid mixtures.[3, 5, 10] This is due to the combined effects of the tortuosity of the charge transport pathways, the need to be above a concentration threshold to form a percolated ionic liquid network, and the dependence of the glass transition temperature, T_g, of the conducting phase on ionic liquid concentration.

Recently, we showed that the ionic conductivity of mixtures of poly(styrene-*b*-2-vinyl pyridine) (PS-*b*-P2VP) with two different ionic liquids selective for the P2VP phase, imidazolium bis(trifluoromethylsulfonyl)imide ([Im][TFSI]) and 1-ethyl-3-

methylimidazolium bis(trifluoromethylsulfonyl)imide ([EMIm][TFSI], can be described by a single expression:[3]

$$\sigma = \sigma_0 (\phi_{IL} - 0.15)^{1.5} * \exp\left\{ \frac{-B}{R[T - (T_g(w_{IL}) - 50)]} \right\} \quad (4.1)$$

The influence of T_g on conductivity is encompassed in the second term in Equation 4.1, which describes the temperature dependence. This term comes from the Vogel-Tamman-Fulcher (VTF) equation,[13-16]

$$\sigma = A \exp\left(\frac{-B}{R(T - T_0)} \right) \quad (4.2)$$

where A is a fitting parameter that contains the concentration dependence of σ, T_0 is the Vogel temperature, and B is analogous to the activation energy for ion transport in the Arrhenius equation. The value of B was found to be unique for each polymer/ionic liquid pair. A good choice for the value of T_0 for all the PS-*b*-P2VP mixtures was found to be about 50 K below the T_g of the P2VP/ionic liquid phase, where the T_g is a function of the weight fraction of ionic liquid exclusively in the P2VP phase, w_{IL}. The concentration dependence of conductivity, contained in the fitting parameter A, was found to depend on the overall volume fraction of ionic liquid, ϕ_{IL}, according to percolation theory,[17, 18]

$$A = \sigma_0 (\phi_{IL} - \phi_0)^n \quad (4.3)$$

where σ_0 is determined by the ionic conductivity of the neat ionic liquid and ϕ_0 is the percolation threshold volume fraction of ionic liquid. For PS-*b*-P2VP/ionic liquid mixtures, ϕ_0 was found to be close to the theoretical value[19] of 0.15 for an ideal, 3-D, continuous system. The power law exponent, n, is a constant that includes the effect of tortuosity, depends only on the spatial dimensions, and is 1.5 for a 3-D system. Combining Equations 4.2 and 4.3 leads to Equation 4.1. Equation 4.1 was shown to adequately describe the conductivity of PS-*b*-P2VP/[Im][TFSI] mixtures demonstrating a wide variety of isotropically-oriented morphologies having conducting phase continuity.

In this work, we compare the scaling behavior of σ for poly(styrene-*b*-methyl methacrylate) (PS-*b*-PMMA)/[Im][TFSI] mixtures to that of the PS-*b*-P2VP/[Im][TFSI] mixtures to show that the previously developed scaling relationships are general across different block copolymer chemistries. The polymer for which the ionic liquid is selective was modified since the properties of the ionic liquid-containing phase will potentially have the largest impact on ion transport. PMMA was selected as the new ionic liquid-containing phase because the properties of PMMA, for instance its dielectric strength, pKa, and segregation strength with PS, are quite different from those of P2VP.[20-22] Furthermore, it was anticipated that [Im][TFSI] would be selective for PMMA compared to PS since this selectivity has been previously demonstrated for other imidazolium based ionic liquids.[10] We show that the conductivity of PS-*b*-PMMA/[Im][TFSI] mixtures follows the expected scaling relationships with ionic liquid concentration and temperature detailed in Equation 4.1, which demonstrates that the scaling relationships are indeed general for a wide variety of block copolymer and ionic liquid chemistries.

4.2. Experimental Section

Polymer Synthesis and Characterization. Poly(methyl methacrylate) (PMMA) and poly(styrene-*b*-methyl methacrylate) (PS-*b*-PMMA) were synthesized via anionic polymerization as described previously,[23] using LiCl and 1,1-diphenylethylene as described in reference 24. The molecular weight of PMMA was determined using ^{1}H NMR end-group analysis (Bruker DRX 500 MHz). The molecular weights of the polystyrene (PS) blocks of the block copolymers were determined using gel permeation chromatography (GPC), and the total molecular weights of the block copolymers were determined using ^{1}H NMR. GPC was used to assess the polydispersity of each polymer. Synthesis and characterization of poly(2-vinyl pyridine) (P2VP) and poly(styrene-*b*-2-vinyl pyridine) (PS-*b*-P2VP) were described previously.[3] The degree of polymerization of the PMMA or P2VP blocks, N_{PMMA} or N_{P2VP}, the volume fraction of PS, f_{PS}, and the polydispersity index, PDI, of each polymer are given in Table 4.1.

Ionic Liquid Purification and Preparation. Imidazole (≥95%) and bis(trifluoromethylsulfonyl)imide (HTFSI, ≥95%) were purchased from Sigma Aldrich and purified by sublimation under vacuum. The final purity of each starting material was assessed using differential scanning calorimetry (DSC) and ^{1}H NMR. Purified imidazole and HTFSI were combined in an equimolar ratio and heated at 110 ^{o}C for 2 to 3 hours. The composition of the resulting [Im][TFSI] ionic liquid was confirmed by comparing the measured melting temperature, T_m, and ^{1}H NMR profile to literature.[25] Because of their hygroscopic nature, the ionic liquid and its starting materials were handled in an argon atmosphere glove box and sealed sample holders at all times.

Preparation of Polymer/Ionic Liquid Mixtures. Dichloromethane and tetrahydrofuran were degassed using three freeze, pump, thaw cycles, dried by stirring over CaH_2 overnight, then distilled into a collection flask, brought into an argon atmosphere glove box, and stored on molecular sieves. All further sample preparation was performed within an argon atmosphere glove box. Predetermined quantities of [Im][TFSI] and PMMA or PS-*b*-PMMA were weighed into glass vials, ca. 5 wt% solutions were prepared by dissolving in tetrahydrofuran (PMMA mixtures) or dichloromethane with a few drops of tetrahydrofuran (PS-*b*-PMMA mixtures), and the solutions were stirred overnight. Samples were cast one drop at a time into sample holders for differential scanning calorimetry (DSC), small angle X-ray scattering (SAXS), and AC impedance spectroscopy. Samples were then heated in a vacuum oven at 110 ºC for ca. 18 hours to remove remaining solvent before sample holders were sealed shut. Preparation of P2VP and PS-*b*-P2VP mixtures was described previously.[3] Samples were sealed in jars containing desiccant in the glove box for transportation to experimental apparatuses.

Differential Scanning Calorimetry (DSC). DSC samples were crimped in an argon atmosphere glove box using hermetically sealed pans and placed inside a container with desiccant for transfer to the DSC. DSC was performed on a TA Instruments DSC Q20. Indium and dodecane were used as calibration standards. Samples underwent three heating and cooling cycles with a scan rate of 10 ºC per minute, and the measured values of T_g or T_m from the second heating scan were recorded.

Table 4.1. Degree of Polymerization, Volume Fraction, and PDI of PS-*b*-P2VP and PS-*b*-PMMA Polymers Studied.

PMMA and PS-*b*-PMMA				P2VP and PS-*b*-P2VP		
N_{PMMA}	f_{PS}	PDI		N_{P2VP}	f_{PS}	PDI
81	0.00	1.09		118	0.00	1.07
85	0.56	1.07		102	0.29	1.07
92	0.78	1.13		115	0.42	1.02
				108	0.62	1.10
				101	0.72	1.04

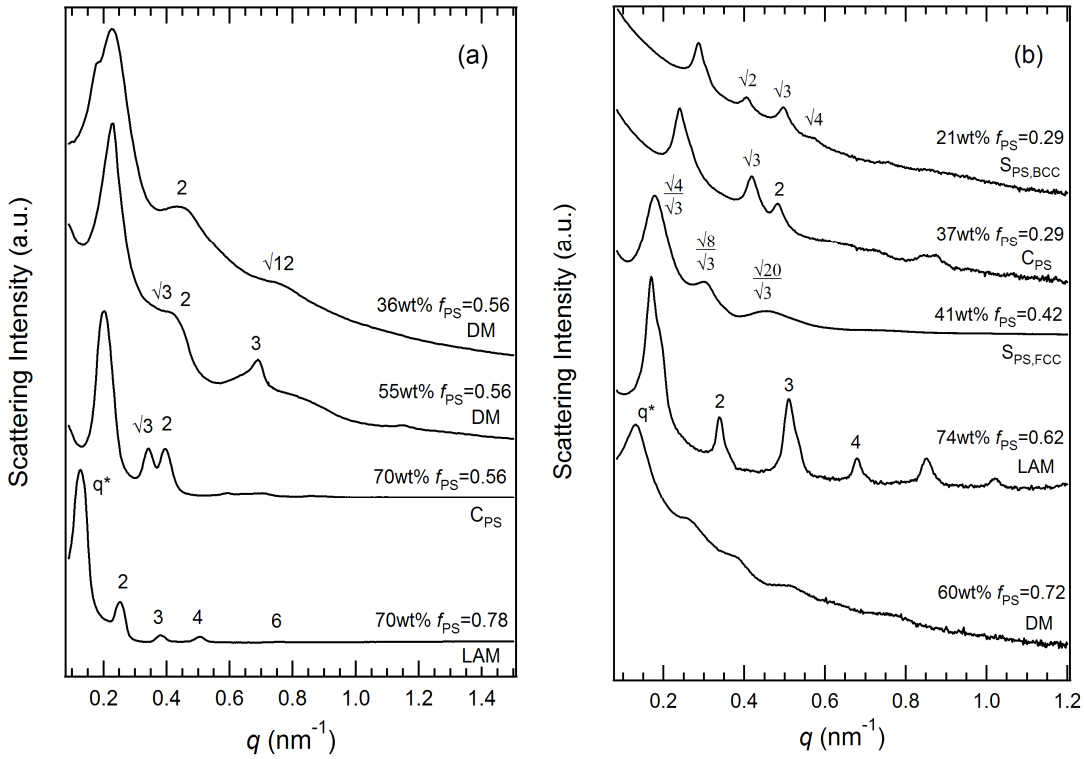


Figure 4.1. SAXS Profiles of Block Copolymer/Ionic Liquid Mixtures. SAXS profiles of (a) PS-*b*-PMMA/[Im][TFSI] mixtures studied as well as (b) representative PS-*b*-P2VP/[Im][TFSI] mixtures. The block copolymer weight percent as well as the assigned morphology of each mixture is indicated next to the corresponding scattering profile.

Morphology Characterization. Mixture morphologies were determined using small angle X-ray scattering (SAXS). Samples were cast in an argon atmosphere glove box into sample cells formed by an aluminum spacer sealed onto a Kapton window on one side until ca. 1 mm solid samples were obtained. After heating to remove solvent, a second Kapton window was glued to seal the samples, and the samples were sealed in jars containing desiccant for transportation to the beamline. SAXS was performed on beamline 7.3.3 of the Advanced Light Source (ALS) and beamline 1-4 of the Stanford Synchrotron Radiation Lightsource (SSRL). Samples were equilibrated within the beamline at 145 ºC for 30 minutes before data were gathered. At the ALS, the beamline was configured with an X-ray wavelength of λ=1.240 Å and focused to a 50 by 300 µm spot. Full two-dimensional scattering patterns were collected on an ADSC CCD detector with an active area of 188 by 188 mm. The scattering patterns were radially averaged, and the scattering intensity corrected with the post-ion chamber intensity using Nika software package.[26] At the SSRL, the beamline was configured with an X-ray wavelength λ=1.488 Å and focused to a 0.5 mm diameter spot. A single quadrant of a two-dimensional scattering pattern was collected on a CCD detector with an active area of 25.4 by 25.4 mm. The scattering patterns were radially averaged and corrected for detector null signal, dark current, and empty cell scattering.

SAXS profiles for the PS-*b*-PMMA mixtures used in the conductivity study are shown in Figure 4.1a. The morphologies of the mixtures all have conducting phase continuity, and include lamellae (LAM), hexagonally packed PS cylinders (C_{PS}), and disordered PS micelles (DM). Morphologies of PS-*b*-P2VP mixtures were reported previously and include LAM, C_{PS}, DM, as well as body-centered cubic (BCC) PS spheres ($S_{PS,BCC}$) and face-centered cubic (FCC) PS spheres ($S_{PS,BCC}$).[7] SAXS profiles for selected mixtures have been reproduced in Figure 4.1b to facilitate comparison to those of the PS-*b*-PMMA mixtures.

Selectivity of [Im][TFSI] for PMMA. Based on the demonstrated selectivity of the ionic liquid 1-ethyl-3-methylimidazolium bis(trifluoromethylsulfonyl)imide ([EMIm][TFSI]) for the PMMA phase of PS-*b*-PMMA block copolymers,[10] it was expected that [Im][TFSI] would also be selective for PMMA. The selectivity of [Im][TFSI] for one phase is confirmed by the shift of the primary SAXS peak of lamellar mixtures to lower q upon ionic liquid addition coupled with the decrease in T_g of only one phase (Figure 4.2). The T_g of the ionic liquid-containing phase collapses as a function of w_{IL} assuming complete segregation of the ionic liquid to the PMMA phase, confirming that [Im][TFSI] is selective for the PMMA phase specifically. The order of lyotropic phase transitions upon ionic liquid addition also reflect this selectivity: for instance, swelling of the PMMA phase leads to the lyotropic phase transition from hexagonally packed PMMA cylinders (C_{P2VP}) in pure PS-*b*-PMMA(f_{PS}=0.78) (characterized by a higher order peak at $\sqrt{3}q^*$) to LAM in a 90wt% mixture (characterized by higher order peaks at integer multiples of q*).

Ionic Conductivity Measurements. Bulk ionic conductivity was measured using four-point probe in-plane AC impedance spectroscopy. Samples were cast and hot-pressed into a home made, air-tight, poly(ether ether ketone) cell, which contained four stainless

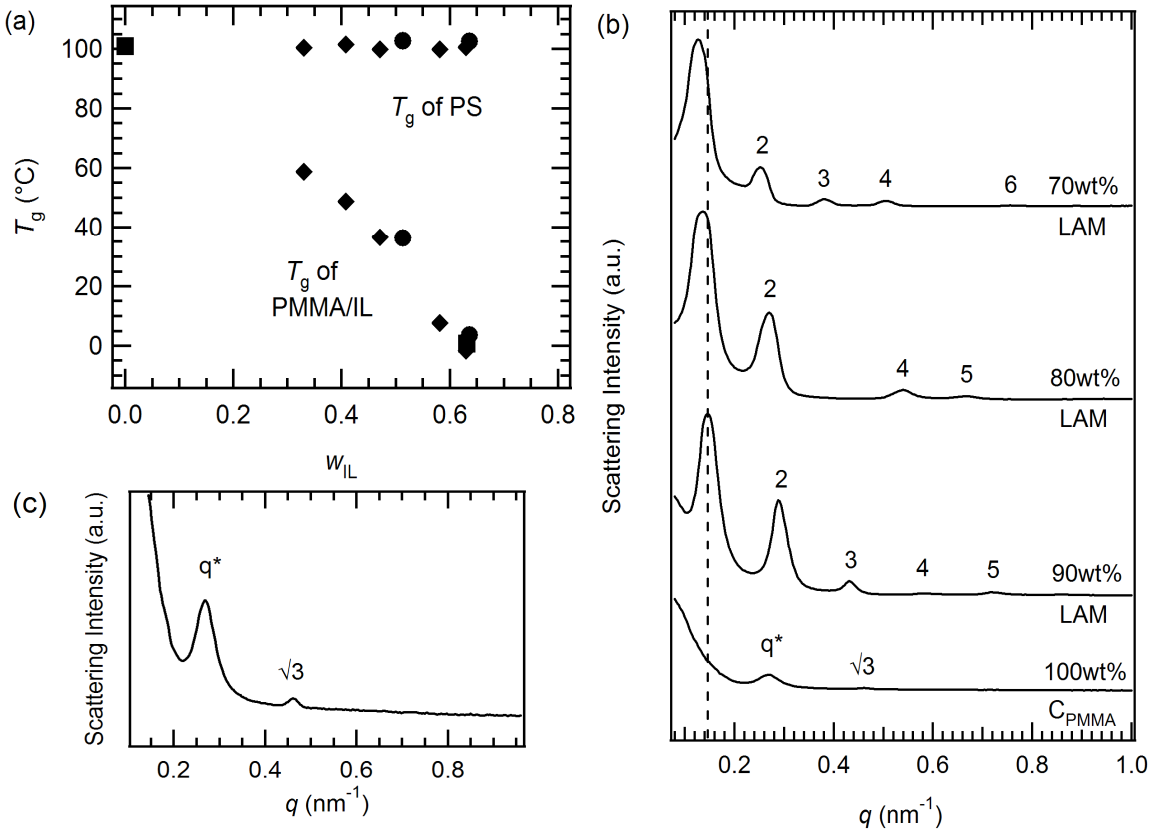


Figure 4.2. Selectivity of [Im][TFSI] for PMMA. (a) T_g, of the PS and PMMA/[Im][TFSI] phases as a function of w_{IL} for mixtures of [Im][TFS] with PMMA (squares), PS-*b*-PMMA(f_{PS}=0.56) (diamonds), and PS-*b*-PMMA(f_{PS}=0.78) (circles). The T_g of the ionic liquid-containing phase decreases upon ionic liquid addition, while the T_g of the PS phase remains close to 100 ºC. (b) SAXS profiles of PS-*b*-PMMA(f_{PS}=0.78)/[Im][TFSI] mixtures, demonstrating the selectivity of [Im][TFSI] for the PMMA phase of the block copolymer. (c) Blown up view of the scattering profile of 100wt% PS-*b*-PMMA(f_{PS}=0.78).

steel electrodes and was screwed shut in an argon atmosphere glove box. The working and reference electrodes were 0.7 cm apart and 1.7 cm long, and the samples were cast to be about 0.04 cm thick (measured after AC impedance measurements). The samples were heated at the highest measurement temperature for 12 hours before measurements were made. Impedance measurements were performed using a Gamry Reference 600 Potentiostat at descending temperatures. An alternating current signal with an amplitude of 5 mV was applied in the frequency range of 100 to 65,000 Hz. Either the nonzero x-intercept or the minimum in the Nyquist plot of the negative imaginary part of the impedance versus the real part of the impedance was taken as the sample resistance, R. The ionic conductivity, σ, was calculated as t/AR, where t and A are the thickness and area of the sample, respectively.

4.3. Results and Discussion

Like the previously reported PS-*b*-P2VP/ionic liquid mixtures,[3] the conductivity of PS-*b*-PMMA/[Im][TFSI] mixtures depends on the overall ion concentration in the mixture as well as how far the temperature is above the T_g of the conducting phase. This is demonstrated in Figure 4.3 for two sets of mixtures, one having fixed w_{IL} and various f_{PS}, and the other having fixed f_{PS} and various w_{IL}. The conductivity of the first set of mixtures decreases with increasing f_{PS} due to the corresponding decrease in the overall charge carrier concentration (Figure 4.3a). They have similar temperature dependence since the T_g of the conducting phase is a function of w_{IL}, which is fixed. The conductivity of the second set increases with increasing w_{IL} due to the increase in charge carrier concentration, and the temperature dependence becomes less steep with increasing w_{IL} since the T_g decreases.

The PS-*b*-PMMA/[Im][TFSI] conductivity data collapses well according to Equation 4.1 (Figure 4.4). This indicates that the form of Equation 4.1, which accounts for total ion concentration and tortuosity of the conducting pathways separately from the plasticization effect of the ionic liquid, is universal in its ability to capture the conductivity behavior of block copolymer/ionic liquid systems.

The slope of the PS-*b*-PMMA/[Im][TFSI] data in Figure 4.4 is slightly lower than that of the PS-*b*-P2VP/[Im][TFSI] data. This reflects the value of B in Equation 4.1, which quantifies the T_g-normalized temperature dependence of conductivity, and is specific to the polymer/ionic liquid pair. We previously showed that B=8.1±1.2 kJ/mol for PS-*b*-P2VP/[Im][TFSI] mixtures.[3] VTF fits (shown in Figure 4.3) reveal that B=7.3±0.6 kJ/mol for PS-*b*-PMMA/[Im][TFSI]. This is quite similar, but slightly lower than B for the PS-*b*-P2VP mixtures.

The data for both types of mixtures begin to collapse with each other at the highest experimental temperatures (lowest values of the normalized x-coordinate), which is the regime in which the concentration dependence described by percolation theory dominates over the temperature dependence. Figure 4.5 shows this directly by comparing the fitted values of the prefactor A from VTF fits, which contains the concentration dependence of

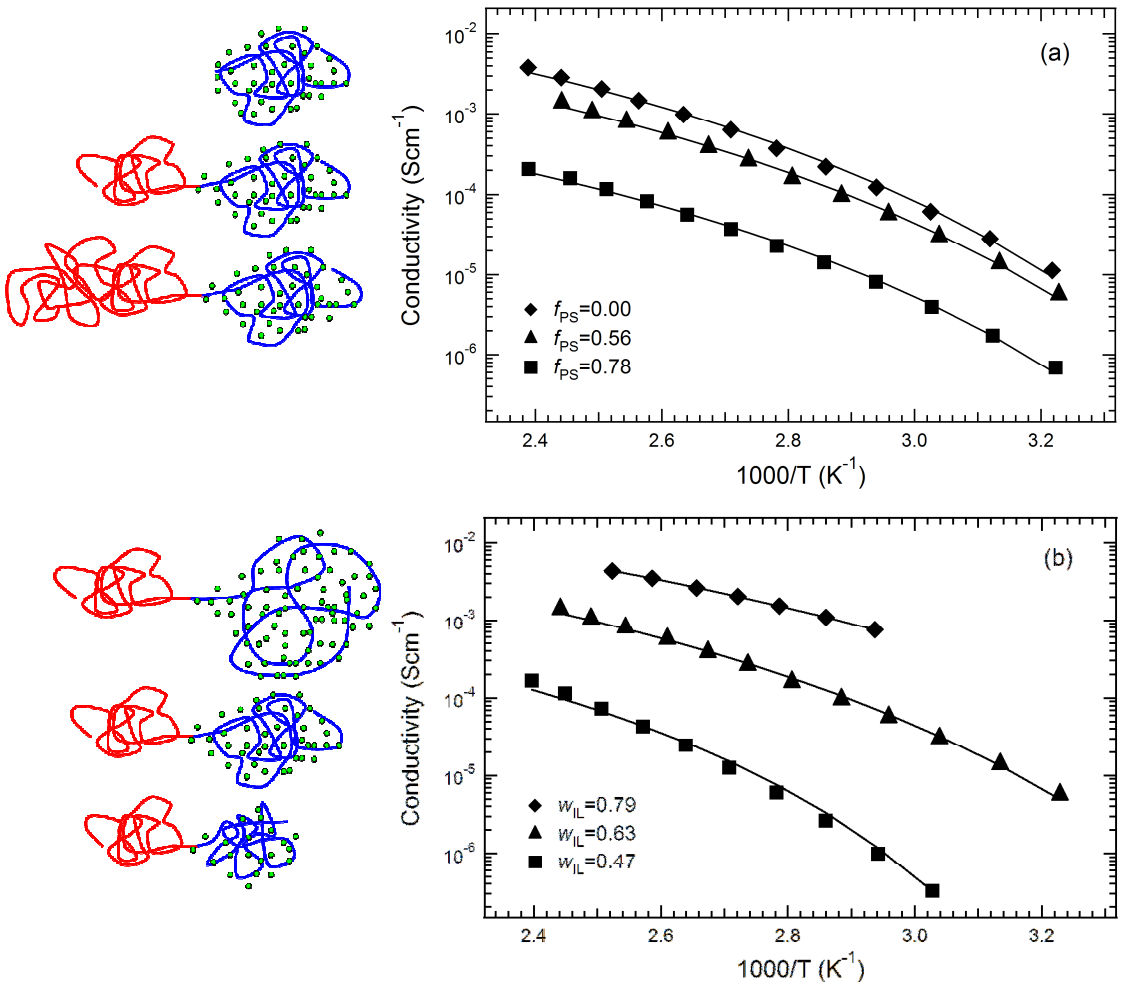


Figure 4.3. Ionic Conductivity of PS-*b*-PMMA/[Im][TFSI] Mixtures. Ionic conductivity as a function of temperature for PS-*b*-PMMA/[Im][TFSI] mixtures having (a) fixed w_{IL}=0.63 and various f_{PS}, and (b) fixed f_{PS}=0.56 and various w_{IL}. Solid curves are VTF fits. Red depicts PS regions, blue depicts PMMA regions, and

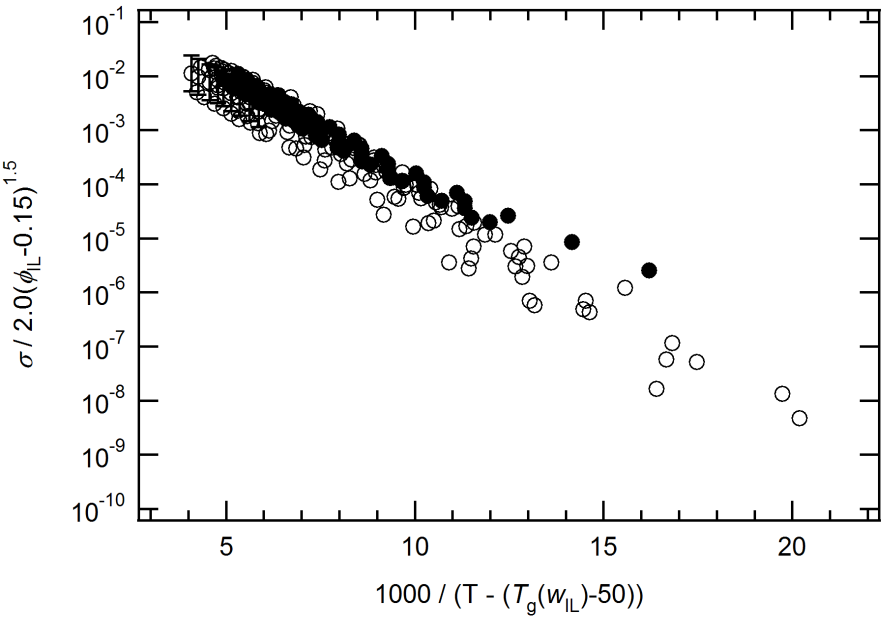


Figure 4.4. Normalized Ionic Conductivity. Conductivity of PS-*b*-PMMA/[Im][TFSI] mixtures (solid symbols) and PS-*b*-P2VP/[Im][TFSI] mixtures (open symbols), plotted according to Equation 4.1. For graphical clarity, the error bars are shown only for one sample. They represent a reasonable estimate based on the accuracy of AC Impedance measurements and can be extended to all data points.

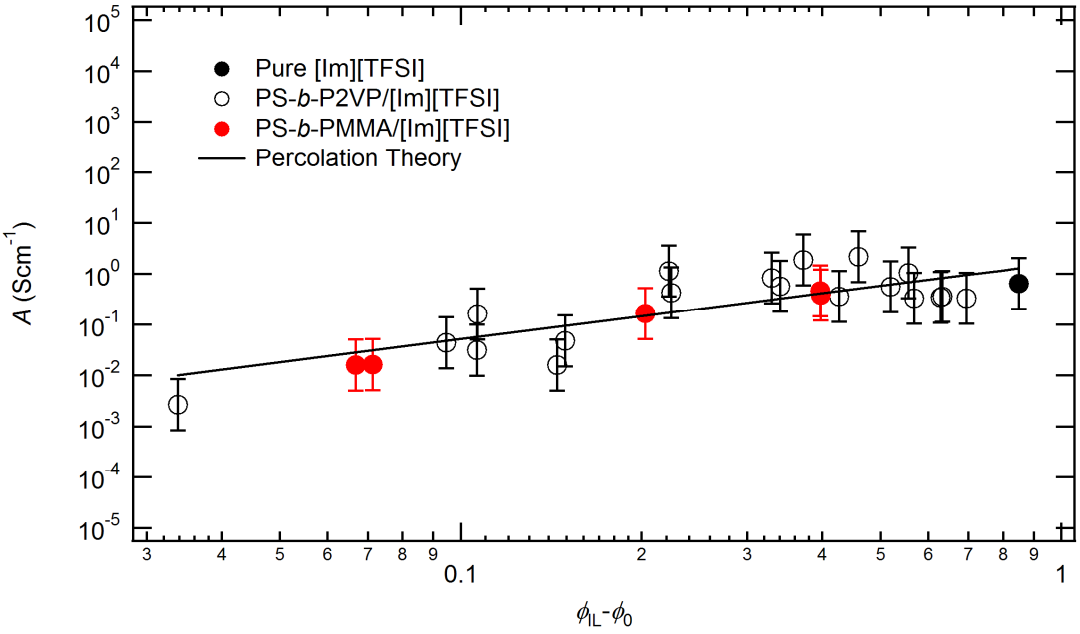


Figure 4.5. Concentration Dependence of Ionic Conductivity. *A* as a function of ϕ_{IL}-ϕ_0 for PS-*b*-PMMA/[Im][TFSI] mixtures, compared to *A* for PS-*b*-P2VP/[Im][TFSI] mixtures and the percolation theory (Equation 4.3) fit to PS-*b*-P2VP/[Im][TFSI] data.

conductivity. The data for both mixtures are found to be described well by the same percolation curve fit (Equation 4.3), as expected.

The ability of percolation theory to describe the conductivity of block copolymer/ionic liquid mixtures with many different morphologies as well as homopolymer/ionic liquid mixtures indicates the dominance of ionic liquid volume fraction in determining conductivity. The morphology imparted to the membrane via block copolymer self-assembly, while being a handle for improving mechanical and other desirable properties of the membrane, has little effect on conductivity so long as the ion-conducting domains are well-connected (and confinement does not actually influence the mechanism of ion conduction in the ionic liquid[12]). Alignment of isotropic grains could increase conductivity in the direction of alignment, but these effects are modest compared to the multiple-order-of-magnitude effect of varying ionic liquid volume fraction. For instance, aligning membranes with lamellar channels theoretically enhances conductivity in the direction of alignment by a factor of 1.5, which is consistent with experiment.[27, 28]

Equation 4.1 paints a picture of how ion conduction occurs in block copolymer/ionic liquid mixtures. The main effect of the block copolymer on ionic conductivity is its influence on the T_g of the conducting phase. It is possible to increase greatly the conductivity by choosing a polymer/ionic liquid pair with a low T_g compared to the desired operating temperature. Additional factors such as specific molecular interactions between the polymer and ionic liquid[3] or ion aggregation in the presence of the polymer[29, 30] affect the temperature dependence of conductivity through the parameter B, but the value of B has not been shown to vary greatly among the systems studied thus far. Other than these effects, the polymer serves only as a mechanical matrix for the ionic liquid, as evidenced by the concentration dependence term being described well by percolation theory. Thus, there is enormous flexibility in designing block copolymer/ionic liquid systems for applications requiring high ionic conductivity. This is in contrast to block copolymer/salt polymer electrolytes, for instance, where the conductivity mechanism is intimately related to specific coordination between the polymer and salt, and is thus extremely chemistry dependent.[31]

4.4. Conclusion

Membranes composed of phase separated mixtures of ionic liquids and polymers are of great interest for a wide variety of electrochemical applications. Understanding the relationship between membrane composition, structure, and ionic conductivity is essential for optimizing their properties. It was previously demonstrated that the conductivity of PS-*b*-P2VP/ionic liquid mixtures can be described by a single expression (Equation 4.1), in which the concentration dependence is described by percolation theory, and the temperature dependence is described by the VTF equation. In this work, we show that the conductivity of PS-*b*-PMMA/[Im][TFSI] mixtures follows the same scaling relationships as that of PS-*b*-P2VP mixtures, demonstrating that they are general across a wide variety of block copolymer/ionic liquid chemistries.

4.5. Acknowledgements

This material is based upon work performed by the Joint Center for Artificial Photosynthesis, a DOE Energy Innovation Hub, as follows: Material preparation and investigation of mixture morphology and conductivity was supported by the Assistant Secretary for Energy Efficiency and Renewable Energy, Office of Hydrogen, Fuel Cell, and Infrastructure Technologies of the U.S. Department of Energy under Contract No. DE-AC02-05CH11231; Continued investigation of mixture conductivity and interpretation of conductivity data was supported through the Office of Science of the U.S. Department of Energy under Award Number DE-SC0004993. M.L. Hoarfrost thanks support from an NSF Graduate Research Fellowship. SAXS experiments were performed at the Advanced Light Source (ALS) and the Stanford Synchrotron Radiation Laboratory (SSRL). Both are national user facilities supported by the Department of Energy, Office of Basic Energy Sciences. We gratefully acknowledge Dr. Alexander Hexemer, Dr. Cheng Wang, and Dr. Eric Schaible for experimental assistance at the ALS, and Dr. John Pople for experimental assistance at the SSRL. This report was prepared as an account of work sponsored by an agency of the United States Government. Neither the United States Government nor any agency thereof, nor any of their employees, makes any warranty, express or implied, or assumes any legal liability or responsibility for the accuracy, completeness, or usefulness of any information, apparatus, product, or process disclosed, or represents that its use would not infringe privately owned rights. Reference herein to any specific commercial product, process, or service by trade name, trademark, manufacturer, or otherwise does not necessarily constitute or imply its endorsement, recommendation, or favoring by the United States Government or any agency thereof. The views and opinions of authors expressed herein do not necessarily state or reflect those of the United States Government or any agency thereof.

4.6. References

1. Wasserscheid, P.; Welton, T., *Ionic Liquids in Synthesis*. WILEY-VCH Verlag: Weinheim, 2003.
2. Ohno, H., *Electrochemical Aspects of Ionic Liquids*. Wiley-Interscience: New York, 2005.
3. Hoarfrost, M. L.; Segalman, R. A. *Macromolecules* **2011,** 44, (13), 5281-5288.
4. Simone, P. M.; Lodge, T. P. *Macromolecules* **2008,** 41, (5), 1753-1759.
5. Simone, P. M.; Lodge, T. P. *Acs Applied Materials & Interfaces* **2009,** 1, (12), 2812-2820.
6. Virgili, J. M.; Hexemer, A.; Pople, J. A.; Balsara, N. P.; Segalman, R. A. *Macromolecules* **2009,** 42, (13), 4604-4613.
7. Virgili, J. M.; Hoarfrost, M. L.; Segalman, R. A. *Macromolecules* **2010,** 43, (12), 5417-5423.
8. Virgili, J. M.; Nedoma, A. J.; Segalman, R. A.; Balsara, N. P. *Macromolecules* **2010,** 43, (8), 3750-3756.
9. Kim, S. Y.; Kim, S.; Park, M. J. *Nature Communications* **2010,** 1.
10. Gwee, L.; Choi, J. H.; Winey, K. I.; Elabd, Y. A. *Polymer* **2010,** 51, (23), 5516-5524.

11. Kim, S. Y.; Yoon, E.; Joo, T.; Park, M. J. *Macromolecules* **2011,** 44, (13), 5289-5298.
12. Hoarfrost, M. L.; Tyagi, M. S.; Segalman, R. A.; Reimer, J. A. *Macromolecules* **2012,** 45, (7), 3112-3120.
13. Fulcher, G. S. *Journal of the American Ceramic Society* **1925,** 8, (12), 789-794.
14. Fulcher, G. S. *Journal of the American Ceramic Society* **1925,** 8, (6), 339-355.
15. Tammann, G.; Hesse, W. *Zeitschrift Fur Anorganische Und Allgemeine Chemie* **1926,** 156, (4).
16. Vogel, H. *Physikalische Zeitschrift* **1921,** 22, 645-646.
17. Hunt, A. G.; Ewing, R. P., *Percolation Theory for Flow in Porous Media, Lecture Notes in Physics*. Springer: Berlin, 2009.
18. Kirkpatr.S. *Reviews of Modern Physics* **1973,** 45, (4), 574-588.
19. Scher, H.; Zallen, R. *Journal of Chemical Physics* **1970,** 53, (9), 3759-&.
20. *CRC Handbook of Chemistry and Physics*. 92 ed.; Taylor and Francis Group, LLC: 2011-2012.
21. Zhao, Y.; Sivaniah, E.; Hashimoto, T. *Macromolecules* **2008,** 41, (24), 9948-9951.
22. Schulz, M. F.; Khandpur, A. K.; Bates, F. S.; Almdal, K.; Mortensen, K.; Hajduk, D. A.; Gruner, S. M. *Macromolecules* **1996,** 29, (8), 2857-2867.
23. Yokoyama, H.; Mates, T. E.; Kramer, E. J. *Macromolecules* **2000,** 33, (5), 1888-1898.
24. Varshney, S. K.; Hautekeer, J. P.; Fayt, R.; Jerome, R.; Teyssie, P. *Macromolecules* **1990,** 23, (10), 2618-2622.
25. Noda, A.; Susan, A. B.; Kudo, K.; Mitsushima, S.; Hayamizu, K.; Watanabe, M. *Journal of Physical Chemistry B* **2003,** 107, (17), 4024-4033.
26. Ilavsky, J. *Journal of Applied Crystallography* 45, (2), 324-328.
27. Li, J.; Park, J. K.; Moore, R. B.; Madsen, L. A. *Nature Materials* **2011,** 10, (7), 507-511.
28. Park, M. J.; Balsara, N. P. *Macromolecules* **2010,** 43, (1), 292-298.
29. Noda, A.; Hayamizu, K.; Watanabe, M. *Journal of Physical Chemistry B* **2001,** 105, (20), 4603-4610.
30. Susan, M. A.; Kaneko, T.; Noda, A.; Watanabe, M. *Journal of the American Chemical Society* **2005,** 127, (13), 4976-4983.
31. Gray, F. M., *Solid Polymer Electrolytes: Fundamentals and Technological Applications*. VCH Publishers, Inc.: New York, 1991.

Chapter 5. Proton Hopping and Long-range Transport in the Protic Ionic Liquid [Im][TFSI], Probed by Pulsed-Field Gradient NMR and Quasi-Elastic Neutron Scattering

Reproduced with permission from Megan L. Hoarfrost, Madhu S. Tyagi, Rachel A. Segalman, and Jeffrey A. Reimer (2012) *In Preparation.*

The management of proton conductivity in the protic ionic liquid imidazolium bis(trifluoromethylsulfonyl)imide ([Im][TFSI]) is investigated via the use of quasi-eleastic neutron scattering and pulsed-field gradient NMR. The introduction of excess neutral imidazole to [Im][TFSI] leads to enhanced conductivity. We find that proton dynamics in [Im][TFSI] with excess imidazole are characterized by proton hopping that is encompassed in the slower of two translational processes, as identified by quasi-elastic neutron scattering (QENS). This relatively slow process contributes most to long-range diffusion. NMR diffusion measurements show that proton hopping decreases with increasing temperature, but significant proton hopping persists even at the maximum experimental temperature of 120 ºC. This, in combination with minimal ion aggregation, leads to high proton conductivity and a high H^+ transference number over a wide temperature range.

5.1. Introduction

Protic ionic liquids are characterized by proton conductivity, negligible volatility, and good thermal and electrochemical stability. These features make them promising candidates for a wide variety of electrochemical applications, particularly those that operate at elevated temperatures (i.e. above the boiling point of water).[1] Systematic management of the proton conductivity in these ionic liquids is an important goal for many technologies, yet the scientific underpinnings for such management warrants further attention, in particular the relationship between ionic liquid composition and the atomistic mechanism by which protons move. For example, proton conductivity in imidazolium bis(trifluoromethylsulfonyl)imide ([Im][TFSI]) is known to be enhanced when prepared with an excess of imidazole.[2] In this scenario proton hopping between hydrogen-bonded imidazole molecules is facilitated, where the excess imidazole fulfills the role of proton "acceptor".[2-4] Proton hopping is presumed to decouple proton transport from molecular diffusion, leading to a high proton transference number in addition to overall faster proton conductivity.[5] A high proton transference number is desirable for applications such as proton exchange membrane fuel cells, as well as actuator applications that require asymmetric charge transport. We submit that a greater understanding of the mechanism of proton hopping in crafted imidazole-based ionic liquids will facilitate their use as electrolytes in these applications.

It has been understood for decades that imidazole molecules shuttle protons through biological membranes.[6] The observation of enhanced acidic proton diffusion coefficients in imidazole/acid mixtures[3] was the first demonstration that imidazole facilitates fast proton hopping in an electrolyte. Since that demonstration several theoretical studies have shed light on the details of the proton hopping mechanism in imidazole.[4, 7-10] These

studies have mapped out the predicted hydrogen bond network and intermolecular distances and shown that proton hopping involves two steps: a fast proton transfer step and a slow, rate-limiting reorientation step. These simulations are computationally demanding, and only recently has a simulation been performed using long enough time scales and a sufficient number of molecules to observe multiple hopping events.[7] The reorientation time scale was calculated to be ca. 20 ps and the hop rate was calculated to be 1/36 ps^{-1}, the latter of which appears consistent with bulk transport measurements.[3] Solid state nuclear magnetic resonance (NMR) experiments have observed imidazole ring flipping and quantified the activation energy to be similar to that of proton conductivity, confirming that ring flipping is an important part of the reorientation step.[11-13]

Direct experimental probes are desired to improve understanding of proton hopping in imidazole and its relationship to macroscopic proton conductivity. Using NMR to measure self-diffusion is an invaluable tool for quantifying the amount of proton hopping and determining the proton transference number. For example, by comparing the diffusion coefficients of acidic protons to the diffusion coefficients of protons covalently bound to the carbon atoms on imidazole in [Im][TFSI], it has been shown that proton hopping increases acidic proton diffusion by a factor of 1.4 at 30 ºC when the ratio of imidazole to HTFSI is 4:1.[2] Furthermore, comparing proton diffusion to anion diffusion revealed that the proton transference number reaches 0.69 at this temperature and composition.[2] Quasi-elastic neutron scattering (QENS) has provided more detailed information about proton dynamics in protic and aprotic ionic liquids,[14-18] and has proven very useful for studying proton hopping mechanisms in water,[19, 20] metals,[21, 22] oxides,[23] and oxo-acid salts.[24] This method has not yet been employed to study proton hopping in ionic liquids.

In this work, we study [Im][TFSI] having a 4:1 ratio of imidazole to HTFSI in order to provide insight into the proton hopping conductivity mechanism. 3:7 and 1:1 [Im][TFSI], which are not expected to exhibit proton hopping, are studied for comparison. Given the desire to utilize protic ionic liquids as electrolytes at elevated temperatures, we investigate how the degree of proton hopping, ion aggregation, and the proton transference number vary with temperature. Proton hopping is shown to persist even at 120 ºC, leading to a proton transference number of 0.66. We employ QENS to show that hopping is encompassed in the slower of two translational processes, and that this relatively slow process contributes most to long-range diffusion. Information about local dynamics is compared to bulk ionic conductivity measurements to provide insight into the effect of proton hopping on macroscopic conductivity.

5.2. Experimental Section

Ionic Liquid Purification and Preparation. Imidazole (≥95%), *d*4-imidazole (≥98% deuteration), and bis(trifluoromethylsulfonyl)imide (HTFSI, ≥95%) were purchased from Sigma Aldrich and purified by sublimation under vacuum. The final purity of each starting material was assessed using differential scanning calorimetry (DSC) and ^{1}H NMR (Bruker DRX 500 MHz). Purified imidazole or *d*4-imidazole and HTFSI were combined in 3:7, 1:1, and 4:1 molar ratios and heated at 100 $^{\circ}C$ for 2 to 3 hours. The

compositions of the resulting [Im][TFSI] and [*d*Im][TFSI] ionic liquids were confirmed by comparing the measured thermal transitions and ^{1}H NMR profiles to literature.[2] Thermal transitions were measured by differential scanning calorimetry (DSC) on a TA Instruments DSC Q20 to check the purity of the samples. Samples were crimped in an argon atmosphere glove box using hermetically sealed pans and placed inside a container with desiccant for transfer to the DSC. Indium and dodecane were used as calibration standards. Samples underwent three heating and cooling cycles with a scan rate of 10 ºC per minute, and thermal transitions from the second heating scan were recorded. The structures of the ionic liquid molecules are shown in Figure 5.1. Because of their hygroscopic nature, the ionic liquids and their starting materials were handled in an argon atmosphere glove box and sealed sample holders at all times.

Diffusion Coefficient Measurements. Self-diffusion coefficients of [Im][TFSI] were measured with pulsed-field gradient spin echo (PGSE) and pulsed-field gradient stimulated echo (PGStE) NMR experiments using a Doty Scientific single-axis diffusion probe with temperature control. The applied gradients were calibrated using water[25] and glycerol[26] standards, and were found to reach 1.7 T/m. ^{1}H diffusion coefficients were measured in a 7 T superconducting magnet with a 300 MHz Tecmag Apollo spectrometer and gradient control, and ^{19}F diffusion coefficients were measured in a 1.5 T superconducting magnet with a 61.2 MHz Tecmag LapNMR spectrometer and gradient control. Experiments were performed between 25 and 120 ºC, where the temperature was calibrated[27] using an ethylene glycol standard between 24 and 83 ºC and extrapolation to higher temperatures.

The NMR signal attenuation in PGSE and PGStE experiments is described by

$$I = I_0 e^{-D\gamma^2 g^2 \delta^2 \left(\Delta - \delta/3\right)} \tag{5.1}$$

where I is the spin-echo signal intensity, I_0 is the signal intensity with zero gradient, γ is the magnetogyric ratio of the probe nucleus, g is the magnitude of the gradient pulse, δ is the duration of the gradient pulse, Δ is the duration of time between the leading edges of the two gradient pulses, and D is the self-diffusion coefficient of the probe nucleus. I was measured as a function of g, and Equation 5.1 was used to determine D. An example plot of I/I_0 as a function of $\gamma^2 g^2 \delta^2(\Delta - \delta/3)$ is shown in Figure 5.A.1 in the Appendix. PGSE and PGStE experiments performed on each sample resulted in consistent measurements of D. Some ^{1}H NMR spectra are reported that were derived from PGSE experiments at the lowest gradient strength.

The diffusion coefficients for protons covalently bound to the carbon atoms on imidazole (C-H protons), $D_{\text{C-H}}$, and protons bound to nitrogen atoms on imidazole (N-H protons), $D_{\text{N-H}}$, were measured separately owing to their chemical shift contrast. The diffusion coefficients of acidic protons, $D_{\text{H+}}$, were calculated according to

$$D_{N-H} = xD_{H+} + (1-x)D_{C-H} \tag{5.2}$$

where x is the mole fraction of imidazolium.[2] For ^{19}F experiments, a single peak was observed corresponding to fluorine atoms on the TFSI anion, and a single diffusion coefficient was therefore measured, D_{TFSI}.

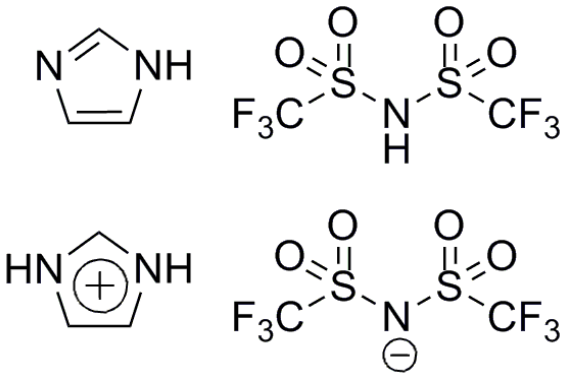


Figure 5.1. Chemical structure of Imidazole, HTFSI, and Imidazolium and TFSI Ions.

Neutron Scattering. Neutron scattering experiments were performed at the National Institute for Standards and Technology (NIST) Center for Neutron Research (NCNR). [Im][TFSI] and [*d*Im][TFSI] samples were loaded into sample cans with an annular geometry and the sample transmission was set to about 90% to minimize multiple scattering on both spectrometers. Reduction, visualization, and analysis of data were performed using the DAVE software package developed at NCNR.[28] Fixed window scans (FWS) were performed on the high flux backscattering spectrometer (HFBS) with an incident neutron wavelength of λ=6.271 Å and an energy resolution of about 0.8 μeV. Elastic scattering intensity was recorded as the temperature was increased steadily from 70 K at a rate of 1 K/min. Data were collected every minute from all 16 detectors, together probing a *q*-range from 0.25 to 1.75 $Å^{-1}$. The mean squared displacement of protons as a function of temperature was calculated from the loss in elastic scattering intensity using DAVE. QENS experiments were performed on the HFBS as well as on the disc chopper spectrometer (DCS). An incident neutron wavelength of λ=6 Å and an energy resolution of 64 μeV were used for DCS experiments. Data were binned into nine bins having average *q* values ranging from 0.35 to 1.8 $Å^{-1}$, and the data were corrected for empty cell scattering. An incident neutron wavelength of λ=6.271 Å and an energy resolution of about 0.8 μeV were used for HFBS experiments. Data from all 16 detectors were used to probe a *q*-range from 0.25 to 1.75 $Å^{-1}$. The acquired data were corrected for detector efficiencies (determined using a vanadium standard), and the resolution functions of the instruments were determined by measuring scattering from 4:1 [*d*Im][TFSI] at 35 K (on the DCS) and 4:1 [Im][TFSI] at 30 K (on the HFBS) where all the signal is expected to be elastic.

Ionic Conductivity Measurements. Bulk ionic conductivity was measured using two-point probe through-plane AC impedance spectroscopy. An annular ionic liquid-containing spacer was placed between two stainless steel electrodes. The spacers were made from Kapton™ or Teflon, and had thicknesses ranging from 25 μm to 0.3 cm and inner diameters ranging from 0.3 to 0.7 cm. The samples were then placed in home made, air-tight, stainless steel cells with Teflon flanges. The cells were screwed together in the glove box, and then clamped to maintain constant pressure in an oven outside the glove box and heated at the maximum measurement temperature for 12 hours before measurements were made. Impedance measurements were performed using a Gamry Reference 600 Potentiostat at descending temperatures. An alternating current signal with an amplitude of 5 mV was applied in the frequency range of 100 to 65,000 Hz. The nonzero x-intercept in the Nyquist plot of the negative imaginary part of the impedance versus the real part of the impedance was taken as the sample resistance, R. The ionic conductivity, σ, was calculated as t/AR, where t and A are the thickness and area of the sample, respectively.

5.3. Results and Discussion

Comparing D_{H+} to $D_{C\text{-}H}$ provides a quantitative description of how proton hopping increases proton transport vis-à-vis vehicle diffusion alone (Figure 5.2a). A ratio of approximately unity is expected and observed in cases were there is no excess imidazole to act as proton acceptors (3:7 and 1:1 [Im][TFSI]). Also as expected, this ratio is greater

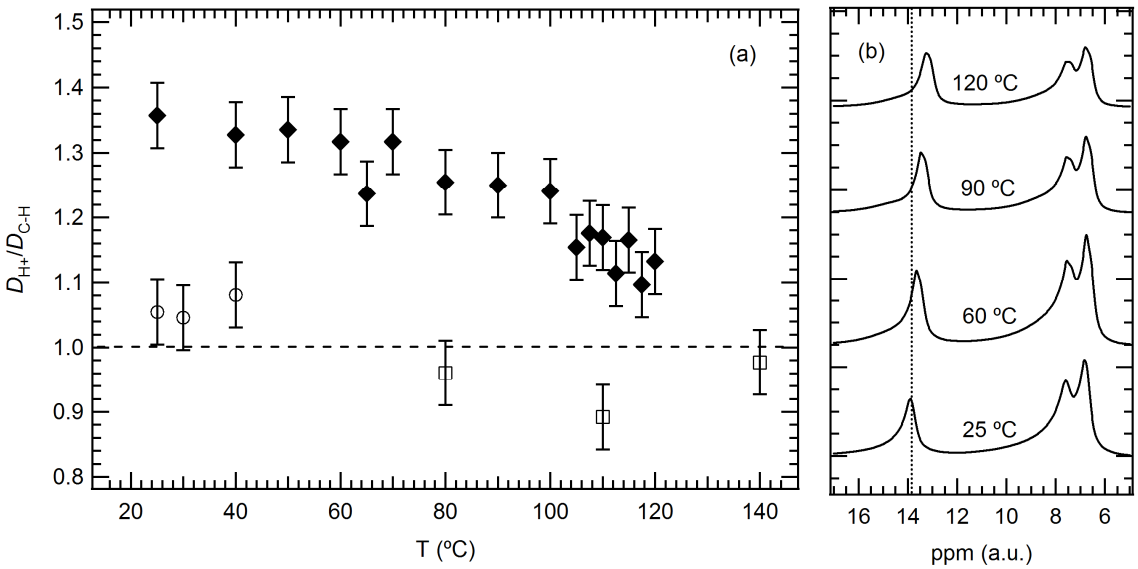


Figure 5.2. Proton Hopping in [Im][TFSI]. (a) D_{H+}/D_{C-H} as a function of temperature for 4:1 [Im][TFSI] (solid diamonds), 1:1 [Im][TFSI] (open squares) and 3:7 [Im][TFSI] (open circles). D_{H+}/D_{C-H} is greater than one in 4:1 [Im][TFSI], indicating proton hopping. (b) ^{1}H NMR spectra of 4:1 [Im][TFSI] at various temperatures, derived from PGSE experiments at the lowest gradient strength. The N-H proton peak shifts to lower ppm at higher temperatures, reflecting changes in the hydrogen bond structure with temperature.

than one in 4:1 [Im][TFSI] (D_{H+}/D_{C-H}=1.36 at 25 ºC, in close agreement with previous work[2]). Proton hopping decreases with increasing temperature, but persists over the entire experimental temperature range; D_{H+}/D_{C-H} decreases to about 1.1 at 120 ºC. Since proton hopping relies on hydrogen bonding between imidazole molecules,[4, 7-10] it is expected that the decrease in proton hopping at elevated temperatures is related to a number of changes that occur in the imidazole hydrogen bond structure with increased temperature. These include an increased hydrogen bond length, shortened average lifetime, or decreased number of hydrogen bonds.[29, 30] Figure 5.2b shows how the NMR spectrum of 4:1 [Im][TFSI] evolves with increasing temperature. The peak that corresponds to N-H protons, which is farthest downfield, shifts upfield with increasing temperature. This peak shift reflects the overall increased electron density surrounding the nuclei of the N-H protons that accompanies the changes in hydrogen bond structure.[2]

The relationship between hydrogen bond character and proton transport is complex because proton hopping relies on the existence of hydrogen bonds as well as the ability of hydrogen bonds within the network to break and reform.[4, 7-10] Proton diffusion enhancement due to the analogous Grotthuss mechanism in water increases with increasing temperature between about 0 and 150 ºC, and decreases at higher temperatures; hydrogen bond reconstruction is the limiting process at low temperatures, whereas the diminished extent of hydrogen bonding is the limiting factor at high temperatures.[31, 32] In contrast, proton hopping in 4:1 [Im][TFSI] decreases monotonically with increasing temperature between 25 and 120 ºC, implying that the overall weakening of the hydrogen bond network is the limiting factor for proton hopping in this entire temperature range.

QENS experiments provide more details about proton dynamics in [Im][TFSI]. The relatively large incoherent neutron scattering cross section of ^{1}H compared to other atoms leads to the selective observation of self-correlated hydrogen motion in QENS experiments, making QENS an ideal tool for studying proton transport mechanisms. Ionic liquids synthesized from deuterated imidazole were used for QENS experiments in order to selectively observe acidic proton dynamics, although some exchange between acidic protons and N-H protons was expected to occur. Fixed window scans (FWS) were performed on the HFBS first to ascertain how the proton dynamics are affected by thermal transitions in all the samples including pure *d*4-imidazole and HTFSI. The mean squared displacements of protons, $\langle u^2(T)\rangle$, were calculated from FWS experiments using the following expression relating $\langle u^2(T)\rangle$ to the elastic scattering intensity, I(q,T):

$$I(q,T) = \exp\left[-\frac{q^2\langle u^2(T)\rangle}{3}\right] \tag{5.3}$$

Equation 5.3 makes use of the Gaussian approximation, which presumes that the distribution of particle displacements at long times is Gaussian, as it would be in a system made up of harmonic oscillators in thermal equilibrium.[33] Figure 5.3 shows $\langle u^2(T)\rangle$ as a function of temperature for 3:7 and 4:1 [*d*Im][TFSI]. At the lowest temperatures, the mean squared displacements of the two ionic liquids are similar, and increase slowly and linearly with temperature, consistent with the Debye-Waller factor. The mean squared displacements begin to diverge near the known[2] glass transition temperature, T_g, of each

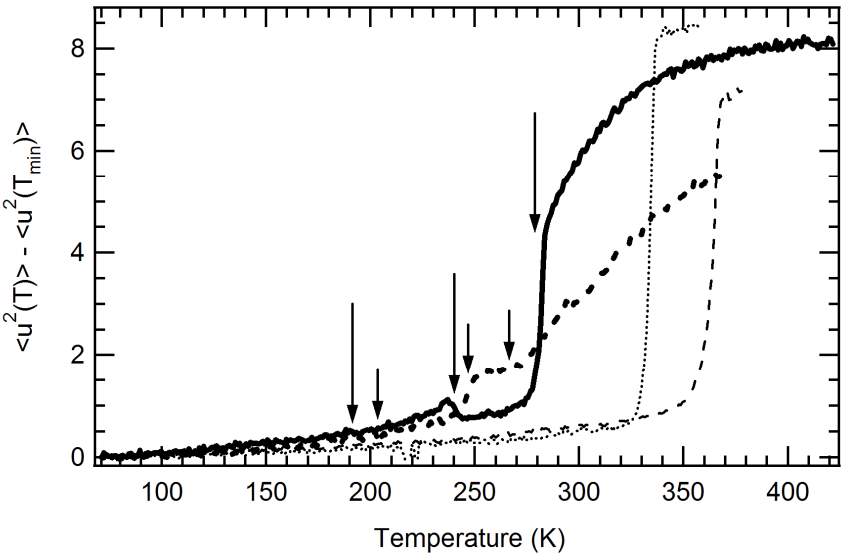


Figure 5.3. Mean Squared Displacement of Protons in [Im][TFSI]. Mean squared displacement of protons as a function of temperature for 3:7 [*d*Im][TFSI] (thick dashed line), 4:1 [*d*Im][TFSI] (thick solid line), *d*4-imidazole (thin dashed line), and HTFSI (thin dotted line). T_g, T_c, and T_m from reference 2 are indicated with short and long arrows for 3:7 and 4:1 [*d*Im][TFSI], respectively, where the transitions increase in temperature in the order $T_g<T_c<T_m$.

ionic liquid. The observed crystallization and melting temperatures of each ionic liquid, T_c and T_m, respectively, agree well with DSC experiments.[2] QENS experiments on the HFBS were performed above the T_m of each ionic liquid in the temperature regimes where the mean squared displacements increase steadily with temperature. Higher temperatures could be probed using the DCS because it measures higher-energy scattering corresponding to faster motions. QENS experiments were also performed on 4:1 [*d*Im][TFSI] between T_c and T_m by cooling the sample down from above T_m. For comparison, the mean squared displacements of *d*4-imidazole and HTFSI are also shown in Figure 5.3. The much sharper transitions at T_m and the plateaus in mean squared displacements above T_m indicate truly first-order transitions. Therefore, quasi-elastic scattering for these compounds above the transition temperatures are too high in energy to be measured by QENS experiments on the HFBS.

QENS experiments were performed using both the DCS and HFBS to probe proton dynamics over a wide energy range. Representative HFBS scattering profiles are shown in Figure 5.4. As the scattering vector q increases, the full-width at half maximum (FWHM) of quasi-elastic scattering increases, indicating translational motion processes in each energy range. Quasi-elastic scattering was modeled to quantify its q-dependence, and example fits are shown in Figure 5.5. Similar scattering profiles and fits were obtained for DCS data, and examples are shown in Figures 5.A.2 and 5.A.3 in the Appendix. Two Lorentzian functions were used to fully capture the scattering profiles, consistent with previous QENS studies of ionic liquids above T_m.[14, 16] In the case of DCS profiles, one Lorentzian describes the main quasi-elastic scattering contribution, and one describes the high-energy background signal. In the case of HFBS profiles, lower-energy processes are resolved compared to DCS profiles. One Lorentzian describes the main quasi-elastic scattering contribution in this energy range, and the second, broader Lorentzian is the same as the main Lorentzian in the DCS energy range.

The q-dependence of the FWHM of the quasi-elastic scattering contributions, Γ, provides information regarding the mechanism of translational proton motion. When diffusion is purely Fickian, Γ is expected to vary linearly with q^2 according to[34]

$$\Gamma/2 = \hbar D q^2 \tag{5.4}$$

Equation 5.4 adequately describes simple liquids such as argon[35] and even some more complex liquids such as the ionic liquid 1-butyl-3-methylimidazolium:chloride.[15] When molecular interactions are significant, for instance in the case of the ionic liquids 1-ethyl-3-methylimidazolium:bromide[14] and N,N,N',N'-tetramethylguanidinium: bis(perfluoroethylsulfonyl)imide ($[H_2NC(dma)_2][BETI]$)[16], deviations from Equation 5.4 are observed at high values of q corresponding to length scales smaller than the interaction distance. In these cases, the Jump-Diffusion model[36] is often used to describe the variation of Γ with q^2 as

$$\Gamma/2 = \frac{\hbar D q^2}{1 + D q^2 \tau_0} \tag{5.5}$$

where τ_0 is the residence time between jumps, or the molecular interaction time. Furthermore, the Jump-Diffusion model describes the complex dynamics of protons in supercooled water, which are dominated by Grotthuss proton transfer between water

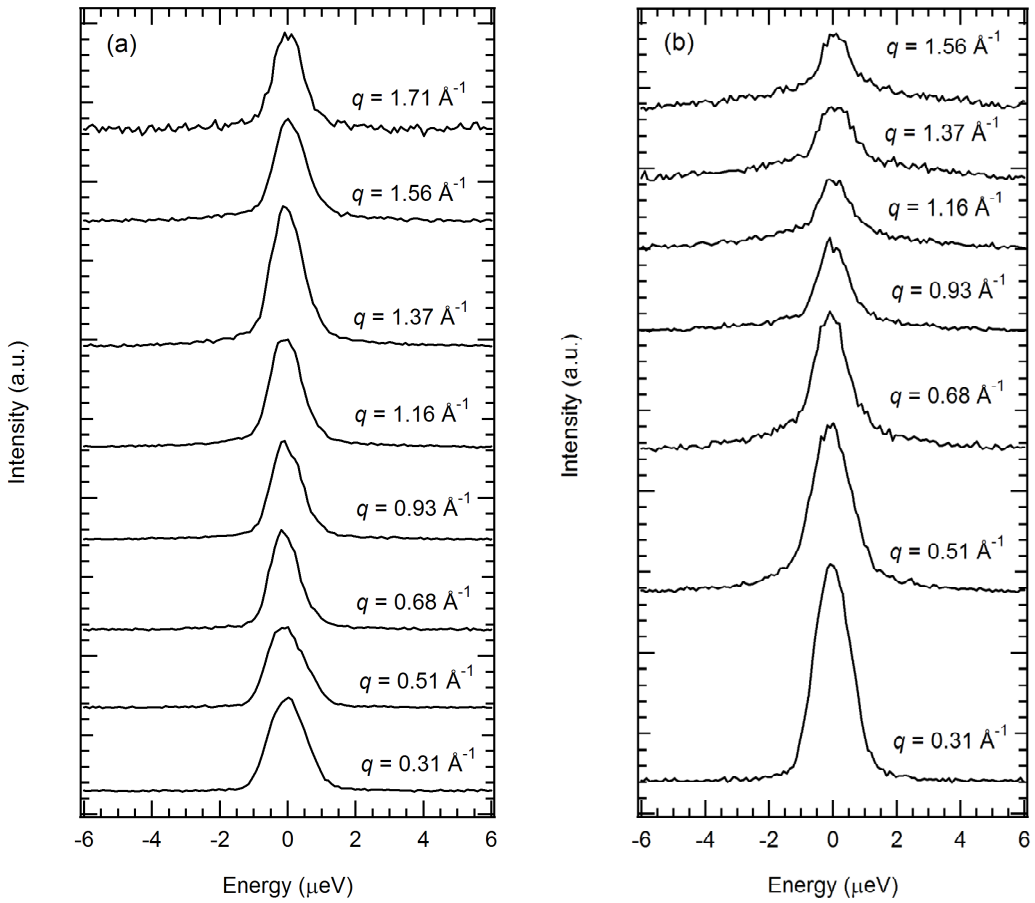


Figure 5.4. HFBS QENS Profiles for [Im][TFSI]. Example HFBS QENS profiles of (a) 3:7 [*d*Im][TFSI] and (b) 4:1 [*d*Im][TFSI] at 290 K. The full-width at half maximum (FWHM) of quasi-elastic scattering increases with increasing q, indicating translational motion processes.

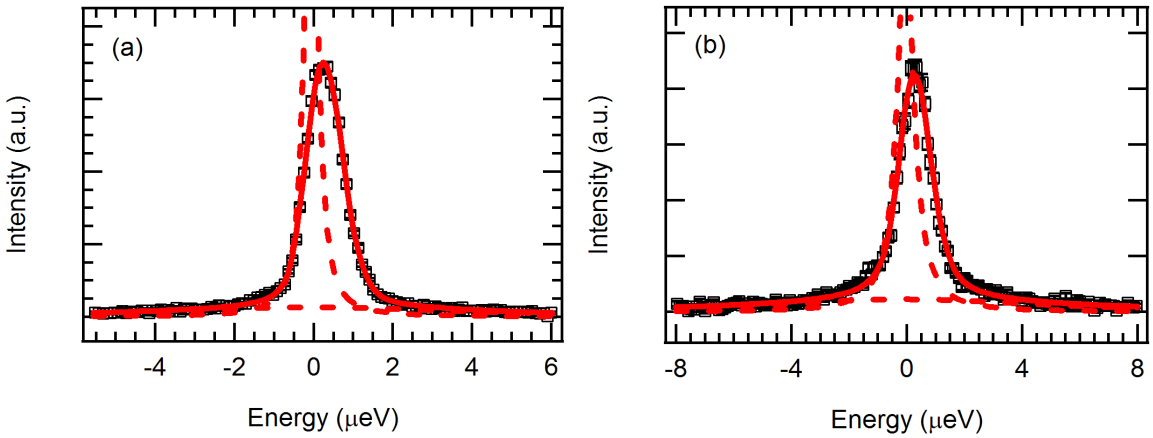


Figure 5.5. HFBS QENS Fits for [Im][TFSI]. Representative HFBS QENS profiles of (a) 3:7 [*d*Im][TFSI] at T=290 K and q=1.16 Å^{-1} and (b) 4:1 [*d*Im][TFSI] at T=270 K and q=0.99 Å^{-1}. The solid lines are the total fits to the data, while the dashed lines are the component fits (two Lorentzian functions).

molecules through hydrogen bonds.[19, 20] τ_0 in this case is the time between proton transfer events.

The FWHMs of the Lorentzians describing the main quasi-elastic scattering contributions to DCS and HFBS scattering profiles for 3:7 and 4:1 [*d*Im][TFSI] are plotted as a function of q^2 in Figures 5.6 and 5.7 at several temperatures. (The high energy background signal in DCS has very little q or temperature dependence.) Based on the complex diffusion observed previously in ionic liquids and water, it is unsurprising that the data for both ionic liquids deviate from linear behavior, and are described well by Equation 5.5. The nonlinearity probably reflects a combination of strong molecular interactions and proton hopping in the case of 4:1 [*d*Im][TFSI].

It is interesting that there are two distinct contributions to translational motion with different characteristic energies, one in the main energy range of the DCS and one in the main energy range of the HFBS. The diffusion coefficients associated with each process were estimated from the Equation 5.4 fits to the data, and are plotted in Figure 5.8 as a function of temperature along with $D_{N\text{-}H}$ measured by NMR. $D_{N\text{-}H}$ falls in between the diffusion coefficients associated with each process identified by QENS, confirming that both contribute to long-range proton diffusion. The lower-energy diffusion process (in the main energy range of HFBS) is the slower of the two. These data points fall closest to $D_{N\text{-}H}$ and have more similar activation energies to $D_{N\text{-}H}$, indicating that protons participating in the slower process contribute more to long-range N-H proton diffusion than those participating in the faster process. This suggests that either the faster diffusion process is spatially restricted and/or a greater population of N-H protons is able to participate in the slower diffusion process. Comparing the areas of the Lorentzians associated with each diffusion process in the HFBS scattering profiles confirms that both phenomena play a role. At low temperatures, the fraction of protons participating in the faster process is significantly smaller than that participating in the slower process (Figure 5.9). In addition, the number of protons participating in the faster process increases with increasing q, especially at high temperatures. This is indicative of a spatially confined process on the length scale of Angstroms.

Two translational diffusion processes have also been observed previously in the protic ionic liquid $[H_2NC(dma)_2][BETI]$, where the faster process was attributed to the motion of ions in structurally well-defined clusters with an associated length scale of 8 Å.[16] Such clusters have been observed in imidazolium based ionic liquids experimentally[37-40] and theoretically.[41-43] It is likely that this type of spatial heterogeneity also explains the existence of two translational diffusion processes in [*d*Im][TFSI]. In the case of $[H_2NC(dma)_2][BETI]$, the spatial confinement of the fast process was evidenced by a low-q (q^2<0.25 Å^{-2}) plateau in the FWHM of the higher-energy quasi-elastic signal. No such plateau is observed for [*d*Im][TFSI in Figure 5.6, but reliable DCS data below q^2=0.24 were not obtained.

The energetics of proton hopping are illuminated by comparing the proton dynamics of 4:1 [*d*Im][TFSI] and [Im][TFSI]. The quasi-elastic signal is more affected by proton hopping in the deuterated ionic liquid, which contains only N-H protons that come from

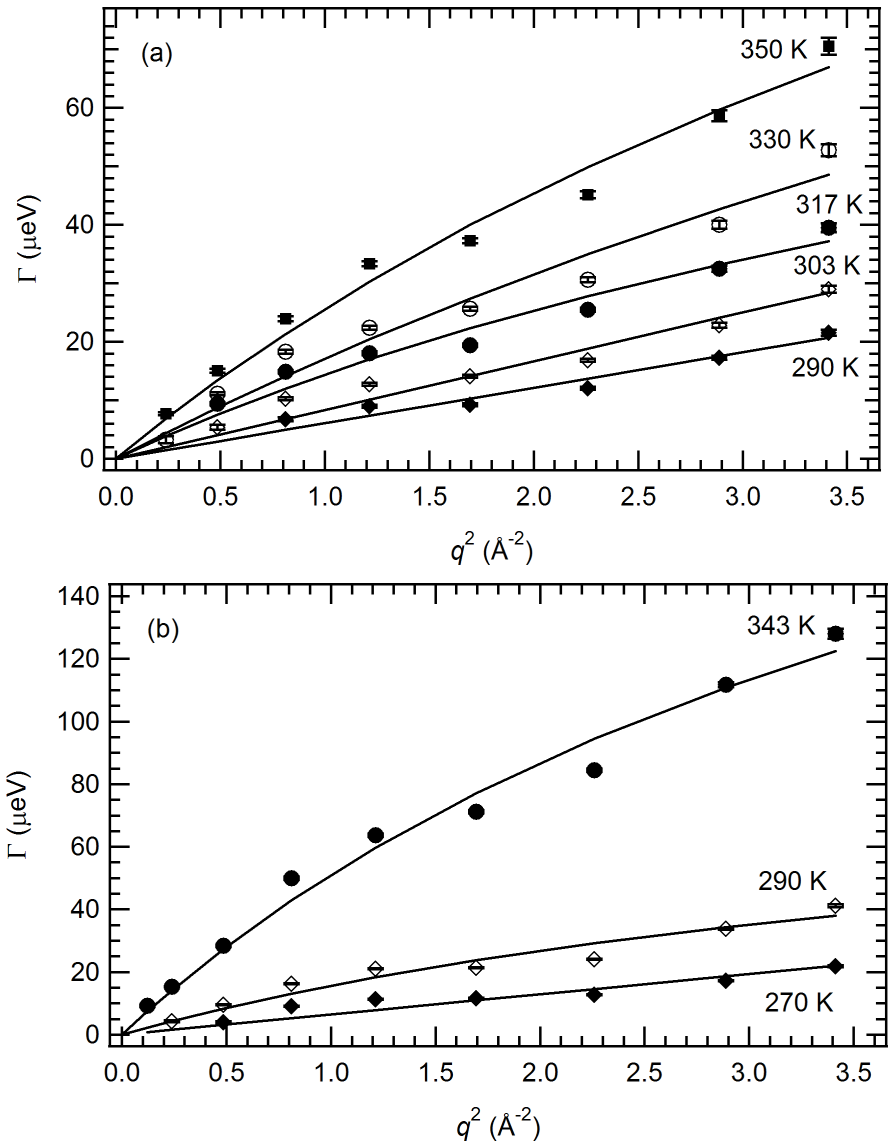


Figure 5.6. Dependence of DCS Quasi-elastic Scattering on Scattering Vector. Γof the main Lorentzian peak fit to the DCS QENS signal as a function of q^2 for (a) 3:7 [*d*Im][TFSI] and (b) 4:1 [*d*Im][TFSI] at various temperatures. Error bars represent one standard deviation of the Lorentzian fits. Solid curves are fits to the data using Equation 5.4.

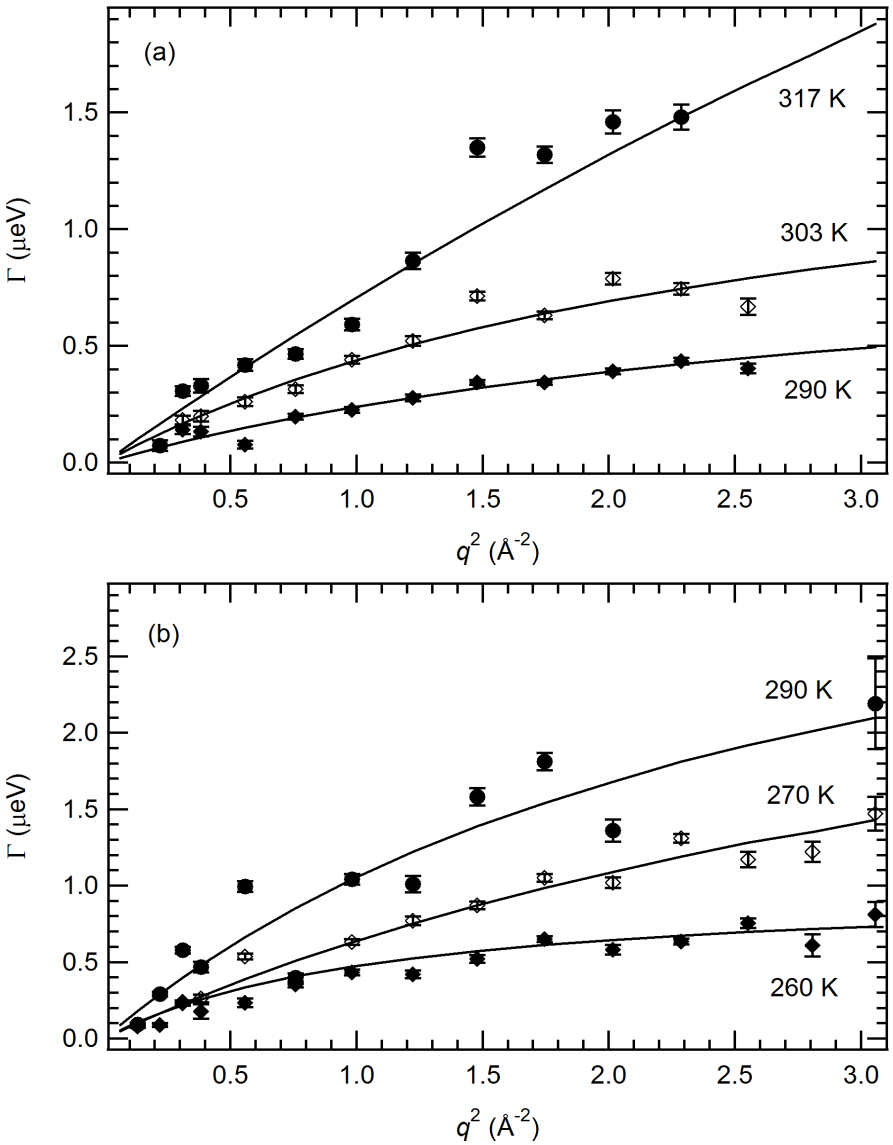


Figure 5.7. Dependence of HFBS Quasi-elastic Scattering on Scattering Vector. Γof the main Lorentzian peak fit to the HFBS QENS signal as a function of q^2 for (a) 3:7 [*d*Im][TFSI] and (b) 4:1 [*d*Im][TFSI] at various temperatures. Error bars represent one standard deviation of the Lorentzian fits. Solid curves are fits to the data using Equation 5.4.

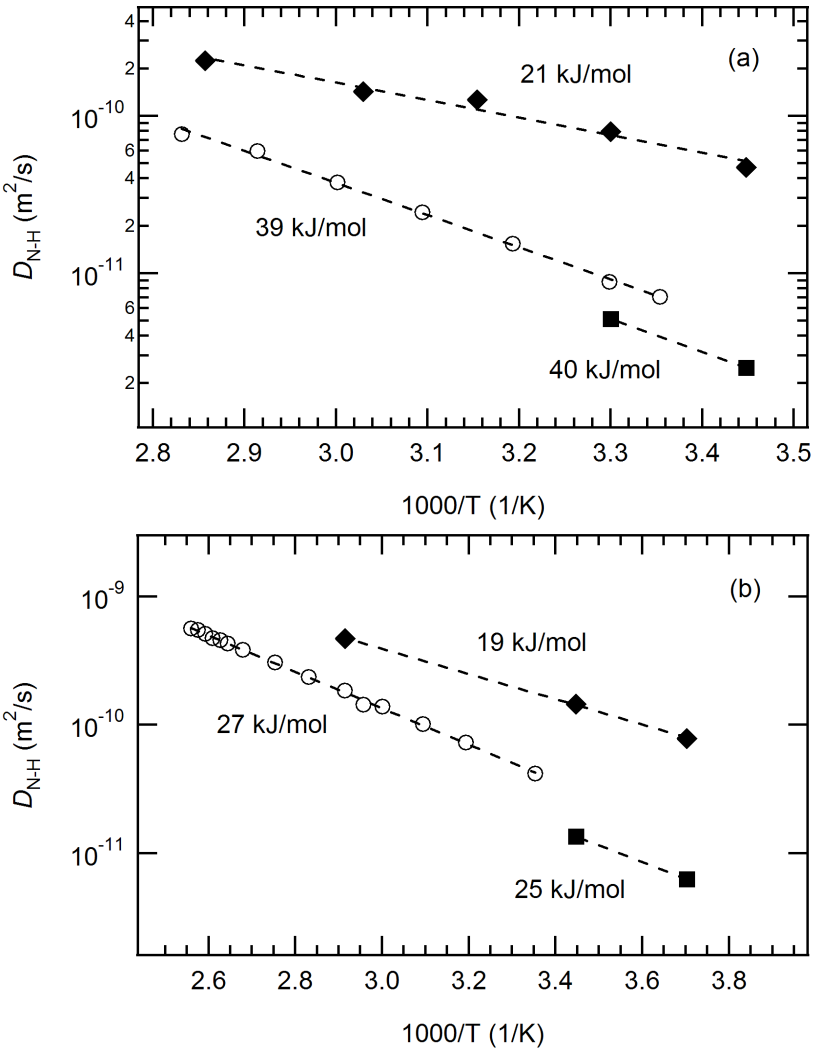


Figure 5.8. Proton Diffusion in [Im][TFSI]. $D_{N\text{-}H}$ measured with NMR (open circles) compared to D calculated from DCS (closed diamonds) and HFBS (closed squares) measurements for (a) 3:7 [*d*Im][TFSI] and (b) 4:1 [*d*Im][TFSI]. Arrhenius fits are shown with dashed lines, and activation energies determined by the fits are labeled.

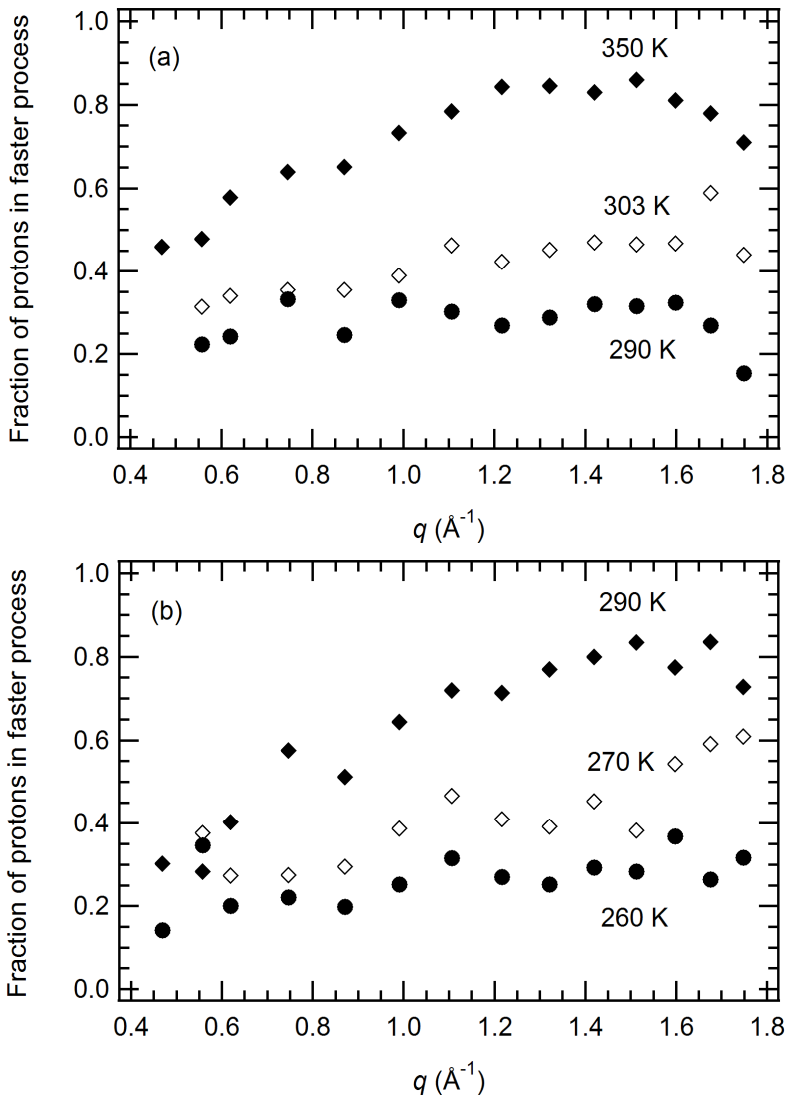


Figure 5.9. Fraction of Fast Proton Diffusion Process. Fraction of quasi-elastic scattering due to proton participating in faster, high-energy process as a function of q for (a) 3:7 [*d*Im][TFSI] and (b) 4:1 [*d*Im][TFSI] at various temperatures. The fractions were determined by comparing the peak areas of each Lorentzian in HFBS scattering profiles.

HTFSI, than in the hydrogenated ionic liquid, which contains C-H and N-H protons. Figure 5.10 shows Γ vs q^2 from DCS and HFBS experiments on both samples at 290 K. There is a much greater discrepancy between the HFBS data for the hydrogenated and deuterated ionic liquids than between the DCS data sets, implying that proton hopping is mostly contained in the slower, unconfined process that contributes most to long-range proton diffusion. This result is reasonable since it is clear that proton hopping strongly influences long-range proton diffusion.[2, 3] While the Γ vs q^2 data for both 4:1 [*d*Im][TFSI] and [Im][TFSI] demonstrate nonlinear behavior, the data for the deuterated ionic liquid clearly exhibit a greater deviation from linearity due to proton hopping.

To our knowledge, this is the first time that the proton hopping mechanism in imidazole has been observed by QENS. It is expected that with improved signal-to-noise in combination with more sophisticated mathematical models and/or numerical simulation, future QENS experiments could quantify the degree of proton hopping and characterize important hopping parameters including hop distance, time scale for proton hopping and imidazole reorientation, and activation energy for hops. This would not only be useful for providing insight into proton transport mechanisms in ionic liquids, but would also be invaluable for evaluating ionic liquid-containing membranes of interest for electrochemical applications.[44]

As a result of proton hopping, 4:1 [Im][TFSI] achieves greater proton transport as well as a higher H^+ transference number than the ionic liquids without excess imidazole. As shown in Figure 5.11, molecular diffusion is already greatest in 4:1 [Im][TFSI], most likely because it has the lowest T_g (T_g=-81 ºC, compared to T_g=-68 ºC for 3:7 [Im][TFSI] and T_m=73 ºC for 1:1 [Im][TFSI], which does not have a measurable T_g[2]). D_{H+} is further enhanced as a result of proton hopping. Furthermore, since proton transport becomes somewhat decoupled from simple vehicle diffusion of imidazolium cations, the H^+ transference number is high, ranging between 0.66 and 0.78 in the experimental temperature range. Without proton hopping, the transference number would be much closer to 0.50 since $D_{C\text{-}H}$ and D_{TFSI} are very similar.

In addition to having high proton diffusion and a high H^+ transference number, there is very little ion aggregation in 4:1 [Im][TFSI], allowing very high ionic conductivity to be achieved. The degree of ion aggregation is estimated by comparing the measured bulk ionic conductivity to that predicted by the ion diffusion coefficients measured by NMR and the Nernst Einstein equation:

$$\sigma = \frac{F^2}{RT}\left(c_{m,H+}D_{H+} + c_{m,TFSI}D_{TFSI}\right) \tag{5.6}$$

where $c_{m,H+}$ and $c_{m,TFSI}$ are the molar concentrations of acidic protons and TFSI anions, respectively. The predicted conductivity of 4:1 [Im][TFSI] is very close to the actual conductivity (Figure 5.12), indicating that there is very little ion aggregation. In contrast, ion aggregation in 3:7 and 1:1 [Im][TFSI] causes the ionic conductivity to be lower than that predicted by Equation 5.6.

5.4. Conclusion

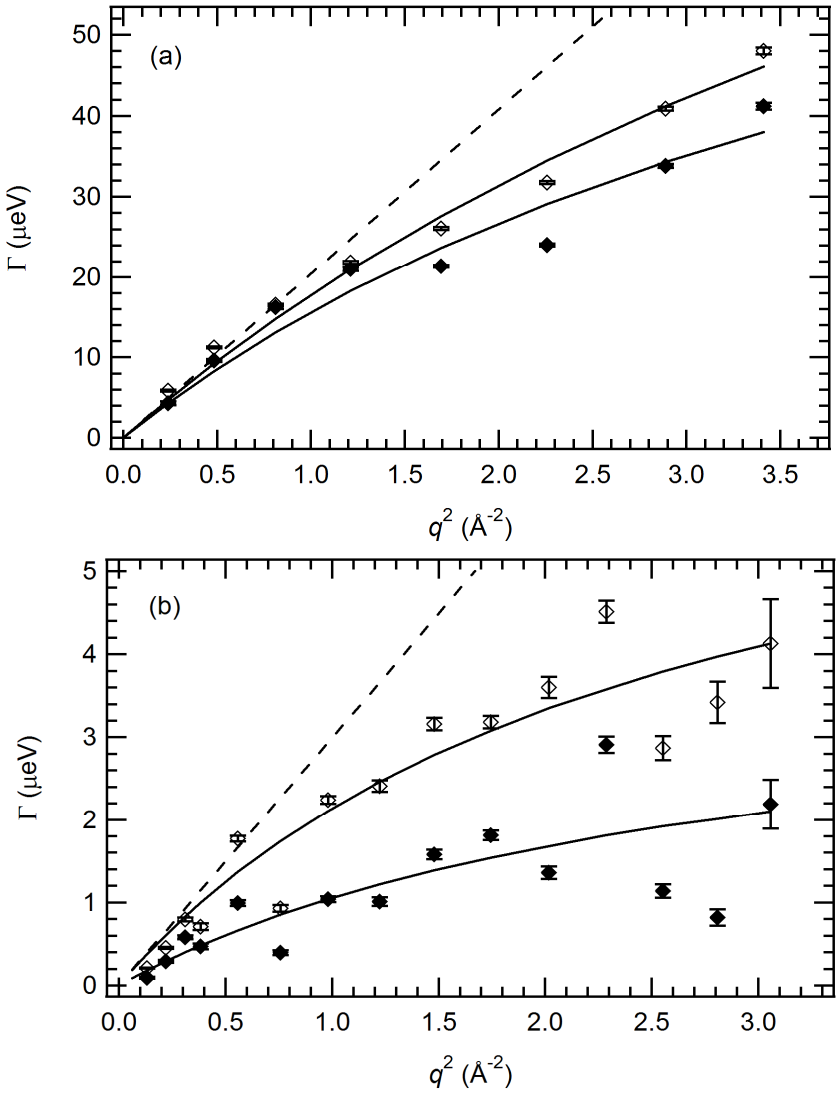


Figure 5.10. Quasi-elastic Scattering of 4:1 [Im][TFSI] and 4:1 [*d*Im][TFSI]. Γof the main Lorentzian peak fit to the (a) DCS and (b) HFBS QENS signal as a function of q^2 for 4:1 [*d*Im][TFSI] (closed symbols) and 4:1 [Im][TFSI] (open symbols) at 290 K. Error bars represent one standard deviation of the Lorentzian fits. Solid curves are fits to the data using Equation 5.4. Dashed curves are Fickian diffusion curves (Equation 5.3) using the diffusion coefficients derived from Equation 5.4 fits to 4:1 [*d*Im][TFSI] data.

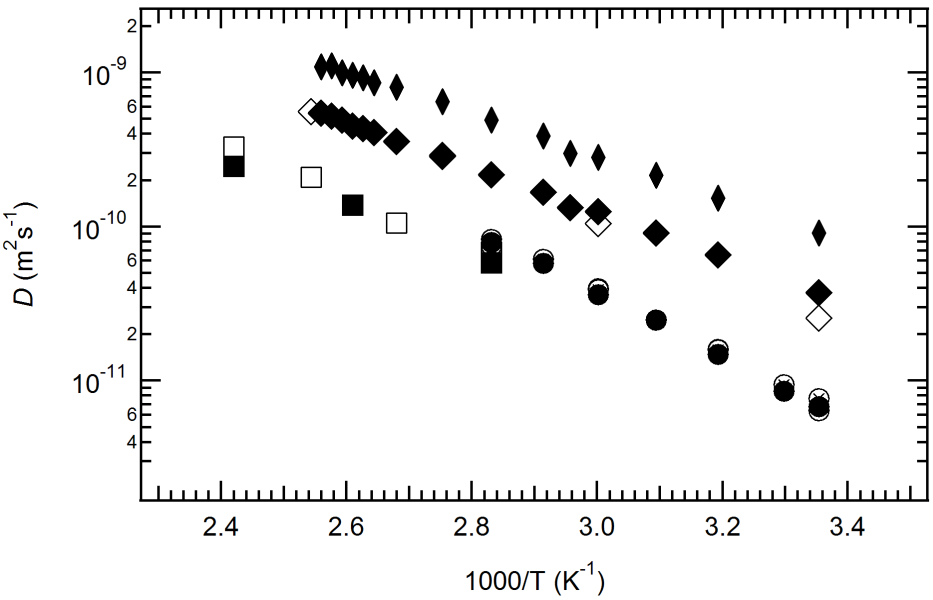


Figure 5.11. Diffusion in [Im][TFSI]. $D_{C\text{-}H}$ (closed symbols) and D_{TFSI} (open symbols) for 4:1 [Im][TFSI] (diamonds), 1:1 [Im][TFSI] (squares) and 3:7 [Im][TFSI] (circles). For 3:7 [Im][TFSI], D_{TFSI} was measured by ^{19}F and ^{1}H (circles marked with X) NMR. D_{H+} for 4:1 [Im][TFSI] are represented by narrow closed diamonds.

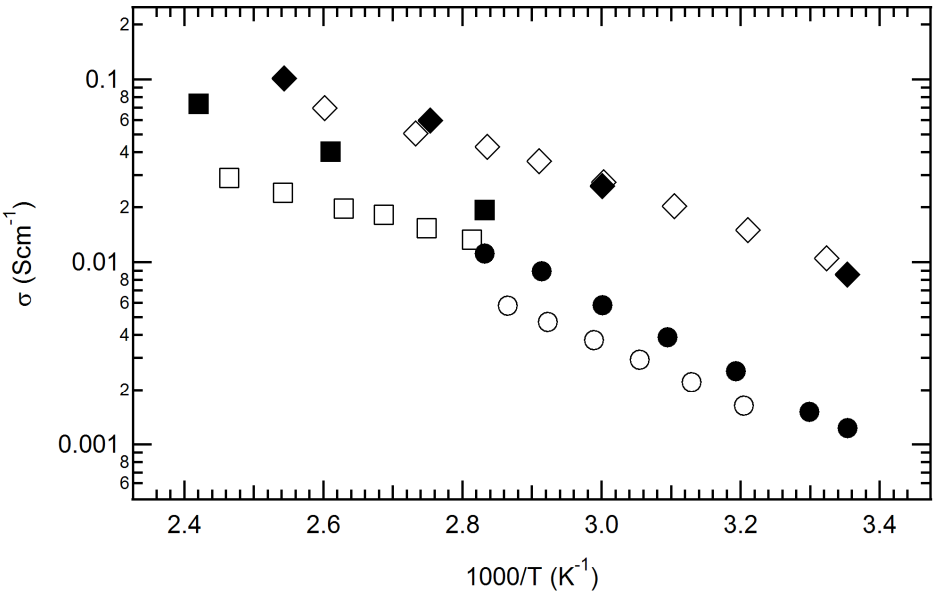


Figure 5.12. Ionic Conductivity of [Im][TFSI]. Measured σ (open symbols) and σ calculated from NMR diffusion coefficients and Nernst-Einstein equation (closed symbols) for 4:1 [Im][TFSI] (diamonds), 1:1 [Im][TFSI] (squares) and 3:7 [Im][TFSI] (circles). Measured σ is in good agreement with previously reported measurements.[2]

Proton transport in [Im][TFSI] ionic liquids was investigated using NMR and QENS, with specific focus on the proton hopping mechanism that occurs when the ionic liquid contains excess imidazole. Proton hopping was found to decrease with increasing temperature, but significant proton hopping exists even at the maximum experimental temperature of 120 ºC. This, in combination with minimal ion aggregation, leads to high proton conductivity over a wide temperature range. Furthermore, proton hopping results in a partial decoupling of proton transport from imidazole diffusion, which leads to a high H^+ transference number.

Proton hopping was shown to be characterized by a deviation from a linear Γ vs q^2 relationship in QENS experiments, opening the door for future QENS studies of proton hopping in ionic liquids and ionic liquid composite materials. In addition, two contributions to translational diffusion were identified. Proton hopping is mostly encompassed in the slower, lower-energy process, which contributes most to long-range proton diffusion.

5.5. Acknowledgements

This material is based upon work performed by the Joint Center for Artificial Photosynthesis, a DOE Energy Innovation Hub, as follows: Material preparation and investigation of ionic liquid dynamics was supported by the Assistant Secretary for Energy Efficiency and Renewable Energy, Office of Hydrogen, Fuel Cell, and Infrastructure Technologies of the U.S. Department of Energy under Contract No. DE-AC02-05CH11231; Continued investigation of ionic liquid dynamics and interpretation of dynamical data was supported through the Office of Science of the U.S. Department of Energy under Award Number DE-SC0004993. M.L. Hoarfrost thanks support from an NSF Graduate Research Fellowship. This work utilized facilities at the NIST Center for Neutron Research (NCNR) supported in part by the National Science Foundation under Agreement No. DMR-0944772. We gratefully acknowledge Dr. Timothy Jenkins and Dr. Craig Brown for experimental assistance at the NCNR as well as Dr. Joel Stettler for technical assistance with NMR experiments. This report was prepared as an account of work sponsored by an agency of the United States Government. Neither the United States Government nor any agency thereof, nor any of their employees, makes any warranty, express or implied, or assumes any legal liability or responsibility for the accuracy, completeness, or usefulness of any information, apparatus, product, or process disclosed, or represents that its use would not infringe privately owned rights. Reference herein to any specific commercial product, process, or service by trade name, trademark, manufacturer, or otherwise does not necessarily constitute or imply its endorsement, recommendation, or favoring by the United States Government or any agency thereof. The views and opinions of authors expressed herein do not necessarily state or reflect those of the United States Government or any agency thereof.

5.6. Appendix: Supporting PGSE NMR and QENS

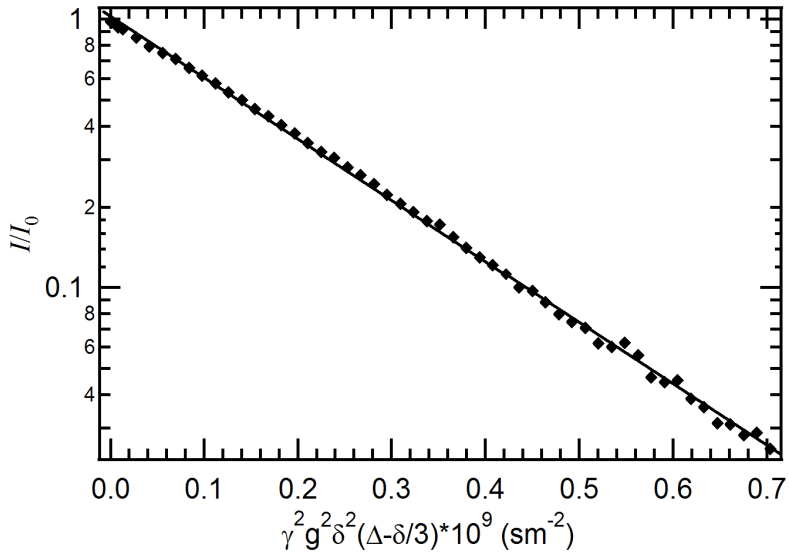


Figure 5.A.1. PGSE NMR Data for [Im][TFSI]. Representative ^{1}H PGSE data and fits for N-H protons in 8:2 [Im][TFSI] at 70 ºC. The log of the signal attenuation has the expected linear decay with $\gamma^2g^2\delta^2(\Delta-\delta/3)$.

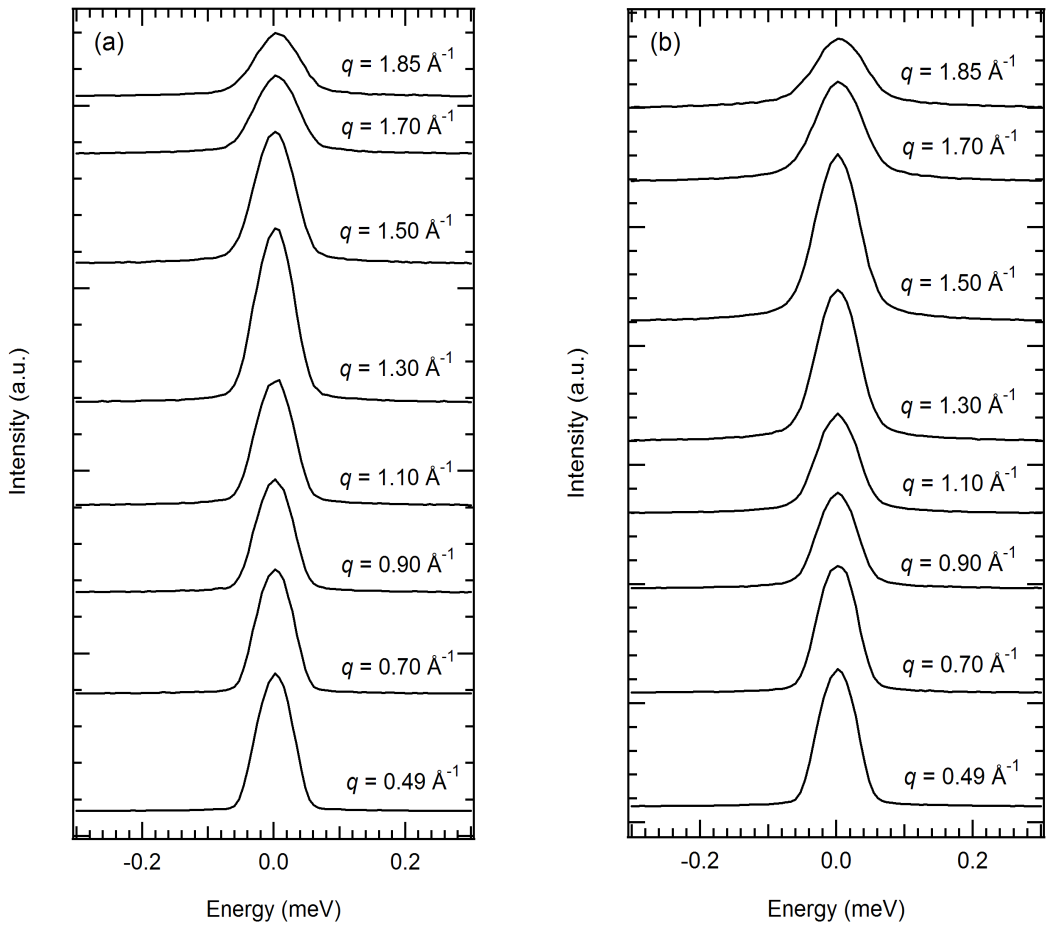


Figure 5.A.2. DCS QENS Profiles for [Im][TFSI]. Example DCS QENS scattering profiles of (a) 3:7 [*d*Im][TFSI] and (b) 4:1 [*d*Im][TFSI] at 290 K.

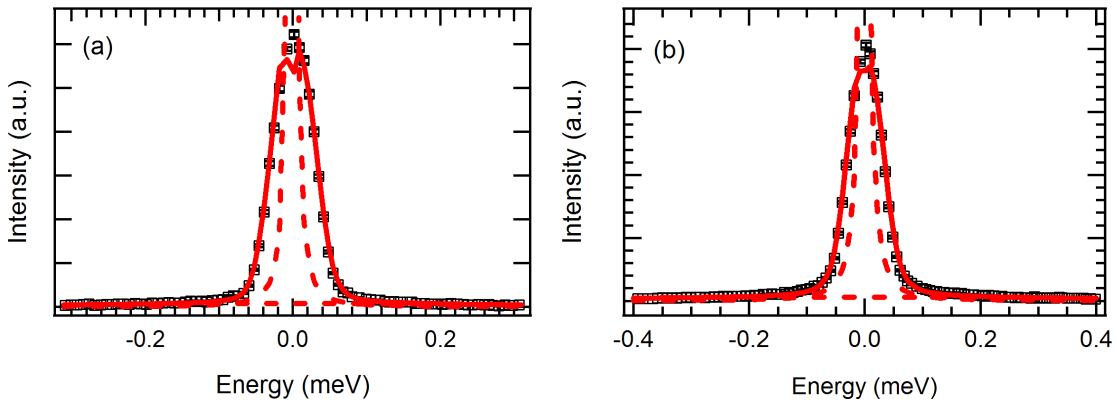


Figure 5.A.3. DCS QENS Fits for [Im][TFSI]. Representative DCS QENS profiles of (a) 3:7 [*d*Im][TFSI] at T=290 K and q=1.16 Å^{-1}and (b) 4:1 [*d*Im][TFSI] at T=270 K and q=0.99 Å^{-1}. The solid lines are the total fits to the data, while the dashed lines are the component fits (two Lorentzian functions).

5.7. References

1. Ohno, H., *Electrochemical Aspects of Ionic Liquids*. Wiley-Interscience: New York, 2005.
2. Noda, A.; Susan, A. B.; Kudo, K.; Mitsushima, S.; Hayamizu, K.; Watanabe, M. *Journal of Physical Chemistry B* **2003,** 107, (17), 4024-4033.
3. Kreuer, K. D.; Fuchs, A.; Ise, M.; Spaeth, M.; Maier, J. *Electrochimica Acta* **1998,** 43, (10-11), 1281-1288.
4. Munch, W.; Kreuer, K. D.; Silvestri, W.; Maier, J.; Seifert, G. *Solid State Ionics* **2001,** 145, (1-4), 437-443.
5. Ueki, T.; Watanabe, M. *Macromolecules* **2008,** 41, (11), 3739-3749.
6. Riehl, N. *Transactions of the New York Academy of Sciences* **1965,** 27, (7), 772-&.
7. Hen, H.; Yan, T. Y.; Voth, G. A. *Journal of Physical Chemistry A* **2009,** 113, (16), 4507-4517.
8. Iannuzzi, M. *Journal of Chemical Physics* **2006,** 124, (20).
9. Iannuzzi, M.; Parrinello, M. *Physical Review Letters* **2004,** 93, (2).
10. Yan, S. H.; Bu, Y. X.; Cao, Z. H.; Li, P. *Journal of Physical Chemistry A* **2004,** 108, (34), 7038-7049.
11. Daycock, J. T.; Jones, G. P.; Evans, J. R. N.; Thomas, J. M. *Nature* **1968,** 218, (5142), 672-&.
12. Goward, G. R.; Saalwachter, K.; Fischbach, I.; Spiess, H. W. *Solid State Nuclear Magnetic Resonance* **2003,** 24, (2-3), 150-162.
13. Fischbach, I.; Spiess, H. W.; Saalwachter, K.; Goward, G. R. *Journal of Physical Chemistry B* **2004,** 108, (48), 18500-18508.
14. Aoun, B.; Gonzalez, M. A.; Ollivier, J.; Russina, M.; Izaola, Z.; Price, D. L.; Saboungi, M. L. *Journal of Physical Chemistry Letters* **2010,** 1, (17), 2503-2507.
15. Inamura, Y.; Yamamuro, O.; Hayashi, S.; Hamaguchi, H. O. *Physica B-Condensed Matter* **2006,** 385, 732-734.
16. Mamontov, E.; Luo, H. M.; Dai, S. *Journal of Physical Chemistry B* **2009,** 113, (1), 159-169.
17. Triolo, A.; Russina, O.; Arrighi, V.; Juranyi, F.; Janssen, S.; Gordon, C. M. *Journal of Chemical Physics* **2003,** 119, (16), 8549-8557.
18. Triolo, A.; Russina, O.; Hardacre, C.; Nieuwenhuyzen, M.; Gonzalez, M. A.; Grimm, H. *Journal of Physical Chemistry B* **2005,** 109, (46), 22061-22066.
19. Chen, S. H.; Teixeira, J.; Nicklow, R. *Physical Review A* **1982,** 26, (6), 3477-3482.
20. Teixeira, J.; Bellissentfunel, M. C.; Chen, S. H.; Dianoux, A. J. *Physical Review A* **1985,** 31, (3), 1913-1917.
21. Skold, K.; Nelin, G. *Journal of Physics and Chemistry of Solids* **1967,** 28, (12), 2369-&.
22. Rowe, J. M.; Skold, K.; Flotow, H. E.; Rush, J. J. *Journal of Physics and Chemistry of Solids* **1971,** 32, (1), 41-&.
23. Hempelmann, R.; Karmonik, C.; Matzke, T.; Cappadonia, M.; Stimming, U.; Springer, T.; Adams, M. A. *Solid State Ionics* **1995,** 77, 152-156.
24. Ishikawa, A.; Maekawa, H.; Yamamura, T.; Kawakita, Y.; Shibata, K.; Kawai, M. *Solid State Ionics* **2008,** 179, (40), 2345-2349.

25. Price, W. S. *Concepts in Magnetic Resonance* **1998,** 10, (4), 197-237.
26. Stejskal, E. O.; Tanner, J. E. *Journal of Chemical Physics* **1965,** 42, (1), 288-292.
27. Raiford, D. S.; Fisk, C. L.; Becker, E. D. *Analytical Chemistry* **1979,** 51, (12), 2050-2051.
28. Azuah, R. T.; Kneller, L. R.; Qiu, Y. M.; Tregenna-Piggott, P. L. W.; Brown, C. M.; Copley, J. R. D.; Dimeo, R. M. *Journal of Research of the National Institute of Standards and Technology* **2009,** 114, (6), 341-358.
29. Cavalcanti, W. L.; Portaluppi, D. F.; Joswig, J. O. *Journal of Chemical Physics* **2010,** 133, (10).
30. Kanaskov.Yd; Sukhoruk.Bi; Pentin, Y. A.; Komarovs.Gv. *Izvestiya Akademii Nauk Sssr-Seriya Khimicheskaya* **1970**, (8), 1735.
31. Gierer, A.; Wirtz, K. *Journal of Chemical Physics* **1949,** 17, (8), 745-746.
32. Gileadi, E.; Kirowa-Eisner, E. *Electrochimica Acta* **2006,** 51, (27), 6003-6011.
33. Zorn, R. *Nuclear Instruments & Methods in Physics Research Section a-Accelerators Spectrometers Detectors and Associated Equipment* **2007,** 572, (2), 874-881.
34. Bee, M., *Quasielastic Neutron Scattering: Principles and Applications in Solid State Chemistry, Biology and Materials Science*. IOP Publishing Ltd: 1988.
35. Dasannacharya, B. A.; Rao, K. R. *Physical Review* **1965,** 137, (2A), A417-A427.
36. Chudley, C. T.; Elliott, R. J. *Proceedings of the Physical Society of London* **1961,** 77, (494), 353-361.
37. AbdulSada, A. K.; Elaiwi, A. E.; Greenway, A. M.; Seddon, K. R. *European Mass Spectrometry* **1997,** 3, (3), 245-247.
38. Dupont, J. *Journal of the Brazilian Chemical Society* **2004,** 15, (3), 341-350.
39. Gozzo, F. C.; Santos, L. S.; Augusti, R.; Consorti, C. S.; Dupont, J.; Eberlin, M. N. *Chemistry-a European Journal* **2004,** 10, (23), 6187-6193.
40. Kuang, Q. L.; Zhang, J.; Wang, Z. G. *Journal of Physical Chemistry B* **2007,** 111, (33), 9858-9863.
41. Del Popolo, M. G.; Voth, G. A. *Journal of Physical Chemistry B* **2004,** 108, (5), 1744-1752.
42. Habasaki, J.; Ngai, K. L. *Journal of Chemical Physics* **2008,** 129, (19).
43. Morrow, T. I.; Maginn, E. J. *Journal of Physical Chemistry B* **2002,** 106, (49), 12807-12813.
44. Hoarfrost, M. L.; Tyagi, M. S.; Segalman, R. A.; Reimer, J. A. *Macromolecules* **2012,** 45, (7), 3112-3120.

Chapter 6. Effect of Confinement on Proton Transport Mechanisms in Block Copolymer/Ionic Liquid Membranes

Reproduced with permission from Megan L. Hoarfrost, Madhu S. Tyagi, Rachel A. Segalman, and Jeffrey A. Reimer, Macromolecules, 2012, 45(7), pp. 3112-3120. 2012 American Chemical Society

Nanostructured membranes containing structural and proton-conducting domains are of great interest for a wide range of applications requiring high conductivity coupled with high thermal stability. Understanding the effect of nanodomain confinement on proton-conducting properties in such materials is essential for designing new, improved membranes. This relationship has been investigated for a lamellae-forming mixture of poly(styrene-*b*-2-vinyl pyridine) (PS-*b*-P2VP) with ionic liquid composed of imidazole and bis(trifluoromethylsulfonyl)imide, where the ionic liquid selectively resides in the P2VP domains of the block copolymer. Quasi-elastic neutron scattering and NMR diffusion measurements reveal increased prevalence of a fast proton hopping transport mechanism, which we hypothesize is due to changes in the hydrogen bond structure of the ionic liquid under confinement. This, in combination with unique ion aggregation behavior, leads to a lower activation energy for macroscopic ion transport compared to that in a mixture of ionic liquid with P2VP homopolymer. The proton transference number in both samples is significantly higher than in the neat ionic liquid, which could be taken advantage of for applications such as proton exchange membrane fuel cells and actuators. These results portend the rational design of nanostructured membranes having improved mechanical properties and conductivity.

6.1. Introduction

Nanostructured membranes containing structural and ion-conducting phases are of great interest for a wide variety of applications requiring high ionic conductivity coupled with mechanical durability. Such membranes may be designed to exhibit continuous ion-conducting channels that lead to enhanced conductivity compared to non-ordered materials. For instance, Nafion™ (Dupont) is currently the industry standard proton-conducting polymer membrane for many applications due to its exceptional conductivity and mechanical properties that have been attributed to its nanoscale phase separation into conducting, water-filled domains and structural, hydrophobic domains.[1] Furthermore, materials designed to have well-ordered, continuous nanostructures have significantly higher conductivities than comparable nonordered materials.[2, 3] Understanding the effect of morphology on conductivity has become increasingly important in recent years as a tool for designing new, improved membranes.[4-9]

Of the many factors contributing to improved conductivity in nanostructured membranes (including conducting phase continuity and increased contrast between conducting and structural phases[4, 8, 9]), we expect differences in the local charge carrier environment near the "walls" of conducting phases to have a significant impact on the mechanism of conductivity. It has been shown, for example, that hydrogen bonding is significantly different at the walls of confined water domains,[10-13] and that such effects have

significant implications for proton transport in hydrated Nafion.[14-18] A few studies of nanostructured materials with ion carriers other than water have also identified wall effects on the mechanism of conductivity.[19, 20] These effects were deduced largely based on bulk conductivity measurements. In one case, NMR experiments also provided clues as to how the local dynamics change,[20] but determining exactly how confinement affects the molecular mechanisms of conductivity remains difficult.

Mixing a block copolymer with an ionic liquid is one route to obtaining nanostructured, ion-conducting membranes having high ionic conductivity coupled with favorable mechanical durability. Ionic liquids have been selectively incorporated into one phase of a diblock copolymer, where the second phase imparts mechanical durability to the membrane.[21-26] Such membranes self-assemble into well-defined nanostructures, making them ideal materials for studying the relationship between structure and conductivity. In this work, the effect of confinement on the mechanism of conductivity has been investigated for mixtures of the diblock copolymer poly(styrene-*b*-2-vinyl pyridine) (PS-*b*-P2VP) with the proton-conducting ionic liquid, imidazolium:bis(trifluoromethylsulfonyl)imide ([Im][TFSI]) having an excess of imidazole, in which the ionic liquid is selective for the P2VP phase of the block copolymer.

Nonstoichiometric [Im][TFSI] containing excess imidazole conducts protons via two mechanisms: a vehicle mechanism whereby protons are carried by imidazolium cations, and a proton hopping mechanism whereby protons are transferred between hydrogen bonded imidazole molecules.[27] Excess imidazole molecules act as proton "acceptors" that facilitate proton hopping, increasing proton conduction vis-à-vis conduction by vehicle diffusion alone.[28, 29] Since the proton hopping mechanism is strongly related to the hydrogen bond network of imidazole and hydrogen bonding is known to be affected by confinement, we surmise that proton hopping in imidazole will also be affected by confinement (i.e. to block copolymer nanodomains).

Previous studies of block copolymer/ionic liquid membranes have focused on bulk conductivity measurements.[7, 21, 26, 30, 31] These measurements have provided insight into the relationship between structure and conductivity, but afford limited information regarding the mechanism of ionic liquid conductivity. Combined conductivity and NMR studies of mixtures of ionic liquids with homopolymers and random copolymers have shown that specific interactions between the ionic liquid and polymers greatly affect the prevalence of ion aggregation and the number of effective charge carriers,[32, 33] yet there have been no similar studies on mixtures containing protic ionic liquids or having well-defined nanostructures. In this work, we employ a combination of experimental techniques that together probe the dynamics of a variety of molecular and atomic species on length scales ranging from tenths of nanometers to microns to millimeters in order to determine the effect of confinement on the mechanisms of proton transport in a self-assembled mixture of PS-*b*-P2VP block copolymer with nonstoichiometric [Im][TFSI] ionic liquid, where the ionic liquid is confined to P2VP domains. A mixture of nonstoichiometric [Im][TFSI] with P2VP homopolymer has been studied in addition to the block copolymer mixture in order to discriminate effects of confinement from effects

of mixing with P2VP. We show that combining the ionic liquid with both P2VP and PS-*b*-P2VP has significant effects on ion aggregation and the proton transference number and, most strikingly, that the amount of proton hopping compared to vehicle diffusion is greatly increased in the nanostructured membrane. These results portend the rational design of nanostructured membranes having improved mechanical properties and conductivity.

6.2. Experimental Section

Polymer Synthesis and Characterization. Hydrogenated and deuterated poly(2-vinyl pyridine) (P2VP and *d*P2VP) and poly(styrene-*b*-2-vinyl pyridine) (PS-*b*-P2VP and *d*PS-*b*-*d*P2VP) were synthesized via anionic polymerization as described previously.[34] *d*8-styrene monomer (Polymer Source) and *d*7-2-vinyl pyridine monomer (Isotec) were used to synthesize deuterated polymers. The molecular weights of the polystyrene blocks (PS or *d*PS) were determined using gel permeation chromatography (GPC) and the total molecular weights of the block copolymers were determined using ^{1}H NMR (Bruker AVB 300 MHz). The molecular weight of P2VP was determined using ^{1}H NMR end-group analysis, and the molecular weight of *d*P2VP was determined using GPC. GPC was used to assess the polydispersity of each polymer. The degree of polymerization of the P2VP or *d*P2VP block, N_{P2VP}, the volume fraction of PS or *d*PS, f_{PS}, and the polydispersity index, PDI, of each polymer are given in Table 6.1.

Ionic Liquid Purification and Preparation. Imidazole (≥95%), *d*4-imidazole (≥98% deuteration), and bis(trifluoromethylsulfonyl)imide (HTFSI, ≥95%) were purchased from Sigma Aldrich and purified by sublimation under vacuum. The final purity of each starting material was assessed using differential scanning calorimetry (DSC) and ^{1}H NMR. Purified imidazole or *d*4-imidazole and HTFSI were combined in a 4:1 molar ratio and heated at 100 ºC for 2 to 3 hours. The compositions of the resulting nonstoichiometric [Im][TFSI] and [*d*Im][TFSI] ionic liquids were confirmed by comparing the measured melting points and ^{1}H NMR profiles to literature.[28] The structures of the ionic liquid molecules are shown in Figure 6.1. Because of their hygroscopic nature, the ionic liquids and their starting materials were handled in an argon atmosphere glove box and sealed sample holders at all times.

Preparation of Polymer/Ionic Liquid Mixtures. Dichloromethane and tetrahydrofuran were degassed using three freeze, pump, thaw cycles, dried by stirring over CaH_2 overnight, and stored on molecular sieves in an argon atmosphere glove box. All further sample preparation was performed within the glove box. Predetermined masses of ionic liquids and polymers were added to glass vials. Ca. 5 wt% solutions were prepared by dissolving in dichloromethane (block copolymer mixtures) or tetrahydrofuran (homopolymer mixtures), and the solutions were stirred overnight. Samples were cast one drop at a time into sample holders for DSC, small angle X-ray scattering (SAXS), quasi-elastic neutron scattering (QENS), and AC impedance spectroscopy. Samples were cast onto pieces of Kapton™ for NMR. Solvent was removed carefully so as not to simultaneously remove excess imidazole. Block copolymer samples were heated to 65 ºC for precisely 30 minutes. Homopolymer samples were dried at 35 ºC for three days.

Table 6.1. Degree of Polymerization, Volume Fraction, and PDI of Polymers Studied.

Polymer	N_{P2VP}	f_{PS}	PDI
*d*P2VP	82	0.00	1.07
*d*PS-*b*-P2VP	72	0.71	1.04
P2VP	118	0.00	1.07
PS-*b*-P2VP	101	0.72	1.04

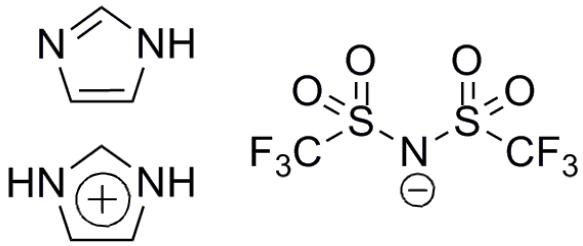


Figure 6.1. Chemical Structure of Nonstoichiometric [Im][TFSI].

Complete solvent removal and negligible imidazole loss was confirmed by ^{1}H NMR. After solvent removal, DSC, SAXS, QENS and conductivity sample holders were sealed shut, while NMR samples were scraped off of the Kapton™ and into sealable NMR tubes (for diffusion measurements) or 4 mm (outer diameter) magic angle spinning (MAS) rotors. Samples were sealed in jars containing desiccant for transportation to experimental apparatuses. The exclusion of water from samples was confirmed by ^{1}H NMR.

Both homopolymer and block copolymer samples were prepared and studied in order to distinguish the effects of mixing the ionic liquid with P2VP from the effects of confining the ionic liquid to nanodomains. The ratio of imidazole molecules to 2VP monomer units was held constant at 1.16:1 for all samples, which translates into 30 wt% ionic liquid in the block copolymer samples and 59 wt% ionic liquid in the homopolymer samples. This ensured that the glass transition temperature of the P2VP/ionic liquid phase, $T_{g,P2VP}$, was constant at about 4 ºC for each sample. The specific ionic liquid loading was chosen to maximize the number of ionic liquid protons so as to maximize the signal-to-noise ratio in NMR and QENS experiments, while limiting the ionic liquid concentration to the range in which the block copolymer mixtures form lamellar nanostructures. Deuterated polymers were used for NMR experiments so that the ionic liquid protons could be easily resolved in NMR spectra. Deuterated polymers as well as deuterated imidazole were used for QENS experiments so that the dynamics studied were dominated by the acidic proton. Hydrogenated materials were used for AC impedance ionic conductivity measurements.

Differential Scanning Calorimetry (DSC). DSC samples were crimped in an argon atmosphere glove box using hermetically sealed pans and placed inside a container with desiccant for transfer to the DSC. DSC was performed on a TA Instruments DSC Q20. Indium and dodecane were used as calibration standards. Samples underwent three heating and cooling cycles with a scan rate of 10 ºC per minute, and thermal transition temperatures from the second heating scan were recorded.

Morphology Characterization. Mixture morphologies were determined using small angle X-ray scattering (SAXS). Samples of ca. 1 mm thickness were cast in an argon atmosphere glove box into sample cells formed by an aluminum spacer sealed onto a Kapton window on one side. After heating to remove solvent, a second Kapton window was glued to seal the sample cells, and the cells were sealed in jars containing desiccant for transportation to the beamline. SAXS was performed on beamline 7.3.3 of the Advanced Light Source (ALS) and beamline 1-4 of the Stanford Synchrotron Radiation Lightsource (SSRL). Samples were equilibrated within the beamline at 145 ºC for 30-45 minutes before data were gathered. At the ALS, the X-ray beam was focused to a 50 by 300 μm spot, and the X-ray wavelength was λ=1.240 Å. Full two-dimensional scattering patterns were collected on an ADSC CCD detector with an active area of 188 by 188 mm. The scattering patterns were radially averaged and the scattering intensity was corrected with the post-ion chamber intensity using Nika version 1.18. At the SSRL, the X-ray beam was focused to a 0.5 mm diameter spot, and the X-ray wavelength was λ=1.488 Å. A single quadrant of a two-dimensional scattering pattern was collected on a CCD

detector with an active area of 25.4 by 25.4 mm. The scattering patterns were radially averaged and corrected for detector null signal, dark current, and empty cell scattering.

The block copolymer mixtures in this study have lamellar morphologies. Scattering patterns are shown in Figure 6.A.1 in the Appendix. The deuterated mixture used for NMR and QENS experiments has a lamellar domain size, *d*, of 37 nm, calculated as $2\pi/q^*$, where q* is the primary scattering peak from SAXS data. The size of the *d*P2VP/ionic liquid channel, then, is 17 nm assuming complete segregation of the ionic liquid to the *d*P2VP domains, ideal mixing, and the density of the ionic liquid to be 1.4 g/mL (based on volumetric measurements). The assumption of complete ionic liquid segregation is justified based on the strong selectivity of the ionic liquid for P2VP. The strong selectivity of stoichiometric [Im][TFSI] has been demonstrated previously based on the scaling behavior of *d* with mixture composition.[25] Non-stoichiometric [Im][TFSI] is also very selective for P2VP, as evidenced by an increase in *d* with increased ionic liquid composition (see Figure 6.A.1c in the Appendix) as well as negligible change in the glass transition temperature of the PS phase upon ionic liquid addition. The hydrogenated PS-*b*-P2VP block copolymer used for bulk ionic conductivity measurements has a slightly larger molecular weight than the deuterated version, leading to a larger lamellar domain size of the PS-*b*-P2VP/ionic liquid mixture of *d*=43 nm (P2VP/ionic liquid channel size equal to 19 nm).

Ionic Conductivity Measurements. Bulk ionic conductivity was measured using four-point probe AC impedance spectroscopy. Samples were cast in an argon atmosphere glove box into a home made, air-tight, poly(ether ether ketone) cell equipped with rubber o-rings and four stainless steel electrodes. The working and reference electrodes were 1.7 cm long and placed 0.6 to 0.7 cm apart, and the samples were cast to be about 0.05 cm thick (measured after AC impedance measurements). After solvent removal, the sample cell was screwed shut, removed from the glove box, and heated at 150 ºC for 12 hours before measurements were made. AC impedance measurements were performed using a Gamry Reference 600 Potentiostat at descending temperatures. An alternating current signal with an amplitude of 5 mV was applied in the frequency range of 0.1 to 65,000 Hz. The non-zero x-intercept in the Nyquist plot of the negative imaginary part of the impedance versus the real part of the impedance was taken as the sample resistance, *R*. The ionic conductivity, σ, was calculated as t/AR, where t and A are the thickness and area of the sample (with respect to electrode placement), respectively, measured after the AC impedance measurements.

Diffusion Coefficient Measurements. Self-diffusion coefficients were measured with pulsed-field gradient spin echo (PGSE) and pulsed-field gradient stimulated echo (PGStE) NMR experiments using a Doty Scientific single-axis diffusion probe with temperature control. The applied gradients were calibrated using water[35] and glycerol[36] standards, and were found to reach 1.7 T/m. ^{1}H diffusion coefficients were measured in a 7 T superconducting magnet with a 300 MHz Tecmag Apollo spectrometer and gradient control, and ^{19}F diffusion coefficients were measured in a 1.5 T superconducting magnet with a 61.2 MHz Tecmag LapNMR spectrometer and gradient control. Experiments

were performed between 25 and 132 ºC, where the temperature was calibrated[37] using an ethylene glycol standard between 24 and 83 ºC and extrapolation to higher temperatures.

The NMR signal attenuation for Fickian diffusion in both PGSE and PGStE experiments is described by

$$I = I_0 e^{-D\gamma^2 g^2 \delta^2 \left(\Delta - \delta/3\right)} \tag{6.1}$$

where I is the spin-echo signal intensity, I_0 is the signal intensity with zero gradient, γ is the magnetogyric ratio of the probe nucleus, g is the magnitude of the gradient pulse, δ is the duration of the gradient pulse, Δ is the duration of time between the leading edges of the two gradient pulses, and D is the self-diffusion coefficient of the probe nucleus. I was measured as a function of g, and Equation 6.1 was used to determine D. Example plots of I/I_0 as a function of $\gamma^2 g^2 \delta^2(\Delta - \delta/3)$ are shown in Figure 6.A.2 in the Appendix. Experiments were repeated on the block copolymer sample using values of Δ ranging from 0.02 to 0.11 seconds, corresponding to root mean squared diffusion path lengths of ionic liquid ions ranging from 0.2 to 2.2 μm, resulting in consistent measurements of D (see, for example, Figure 6.A.3 in the Appendix). PGSE and PGStE experiments performed on each sample also resulted in consistent measurements of D.

Spectroscopic resolution of ionic liquid protons was possible in ^{1}H experiments because the polymers were deuterated. Thus, the diffusion coefficients for protons covalently bound to the carbon atoms on the imidazole (involved only in vehicle diffusion), $D_{C\text{-}H}$, and protons bound to nitrogen atoms on imidazole (involved in vehicle diffusion and proton hopping), $D_{N\text{-}H}$, were measured separately. For ^{19}F experiments, a single peak was observed corresponding to fluorine atoms on the TFSI anion, and a single diffusion coefficient measured, D_{TFSI}.

Magic Angle Spinning (MAS) NMR. High resolution ^{1}H NMR spectra were obtained for ionic liquid/polymer mixtures using MAS NMR. MAS experiments were performed in a 7 T superconducting magnet using a Doty Scientific MAS probe and 300 MHz Tecmag Apollo spectrometer. Samples were annealed in sealed 4 mm (outer diameter) MAS rotors at 150 ºC for 12 hours before MAS experiments. During MAS experiments, samples were spun at 13 kHz. Spectra were acquired between 93 and 132 ºC, where the temperature was calibrated in the same manner as they were for diffusion measurements. Samples equilibrated slowly at each temperature due to fast spinning, so samples were annealed at each temperature for 1 to 9 hours until the spectra did not change between consecutive acquisitions.

Quasi-elastic Neutron Scattering (QENS). QENS experiments were performed at the National Institute for Standards and Technology (NIST) Center for Neutron Research (NCNR) on the high flux backscattering spectrometer (HFBS). An incident neutron wavelength of λ=6.271 Å and an energy resolution of about 0.8 μeV were used. Data from all 16 detectors were used to probe a q-range from 0.25 to 1.75 Å^{-1}. Polymer/ionic liquid samples were loaded into sample cans with an annular geometry and the sample transmission was set to about 90% to minimize multiple scattering. All experiments were performed at 140 ºC. The acquired data were corrected for detector efficiencies (determined using a vanadium standard), and the resolution function of the instrument

was determined by measuring scattering from the *d*P2VP/[*d*Im][TFSI] mixture at 15 K where all the signal is expected to be elastic.

Elastic and quasi-elastic scattering contribute to the observed scattering profiles, $S(q,\omega)$. Quasi-elastic scattering in $S(q,\omega)$ reflects self-correlated motion, and appears as broad signal over a sharp, elastic scattering peak centered around ω=0. Reduction, visualization, and analysis of HFBS data were performed using the DAVE software package developed at NCNR.[38] The elastic scattering contributions were modeled using a Delta function convoluted with the resolution function of the instrument. The quasi-elastic scattering contributions were modeled using two Lorentzian functions, one for the high energy background signal, and one for the main quasi-elastic contribution in the energy range of the instruments. The full-width-at-half-maximum (FWHM) values of the high energy background signals were found to be essentially constant at 30 μeV for all q. Fitted FWHMs of the main quasi-elastic contributions in HFBS profiles were reported, with the standard deviation of the fits reported as the error.

6.3. Results and Discussion

Relative cation and anion diffusion in nonstoichiometric [Im][TFSI] was found to be dramatically affected both by combining the ionic liquid with polymer as well as confining it to lamellar block copolymer nanodomains. While the anion and cation diffuse at similar rates in the neat ionic liquid,[28, 39] the cation diffuses much more quickly than the anion when the ionic liquid is added to the homopolymer or block copolymer, as shown in Figure 6.2. Faster cation diffusion can be attributed to the prevalence of anionic aggregates in the membrane or to specific interactions between the TFSI anions and the 2VP repeat units. The presence of anionic aggregates has been shown to cause relatively fast cation diffusion in ionic liquid-impregnated Nafion at low hydration levels.[32] Alternatively, specific polymer/anion interactions may slow down anion diffusion. This effect has been previously observed in mixtures of 1-ethyl-3-methylimidazolium:TFSI with poly(methyl methacrylate) (PMMA).[33] The 2VP repeat unit is basic, so this type of specific interaction with TFSI is not anticipated. It is possible, however, that some 2VP moieties are protonated by imidazolium, leading to interactions between protonated 2VP moieties and the TFSI anion.

Cation diffusion is deduced from $D_{C\text{-}H}$, which is actually a molar weighted average of the diffusion coefficients of imidazolium cations and neutral imidazole.[28] It is possible, then, that an increase in ion aggregation upon mixing the ionic liquid with the lower dielectric polymer could lead to a larger decrease in D_{TFSI} than $D_{C\text{-}H}$ and explain the results in Figure 6.2. $D_{TFSI,St}$ and $D_{C\text{-}H,St}$ were also measured for mixtures of stoichiometric [Im][TFSI] with *d*P2VP and *d*PS-*b*-*d*P2VP, in which the ratio of Im:*d*2VP was held constant to that in the nonstoichiometric mixtures. When a stoichiometric ionic liquid is used, diffusion is dominated by the diffusion of ions. At high temperatures the difference in the diffusion rate of the anion and cation is similar to that in the nonstoichiometric mixtures (Figure 6.A.4 in the Appendix), confirming that the high cation diffusion in the nonstoichiometric mixtures is real and not due to fast diffusion of neutral imidazole.

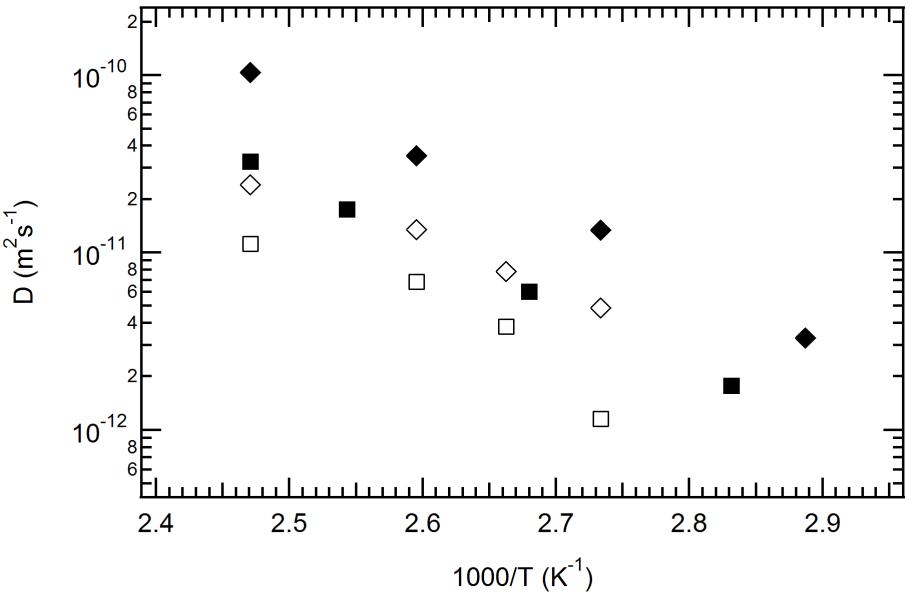


Figure 6.2. Cation and Anion Diffusion as a Function of Temperature. $D_{C\text{-}H}$ (diamonds) and D_{TFSI} (squares) as a function of temperature for *d*P2VP/nonstoichiometric [Im][TFSI] (solid symbols) and *d*PS-*b*-*d*P2VP/nonstoichiometric [Im][TFSI] (open symbols).

The discrepancy between anion and cation diffusion is smaller in the block copolymer mixture than in the homopolymer mixture. For instance, at 132 ºC, $D_{C\text{-}H}/D_{TFSI}$=3.2 for the homopolymer mixed with ionic liquid compared to $D_{C\text{-}H}/D_{TFSI}$=2.3 for the analogous block copolymer mixture. This is not surprising given that in the block copolymer, portions of the *d*P2VP block close to the block copolymer interface are highly stretched, which appears to affect ion coordination.[19] Similarly, coordination of P2VP with metal chlorides has also been shown to be intimately related to chain conformation.[40] Both $D_{C\text{-}H}$ and D_{TFSI} are smaller in the block copolymer mixture than in the homopolymer mixture due to the confinement of the ionic liquid diffusion path to interconnected, isotropically-oriented lamellar domains with long-range order defects on the length scale of the NMR experiments, including point defects and grain boundaries.[41]

The most striking difference between the mechanism of proton conductivity in mixtures of nonstoichiometric [Im][TFSI] with homopolymer and block copolymer is the greatly increased amount of proton hopping that occurs in the block copolymer sample. The amount of proton hopping was probed by measuring the ratio of the diffusion coefficient of the acidic ionic liquid proton, D_{H+}, to cation diffusion ($D_{C\text{-}H}$), where D_{H+} was calculated by assuming $D_{N\text{-}H}$ is a molar weighted average of the diffusion of protons bound to nitrogen atoms on charged imidazolium and neutral imidazole:

$$D_{N-H} = xD_{H+} + (1-x)D_{C-H} \tag{6.2}$$

where x is the mole fraction of imidazolium.[28] As shown in Figure 6.3, the fact that the proton diffusion coefficient is much larger than $D_{C\text{-}H}$ suggests there is a significant amount of proton hopping in the neat nonstoichiometric ionic liquid over the entire experimental temperature range (25 to 120 ºC). The amount of proton hopping decreases with increasing temperature. This decrease may be related to a number of mechanisms, including increased hydrogen bond length and/or shortened average lifetime, or decreased number of imidazole hydrogen bonds accompanying an increase in temperature.[42, 43] Mixing the ionic liquid with *d*P2VP homopolymer does not appear to affect proton hopping mechanisms. However, the ratio of $D_{H+}/D_{C\text{-}H}$ is considerably greater for the block copolymer mixture, suggesting the influence of confinement on the mechanism of proton transport. Despite the larger error bars for the block copolymer sample (which reflect a decrease in signal following the decrease in proton concentration in these samples), the significant enhancement of acidic proton diffusion is clear.

Further evidence for increased proton hopping in the block copolymer sample comes from QENS experiments. QENS is an ideal tool for studying proton transport mechanisms because the relatively large incoherent neutron scattering cross section of ^{1}H compared to other atoms leads to the selective observation of self-correlated hydrogen motion (i.e. diffusion). Motion is probed on the length scale of tenths of nanometers to nanometers, so the local information derived from these experiments compliments NMR diffusion measurements, which are on the μm length scale, and bulk ionic conductivity measurements, which are on the mm length scale. Representative QENS scattering profiles for mixtures of nonstoichiometric [*d*Im][TFSI] with *d*P2VP homopolymer and *d*PS-*b*-*d*P2VP block copolymer are shown in Figure 6.4. As the scattering vector *q* increases, the elastic scattering contribution decreases and the FWHM of the quasi-elastic scattering contribution increases, indicating diffusive motion.[44] This is clearly seen in

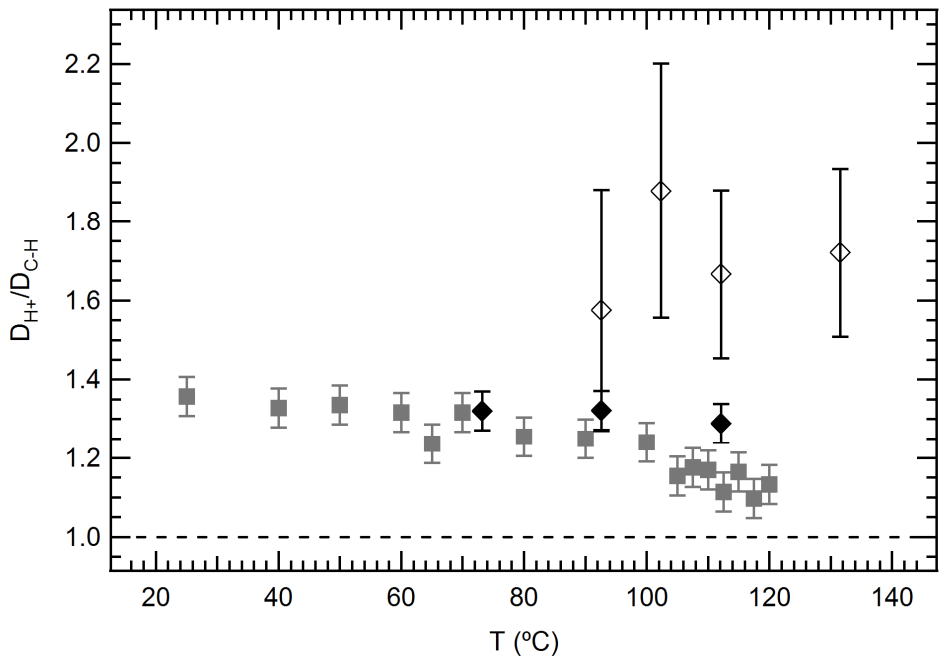


Figure 6.3. Proton Diffusion Enhancement due to Proton Hopping. The ratio of acidic proton diffusion to cation diffusion as a function of temperature for *d*P2VP/nonstoichiometric [Im][TFSI] (solid diamonds), *d*PS-*b*-*d*P2VP/nonstoichiometric [Im][TFSI] (open diamonds), and neat nonstoichiometric [Im][TFSI] (gray squares). The degree of proton hopping is greatly enhanced in the nanostructured sample. Error bars on data for the neat ionic liquid and the *d*P2VP mixture represent a reasonable estimate based on the reproducibility of experiments, and error bars on data for the *d*PS-*b*-*d*P2VP mixture represent one standard deviation of the mean obtained from many experiments.

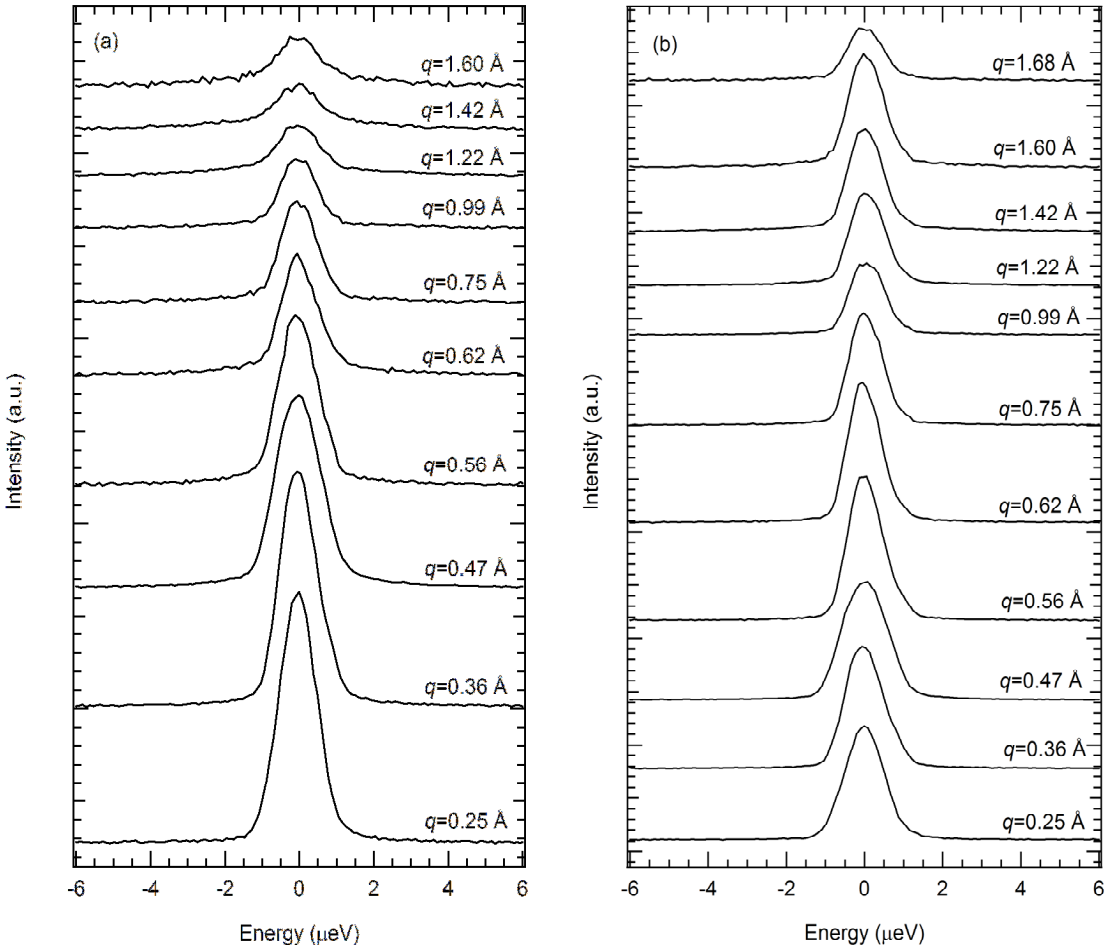


Figure 6.4. QENS Profiles of Polymer/Ionic Liquid Mixtures. QENS profiles of (a) *d*P2VP/nonstoichiometric [*d*Im][TFSI] and (b) *d*PS-*b*-*d*P2VP/nonstoichiometric [*d*Im][TFSI] at 140 ºC. The full-width at half maximum (FWHM) of quasi-elastic scattering increases with increasing q, indicating translational motion processes.

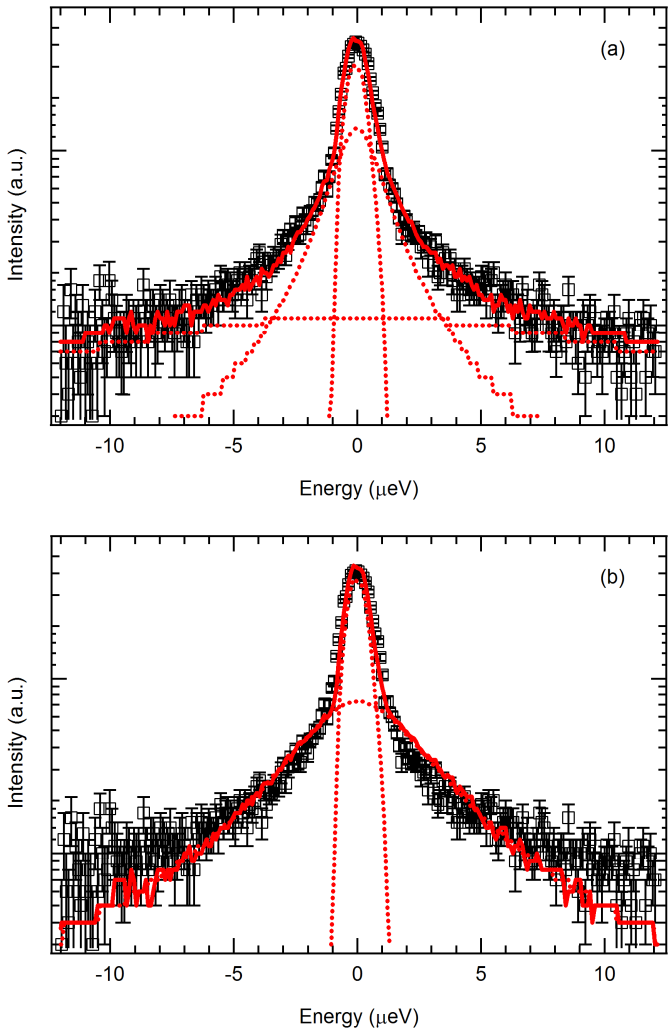


Figure 6.5. QENS Fits of *d*P2VP/[*d*Im][TFSI] Mixtures. QENS profiles of *d*P2VP/nonstoichiometric [*d*Im][TFSI] at T=140 ºC and q=0.99 Å^{-1}. The solid lines are the total fits to the data, while the dotted lines are the component fits. The fit using two Lorentzians in addition to a delta function convoluted with the resolution function that captures elastic scattering (a) is clearly better than the fit using a single Lorentzian (b).

Figure 6.4a for the homopolymer sample. The trends are less obvious for the block copolymer sample scattering profiles (Figure 6.4b) due to a combination of increased *q*-dependent elastic scattering resulting from increased order as well as increased influence of *q*-dependent coherent scattering resulting from a higher concentration of deuterium atoms.[44] The quasi-elastic contributions were modeled to quantify their dependence on *q*. Example fits of the homopolymer sample are shown in Figure 6.5, where it is clear that two Lorentzian functions are necessary to fully capture the scattering profile: one to describe the main quasi-elastic scattering contribution stemming from diffusive motion, and one to describe the high-energy background signal. Similar plots of data and fits for the block copolymer sample are shown in Figure 6.A.5 in the Appendix.

The *q*-dependence of the FWHM of the main quasi-elastic scattering contribution, Γ, provides information regarding the mechanism of proton diffusion. When there is purely Fickian diffusion, Γ is expected to vary linearly with q^2 according to[44]

$$\Gamma/2 = \hbar D q^2 \tag{6.3}$$

Equation 6.3 adequately describes simple liquids such as argon[45] and even some more complex liquids such as the ionic liquid 1-butyl-3-methylimidazolium:chloride[46]. When molecular interactions are significant, for instance in the case of the ionic liquids 1-ethyl-3-methylimidazolium:bromide[47] and N,N,N',N'-tetramethylguanidinium: bis(perfluoroethylsulfonyl)imide[48], deviations from Equation 6.3 have been observed at high values of *q* corresponding to length scales smaller than the interaction distance. In these cases, the Jump-Diffusion model[49] has been used to describe the variation of Γ with q^2 as

$$\Gamma/2 = \frac{\hbar D q^2}{1 + D q^2 \tau_0} \tag{6.4}$$

where τ_0 is the residence time between jumps, or the molecular interaction time. Specifically, the Jump-Diffusion model describes the complex dynamics of protons in supercooled water, which are dominated by Grotthuss proton transfer between water molecules through hydrogen bonds.[50, 51] τ_0 in this case is the time between proton transfer events. Similarly, Equation 6.4 is a good model for describing quasi-elastic scattering from the combination of diffusion and proton hopping in nonstoichiometric [*d*Im][TFSI], where the interpretation of τ_0 is complex due to significant contributions of both molecular interactions and proton hopping to the deviation from Fickian behavior.[39] Thus, it is expected that the ionic liquid/polymer mixtures in this study also exhibit non-Fickian behavior that can be estimated by Equation 6.4, and that the magnitude of the departure from Fickian behavior is related to the amount of proton hopping. Figure 6.6 demonstrates that the acidic protons in mixtures of nonstoichiometric [*d*Im][TFSI] with *d*P2VP homopolymer and *d*PS-*b*-*d*P2VP block copolymer undergo non-Fickian diffusion, adequately captured by Equation 6.4. The block copolymer sample shows a greater departure from Fickian diffusion than the homopolymer sample, indicating increased proton hopping in agreement with NMR diffusion experiments.

It is anticipated that increased proton hopping in the block copolymer sample is related to a difference in the imidazole hydrogen bond structure under confinement. The ^{1}H MAS NMR chemical shifts of the protons covalently bound to imidazole/imidazolium

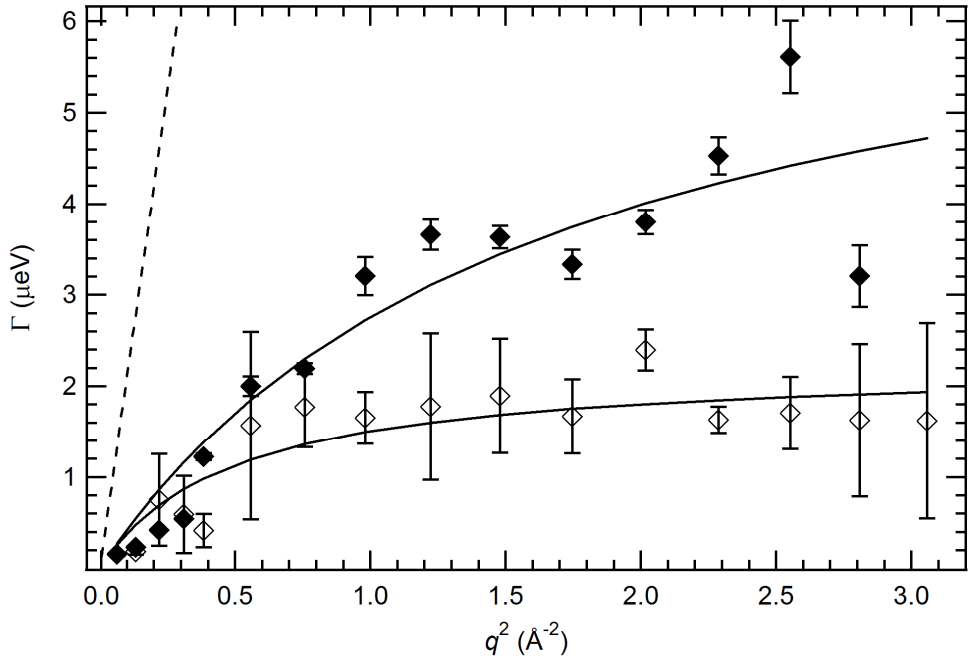


Figure 6.6. Dependence of Quasi-elastic Scattering on Scattering Vector. Γof the main Lorentzian peak fit to HFBS QENS scattering profiles as a function of q^2 for *d*P2VP/nonstoichiometric [*d*Im][TFSI] (solid symbols) and *d*PS-*b*-*d*P2VP/nonstoichiometric [*d*Im][TFSI] (open symbols) at 140 ºC. Error bars represent one standard deviation of the fits. Solid curves are fits to the data using Equation 6.4, and the dashed line is the Fickian Diffusion curve (Equation 6.3) using $D_{N\text{-}H}$ in the homopolymer sample from NMR.

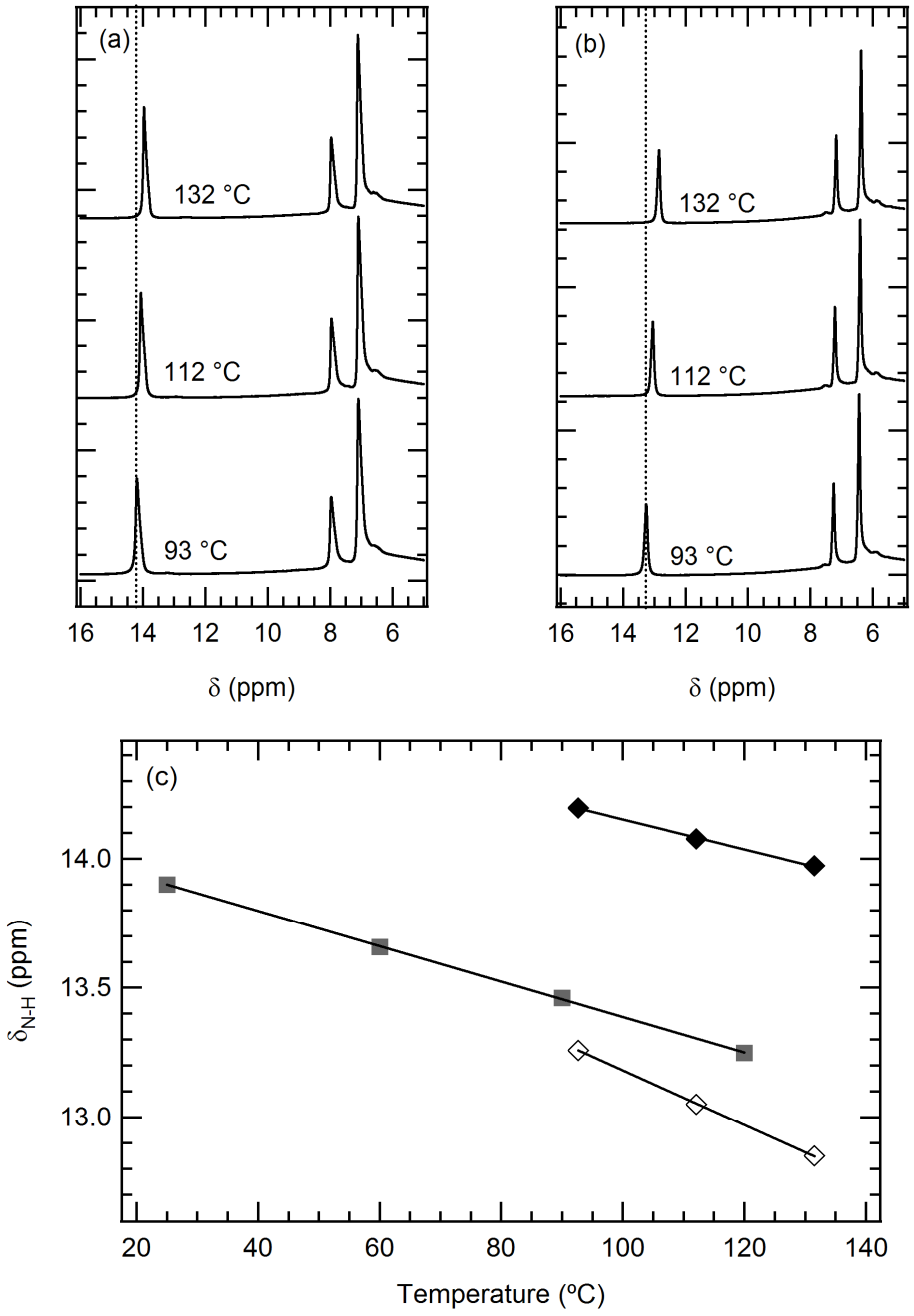


Figure 6.7. MAS ^{1}H NMR Spectra of Polymer/Ionic Liquid Mixtures. MAS ^{1}H NMR spectra of (a) *d*P2VP/nonstoichiometric [Im][TFSI] and (b) *d*PS-*b*-*d*P2VP/nonstoichiometric [Im][TFSI], as well as (c) $\delta_{N\text{-}H}$ as a function of temperature for the *d*P2VP mixture (solid diamonds), *d*PS-*b*-*d*P2VP mixture (open diamonds), and neat nonstoichiometric [Im][TFSI] (gray squares). Lines of best linear fit connect the data points.

nitrogens, $\delta_{N\text{-}H}$, are strongly dependent on hydrogen bonding.[28] In qualitative similarity with the neat ionic liquid,[39] $\delta_{N\text{-}H}$ shifts to lower ppm as the temperature is increased (Figures 6.7a and 6.7b). The temperature dependence of $\delta_{N\text{-}H}$ is steeper for the block copolymer mixture than for the neat ionic liquid sample and the homopolymer mixture (Figure 6.7c), suggesting unique hydrogen bonding behavior. Furthermore, the absolute values of the chemical shifts for the block copolymer sample are unexpected. The higher values for the homopolymer sample compared to those for the neat ionic liquid are unsurprising due to the greater number of molecules that can participate in hydrogen bonding. The same phenomena is observed when excess imidazole is added to stoichiometric ionic liquid.[28] The block copolymer sample, on the other hand, has lower values of $\delta_{N\text{-}H}$ despite containing the same number of molecules that can participate in hydrogen bonding as the homopolymer sample. These unexpected trends indicate that a different hydrogen bond network exists in the ionic liquid when confined to block copolymer domains, which affects the amount of proton hopping that occurs.

Polymer chain stretching near the block copolymer interface likely affects how *d*2VP units interact with the imidazole hydrogen bond network. Previous studies have already demonstrated the relationship between polymer chain conformation and ion and metal chloride coordination.[19, 40] Additionally, the presence of the interface itself likely alters the near-interface hydrogen bond structure, the effects of which could propagate several nanometers into either side of the 17 nm *d*P2VP/ionic liquid channels. Such confinement effects on hydrogen bonding in water are well documented.[10-13]

The mechanistic differences in proton transport in the nanostructured and non-ordered samples lead to differences in bulk ionic conductivity, σ. In Figure 6.8, σ is plotted as a function of temperature for mixtures of nonstoichiometric [Im][TFSI] with homopolymer and block copolymer. The conductivity of the block copolymer sample is lower than that of the homopolymer sample due to the overall lower ion concentration in the block copolymer membrane, in addition to the lack of long-range order characterizing its lamellar domains. Ion aggregation in each sample is investigated by comparing the measured conductivity to the conductivity predicted by the Nernst-Einstein equation using ion diffusion coefficients measured by NMR. The Nernst-Einstein equation is given by

$$\sigma = \frac{F^2}{RT}\left(c_{m,H+}D_{H+} + c_{m,TFSI}D_{TFSI}\right) \tag{6.5}$$

where $c_{m,H+}$ and $c_{m,TFSI}$ are the molar concentrations of acidic protons and TFSI anions, respectively. The predicted conductivities for both samples are plotted along with the measured bulk conductivities as a function of temperature in Figure 6.8. Equation 6.5 over-predicts the measured ionic conductivity of the block copolymer sample by a factor of 3 to 4 while predicting the homopolymer conductivity relatively well. Since NMR measures diffusion over micron lengthscales and bulk conductivity measurements probe a millimeter dimension, the large discrepancy for the block copolymer sample is likely attributed to a combination of ion aggregation and differences in long range order. The increasing overprediction of the conductivity of the homopolymer sample at lower temperatures suggests an increase in the degree of ion aggregation with decreasing temperature. The strong temperature dependence suggests that anionic aggregates are not

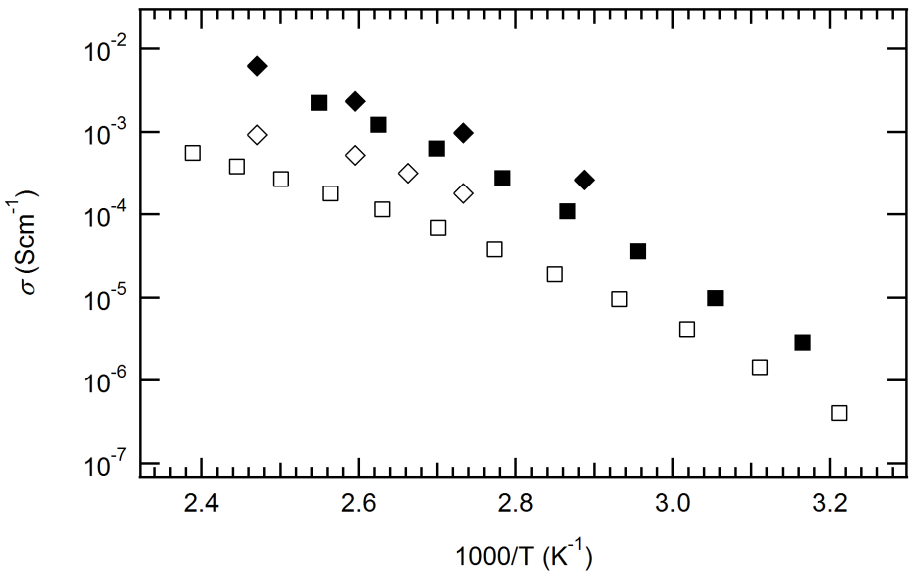


Figure 6.8. Comparison of Conductivity and NMR Experiments. Measured σ (squares) and σ calculated from NMR diffusion coefficients and Nernst-Einstein equation (diamonds) for mixtures of nonstoichiometric [Im][TFSI] with homopolymer (solid symbols) and block copolymer (open symbols).

the major cause of faster relative cation diffusion in the homopolymer sample. (If the ion aggregates were anionic aggregates, the temperature dependence would be reflected in Figure 6.2.) In the block copolymer sample, on the other hand, no temperature dependence is observed, so anionic aggregates in this sample are still a possibility.

The result of different ion aggregation behavior, as well as different amounts of proton hopping in the homopolymer and block copolymer samples, is that the activation energy for bulk ionic conductivity is lower in the block copolymer sample. This is clearly observed on Figure 6.8, where the temperature dependence for the measured conductivity is much less steep.

6.4. Conclusions

Proton transport in ionic liquids is clearly affected when the ionic liquid is mixed with a polymer, and especially when the ionic liquid is confined to block copolymer nanodomains. Several specific mechanistic changes have been illuminated in this work using a combination of transport measurements that together probe a variety of length scales and a variety of molecular and atomic species. The relative amount of cation and anion diffusion, for example, has been found to change drastically upon incorporation of ionic liquid into a homopolymer and block copolymer. In the case presented here of nonstoichiometric [Im][TFSI] mixed with *d*P2VP and *d*PS-*b*-*d*P2VP, specific interactions between TFSI and *d*2VP moieties or the prevalence of anionic aggregates cause the cation to diffuse significantly faster than the anion, which is in stark contrast to the neat ionic liquid. This asymmetric charge transport could be taken advantage of for a variety of applications, including proton exchange membrane fuel cells or actuators.

The temperature dependence of ion aggregation has been found to be significantly different in the homopolymer and block copolymer samples, contributing to a lower activation energy for ion transport in the block copolymer sample. Determining the degree of ion aggregation in the block copolymer sample as well as understanding the source of its temperature independence could lead to the design of nanostructured membranes with increased conductivity.

The most striking change in proton transport upon incorporation of nonstoichiometric [Im][TFSI] into a block copolymer is that the amount of diffusion-enhancing proton hopping drastically increases. We propose that block copolymer chain stretching and/or confinement affect the hydrogen bond structure of the ionic liquid, leading to this increase. Long-range proton diffusion in the block copolymer/ionic liquid membrane is still not as high as in the homopolymer/ionic liquid membrane due to the lack of long-range order characterizing the lamellar domains. However, highly conductive, mechanically durable membranes could be designed by combining the enhancement of acidic proton diffusion due to block copolymer self-assembly with increased long-range order obtained using one of many channel-aligning techniques.[52]

6.5. Acknowledgements

We gratefully acknowledge support from the Assistant Secretary for Energy Efficiency and Renewable Energy, Office of Hydrogen, Fuel Cell, and Infrastructure Technologies of the U.S. Department of Energy under Contract DE-AC02-05CH11231. M.L. Hoarfrost thanks support from an NSF Graduate Research Fellowship. SAXS experiments were performed at the Advanced Light Source (ALS) and the Stanford Synchrotron Radiation Lightsource (SSRL). Both are national user facilities supported by the Department of Energy, Office of Basic Sciences. We gratefully acknowledge Dr. Alexander Hexemer, Dr. Cheng Wang, and Dr. Eric Schaible for experimental assistance at the ALS and Dr. John Pople for experimental assistance at the SSRL. This work also utilized facilities at the NIST Center for Neutron Research (NCNR) supported in part by the National Science Foundation under Agreement No. DMR-0944772. We gratefully acknowledge Dr. Timothy Jenkins for experimental assistance at the NCNR. Finally, the authors thank Dr. Joel Stettler for technical assistance with NMR experiments. Certain commercial equipment, instruments, materials or material suppliers are identified in this paper to foster understanding. Such identification does not imply recommendation or endorsement by the National Institute of Standards and Technology, nor does it imply that the materials or equipment identified are necessarily the best available for the purpose.

6.6. Appendix: Supporting SAXS, PGSE NMR, and QENS

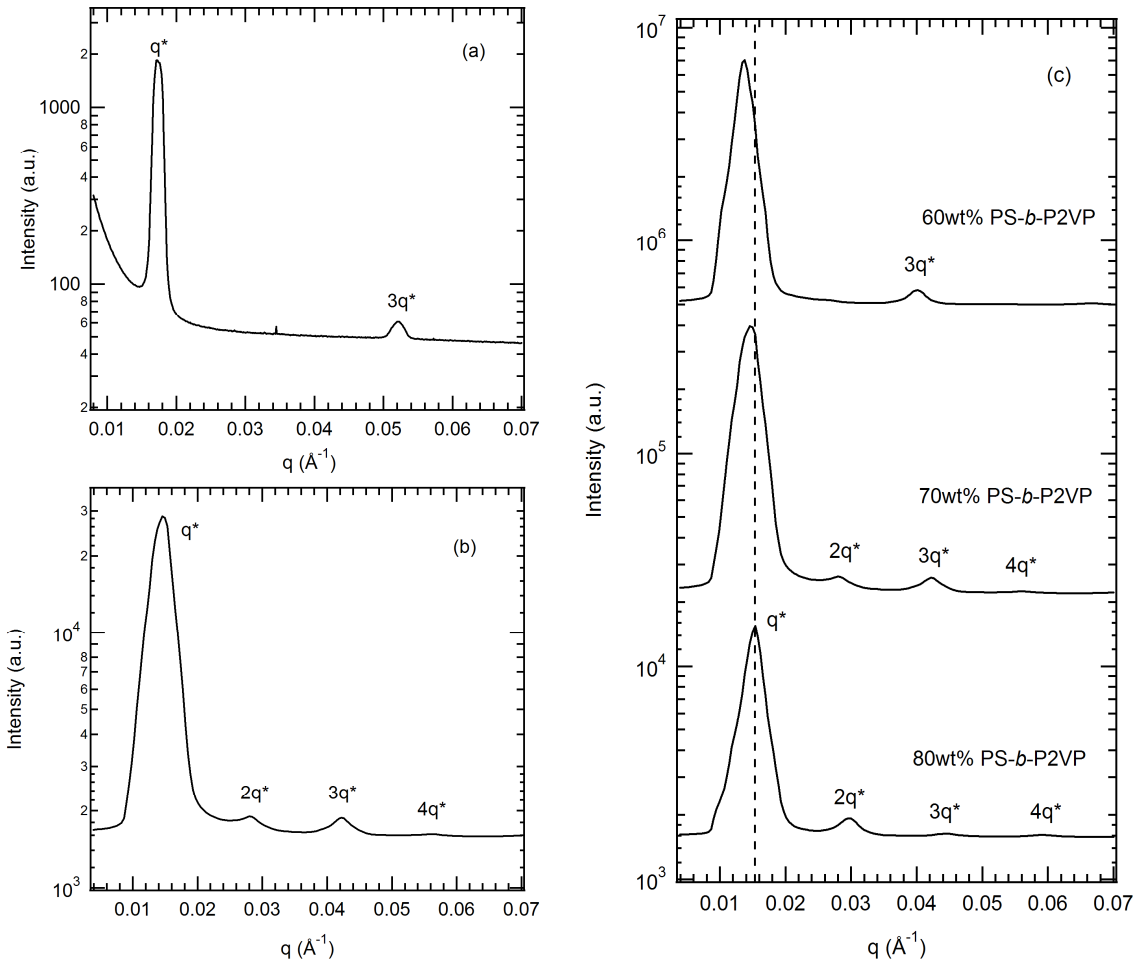


Figure 6.A.1. SAXS Profiles of Mixtures of PS-*b*-P2VP with Nonstoichiometric [Im][TFSI]. SAXS profile for (a) *d*PS-*b*-*d*P2VP/nonstoichiometric [Im][TFSI] (b) PS-*b*-P2VP/nonstoichiometric [Im][TFSI] at 130 ºC. Both mixtures have Imidazole:2VP=1.16, corresponding to 30 mass percent ionic liquid. The mixtures have lamellar morphologies with *d*=37 and 43 nm, respectively. The strong selectivity of nonstoichiometric [Im][TFSI] for one phase of the block copolymer is demonstrated in (c), where *d* increases with increasing ionic liquid loading.

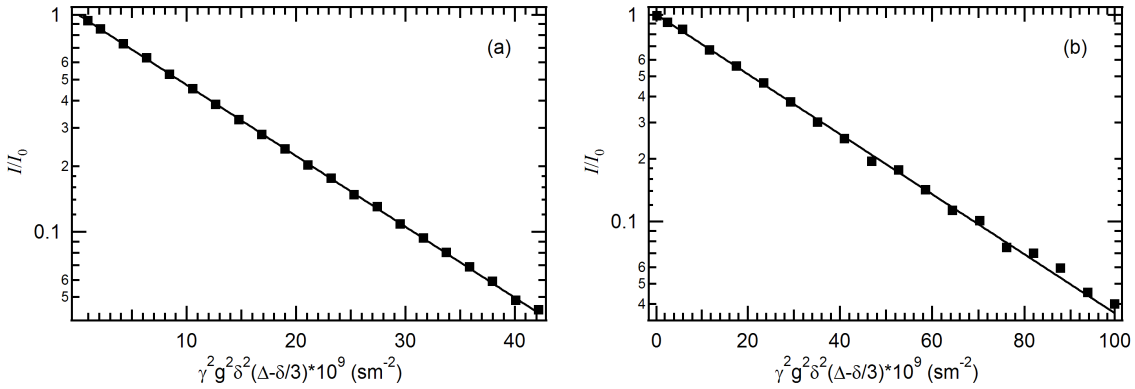


Figure 6.A.2. PGSE NMR Data and Fits. Representative ^{1}H PGSE data and fits for (a) *d*P2VP/nonstoichiometric [Im][TFSI] and (b) *d*PS-*b*-*d*P2VP/nonstoichiometric [Im][TFSI]. The logs of the signal attenuations have the expected linear decay with $\gamma^2 g^2 \delta^2 (\Delta - \delta/3)$.

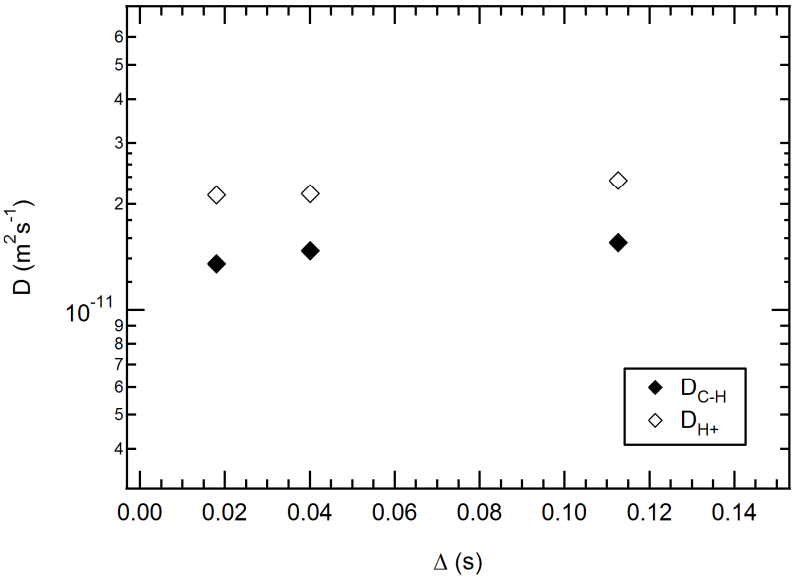


Figure 6.A.3. Evidence that Diffusion Coefficients Do Not Depend on Diffusion Time in PGSE NMR Experiments. $D_{C\text{-}H}$ and D_{H+} as a function of Δ for *d*PS-*b*-*d*P2VP/nonstoichiometric [Im][TFSI] at 112 ºC. Diffusion coefficients do not change significantly as a function of Δ.

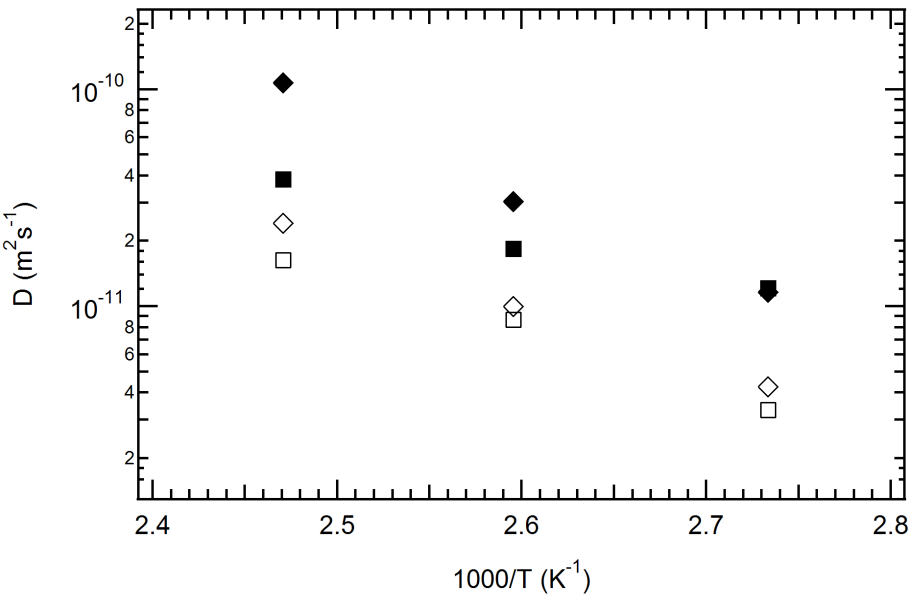


Figure 6.A.4. Cation and Anion Diffusion of Stoichiometric Mixtures. $D_{C\text{-}H,St}$ (diamonds) and $D_{TFSI,St}$ (squares) as a function of temperature for *d*P2VP/[Im][TFSI] (solid symbols) and *d*PS-*b*-*d*P2VP/[Im][TFSI] (open symbols). At high temperatures, the differences between $D_{C\text{-}H,St}$ and $D_{TFSI,St}$ is similar to the differences between $D_{C\text{-}H}$ and D_{TFSI} (in nonstoichiometric mixtures), confirming that $D_{C\text{-}H}>D_{TFSI}$ is not due to fast diffusion of neutral imidazole. Note that at low temperatures, hydrogen bonding or other interactions between *d*2VP moieties and imidazolium in the stoichiometric mixtures leads to decreased $D_{C\text{-}H,St}$ so that $D_{C\text{-}H,St}$ and $D_{TFSI,St}$ are similar, a phenomena avoided in the nonstoichiometric mixtures since excess imidazole molecules have a much higher pKa than pyridine (6.99 compared to 5.23, according to the *CRC Handbook of Chemistry and Physics*).

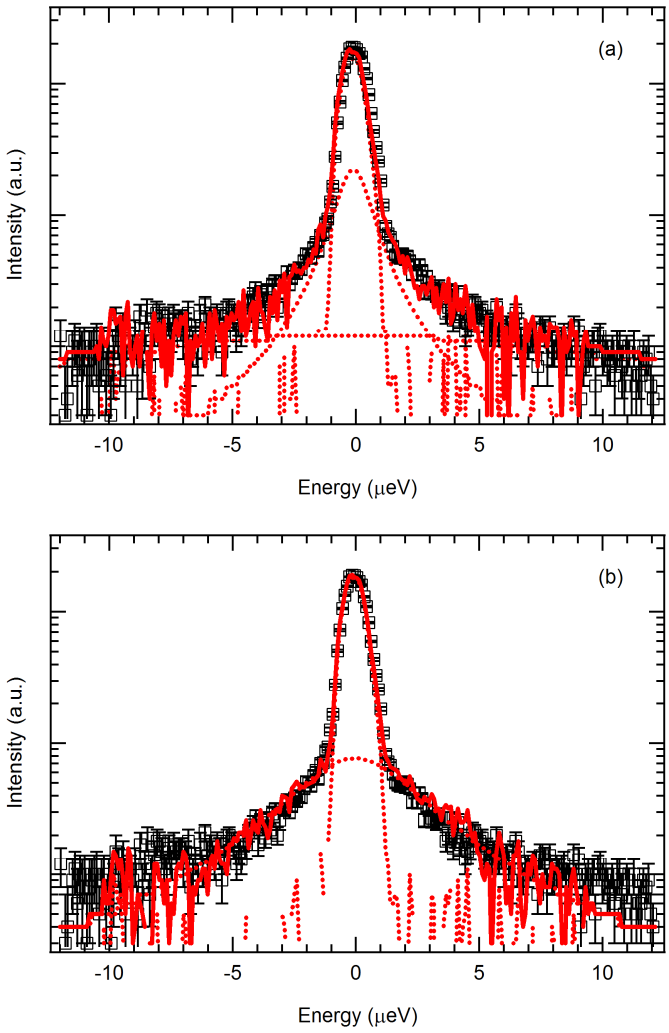


Figure 6.A.5. QENS Scattering Fits of *d*PS-*b*-*d*P2VP/[*d*Im][TFSI] Mixtures. QENS profiles of *d*PS-*b*-*d*P2VP/nonstoichiometric [*d*Im][TFSI] at T=140 ºC and Q=0.99 $Å^{-1}$. The solid lines are the total fits to the data, while the dotted lines are the component fits. The fit using two Lorentzians in addition to a delta function convoluted with the resolution function (a) is clearly better than the fit using a single Lorentzian (b).

6.7. References

1. Mauritz, K. A.; Moore, R. B. *Chemical Reviews* **2004,** 104, (10), 4535-4585.
2. Chen, Y. B.; Thorn, M.; Christensen, S.; Versek, C.; Poe, A.; Hayward, R. C.; Tuominen, M. T.; Thayumanavan, S. *Nature Chemistry* **2010,** 2, (6), 503-508.
3. Ichikawa, T.; Yoshio, M.; Hamasaki, A.; Mukai, T.; Ohno, H.; Kato, T. *Journal of the American Chemical Society* **2007,** 129, (35), 10662-10663.
4. Wanakule, N. S.; Panday, A.; Mullin, S. A.; Gann, E.; Hexemer, A.; Balsara, N. P. *Macromolecules* **2009,** 42, (15), 5642-5651.
5. Rubatat, L.; Li, C. X.; Dietsch, H.; Nykanen, A.; Ruokolainen, J.; Mezzenga, R. *Macromolecules* **2008,** 41, (21), 8130-8137.
6. Ruzette, A. V. G.; Soo, P. P.; Sadoway, D. R.; Mayes, A. M. *Journal of the Electrochemical Society* **2001,** 148, (6), A537-A543.
7. Hoarfrost, M. L.; Segalman, R. A. *Macromolecules* **2011,** 44, (13), 5281-5288.
8. Cho, B. K.; Jain, A.; Gruner, S. M.; Wiesner, U. *Science* **2004,** 305, (5690), 1598-1601.
9. Kim, Y. S.; Pivovar, B. S. *Annual Review of Chemical and Biomolecular Engineering, Vol 1* **2010,** 1, 123-148.
10. Scatena, L. F.; Brown, M. G.; Richmond, G. L. *Science* **2001,** 292, (5518), 908-912.
11. Piletic, I. R.; Moilanen, D. E.; Spry, D. B.; Levinger, N. E.; Fayer, M. D. *Journal of Physical Chemistry A* **2006,** 110, (34), 10369-10369.
12. Moilanen, D. E.; Levinger, N. E.; Spry, D. B.; Fayer, M. D. *Journal of the American Chemical Society* **2007,** 129, (46), 14311-14318.
13. Guegan, R. *Journal of Colloid and Interface Science* **2011,** 358, (2), 485-490.
14. Moilanen, D. E.; Piletic, I. R.; Fayer, M. D. *Journal of Physical Chemistry C* **2007,** 111, (25), 8884-8891.
15. Choi, P.; Jalani, N. H.; Datta, R. *Journal of the Electrochemical Society* **2005,** 152, (3), E123-E130.
16. Eikerling, M.; Kornyshev, A. A.; Kuznetsov, A. M.; Ulstrup, J.; Walbran, S. *Journal of Physical Chemistry B* **2001,** 105, (17), 3646-3662.
17. Mafe, S.; Manzanares, J. A.; Ramirez, P. *Physical Chemistry Chemical Physics* **2003,** 5, (2), 376-383.
18. Paddison, S. J.; Paul, R. *Physical Chemistry Chemical Physics* **2002,** 4, (7), 1158-1163.
19. Singh, M.; Odusanya, O.; Wilmes, G. M.; Eitouni, H. B.; Gomez, E. D.; Patel, A. J.; Chen, V. L.; Park, M. J.; Fragouli, P.; Iatrou, H.; Hadjichristidis, N.; Cookson, D.; Balsara, N. P. *Macromolecules* **2007,** 40, (13), 4578-4585.
20. Bureekaew, S.; Horike, S.; Higuchi, M.; Mizuno, M.; Kawamura, T.; Tanaka, D.; Yanai, N.; Kitagawa, S. *Nature Materials* **2009,** 8, (10), 831-836.
21. Simone, P. M.; Lodge, T. P. *Acs Applied Materials & Interfaces* **2009,** 1, (12), 2812-2820.
22. Simone, P. M.; Lodge, T. P. *Macromolecules* **2008,** 41, (5), 1753-1759.
23. Virgili, J. M.; Hexemer, A.; Pople, J. A.; Segalman, R. A.; Balsara, N. P. *Macromolecules* **2009,** 42, (13), 4604-4613.

24. Virgili, J. M.; Nedoma, A. J.; Segalman, R. A.; Balsara, N. P. *Macromolecules* **2010,** 43, (8), 3750-3756.
25. Virgili, J. M.; Hoarfrost, M. L.; Segalman, R. A. *Macromolecules* **2010,** 43, (12), 5417-5423.
26. Gwee, L.; Choi, J. H.; Winey, K. I.; Elabd, Y. A. *Polymer* **2010,** 51, (23), 5516-5524.
27. Munch, W.; Kreuer, K. D.; Silvestri, W.; Maier, J.; Seifert, G. *Solid State Ionics* **2001,** 145, (1-4), 437-443.
28. Noda, A.; Susan, A. B.; Kudo, K.; Mitsushima, S.; Hayamizu, K.; Watanabe, M. *Journal of Physical Chemistry B* **2003,** 107, (17), 4024-4033.
29. Kreuer, K. D.; Fuchs, A.; Ise, M.; Spaeth, M.; Maier, J. *Electrochimica Acta* **1998,** 43, (10-11), 1281-1288.
30. Kim, S. Y.; Kim, S.; Park, M. J. *Nature Communications* **2010,** 1:88.
31. Kim, S. Y.; Yoon, E.; Joo, T.; Park, M. J. *Macromolecules* **2011,** 44, (13), 5289-5298.
32. Hou, J. B.; Zhang, Z. Y.; Madsen, L. A. *Journal of Physical Chemistry B* **2011,** 115, (16), 4576-4582.
33. Susan, M. A.; Kaneko, T.; Noda, A.; Watanabe, M. *Journal of the American Chemical Society* **2005,** 127, (13), 4976-4983.
34. Yokoyama, H.; Mates, T. E.; Kramer, E. J. *Macromolecules* **2000,** 33, (5), 1888-1898.
35. Price, W. S. *Concepts in Magnetic Resonance* **1998,** 10, (4), 197-237.
36. Stejskal, E. O.; Tanner, J. E. *Journal of Chemical Physics* **1965,** 42, (1), 288-292.
37. Raiford, D. S.; Fisk, C. L.; Becker, E. D. *Analytical Chemistry* **1979,** 51, (12), 2050-2051.
38. Azuah, R. T.; Kneller, L. R.; Qiu, Y. M.; Tregenna-Piggott, P. L. W.; Brown, C. M.; Copley, J. R. D.; Dimeo, R. M. *Journal of Research of the National Institute of Standards and Technology* **2009,** 114, (6), 341-358.
39. Hoarfrost, M. L.; Tyagi, M. S.; Segalman, R. A.; Reimer, J. A. *In Preparation*.
40. Lee, D. H.; Kim, H. Y.; Kim, J. K.; Huh, J.; Ryu, D. Y. *Macromolecules* **2006,** 39, (6), 2027-2030.
41. Hou, J. B.; Li, J.; Madsen, L. A. *Macromolecules* **2010,** 43, (1), 347-353.
42. Kanaskov.Yd; Sukhoruk.Bi; Pentin, Y. A.; Komarovs.Gv. *Izvestiya Akademii Nauk Sssr-Seriya Khimicheskaya* **1970**, (8), 1735.
43. Cavalcanti, W. L.; Portaluppi, D. F.; Joswig, J. O. *Journal of Chemical Physics* **2010,** 133, (10).
44. Bee, M., *Quasielastic Neutron Scattering: Principles and Applications in Solid State Chemistry, Biology and Materials Science*. IOP Publishing Ltd: 1988.
45. Dasannacharya, B. A.; Rao, K. R. *Physical Review* **1965,** 137, (2A), A417-A427.
46. Inamura, Y.; Yamamuro, O.; Hayashi, S.; Hamaguchi, H. O. *Physica B-Condensed Matter* **2006,** 385, 732-734.
47. Aoun, B.; Gonzalez, M. A.; Ollivier, J.; Russina, M.; Izaola, Z.; Price, D. L.; Saboungi, M. L. *Journal of Physical Chemistry Letters* **2010,** 1, (17), 2503-2507.
48. Mamontov, E.; Luo, H. M.; Dai, S. *Journal of Physical Chemistry B* **2009,** 113, (1), 159-169.

49. Chudley, C. T.; Elliott, R. J. *Proceedings of the Physical Society of London* **1961,** 77, (494), 353-361.
50. Chen, S. H.; Teixeira, J.; Nicklow, R. *Physical Review A* **1982,** 26, (6), 3477-3482.
51. Teixeira, J.; Bellissentfunel, M. C.; Chen, S. H.; Dianoux, A. J. *Physical Review A* **1985,** 31, (3), 1913-1917.
52. Li, J.; Park, J. K.; Moore, R. B.; Madsen, L. A. *Nature Materials* **2011,** 10, (7), 507-511.

Chapter 7. Conclusion and Future Outlook

Combining ionic liquids with block copolymers is a promising route to obtaining nanostructured membranes having high conductivity in combination with other desirable properties such as mechanical durability and selective gas permeability. Through investigation of model block copolymer/ionic liquid systems, we have furthered the understanding of the relationship between composition, structure, and ion transport in such membranes. Our findings suggest a roadmap for the rational design of nanostructured membranes for a variety of applications, especially electrochemical devices. Knowledge of how conductivity depends on ionic liquid concentration and membrane structure will guide the optimization of membranes to meet the specific property requirements of various devices.

An important area of future fundamental research is gaining further understanding of how interactions between the host polymer and the ionic liquid affect conductive properties. We have developed general scaling relationships for the bulk ionic conductivity of block copolymer/ionic liquid membranes, where certain proportionality constants vary depending on the polymer and ionic liquid chemistries, presumably due to specific chemical interactions. For instance, the conductivities of PS-*b*-P2VP/[Im][TFSI] mixtures have stronger temperature dependence than any other type of mixture, which is likely due to hydrogen bonding between imidazolium cations and P2VP repeat units slowing down cation transport. Furthermore, in Chapter 6 we described how specific interactions between the polymer and the ionic liquid drastically changes the anion and cation transference numbers compared to the neat ionic liquid, and that ion aggregation is affected by combination with a polymer as well. While the general conductivity scaling relationships developed in this work are invaluable for optimizing the design of nanostructured membranes for electrochemical applications, it will also be important to understand how the choices of polymer and ionic liquid affect conductive properties in order to optimize the chemistry of the membranes.

Furthermore, it is important for continuing efforts to be directed towards understanding how membrane composition and structure are related not only to ionic conductivity, but to other important properties for electrochemical applications, specifically mechanical properties and gas permeability. For most applications, it is critical to have a durable membrane. In general, it is expected that mechanical properties worsen with increasing ionic liquid concentration. Thus, there is a tradeoff between improving conductivity and worsening mechanical durability with increasing ionic liquid concentration. Managing gas permeability is also very important in membranes for devices such as fuel cells and solar-to-fuel devices. It is not immediately obvious how gas permeability is related to structure and ionic liquid concentration since both the polymer and ionic liquid can be designed to contribute to gas blocking. The chemistry of the ionic liquid itself can be tuned to provide the desired gas selectivity, and a gas-impermeable component can be incorporated into the non-ionic-liquid-containing section of the block copolymer. Intimate knowledge of how mechanical properties and gas permeability depend on membrane composition and structure is required for the optimization of membranes for

specific applications requiring different combinations of these properties with ionic conductivity.

While studying model diblock copolymer/ionic liquid systems provides invaluable insight into structure-property relationships, the development of membranes for practical application will require several improvements, particularly with regard to the long-term stability of the membranes. The mechanical properties can be greatly improved by utilizing multiblock copolymers or exploiting physical or chemical crosslinking and/or crystallinity in nonconductive microphases. The chemical stability of the membranes in harsh device environments must be addressed by incorporating fluorinated or other chemically robust polymer chemistries. The conductivity scaling relationships developed in this work will also be useful for optimizing the design of practical membranes with enhanced mechanical and chemical resilience.

A major practical limitation of the model block copolymer/ionic liquid membranes is that the ionic liquid may easily leach out of the membrane or be washed away during device operation. In the future, it is desirable to design completely solid-state membranes where ionic liquid molecules are covalently bound to the polymer chain. There are many potential challenges associated with this strategy, especially the decreased vehicular mobility of the tethered ions. Taking advantage of the demonstrated effect of block copolymer nanoconfinement on ion conduction mechanisms is a promising tactic for overcoming decreased mobility in such membranes.

The development of nanostructured, ion-conducting membranes will continue to be an important area of research, especially for the design of advanced electrochemical devices. Our newly-developed understanding of the relationship between membrane composition, structure, and ion-transport provides a valuable framework for the rational design of membranes with enhanced conductivity.